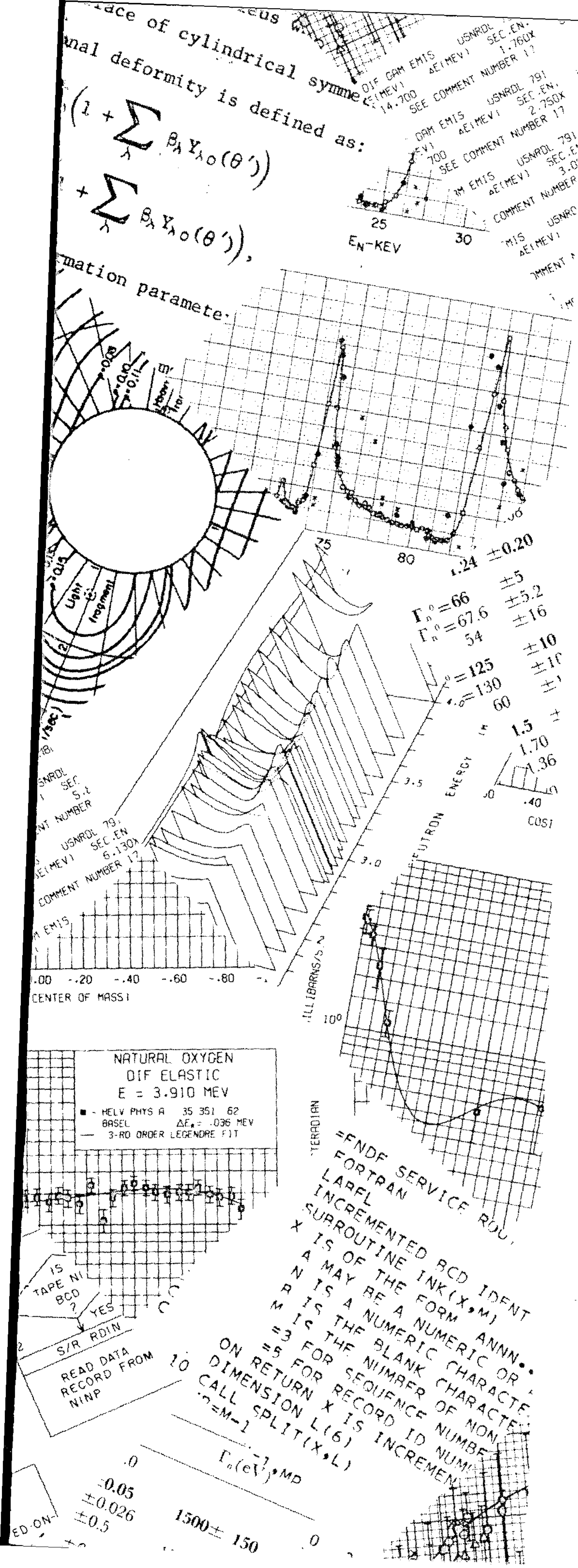

1135

BNL-NCS—29426
DOE/NDC-24/U
NEANDC(US)-210/U
INDC(USA)-86/L
Informal Report
Limited Distribution

REPORTS TO THE DOE NUCLEAR DATA COMMITTEE

Compiled by
NATIONAL NUCLEAR DATA CENTER
for the
U.S. Department of Energy
Nuclear Data Committee

May 1981

BROOKHAVEN NATIONAL LABORATORY
ASSOCIATED UNIVERSITIES
UPTON, NEW YORK 11973

national nuclear data center

BNL-NCS-29426
DOE/NDC-24/U

REPORTS TO THE DOE NUCLEAR DATA COMMITTEE

May 1981

Compiled by
NATIONAL NUCLEAR DATA CENTER
for the
U.S. Department of Energy
Nuclear Data Committee

NATIONAL NUCLEAR DATA CENTER

BROOKHAVEN NATIONAL LABORATORY
ASSOCIATED UNIVERSITIES, INC.

UNDER CONTRACT NO. DE-AC02-76CH00016 WITH THE

UNITED STATES DEPARTMENT OF ENERGY

Printed in the United States of America
Available from
National Technical Information Service
U.S. Department of Commerce
5285 Port Royal Road
Springfield, VA 22161

NTIS price codes:
Printed Copy: A10; Microfiche Copy: A01

PREFACE

The reports in this document were submitted to the Department of Energy, Nuclear Data Committee (DOE-NDC) in April, 1981. The reporting laboratories are those having a substantial effort in measuring neutron and nuclear cross sections of relevance to the U.S. applied nuclear energy program.

The authors of the Status Report contributions are responsible for collecting and editing individual contributions from their laboratory and are not necessarily the sole authors of the contributions. The scientists responsible for the work described in each individual contribution are listed at the beginning of the contribution.

The material contained in these reports is to be regarded as comprised of informal statements of recent developments and preliminary data. Persons wishing to make use of these data should contact the individual experimenter for further details. The data which appear in this document should be quoted only by permission of the contributor and should be referenced as private communication, and not by this document number. Appropriate subjects are listed as follows:

1. Microscopic neutron cross sections relevant to the nuclear energy program, including shielding. Inverse reactions where pertinent are included.

2. Charged-particle cross sections, where they are relevant to "1" above, and where relevant to developing and testing nuclear models.

3. Gamma ray production, radioactive decay, and theoretical developments in nuclear structure which are applicable to nuclear energy programs.

4. Proton and alpha-particle cross sections, at energies of up to 1 GeV, which are of interest to the space program.

These reports cannot be regarded as a complete summary of the nuclear research efforts in the U.S. A number of laboratories, whose research is less programmatically oriented do not submit reports; neither do the submitted reports reflect all the work related to nuclear data in progress at the submitting laboratory.

This compilation has been produced almost completely from master copies prepared by the individual contributors listed in the Table of Contents.

The CINDA-type index and CPND-type index, which follow the Table of Contents, were prepared by Gail Wyant and Thomas Burrows, respectively, of the National Nuclear Data Center, Brookhaven National Laboratory, Upton, Long Island, New York.

TABLE OF CONTENTS

TABLE OF CONTENTS (cont.)

NEUTRON DATA REFERENCES

Element	Quantity	Energy (eV) Min	Max	Type	Documentation Ref	Page	Date	Lab	Comments
^{1}H	σ_{tot}	5.0+5	2.0+6	Expt	DOE-NDC-24	6	Apr81	ANL	Poenitz+3 ES.PRELIM TBL.CFD ENDF OK.
^{1}H	σ_{el}	5.0+5	2.0+6	Theo	DOE-NDC-24	6	Apr81	ANL	Poenitz+TRIPLET,SINGLET SCT LENGTH.
^{1}H	σ_{pol}	1.4+7	1.7+7	Expt	DOE-NDC-24	169	Apr81	TNL	Beyerle+ANAL PWR.SEE NP/A 340,P.34.
C_6H_6	σ_{tsl}	1.2+0	9.6+0	Expt	DOE-NDC-24	106	Apr81	NBS	Johnson+INEL SCT SPEC GRPH.TBC.
^{3}He	σ_{pol}	9.0+6		Expt	DOE-NDC-24	185	Apr81	TNL	Roberson+ANGDIST,ANAL PWR GRPH.CFD.
^{3}He	$\sigma_{n,\gamma}$	6.0+6	1.6+7	Expt	DOE-NDC-24	185	Apr81	TNL	Roberson+GN DRVD.GRPH CFD (P,G).
^{4}He	$\sigma_{\gamma,n}$	2.3+7	3.3+7	Expt	DOE-NDC-24	185	Apr81	TNL	Roberson+INVERSE.GRPH CFD OTHS.
^{6}Li	σ_{tot}		4.0+6	Expt	DOE-NDC-24	2	Apr81	ANL	Guenther+NDG.TBP IN JOURNAL SOON.
^{6}Li	σ_{tot}	1.0+1		Expt	DOE-NDC-24	105	Apr81	NBS	Carlson+TRNS.TBD.NDG.
^{6}Li	σ_{el}	1.4+7		Expt	DOE-NDC-24	72	Apr81	LAS	Drake.SPEC,ANGDIST MEAS.TBL.CFD.
^{6}Li	$\sigma_{el}(\theta)$		4.0+6	Expt	DOE-NDC-24	2	Apr81	ANL	Guenther+NDG.TBP IN JOURNAL SOON.
^{6}Li	$\sigma_{el}(\theta)$	1.4+7		Expt	DOE-NDC-24	72	Apr81	LAS	Drake.SPEC,ANGDIST MEAS.TBL.CFD.
^{6}Li	$\sigma_{el}(\theta)$	4.5+6	6.4+6	Expt	DOE-NDC-24	137	Apr81	OHO	Knox+4 ES.2 ES TBD.NDG.SEE P141.
^{6}Li	$\sigma_{dif.inl}$		4.0+6	Expt	DOE-NDC-24	2	Apr81	ANL	Guenther+NDG.TBP IN JOURNAL SOON.
^{6}Li	$\sigma_{dif.inl}$	1.4+7		Expt	DOE-NDC-24	72	Apr81	LAS	Drake.SPEC,ANGDIST MEAS.TBL.CFD.
^{6}Li	$\sigma_{dif.inl}$	4.5+6	6.4+6	Expt	DOE-NDC-24	137	Apr81	OHO	Knox+4 ES.2 ES TBD.NDG.SEE P141.
^{6}Li	$\sigma_{n,t}$	1.0+0	5.0+3	Expt	DOE-NDC-24	75	Apr81	LAS	Auchampaugh+FLUX SHAPE.NDG.
^{6}Li	$\sigma_{n,t}$	1.0+1		Expt	DOE-NDC-24	105	Apr81	NBS	Carlson+LI-6/B-10 RATIO TBD.NDG.
^{6}Li	$\sigma_{n,t}$	2.0+6		Expt	DOE-NDC-24	141	Apr81	OHO	Knox+EXPT,ANAL TBD.NDG.
^{7}Li	σ_{el}	1.4+7		Expt	DOE-NDC-24	72	Apr81	LAS	Drake.SPEC,ANGDIST MEAS.TBL.CFD.
^{7}Li	$\sigma_{el}(\theta)$	1.4+7		Expt	DOE-NDC-24	72	Apr81	LAS	Drake.SPEC,ANGDIST MEAS.TBL.CFD.
^{7}Li	$\sigma_{el}(\theta)$		8.0+6	Expt	DOE-NDC-24	141	Apr81	OHO	Knox+R-MATRIX.NDG.TBP NP/A.
^{7}Li	$\sigma_{dif.inl}$	1.4+7		Expt	DOE-NDC-24	72	Apr81	LAS	Drake.SPEC,ANGDIST MEAS.TBL.CFD.
^{7}Li	$\sigma_{dif.inl}$		8.0+6	Expt	DOE-NDC-24	141	Apr81	OHO	Knox+R-MATRIX.NDG.TBP NP/A.
^{7}Li	$\sigma_{n,n'\gamma}$	1.0+5	2.0+7	Revw	DOE-NDC-24	121	Apr81	ORL	Larson.ABST BNL 80 P.277.NDG.
^{7}Li	σ_{nem}	1.0+6	2.0+7	Revw	DOE-NDC-24	121	Apr81	ORL	Larson.ABST BNL 80 P.277.NDG.
^{7}Li	$\sigma_{n,nt}$	7.0+6	9.0+6	Expt	DOE-NDC-24	1	Apr81	ANL	Smith+GRPH.CFD ENDF.TBP ANL-NDM-55.
^{9}Be	$\sigma_{el}(\theta)$	9.0+6	1.5+7	Expt	DOE-NDC-24	158	Apr81	TNL	Beyerle+OPTMDL FIT TO DATA.GRPH.
^{9}Be	σ_{pol}	1.1+7	1.5+7	Theo	DOE-NDC-24	177	Apr81	TNL	Byrd+ANAL PWR CALCS. GRPHS.CFD.
^{9}Be	σ_{pol}	9.0+6	1.5+7	Expt	DOE-NDC-24	169	Apr81	TNL	Beyerle+5 ES.ANAL PWR.CFD MDL.NDG.
^{9}Be	$\sigma_{n,p}$	1.4+7		Expt	DOE-NDC-24	51	Apr81	LRL	Haight+EMISSION CS.NDG.
^{9}Be	$\sigma_{n,\alpha}$	1.5+7		Expt	DOE-NDC-24	155	Apr81	AI	Kneff+HE PROD CS.NDG.ANAL TBD.
^{9}Be	$\sigma_{n,\alpha}$	1.4+7		Expt	DOE-NDC-24	51	Apr81	LRL	Haight+ALPHA SPEC GRPH GVN.

NEUTRON DATA REFERENCES

Element	Quantity	Energy (eV) Min	Max	Type	Documentation Ref	Page	Date	Lab	Comments
^{10}B	$\sigma_{el}(\theta)$	8.0+6	1.4+7	Expt	DOE-NDC-24	158	Apr81	TNL	Beyerle+TOF.GRPHS.TBP NSE.OPTMDL.
^{10}B	$\sigma_{dif.inl}$	8.0+6	1.4+7	Expt	DOE-NDC-24	158	Apr81	TNL	Beyerle+TOF.GRPHS.TBP NSE.OPTMDL.
^{10}B	$\sigma_{n,\alpha}$	1.0+1		Expt	DOE-NDC-24	105	Apr81	NBS	Carlson+LI-6/B-10 RATIO TBD.NDG.
^{11}B	$\sigma_{el}(\theta)$	5.3+6	6.4+6	Expt	DOE-NDC-24	137	Apr81	OHO	Koehler+3 ES.CFD OTHS.R MATRIX.NDG.
^{11}B	$\sigma_{el}(\theta)$	8.0+6	1.4+7	Expt	DOE-NDC-24	158	Apr81	TNL	Beyerle+TOF.GRPHS.TBP NSE.OPTMDL.
^{11}B	$\sigma_{dif.inl}$	5.3+6	6.4+6	Expt	DOE-NDC-24	137	Apr81	OHO	Koehler+3 ES.CFD OTHS.R MATRIX.NDG.
^{11}B	$\sigma_{dif.inl}$	8.0+6	1.4+7	Expt	DOE-NDC-24	158	Apr81	TNL	Beyerle+TOF.GRPHS.TBP NSE.OPTMDL.
^{12}C	σ_{tot}	5.0+5	2.0+6	Expt	DOE-NDC-24	6	Apr81	ANL	Poenitz+3 ES.NDG.PRELIM.
^{12}C	σ_{tot}	2.0+6	8.0+7	Revw	DOE-NDC-24	121	Apr81	ORL	Larson.ABST BNL 80 P.277.NDG.
^{12}C	$\sigma_{el}(\theta)$	2.4+7		Expt	DOE-NDC-24	138	Apr81	OHO	Mellema+TOF.EXPT,ANAL TBC.NDG.
^{12}C	σ_{pol}	1.1+7	1.5+7	Expt	DOE-NDC-24	169	Apr81	TNL	Beyerle+ANAL PWR MEAS.OPTMDL.GRPH.
^{12}C	$\sigma_{dif.inl}$	2.4+7		Expt	DOE-NDC-24	138	Apr81	OHO	Mellema+TOF.EXPT,ANAL TBC.NDG.
^{12}C	$\sigma_{n,X}$	4.0+7	5.0+7	Expt	DOE-NDC-24	31	Apr81	DAV	Brady+2 ES.TRANS TECHNIQUE.TBL.
^{12}C	$\sigma_{n,n'\gamma}$	1.0+5	2.0+7	Revw	DOE-NDC-24	121	Apr81	ORL	Larson.ABST BNL 80 P.277.NDG.
^{12}C	$\sigma_{n,p}$	2.7+7	6.1+7	Expt	DOE-NDC-24	33	Apr81	DAV	Subramanian+CONTINUUM DIF CS.NDG.
^{12}C	$\sigma_{n,d}$	2.7+7	6.1+7	Expt	DOE-NDC-24	33	Apr81	DAV	Subramanian+CONTINUUM DIF CS.NDG.
^{12}C	$\sigma_{n,t}$	2.7+7	6.1+7	Expt	DOE-NDC-24	33	Apr81	DAV	Subramanian+CONTINUUM DIF CS.NDG.
^{12}C	$\sigma_{n,^3He}$	2.7+7	6.1+7	Expt	DOE-NDC-24	33	Apr81	DAV	Subramanian+CONTINUUM DIF CS.NDG.
^{12}C	$\sigma_{n,\alpha}$	2.7+7	6.1+7	Expt	DOE-NDC-24	33	Apr81	DAV	Subramanian+CONTINUUM DIF CS.NDG.
^{12}C	$\sigma_{n,\alpha}$	9.5+6	2.4+7	Expt	DOE-NDC-24	140	Apr81	OHO	Finlay+3 ES.DBL DIFF.GRPHS.TBC.
^{12}C	$\sigma_{n,n\alpha}$	9.5+6	2.4+7	Expt	DOE-NDC-24	140	Apr81	OHO	Finlay+3 ES.DBL DIFF.GRPHS.TBC.
^{12}C	Res.Params.		8.5+6	Expt	DOE-NDC-24	141	Apr81	OHO	Knox+R-MATRIX ANAL.I,PI.NDG.TBP.
^{13}C	σ_{tot}		6.5+6	Expt	DOE-NDC-24	142	Apr81	OHO	Lane+R-MATRIX.NDG.TBP PR/C.
^{13}C	$\sigma_{el}(\theta)$		6.5+6	Expt	DOE-NDC-24	142	Apr81	OHO	Lane+R-MATRIX.NDG.TBP PR/C.
^{13}C	$\sigma_{el}(\theta)$	4.6+6	4.9+6	Expt	DOE-NDC-24	138	Apr81	OHO	Resler+6 ES.ANAL,EXPT TBC.NDG.
^{13}C	$\sigma_{el}(\theta)$	1.0+7	1.8+7	Expt	DOE-NDC-24	158	Apr81	TNL	Beyerle+TOF.20-155 DEG.NDG.TBC.
^{13}C	$\sigma_{dif.inl}$	4.6+6	4.9+6	Expt	DOE-NDC-24	138	Apr81	OHO	Resler+6 ES.ANAL,EXPT TBC.NDG.
^{13}C	$\sigma_{dif.inl}$	1.0+7	1.8+7	Expt	DOE-NDC-24	158	Apr81	TNL	Beyerle+TOF.20-155 DEG.NDG.TBC.
^{13}C	$\sigma_{n,\gamma}$	5.0+6	1.4+7	Expt	DOE-NDC-24	184	Apr81	TNL	Roberson+EXPT CFD CALC.GRPH P.188.
^{13}C	$\sigma_{\gamma,n}$	7.5+6	4.0+7	Expt	DOE-NDC-24	51	Apr81	LRL	Berman+(G,N),(G,2N).NDG.
^{14}N	$\sigma_{n,\gamma}$	NDG		Expt	DOE-NDC-24	184	Apr81	TNL	Roberson+EXPT CFD CALC.NDG.
^{14}N	$\sigma_{n,X\gamma}$	1.0+5	2.0+7	Revw	DOE-NDC-24	121	Apr81	ORL	Larson.ABST BNL 80 P.277.NDG.
^{14}N	$\sigma_{n,p}$	2.7+7	6.1+7	Expt	DOE-NDC-24	33	Apr81	DAV	Subramanian+CONTINUUM DIF CS.NDG.

NEUTRON DATA REFERENCES

Element	Quantity	Energy (eV) Min	Max	Type	Documentation Ref	Page	Date	Lab	Comments
^{14}N	$\sigma_{n,p}$	1.4+7		Expt	DOE-NDC-24	51	Apr81	LRL	Haight+EMISSION CS.NDG.
^{14}N	$\sigma_{n,d}$	2.7+7	6.1+7	Expt	DOE-NDC-24	33	Apr81	DAV	Subramanian+CONTINUUM DIF CS.NDG.
^{14}N	$\sigma_{n,d}$	1.4+7		Expt	DOE-NDC-24	51	Apr81	LRL	Haight+EMISSION CS.NDG.
^{14}N	$\sigma_{n,t}$	2.7+7	6.1+7	Expt	DOE-NDC-24	33	Apr81	DAV	Subramanian+CONTINUUM DIF CS.NDG.
^{14}N	$\sigma_{n,^{3}He}$	2.7+7	6.1+7	Expt	DOE-NDC-24	33	Apr81	DAV	Subramanian+CONTINUUM DIF CS.NDG.
^{14}N	$\sigma_{n,\alpha}$	2.7+7	6.1+7	Expt	DOE-NDC-24	33	Apr81	DAV	Subramanian+CONTINUUM DIF CS.NDG.
^{14}N	$\sigma_{n,\alpha}$	1.4+7		Expt	DOE-NDC-24	51	Apr81	LRL	Haight+EMISSION CS.NDG.
^{16}O	σ_{tot}	2.0+6	8.0+7	Revw	DOE-NDC-24	121	Apr81	ORL	Larson.ABST BNL 80 P.277.NDG.
^{16}O	$\sigma_{n,X}$	4.0+7	5.0+7	Expt	DOE-NDC-24	31	Apr81	DAV	Brady+2 ES.TRANS TECHNIQUE.TBL.
^{16}O	$\sigma_{n,X\gamma}$	1.0+5	2.0+7	Revw	DOE-NDC-24	121	Apr81	ORL	Larson.ABST BNL 80 P.277.NDG.
^{16}O	$\sigma_{n,p}$	2.7+7	6.1+7	Expt	DOE-NDC-24	33	Apr81	DAV	Subramanian+CONTINUUM DIF CS.NDG.
^{16}O	$\sigma_{n,p}$	1.4+7		Expt	DOE-NDC-24	51	Apr81	LRL	Haight+EMISSION CS.NDG.
^{16}O	$\sigma_{n,d}$	2.7+7	6.1+7	Expt	DOE-NDC-24	33	Apr81	DAV	Subramanian+CONTINUUM DIF CS.NDG.
^{16}O	$\sigma_{n,d}$	1.4+7		Expt	DOE-NDC-24	51	Apr81	LRL	Haight+EMISSION CS.NDG.
^{16}O	$\sigma_{n,t}$	2.7+7	6.1+7	Expt	DOE-NDC-24	33	Apr81	DAV	Subramanian+CONTINUUM DIF CS.NDG.
^{16}O	$\sigma_{n,^{3}He}$	2.7+7	6.1+7	Expt	DOE-NDC-24	33	Apr81	DAV	Subramanian+CONTINUUM DIF CS.NDG.
^{16}O	$\sigma_{n,\alpha}$	1.5+7		Expt	DOE-NDC-24	155	Apr81	AI	Kneff+HE PROD CS.NDG.ANAL TBD.
^{16}O	$\sigma_{n,\alpha}$	2.7+7	6.1+7	Expt	DOE-NDC-24	33	Apr81	DAV	Subramanian+CONTINUUM DIF CS.NDG.
^{16}O	$\sigma_{n,\alpha}$	1.4+7		Expt	DOE-NDC-24	51	Apr81	LRL	Haight+EMISSION CS.NDG.
^{16}O	$\sigma_{\gamma,n}$	1.7+7	2.1+7	Expt	DOE-NDC-24	191	Apr81	YAL	Firk.90 DEG POL MEAS.
^{17}O	$\sigma_{\gamma,n}$	8.5+6	4.0+7	Expt	DOE-NDC-24	51	Apr81	LRL	Berman+(G,N),(G,2N).NDG.
^{18}O	$\sigma_{el}(\theta)$	6.0+6	6.4+6	Expt	DOE-NDC-24	138	Apr81	OHO	Koehler+5 ES.9 ANGS.ANAL TBD.NDG.
^{18}O	$\sigma_{dif.inl}$	6.0+6	6.4+6	Expt	DOE-NDC-24	138	Apr81	OHO	Koehler+5 ES.9 ANGS.ANAL TBD.NDG.
^{19}F	$\sigma_{n,X\gamma}$	1.0+5	2.0+7	Revw	DOE-NDC-24	121	Apr81	ORL	Larson.ABST BNL 80 P.277.NDG.
^{19}F	$\sigma_{n,\alpha}$	1.5+7		Expt	DOE-NDC-24	155	Apr81	AI	Kneff+HE PROD CS.NDG.ANAL TBD.
^{22}Ne	$\sigma_{n,\gamma}$	NDG		Expt	DOE-NDC-24	120	Apr81	ORL	Macklin.CAPT CS MEAS TBD.NDG.
^{23}Na	Evaluation	1.0-5	2.0+7	Eval	DOE-NDC-24	131	Apr81	ORL	Larson.NDG. ABST ORNL-5662 9/80.
^{23}Na	$\sigma_{dif.inl}$	NDG		Theo	DOE-NDC-24	128	Apr81	ORL	Larson.NDG.H-F CALC.
^{23}Na	$\sigma_{n,X\gamma}$	1.0+5	2.0+7	Revw	DOE-NDC-24	121	Apr81	ORL	Larson.ABST BNL 80 P.277.NDG.
^{23}Na	$\sigma_{n,X\gamma}$	NDG		Theo	DOE-NDC-24	128	Apr81	ORL	Larson.NDG.H-F CALC.
^{23}Na	$\sigma_{n,2n}$	NDG		Theo	DOE-NDC-24	128	Apr81	ORL	Larson.NDG.H-F CALC.CFD EXPT.
^{23}Na	$\sigma_{n,xn}$	1.5+7		Theo	DOE-NDC-24	129	Apr81	ORL	Fu.(N,INEL(N)X) DBL DIFF.NDG.
^{23}Na	σ_{nem}	NDG		Theo	DOE-NDC-24	128	Apr81	ORL	Larson.NDG.H-F CALC.

NEUTRON DATA REFERENCES

Element	Quantity	Energy (eV) Min	Max	Type	Documentation Ref	Page	Date	Lab	Comments
^{23}Na	$\sigma_{n,p}$	NDG		Theo	DOE-NDC-24	128	Apr81	ORL	Larson.NDG.H-F CALC.
^{23}Na	$\sigma_{n,\alpha}$	NDG		Theo	DOE-NDC-24	128	Apr81	ORL	Larson.NDG.H-F CALC.
Mg	σ_{pol}	5.0+4	5.0+5	Expt	DOE-NDC-24	190	Apr81	YAL	Kruk+POL N SOURCE STUDY.NDG.
Mg	$\sigma_{n,n'\gamma}$	1.0+5	2.0+7	Revw	DOE-NDC-24	121	Apr81	ORL	Larson.ABST BNL 80 P.277.NDG.
Mg	$\sigma_{n,X\gamma}$	1.0+5	2.0+7	Revw	DOE-NDC-24	121	Apr81	ORL	Larson.ABST BNL 80 P.277.NDG.
^{26}Mg	$\sigma_{el}(\theta)$	2.4+7		Expt	DOE-NDC-24	139	Apr81	OHO	Tailor+TOF.ANGDIST.OPTMDL ANAL.TBC.
^{26}Mg	$\sigma_{dif.inl}$	2.4+7		Expt	DOE-NDC-24	139	Apr81	OHO	Tailor+TOF.ANGDIST.OPTMDL ANAL.TBC.
^{27}Al	σ_{tot}	2.0+6	8.0+7	Revw	DOE-NDC-24	121	Apr81	ORL	Larson.ABST BNL 80 P.277.NDG.
^{27}Al	$\sigma_{n,X\gamma}$	1.0+5	2.0+7	Revw	DOE-NDC-24	121	Apr81	ORL	Larson.ABST BNL 80 P.277.NDG.
^{27}Al	σ_{nem}	1.0+6	2.0+7	Revw	DOE-NDC-24	121	Apr81	ORL	Larson.ABST BNL 80 P.277.NDG.
Si	σ_{tot}	2.0+6	8.0+7	Revw	DOE-NDC-24	121	Apr81	ORL	Larson.ABST BNL 80 P.277.NDG.
Si	$\sigma_{dif.inl}$	1.0+7	1.2+7	Expt	DOE-NDC-24	164	Apr81	TNL	Beyerle+DBL DIFF.2 ES,5 ANGS.NDG.
Si	$\sigma_{n,X\gamma}$	1.0+5	2.0+7	Revw	DOE-NDC-24	121	Apr81	ORL	Larson.ABST BNL 80 P.277.NDG.
Si	$\sigma_{n,p}$	1.4+7		Expt	DOE-NDC-24	51	Apr81	LRL	Haight+EMISSION CS.NDG.
Si	$\sigma_{n,d}$	1.4+7		Expt	DOE-NDC-24	51	Apr81	LRL	Haight+EMISSION CS.NDG.
Si	$\sigma_{n,\alpha}$	1.5+7		Expt	DOE-NDC-24	155	Apr81	AI	Kneff+HE PROD CS.NDG.ANAL TBD.
Si	$\sigma_{n,\alpha}$	1.4+7		Expt	DOE-NDC-24	51	Apr81	LRL	Haight+EMISSION CS.NDG.
S	$\sigma_{n,\gamma}$	2.5-2		Expt	DOE-NDC-24	73	Apr81	LAS	Jurney+DRVD FROM ISOTOPE CS.PRELIM.
^{32}S	$\sigma_{n,\gamma}$	2.5-2		Expt	DOE-NDC-24	73	Apr81	LAS	Jurney+PRELIM CAPT CS GVN.REL H CS.
^{32}S	$\sigma_{n,\gamma}$	NDG		Expt	DOE-NDC-24	120	Apr81	ORL	Macklin+COMPUTER CODING ERROR CORREC
^{33}S	$\sigma_{n,\gamma}$	2.5-2		Expt	DOE-NDC-24	73	Apr81	LAS	Jurney+PRELIM CAPT CS GVN.REL H CS.
^{34}S	$\sigma_{n,\gamma}$	2.5-2		Expt	DOE-NDC-24	73	Apr81	LAS	Jurney+PRELIM CAPT CS GVN.REL H CS.
^{36}S	$\sigma_{n,\gamma}$	2.5-2		Expt	DOE-NDC-24	73	Apr81	LAS	Jurney+PRELIM CAPT CS GVN.REL H CS.
Ca	σ_{tot}	3.5+7	5.0+7	Expt	DOE-NDC-24	33	Apr81	DAV	Zanelli+3 ES.TOF.CS GVN.TBL.
Ca	σ_{tot}	2.0+6	8.0+7	Revw	DOE-NDC-24	121	Apr81	ORL	Larson.ABST BNL 80 P.277.NDG.
Ca	$\sigma_{n,X}$	4.0+7	5.0+7	Expt	DOE-NDC-24	31	Apr81	DAV	Brady+2 ES.TRANS TECHNIQUE.TBL.
Ca	$\sigma_{n,X\gamma}$	1.0+5	2.0+7	Revw	DOE-NDC-24	121	Apr81	ORL	Larson.ABST BNL 80 P.277.NDG.
^{40}Ca	σ_{pol}	1.0+7	1.4+7	Expt	DOE-NDC-24	170	Apr81	TNL	Beyerle+ANAL PWR,CS MEAS.NDG.
^{40}Ca	$\sigma_{n,\gamma}$	6.0+6	1.7+7	Expt	DOE-NDC-24	187	Apr81	TNL	Roberson+GRPH.CFD OTH.
Ti	$\sigma_{n,X\gamma}$	1.0+5	2.0+7	Revw	DOE-NDC-24	121	Apr81	ORL	Larson.ABST BNL 80 P.277.NDG.
Ti	$\sigma_{n,xn}$	1.0+6	2.0+7	Revw	DOE-NDC-24	121	Apr81	ORL	Larson.ABST BNL 80 P.277.NDG.
^{46}Ti	$\sigma_{n,\alpha}$	1.5+7		Expt	DOE-NDC-24	155	Apr81	AI	Kneff+HE PROD CS.NDG.ANAL TBD.
^{47}Ti	$\sigma_{n,\alpha}$	1.5+7		Expt	DOE-NDC-24	155	Apr81	AI	Kneff+HE PROD CS.NDG.ANAL TBD.

NEUTRON DATA REFERENCES

Element	Quantity	Energy (eV) Min	Max	Type	Documentation Ref	Page	Date	Lab	Comments
^{48}Ti	$\sigma_{n,\alpha}$	1.5+7		Expt	DOE-NDC-24	155	Apr81	AI	Kneff+HE PROD CS.NDG.ANAL TBD.
^{49}Ti	$\sigma_{n,\alpha}$	1.5+7		Expt	DOE-NDC-24	155	Apr81	AI	Kneff+HE PROD CS.NDG.ANAL TBD.
^{50}Ti	$\sigma_{n,\alpha}$	1.5+7		Expt	DOE-NDC-24	155	Apr81	AI	Kneff+HE PROD CS.NDG.ANAL TBD.
^{51}V	$\sigma_{n,X\gamma}$	1.0+5	2.0+7	Revw	DOE-NDC-24	121	Apr81	ORL	Larson.ABST BNL 80 P.277.NDG.
^{51}V	$\sigma_{n,\alpha}$	1.5+7		Expt	DOE-NDC-24	155	Apr81	AI	Kneff+HE PROD CS.NDG.ANAL TBD.
Cr	σ_{tot}	NDG		Expt	DOE-NDC-24	2	Apr81	ANL	Guenther+NDG.TBP ANL-NDM-57.
Cr	σ_{tot}	2.0+6	8.0+7	Revw	DOE-NDC-24	121	Apr81	ORL	Larson.ABST BNL 80 P.277.NDG.
Cr	$\sigma_{el}(\theta)$	NDG		Expt	DOE-NDC-24	2	Apr81	ANL	Guenther+NDG.TBP ANL-NDM-57.
Cr	$\sigma_{dif.inl}$	NDG		Expt	DOE-NDC-24	2	Apr81	ANL	Guenther+NDG.TBP ANL-NDM-57.
Cr	$\sigma_{dif.inl}$	1.0+7	1.2+7	Expt	DOE-NDC-24	164	Apr81	TNL	Beyerle+DBL DIFF.2 ES,5 ANGS.NDG.
Cr	$\sigma_{n,X\gamma}$	1.0+5	2.0+7	Revw	DOE-NDC-24	121	Apr81	ORL	Larson.ABST BNL 80 P.277.NDG.
^{52}Cr	$\sigma_{n,\alpha}$	1.5+7		Expt	DOE-NDC-24	155	Apr81	AI	Kneff+HE PROD CS.NDG.ANAL TBD.
^{53}Cr	$\sigma_{n,p}$		9.4+6	Expt	DOE-NDC-24	3	Apr81	ANL	Smith+ACT.GRPH.U-235 SPEC AVG CALC.
^{53}Cr	$\sigma_{n,\alpha}$	1.5+7		Expt	DOE-NDC-24	155	Apr81	AI	Kneff+HE PROD CS.NDG.ANAL TBD.
^{54}Cr	$\sigma_{n,\alpha}$	1.5+7		Expt	DOE-NDC-24	155	Apr81	AI	Kneff+HE PROD CS.NDG.ANAL TBD.
^{55}Mn	$\sigma_{n,X\gamma}$	1.0+5	2.0+7	Revw	DOE-NDC-24	121	Apr81	ORL	Larson.ABST BNL 80 P.277.NDG.
^{55}Mn	$\sigma_{n,\alpha}$	1.5+7		Expt	DOE-NDC-24	155	Apr81	AI	Kneff+HE PROD CS.NDG.ANAL TBD.
Fe	σ_{tot}	3.5+7	5.0+7	Expt	DOE-NDC-24	33	Apr81	DAV	Zanelli+3 ES.TOF.CS GVN.TBL.
Fe	σ_{tot}	5.0-3	4.0-1	Expt	DOE-NDC-24	107	Apr81	NBS	Johnson+POWDER DIFFRACTION.GRPHS.
Fe	σ_{tot}	2.0+6	8.0+7	Revw	DOE-NDC-24	121	Apr81	ORL	Larson.ABST BNL 80 P.277.NDG.
Fe	$\sigma_{dif.inl}$	7.5+6	1.2+7	Expt	DOE-NDC-24	164	Apr81	TNL	Beyerle+DBL DIFF.3 ES,5 ANGS.CFD.
Fe	$\sigma_{n,X}$	4.0+7	5.0+7	Expt	DOE-NDC-24	31	Apr81	DAV	Brady+2 ES.TRANS TECHNIQUE.TBL.
Fe	$\sigma_{n,X\gamma}$	1.0+5	2.0+7	Revw	DOE-NDC-24	121	Apr81	ORL	Larson.ABST BNL 80 P.277.NDG.
Fe	$\sigma_{n,\alpha}$	1.5+7		Expt	DOE-NDC-24	155	Apr81	AI	Kneff+PRELIM TOTAL HE CS GVN.
^{54}Fe	$\sigma_{el}(\theta)$	2.4+7		Expt	DOE-NDC-24	138	Apr81	OHO	Mellema+TOF.EXPT,ANAL TBC.NDG.
^{54}Fe	$\sigma_{el}(\theta)$	8.0+6	1.4+7	Expt	DOE-NDC-24	161	Apr81	TNL	Beyerle+GRPH.CFD LEG POLY FIT.
^{54}Fe	σ_{pol}	1.0+7	1.2+7	Expt	DOE-NDC-24	171	Apr81	TNL	Beyerle+ANAL PWR 2 ES.GRPH.CFD.
^{54}Fe	$\sigma_{dif.inl}$	2.4+7		Expt	DOE-NDC-24	138	Apr81	OHO	Mellema+TOF.EXPT,ANAL TBC.NDG.
^{54}Fe	$\sigma_{dif.inl}$	8.0+6	1.4+7	Expt	DOE-NDC-24	161	Apr81	TNL	Beyerle+GRPH.CFD LEG POLY FIT.
^{54}Fe	$\sigma_{n,\alpha}$	1.5+7		Expt	DOE-NDC-24	155	Apr81	AI	Kneff+PRELIM TOTAL HE CS GVN.
^{54}Fe	Res.Params.		4.0+5	Eval	DOE-NDC-24	131	Apr81	ORL	Perey+NDG.ABST ORNL-TM-6405 9/80.
^{56}Fe	$\sigma_{el}(\theta)$	8.0+6	1.4+7	Expt	DOE-NDC-24	161	Apr81	TNL	Beyerle+OPTMDL,CC ANAL TBD.NDG.
^{56}Fe	$\sigma_{dif.inl}$	NDG		Expt	DOE-NDC-24	122	Apr81	ORL	Dickens+2+ LVL EXCIT FN.NDG.TBD.

NEUTRON DATA REFERENCES

Element	Quantity	Energy (eV) Min	Max	Type	Documentation Ref	Page	Date	Lab	Comments
^{56}Fe	$\sigma_{dif.inl}$	8.0+6	1.4+7	Expt	DOE-NDC-24	161	Apr81	TNL	Beyerle+OPTMDL,CC ANAL TBD.NDG.
^{56}Fe	$\sigma_{n,\alpha}$	1.5+7		Expt	DOE-NDC-24	155	Apr81	AI	Kneff+PRELIM TOTAL HE CS GVN.
^{56}Fe	Res.Params.		4.0+5	Eval	DOE-NDC-24	131	Apr81	ORL	Perey+NDG.ABST ORNL-TM-6405 9/80.
^{57}Fe	Res.Params.		4.0+5	Eval	DOE-NDC-24	131	Apr81	ORL	Perey+NDG.ABST ORNL-TM-6405 9/80.
^{58}Fe	$\sigma_{n,\alpha}$	1.5+7		Expt	DOE-NDC-24	155	Apr81	AI	Kneff+PRELIM TOTAL HE CS GVN.
^{59}Co	Evaluation	3.0+6	5.0+7	Eval	DOE-NDC-24	79	Apr81	LAS	Arthur+(N,XN),(N,P) CALC.GRPH.
^{59}Co	$\sigma_{n,xn}$	3.0+6	5.0+7	Theo	DOE-NDC-24	79	Apr81	LAS	Arthur+(N,XN),(N,P) CALC.GRPH.
^{59}Co	$\sigma_{n,p}$	3.0+6	5.0+7	Theo	DOE-NDC-24	79	Apr81	LAS	Arthur+(N,XN),(N,P) CALC.GRPH.
^{59}Co	$\sigma_{n,\alpha}$	1.5+7		Expt	DOE-NDC-24	155	Apr81	AI	Kneff+HE PROD CS.NDG.ANAL TBD.
Ni	σ_{tot}	2.0+6	8.0+7	Revw	DOE-NDC-24	121	Apr81	ORL	Larson.ABST BNL 80 P.277.NDG.
Ni	$\sigma_{dif.inl}$	7.5+6	1.2+7	Expt	DOE-NDC-24	164	Apr81	TNL	Beyerle+DBL DIFF.3 ES,5 ANGS.NDG.
Ni	$\sigma_{n,x\gamma}$	1.0+5	2.0+7	Revw	DOE-NDC-24	121	Apr81	ORL	Larson.ABST BNL 80 P.277.NDG.
^{58}Ni	σ_{tot}	1.0+6	4.5+6	Expt	DOE-NDC-24	2	Apr81	ANL	Guenther+E AVG CS.NDG.TBD.
^{58}Ni	$\sigma_{el}(\theta)$	1.0+6	4.5+6	Expt	DOE-NDC-24	2	Apr81	ANL	Guenther+E AVG CS.NDG.ANAL TBD.
^{58}Ni	$\sigma_{el}(\theta)$	8.0+6	1.4+7	Expt	DOE-NDC-24	163	Apr81	TNL	Beyerle+4 ES.GRPH.OPTMDL,CC TBD.
^{58}Ni	σ_{pol}	1.0+7	1.2+7	Expt	DOE-NDC-24	171	Apr81	TNL	Beyerle+ANAL PWR 2ES.NDG.
^{58}Ni	$\sigma_{dif.inl}$	1.0+6	4.5+6	Expt	DOE-NDC-24	2	Apr81	ANL	Guenther+E AVG CS.NDG.ANAL TBD.
^{58}Ni	$\sigma_{dif.inl}$	8.0+6	1.4+7	Expt	DOE-NDC-24	163	Apr81	TNL	Beyerle+4 ES.NDG.OPTMDL CALC TBD.
^{58}Ni	$\sigma_{n,p}$	1.1+7		Expt	DOE-NDC-24	139	Apr81	OHO	Randers-Pehrson+NDG.ANAL TBD.
^{58}Ni	$\sigma_{n,np}$	1.1+7		Expt	DOE-NDC-24	139	Apr81	OHO	Randers-Pehrson+NDG.ANAL TBD.
^{60}Ni	σ_{tot}	NDG		Expt	DOE-NDC-24	127	Apr81	ORL	Larson+TRNS.RES ANAL.NEW CODE.NDG.
^{60}Ni	$\sigma_{el}(\theta)$	8.0+6	1.4+7	Expt	DOE-NDC-24	163	Apr81	TNL	Beyerle+4 ES.NDG.OPTMDL CALC TBD.
^{60}Ni	$\sigma_{dif.inl}$	8.0+6	1.4+7	Expt	DOE-NDC-24	163	Apr81	TNL	Beyerle+4 ES.NDG.OPTMDL CALC TBD.
Cu	σ_{tot}	NDG		Expt	DOE-NDC-24	2	Apr81	ANL	Guenther+MORE INFORMATION.NDG.
Cu	σ_{tot}	2.0+6	8.0+7	Revw	DOE-NDC-24	121	Apr81	ORL	Larson.ABST BNL 80 P.277.NDG.
Cu	$\sigma_{el}(\theta)$	NDG		Expt	DOE-NDC-24	2	Apr81	ANL	Guenther+MORE INFORMATION.NDG.
Cu	$\sigma_{dif.inl}$	NDG		Expt	DOE-NDC-24	2	Apr81	ANL	Guenther+13 INEL GROUP CS.NDG.TBC.
Cu	$\sigma_{dif.inl}$	7.5+6	1.2+7	Expt	DOE-NDC-24	164	Apr81	TNL	Beyerle+DBL DIFF.3 ES,5 ANGS.NDG.
Cu	$\sigma_{n,x\gamma}$	1.0+5	2.0+7	Revw	DOE-NDC-24	121	Apr81	ORL	Larson.ABST BNL 80 P.277.NDG.
Cu	$\sigma_{n,xn}$	1.0+6	2.0+7	Revw	DOE-NDC-24	121	Apr81	ORL	Larson.ABST BNL 80 P.277.NDG.
^{63}Cu	$\sigma_{el}(\theta)$	8.0+6	1.4+7	Expt	DOE-NDC-24	161	Apr81	TNL	Beyerle+OPTMDL,CC ANAL TBD.NDG.
^{63}Cu	$\sigma_{dif.inl}$	8.0+6	1.4+7	Expt	DOE-NDC-24	161	Apr81	TNL	Beyerle+OPTMDL,CC ANAL TBD.NDG.
^{63}Cu	γ Spectra	NDG		Expt	DOE-NDC-24	17	Apr81	BNL	Chrien+NDG.LVL STRUCTURE STUDY.

NEUTRON DATA REFERENCES

Element	Quantity	Energy (eV) Min	Max	Type	Documentation Ref	Page	Date	Lab	Comments
^{65}Cu	$\sigma_{el}(\theta)$	8.0+6	1.4+7	Expt	DOE-NDC-24	161	Apr81	TNL	Beyerle+GRPH.CFD LEG POLY FIT.
^{65}Cu	σ_{pol}	1.0+7	1.2+7	Expt	DOE-NDC-24	171	Apr81	TNL	Beyerle+ANAL PWR 2 ES.GRPH.CFD.
^{65}Cu	$\sigma_{dif.inl}$	8.0+6	1.4+7	Expt	DOE-NDC-24	161	Apr81	TNL	Beyerle+GRPH.CFD LEG POLY FIT.
^{65}Cu	γ Spectra	NDG		Expt	DOE-NDC-24	17	Apr81	BNL	Chrien+NDG.LVL STRUCTURE STUDY.
Zn	$\sigma_{n,X\gamma}$	1.0+5	2.0+7	Revw	DOE-NDC-24	121	Apr81	ORL	Larson.ABST BNL 80 P.277.NDG.
^{64}Zn	$\sigma_{n,\gamma}$	2.5+3	9.0+5	Expt	DOE-NDC-24	120	Apr81	ORL	Garg+TOF.NDG.RES PAR ANAL.
^{64}Zn	Res.Params.	2.5+3	1.3+5	Expt	DOE-NDC-24	120	Apr81	ORL	Garg+CAPT.TOF.RES PAR ANAL.
^{64}Zn	$\langle\Gamma\rangle/D$	2.5+3	1.3+5	Expt	DOE-NDC-24	120	Apr81	ORL	Garg+CAPT,TOF.SI,S2 GVN.
^{76}Se	γ Spectra	NDG		Expt	DOE-NDC-24	17	Apr81	BNL	Chrien+NDG.RES CAPT STUDY.
^{77}Se	γ Spectra	NDG		Expt	DOE-NDC-24	17	Apr81	BNL	Chrien+NDG.RES CAPT STUDY.
^{80}Se	γ Spectra	NDG		Expt	DOE-NDC-24	17	Apr81	BNL	Chrien+NDG.RES CAPT STUDY.
^{86}Kr	$\sigma_{n,\gamma}$	NDG		Expt	DOE-NDC-24	120	Apr81	ORL	Macklin.CAPT CS MEAS.NDG.
^{87}Sr	$\sigma_{n,\gamma}$	2.6+3	2.0+6	Expt	DOE-NDC-24	74	Apr81	LAS	Drake.CS.NDG.LAS AND ORL EXPT.
^{87}Sr	γ Spectra	2.0+3	2.4+3	Expt	DOE-NDC-24	53	Apr81	LRL	Sullivan+2 E.SPEC SHAPE GRPH.
^{87}Sr	γ Spectra	Maxw		Expt	DOE-NDC-24	53	Apr81	LRL	Sullivan+YLD.SPEC SHAPE GRPH.
^{89}Y	σ_{tot}	5.0+4	4.5+6	Expt	DOE-NDC-24	3	Apr81	ANL	Poenitz+PRELIM RESULT GRPH.ANAL TBD.
^{89}Y	$\sigma_{el}(\theta)$	Fast		Expt	DOE-NDC-24	3	Apr81	ANL	Smith+CS MEAS.MDL TBD.NDG.
^{89}Y	$\sigma_{dif.inl}$	Fast		Expt	DOE-NDC-24	3	Apr81	ANL	Smith+MEAS DONE.NDG.
^{89}Y	$\sigma_{n,\gamma}$	1.0+3	3.0+6	Theo	DOE-NDC-24	65	Apr81	LRL	Gardner.VALENCE VS STATMDL.NDG
^{89}Y	$\sigma_{n,p}$	1.5+7		Theo	DOE-NDC-24	80	Apr81	LAS	Arthur.P EMISSION SPEC.GRPH.CFD.
^{89}Y	$\sigma_{n,np}$	1.5+7		Theo	DOE-NDC-24	80	Apr81	LAS	Arthur.P EMISSION SPEC.GRPH.CFD.
^{89}Y	Res.Params.	1.0+3	3.0+6	Theo	DOE-NDC-24	65	Apr81	LRL	Gardner.VALENCE VS STATMDL.NDG
Zr	σ_{tot}	5.0+4	4.5+6	Expt	DOE-NDC-24	3	Apr81	ANL	Poenitz+PRELIM RESULT GRPH.ANAL TBD.
Zr	$\sigma_{el}(\theta)$	Fast		Expt	DOE-NDC-24	3	Apr81	ANL	Smith+CS MEAS.MDL TBD.NDG.
Zr	$\sigma_{n,\alpha}$	1.5+7		Expt	DOE-NDC-24	155	Apr81	AI	Kneff+HE PROD CS.NDG.ANAL TBD.
^{90}Zr	$\sigma_{n,p}$	1.5+7		Theo	DOE-NDC-24	80	Apr81	LAS	Arthur.P EMISSION SPEC.GRPH.CFD.
^{90}Zr	$\sigma_{n,np}$	1.5+7		Theo	DOE-NDC-24	80	Apr81	LAS	Arthur.P EMISSION SPEC.GRPH.CFD.
^{93}Nb	σ_{tot}	5.0+4	4.5+6	Expt	DOE-NDC-24	3	Apr81	ANL	Poenitz+PRELIM RESULT GRPH.ANAL TBD.
^{93}Nb	$\sigma_{el}(\theta)$	Fast		Expt	DOE-NDC-24	3	Apr81	ANL	Smith+CS MEAS.MDL TBD.NDG.
^{93}Nb	$\sigma_{dif.inl}$	Fast		Expt	DOE-NDC-24	3	Apr81	ANL	Smith+MEAS DONE.NDG.
^{93}Nb	$\sigma_{dif.inl}$	1.0+7	1.2+7	Expt	DOE-NDC-24	164	Apr81	TNL	Beyerle+DBL DIFF.2 ES,5 ANGS.NDG.
^{93}Nb	$\sigma_{n,X\gamma}$	1.0+5	2.0+7	Revw	DOE-NDC-24	121	Apr81	ORL	Larson.ABST BNL 80 P.277.NDG.
^{93}Nb	$\sigma_{n,xn}$	1.0+6	2.0+7	Revw	DOE-NDC-24	121	Apr81	ORL	Larson.ABST BNL 80 P.277.NDG.

NEUTRON DATA REFERENCES

Element	Quantity	Energy (eV) Min	Max	Type	Documentation Ref	Page	Date	Lab	Comments
^{93}Nb	$\sigma_{n,\alpha}$	1.5+7		Expt	DOE-NDC-24	155	Apr81	AI	Kneff+HE PROD CS.NDG.ANAL TBD.
Mo	σ_{tot}	5.0+4	4.5+6	Expt	DOE-NDC-24	3	Apr81	ANL	Poenitz+PRELIM RESULT GRPH.ANAL TBD.
Mo	$\sigma_{el}(\theta)$	Fast		Expt	DOE-NDC-24	3	Apr81	ANL	Smith+CS MEAS.MDL TBD.NDG.
Mo	$\sigma_{dif.inl}$	1.0+7	1.2+7	Expt	DOE-NDC-24	164	Apr81	TNL	Beyerle+DBL DIFF.2 ES,5 ANGS.NDG.
Mo	$\sigma_{n,X\gamma}$	1.0+5	2.0+7	Revw	DOE-NDC-24	121	Apr81	ORL	Larson.ABST BNL 80 P.277.NDG.
Mo	$\sigma_{n,\alpha}$	1.5+7		Expt	DOE-NDC-24	155	Apr81	AI	Kneff+PRELIM TOTAL HE CS GVN.
^{92}Mo	$\sigma_{n,p}$	1.5+7		Theo	DOE-NDC-24	80	Apr81	LAS	Arthur.P EMISSION SPEC.GRPH.CFD.
^{92}Mo	$\sigma_{n,np}$	1.5+7		Theo	DOE-NDC-24	80	Apr81	LAS	Arthur.P EMISSION SPEC.GRPH.CFD.
^{92}Mo	$\sigma_{n,\alpha}$	1.5+7		Expt	DOE-NDC-24	155	Apr81	AI	Kneff+PRELIM TOTAL HE CS GVN.
^{94}Mo	$\sigma_{n,\alpha}$	1.5+7		Expt	DOE-NDC-24	155	Apr81	AI	Kneff+PRELIM TOTAL HE CS GVN.
^{96}Mo	$\sigma_{n,\alpha}$	1.5+7		Expt	DOE-NDC-24	155	Apr81	AI	Kneff+PRELIM TOTAL HE CS GVN.
^{97}Mo	$\sigma_{n,\alpha}$	1.5+7		Expt	DOE-NDC-24	155	Apr81	AI	Kneff+PRELIM TOTAL HE CS GVN.
^{98}Mo	$\sigma_{n,\gamma}$	1.0+3	3.0+6	Theo	DOE-NDC-24	65	Apr81	LRL	Gardner.VALENCE VS STATMDL.NDG
^{98}Mo	$\sigma_{n,\alpha}$	1.5+7		Expt	DOE-NDC-24	155	Apr81	AI	Kneff+CS MEAS QUESTIONED.
^{98}Mo	Res.Params.	1.0+3	3.0+6	Theo	DOE-NDC-24	65	Apr81	LRL	Gardner.VALENCE VS STATMDL.NDG
^{100}Mo	$\sigma_{n,\alpha}$	1.5+7		Expt	DOE-NDC-24	155	Apr81	AI	Kneff+PRELIM TOTAL HE CS GVN.
^{99}Tc	$\sigma_{n,\gamma}$	NDG		Expt	DOE-NDC-24	120	Apr81	ORL	Macklin.CAPT CS MEAS TBD.NDG.
^{103}Rh	σ_{tot}	5.0+4	4.5+6	Expt	DOE-NDC-24	3	Apr81	ANL	Poenitz+PRELIM RESULT GRPH.ANAL TBD.
^{103}Rh	$\sigma_{el}(\theta)$	1.5+6	3.8+6	Expt	DOE-NDC-24	3	Apr81	ANL	Smith+GRPH.CFD MDL CALC.
Pd	σ_{tot}	5.0+4	4.5+6	Expt	DOE-NDC-24	3	Apr81	ANL	Poenitz+PRELIM RESULT GRPH.ANAL TBD.
Pd	σ_{el}	5.0+5	3.8+6	Expt	DOE-NDC-24	3	Apr81	ANL	Smith+GRPH.CFD MDL CALC.
Pd	$\sigma_{el}(\theta)$	1.5+6	3.8+6	Expt	DOE-NDC-24	3	Apr81	ANL	Smith+GRPH.CFD MDL CALC.
^{104}Pd	$\sigma_{n,\gamma}$	NDG		Expt	DOE-NDC-24	120	Apr81	ORL	Macklin+COMPUTER CODING ERROR CORREC
^{106}Pd	$\sigma_{n,\gamma}$	NDG		Expt	DOE-NDC-24	120	Apr81	ORL	Macklin+COMPUTER CODING ERROR CORREC
^{108}Pd	$\sigma_{n,\gamma}$	NDG		Expt	DOE-NDC-24	120	Apr81	ORL	Macklin+COMPUTER CODING ERROR CORREC
^{110}Pd	$\sigma_{n,\gamma}$	NDG		Expt	DOE-NDC-24	120	Apr81	ORL	Macklin+COMPUTER CODING ERROR CORREC
Ag	σ_{tot}	5.0+4	4.5+6	Expt	DOE-NDC-24	3	Apr81	ANL	Poenitz+PRELIM RESULT GRPH.ANAL TBD.
Ag	$\sigma_{el}(\theta)$	Fast		Expt	DOE-NDC-24	3	Apr81	ANL	Smith+CS MEAS.MDL TBD.NDG.
Ag	$\sigma_{n,X\gamma}$	1.0+5	2.0+7	Revw	DOE-NDC-24	121	Apr81	ORL	Larson.ABST BNL 80 P.277.NDG.
^{107}Ag	$\sigma_{n,\gamma}$	NDG		Expt	DOE-NDC-24	120	Apr81	ORL	Macklin.CAPT CS MEAS TBD.NDG.
^{109}Ag	$\sigma_{n,\gamma}$	NDG		Expt	DOE-NDC-24	120	Apr81	ORL	Macklin.CAPT CS MEAS TBD.NDG.
Cd	σ_{tot}	5.0+4	4.5+6	Expt	DOE-NDC-24	3	Apr81	ANL	Poenitz+PRELIM RESULT GRPH.ANAL TBD.
Cd	$\sigma_{el}(\theta)$	Fast		Expt	DOE-NDC-24	3	Apr81	ANL	Smith+CS MEAS.MDL TBD.NDG.

NEUTRON DATA REFERENCES

Element	Quantity	Energy (eV) Min	Max	Type	Documentation Ref	Page	Date	Lab	Comments
^{112}Cd	γ Spectra	2.0+3	2.4+4	Expt	DOE-NDC-24	15	Apr81	BNL	Chrien+LVL STRUCT.NDG.ANAL TBD.
^{112}Cd	Res.Params.	7.0+0		Expt	DOE-NDC-24	15	Apr81	BNL	Chrien+NEW RES OBS.NDG.TBC.
In	σ_{tot}	5.0+4	4.5+6	Expt	DOE-NDC-24	3	Apr81	ANL	Poenitz+PRELIM RESULT GRPH.ANAL TBD.
In	$\sigma_{el}(\theta)$	Fast		Expt	DOE-NDC-24	3	Apr81	ANL	Smith+CS MEAS.MDL TBD.NDG.
^{113}In	$\sigma_{dif.inl}$	1.4+7		Expt	DOE-NDC-24	119	Apr81	NBS	Duvall+INDUCED ACT TBD.NDG.
^{115}In	$\sigma_{n,\gamma}$	2.3+4	9.6+5	Expt	DOE-NDC-24	97	Apr81	MHG	Grady+4 ES.PHOTO-NS.ANAL TBD.NDG.
Sn	σ_{tot}	5.0+4	4.5+6	Expt	DOE-NDC-24	3	Apr81	ANL	Poenitz+PRELIM RESULT GRPH.ANAL TBD.
Sn	$\sigma_{el}(\theta)$	Fast		Expt	DOE-NDC-24	3	Apr81	ANL	Smith+CS MEAS.MDL TBD.NDG.
Sn	$\sigma_{n,X\gamma}$	1.0+5	2.0+7	Revw	DOE-NDC-24	121	Apr81	ORL	Larson.ABST BNL 80 P.277.NDG.
Sn	$\sigma_{n,\alpha}$	1.5+7		Expt	DOE-NDC-24	155	Apr81	AI	Kneff+HE PROD CS.NDG.ANAL TBD.
^{112}Sn	$\sigma_{n,\alpha}$	1.5+7		Expt	DOE-NDC-24	155	Apr81	AI	Kneff+HE PROD CS.NDG.ANAL TBD.
^{114}Sn	$\sigma_{n,\alpha}$	1.5+7		Expt	DOE-NDC-24	155	Apr81	AI	Kneff+HE PROD CS.NDG.ANAL TBD.
^{115}Sn	$\sigma_{n,\alpha}$	1.5+7		Expt	DOE-NDC-24	155	Apr81	AI	Kneff+HE PROD CS.NDG.ANAL TBD.
^{116}Sn	$\sigma_{el}(\theta)$	1.1+7		Theo	DOE-NDC-24	53	Apr81	LRL	Wong+LANE MDL CALCS.NDG.
^{116}Sn	$\sigma_{el}(\theta)$	1.0+7	1.4+7	Expt	DOE-NDC-24	163	Apr81	TNL	Beyerle+2 ES.NDG.PRELIM ANAL.CFD.MDL
^{116}Sn	σ_{pol}	1.0+7	1.4+7	Expt	DOE-NDC-24	172	Apr81	TNL	Beyerle+ANAL PWR MEAS.CC TBD.NDG.
^{116}Sn	$\sigma_{dif.inl}$	1.0+7	1.4+7	Expt	DOE-NDC-24	163	Apr81	TNL	Beyerle+2 ES.NDG.PRELIM ANAL.CFD MDL
^{116}Sn	$\sigma_{n,\alpha}$	1.5+7		Expt	DOE-NDC-24	155	Apr81	AI	Kneff+HE PROD CS.NDG.ANAL TBD.
^{118}Sn	$\sigma_{el}(\theta)$	1.1+7		Theo	DOE-NDC-24	53	Apr81	LRL	Wong+LANE MDL CALCS.NDG.
^{118}Sn	$\sigma_{n,\alpha}$	1.5+7		Expt	DOE-NDC-24	155	Apr81	AI	Kneff+HE PROD CS.NDG.ANAL TBD.
^{119}Sn	$\sigma_{n,\alpha}$	1.5+7		Expt	DOE-NDC-24	155	Apr81	AI	Kneff+HE PROD CS.NDG.ANAL TBD.
^{120}Sn	$\sigma_{el}(\theta)$	1.1+7		Theo	DOE-NDC-24	53	Apr81	LRL	Wong+LANE MDL CALCS.GRPH,CFD EXPT.
^{120}Sn	$\sigma_{el}(\theta)$	1.0+7	1.7+7	Expt	DOE-NDC-24	163	Apr81	TNL	Beyerle+3 ES.NDG.PRELIM OPTMDL CALC.
^{120}Sn	σ_{pol}	1.0+7	1.4+7	Expt	DOE-NDC-24	172	Apr81	TNL	Beyerle+ANAL PWR MEAS.CC TBD.NDG.
^{120}Sn	$\sigma_{dif.inl}$	1.0+7	1.7+7	Expt	DOE-NDC-24	163	Apr81	TNL	Beyerle+3 ES.NDG.PRELIM OPTMDL CALC.
^{120}Sn	$\sigma_{n,\alpha}$	1.5+7		Expt	DOE-NDC-24	155	Apr81	AI	Kneff+HE PROD CS.NDG.ANAL TBD.
^{122}Sn	$\sigma_{el}(\theta)$	1.1+7		Theo	DOE-NDC-24	53	Apr81	LRL	Wong+LANE MDL CALCS.NDG.
^{122}Sn	$\sigma_{n,\alpha}$	1.5+7		Expt	DOE-NDC-24	155	Apr81	AI	Kneff+HE PROD CS.NDG.ANAL TBD.
^{124}Sn	$\sigma_{el}(\theta)$	1.1+7		Theo	DOE-NDC-24	53	Apr81	LRL	Wong+LANE MDL CALCS.NDG.
^{124}Sn	$\sigma_{n,\alpha}$	1.5+7		Expt	DOE-NDC-24	155	Apr81	AI	Kneff+HE PROD CS.NDG.ANAL TBD.
Sb	σ_{tot}	5.0+4	4.5+6	Expt	DOE-NDC-24	3	Apr81	ANL	Poenitz+PRELIM RESULT GRPH.ANAL TBD.
Sb	$\sigma_{el}(\theta)$	Fast		Expt	DOE-NDC-24	3	Apr81	ANL	Smith+CS MEAS.MDL TBD.NDG.
Te	σ_{tot}	5.0+4	4.5+6	Expt	DOE-NDC-24	3	Apr81	ANL	Poenitz+PRELIM RESULT GRPH.ANAL TBD.

NEUTRON DATA REFERENCES

Element	Quantity	Energy (eV) Min	Max	Type	Documentation Ref	Page	Date	Lab	Comments
Te	$\sigma_{el}(\theta)$	Fast		Expt	DOE-NDC-24	3	Apr81	ANL	Smith+CS MEAS.MDL TBD.NDG.
^{131}Xe	$\sigma_{n,\gamma}$	NDG		Expt	DOE-NDC-24	120	Apr81	ORL	Macklin.CAPT CS MEAS TBD.NDG.
^{136}Xe	$\sigma_{n,\gamma}$	NDG		Expt	DOE-NDC-24	120	Apr81	ORL	Macklin.CAPT CS MEAS TBD.NDG.
^{135}Ba	γ Spectra	2.0+3	2.4+4	Expt	DOE-NDC-24	15	Apr81	BNL	Chrien+LVL STRUCT STUDY.NDG.TBC.
^{147}Sm	γ Spectra	NDG		Expt	DOE-NDC-24	14	Apr81	BNL	Chrien+RES CAPT.20 NUCLIDES.NDG,TBP.
^{154}Sm	γ Spectra	NDG		Expt	DOE-NDC-24	17	Apr81	BNL	Chrien+NDG,LVL STRUCTURE STUDY.
^{152}Gd	γ Spectra	2.0+3		Expt	DOE-NDC-24	39	Apr81	BNL	Greenwood.PROMPT GAMMA SPEC MEAS.NDG
^{165}Ho	$\sigma_{n,\gamma}$	NDG		Expt	DOE-NDC-24	120	Apr81	ORL	Macklin+COMPUTER CODING ERROR CORREC
^{173}Yb	γ Spectra	Maxw	2.0+3	Expt	DOE-NDC-24	39	Apr81	INL	Greenwood+2ES.G-RAYS,INTS MEAS.NDG.
^{176}Lu	γ Spectra	NDG		Expt	DOE-NDC-24	17	Apr81	BNL	Chrien+NDG.HIGH SPIN STATES.
^{180}Ta	γ Spectra	NDG		Expt	DOE-NDC-24	17	Apr81	BNL	Chrien+NDG.HIGH SPIN STATES.
^{181}Ta	$\sigma_{el}(\theta)$	6.0+6	8.0+6	Expt	DOE-NDC-24	56	Apr81	LRL	Hansen+LANE MDL ANAL (P,N).GRPH.
^{181}Ta	$\sigma_{n,X\gamma}$	1.0+5	2.0+7	Revw	DOE-NDC-24	121	Apr81	ORL	Larson.ABST BNL 80 P.277.NDG.
W	$\sigma_{dif.inl}$	1.0+7	1.2+7	Expt	DOE-NDC-24	164	Apr81	TNL	Beyerle+DBL DIFF.2 ES,5 ANGS.NDG.
W	$\sigma_{n,X\gamma}$	1.0+5	2.0+7	Revw	DOE-NDC-24	121	Apr81	ORL	Larson.ABST BNL 80 P.277.NDG.
W	$\sigma_{n,\alpha}$	1.5+7		Expt	DOE-NDC-24	155	Apr81	AI	Kneff+HE PROD CS.NDG.ANAL TBD.
^{182}W	Evaluation	1.0+5	2.0+7	Eval	DOE-NDC-24	80	Apr81	LAS	Arthur.NEW COMBINED WITH ENDF/B-V.
^{182}W	$\sigma_{n,\gamma}$	2.6+3	2.0+6	Expt	DOE-NDC-24	74	Apr81	LAS	Drake.CS.NDG.LAS AND ORL EXPT.
^{182}W	$\sigma_{n,\gamma}$	NDG		Expt	DOE-NDC-24	120	Apr81	ORL	Macklin.CAPT CS MEAS.NDG.
^{182}W	$\sigma_{n,\alpha}$	1.5+7		Expt	DOE-NDC-24	155	Apr81	AI	Kneff+HE PROD CS.NDG.ANAL TBD.
^{183}W	Evaluation	1.0+5	2.0+7	Eval	DOE-NDC-24	80	Apr81	LAS	Arthur.NEW COMBINED WITH ENDF/B-V.
^{183}W	$\sigma_{n,\gamma}$	2.6+3	2.0+6	Expt	DOE-NDC-24	74	Apr81	LAS	Drake.CS.NDG.LAS AND ORL EXPT.
^{183}W	$\sigma_{n,\gamma}$	NDG		Expt	DOE-NDC-24	120	Apr81	ORL	Macklin.CAPT CS MEAS.NDG.
^{183}W	$\sigma_{n,\alpha}$	1.5+7		Expt	DOE-NDC-24	155	Apr81	AI	Kneff+HE PROD CS.NDG.ANAL TBD.
^{184}W	Evaluation	1.0+5	2.0+7	Eval	DOE-NDC-24	80	Apr81	LAS	Arthur.NEW COMBINED WITH ENDF/B-V.
^{184}W	$\sigma_{n,\gamma}$	2.6+3	2.0+6	Expt	DOE-NDC-24	74	Apr81	LAS	Drake.CS.NDG.LAS AND ORL EXPT.
^{184}W	$\sigma_{n,\gamma}$	NDG		Expt	DOE-NDC-24	120	Apr81	ORL	Macklin.CAPT CS MEAS.NDG.
^{184}W	$\sigma_{n,\alpha}$	1.5+7		Expt	DOE-NDC-24	155	Apr81	AI	Kneff+HE PROD CS.NDG.ANAL TBD.
^{186}W	Evaluation	1.0+5	2.0+7	Eval	DOE-NDC-24	80	Apr81	LAS	Arthur.NEW COMBINED WITH ENDF/B-V.
^{186}W	$\sigma_{n,\gamma}$	2.6+3	2.0+6	Expt	DOE-NDC-24	74	Apr81	LAS	Drake.CS.NDG.LAS AND ORL EXPT.
^{186}W	$\sigma_{n,\gamma}$	NDG		Expt	DOE-NDC-24	120	Apr81	ORL	Macklin.CAPT CS MEAS.NDG.
^{186}W	γ Spectra	NDG		Expt	DOE-NDC-24	15	Apr81	BNL	Chrien+NDG.IN PROGRESS.
^{186}W	$\sigma_{n,\alpha}$	1.5+7		Expt	DOE-NDC-24	155	Apr81	AI	Kneff+HE PROD CS.NDG.ANAL TBD.

NEUTRON DATA REFERENCES

Element	Quantity	Energy (eV) Min	Max	Type	Documentation Ref	Page	Date	Lab	Comments
^{186}Os	$\sigma_{n,\gamma}$	2.6+3	8.0+5	Expt	DOE-NDC-24	121	Apr81	ORL	Winters+GALACTIC NUCLEOSYNTHESIS.NDG
^{186}Os	$\sigma_{n,\gamma}$	NDG		Expt	DOE-NDC-24	120	Apr81	ORL	Macklin+COMPUTER CODING ERROR CORREC
^{187}Os	$\sigma_{dif.inl}$	3.0+4	6.5+4	Expt	DOE-NDC-24	122	Apr81	KTY	Winters+KTY,ORL,KRU EXPT.NDG.TBD.
^{187}Os	$\sigma_{dif.inl}$	3.0+4		Expt	DOE-NDC-24	121	Apr81	ORL	Winters+ESTIMATED LOWER BOUND GVN.
^{187}Os	$\sigma_{dif.inl}$	3.4+4		Expt	DOE-NDC-24	122	Apr81	ORL	Winters+KTY,ORL,KRU EXPT.NDG.TBD.
^{187}Os	$\sigma_{dif.inl}$	3.0+4		Expt	DOE-NDC-24	122	Apr81	KRU	Winters+KTY,ORL,KRU EXPT.CS GVN.
^{187}Os	$\sigma_{n,\gamma}$	2.6+3	8.0+5	Expt	DOE-NDC-24	121	Apr81	ORL	Winters+GALACTIC NUCLEOSYNTHESIS.NDG
^{187}Os	γ Spectra	NDG		Expt	DOE-NDC-24	17	Apr81	BNL	Chrien+NDG. G SPEC STUDY.
^{188}Os	$\sigma_{n,\gamma}$	2.6+3	8.0+5	Expt	DOE-NDC-24	121	Apr81	ORL	Winters+GALACTIC NUCLEOSYNTHESIS.NDG
^{190}Os	γ Spectra	NDG		Expt	DOE-NDC-24	15	Apr81	BNL	Chrien+NDG.TBC.SEE P 17 ALSO.
^{194}Pt	γ Spectra	NDG		Expt	DOE-NDC-24	15	Apr81	BNL	Chrien+NDG.IN PROGRESS.
^{195}Pt	γ Spectra	NDG		Expt	DOE-NDC-24	17	Apr81	BNL	Chrien+NDG. G SPEC STUDY.
^{196}Pt	γ Spectra	NDG		Expt	DOE-NDC-24	15	Apr81	BNL	Chrien+NDG.IN PROGRESS.
^{197}Au	σ_{tot}	2.0+6	8.0+7	Revw	DOE-NDC-24	121	Apr81	ORL	Larson.ABST BNL 80 P.277.NDG.
^{197}Au	$\sigma_{el}(\theta)$	6.0+6	8.0+6	Expt	DOE-NDC-24	56	Apr81	LRL	Hansen+LANE MDL ANAL (P,N).GRPH.
^{197}Au	$\sigma_{n,X\gamma}$	1.0+5	2.0+7	Revw	DOE-NDC-24	121	Apr81	ORL	Larson.ABST BNL 80 P.277.NDG.
Pb	σ_{tot}	2.0+6	8.0+7	Revw	DOE-NDC-24	121	Apr81	ORL	Larson.ABST BNL 80 P.277.NDG.
Pb	$\sigma_{dif.inl}$	7.5+6	1.2+7	Expt	DOE-NDC-24	164	Apr81	TNL	Beyerle+DBL DIFF.3 ES,5 ANGS.NDG.
Pb	$\sigma_{n,X\gamma}$	1.0+5	2.0+7	Revw	DOE-NDC-24	121	Apr81	ORL	Larson.ABST BNL 80 P.277.NDG.
Pb	$\sigma_{n,\alpha}$	1.5+7		Expt	DOE-NDC-24	155	Apr81	AI	Kneff+HE PROD CS.NDG.ANAL TBD.
^{204}Pb	$\sigma_{n,\alpha}$	1.5+7		Expt	DOE-NDC-24	155	Apr81	AI	Kneff+HE PROD CS.NDG.ANAL TBD.
^{206}Pb	$\sigma_{n,\alpha}$	1.5+7		Expt	DOE-NDC-24	155	Apr81	AI	Kneff+HE PROD CS.NDG.ANAL TBD.
^{207}Pb	$\sigma_{n,\alpha}$	1.5+7		Expt	DOE-NDC-24	155	Apr81	AI	Kneff+HE PROD CS.NDG.ANAL TBD.
^{208}Pb	$\sigma_{el}(\theta)$	1.0+7	1.7+7	Expt	DOE-NDC-24	163	Apr81	TNL	Beyerle+3 ES.NDG.PRELIM OPTMDL CALC.
^{208}Pb	σ_{pol}	1.0+7	1.4+7	Expt	DOE-NDC-24	172	Apr81	TNL	Beyerle+ANAL PWR MEAS.GRPH P.168.
^{208}Pb	$\sigma_{dif.inl}$	1.0+7	1.7+7	Expt	DOE-NDC-24	163	Apr81	TNL	Beyerle+3 ES.NDG.PRELIM OPTMDL CALC.
^{208}Pb	$\sigma_{n,\gamma}$	6.0+6	1.5+7	Expt	DOE-NDC-24	187	Apr81	TNL	Roberson+GRPH.CFD OTH.
^{208}Pb	$\sigma_{n,\alpha}$	1.5+7		Expt	DOE-NDC-24	155	Apr81	AI	Kneff+HE PROD CS.NDG.ANAL TBD.
^{209}Bi	$\sigma_{el}(\theta)$	6.0+6	8.0+6	Expt	DOE-NDC-24	56	Apr81	LRL	Hansen+LANE MDL ANAL (P,N).GRPH.
^{209}Bi	σ_{pol}	2.0+6	4.0+6	Expt	DOE-NDC-24	190	Apr81	YAL	Ahmed+ASSYM ANAL 3 TO 30 DEG.
^{229}Th	Fiss.Yield	Maxw		Expt	DOE-NDC-24	124	Apr81	ORL	Dabbs+NDG.ANAL TBD.TBP.
^{230}Th	γ Spectra	1.4+0	2.0+3	Expt	DOE-NDC-24	61	Apr81	BNL	White+2 ES.ILL AND BNL LAB EXPT.
^{230}Th	γ Spectra	MAXW	2.0+3	Expt	DOE-NDC-24	61	Apr81	ILL	White+2 ES.ILL AND BNL LAB EXPT.

NEUTRON DATA REFERENCES

Element	Quantity	Energy (eV) Min	Max	Type	Documentation Ref	Page	Date	Lab	Comments
^{232}Th	σ_{tot}	6.0-3	1.0+5	Expt	DOE-NDC-24	122	Apr81	ORL	Olsen+TRNS,TOF.NDG,CFD.TBC.
^{232}Th	σ_{tot}	6.0-3	1.8+1	Expt	DOE-NDC-24	151	Apr81	RPI	Little+TRANS.CFD ENDF,OTH.NDG.
^{232}Th	$\sigma_{el}(\theta)$	6.5+6		Expt	DOE-NDC-24	56	Apr81	LRL	Hansen+LANE MDL ANAL (P,N).NDG.
^{232}Th	$\sigma_{dif.inl}$	7.0+5	2.1+6	Expt	DOE-NDC-24	87	Apr81	LTI	Beghian+DIN FROM DNG CFD MEAS DIN.
^{232}Th	$\sigma_{dif.inl}$		1.0+6	Expt	DOE-NDC-24	89	Apr81	LTI	Traegde+RING GEOM.TOF.NDG.TBD.
^{232}Th	$\sigma_{dif.inl}$	8.0+5	2.5+6	Theo	DOE-NDC-24	92	Apr81	LTI	Sheldon+PRELIM RESULTS.GRPH CFD.
^{232}Th	$\sigma_{n,\gamma}$	2.4+4		Expt	DOE-NDC-24	99	Apr81	MHG	Grady+ABSOL MEAS.ANAL TBD.NDG.
^{232}Th	$\sigma_{n,\gamma}$	NDG		Expt	DOE-NDC-24	120	Apr81	ORL	Macklin+COMPUTER CODING ERROR CORREC
^{232}Th	$\sigma_{n,\gamma}$	2.6+3	1.0+4	Expt	DOE-NDC-24	121	Apr81	ORL	Macklin.NDG.RES PARS ANAL.
^{232}Th	$\sigma_{n,\gamma}$	6.0-3	1.8+1	Expt	DOE-NDC-24	151	Apr81	RPI	Little+SHAPE MEAS.CFD ENDF,OTH.NDG.
^{232}Th	$\sigma_{n,n'\gamma}$	7.0+5	2.1+6	Expt	DOE-NDC-24	87	Apr81	LTI	Beghian+46 STATES.DIN FROM DNG.
^{232}Th	$\sigma_{n,X\gamma}$	1.0+5	2.0+7	Revw	DOE-NDC-24	121	Apr81	ORL	Larson.ABST BNL 80 P.277.NDG.
^{232}Th	ν_d	0.0+0	3.0+6	Expt	DOE-NDC-24	94	Apr81	LTI	Couchell+TOF.NDG.SPEC TO BE MEAS.
^{232}Th	Spect.fiss n	0.0+0	3.0+6	Expt	DOE-NDC-24	94	Apr81	LTI	Couchell+TOF.NDG.SPEC TO BE MEAS.
^{232}Th	Fiss.Yield	NDG		Expt	DOE-NDC-24	69	Apr81	LRL	Meyer+BR-87,I-137 YLDS.TBP PR/C.
^{232}Th	Res.Params.	2.6+3	1.0+4	Expt	DOE-NDC-24	121	Apr81	ORL	Macklin.CAPT.AVG WG DRVD.
^{232}Th	Res.Params.	9.0+0	4.4+2	Expt	DOE-NDC-24	122	Apr81	ORL	Olsen+TRNS.WN,WG AVG DRVD.TBC.
^{232}Th	$<\Gamma>/D$	2.6+3	1.0+4	Expt	DOE-NDC-24	121	Apr81	ORL	Macklin.S0,S1,S2 GVN.
^{231}Pa	σ_{tot}	1.0-2	1.0+4	Expt	DOE-NDC-24	123	Apr81	ORL	Dabbs+TOF.RES ANAL.NDG.TBP.
^{231}Pa	Res.Params.	1.0-2	1.0+4	Expt	DOE-NDC-24	123	Apr81	ORL	Dabbs+TOF.RES ANAL.NDG.TBP.
^{231}Pa	$<\Gamma>/D$	1.0-2	7.0+0	Expt	DOE-NDC-24	123	Apr81	ORL	Dabbs+TOF.RES ANAL.SO.NDG.TBP.
^{232}U	Fiss.Yield	NDG		Expt	DOE-NDC-24	69	Apr81	LRL	Meyer+BR-87,I-137 YLDS.TBP PR/C.
^{233}U	$\sigma_{n,f}$	2.3+4	9.6+5	Expt	DOE-NDC-24	102	Apr81	MHG	Grady+5 ES.NDG.TBC,TBP.
^{233}U	$\sigma_{n,f}$	1.4+7		Expt	DOE-NDC-24	102	Apr81	MHG	Mahdavi+CS MEAS TBD.NDG.
^{233}U	$\sigma_{n,f}$	NDG		Expt	DOE-NDC-24	127	Apr81	ORL	Larson+EXPT TECHNIQUE EXAMPLE.NDG.
^{233}U	ν_p		3.0+5	Expt	DOE-NDC-24	124	Apr81	ORL	Gwin.REL CF252.HIGHER CFD OTHS.NDG.
^{233}U	ν_p		1.0+0	Expt	DOE-NDC-24	124	Apr81	ORL	Gwin.REL CF-252.TBD.NDG.
^{233}U	ν_d	0.0+0	3.0+6	Expt	DOE-NDC-24	94	Apr81	LTI	Couchell+TOF.NDG.SPEC TO BE MEAS.
^{233}U	Spect.fiss n	0.0+0	3.0+6	Expt	DOE-NDC-24	94	Apr81	LTI	Couchell+TOF.NDG.SPEC TO BE MEAS.
^{233}U	Fiss.Yield	2.6+5	9.6+5	Expt	DOE-NDC-24	101	Apr81	ANL	Grady+ANL,MHG LABS.TBD.NDG.
^{233}U	Fiss.Yield	NDG		Expt	DOE-NDC-24	69	Apr81	LRL	Meyer+BR-87,I-137 YLDS.TBP PR/C.
^{235}U	σ_{tot}	2.5-2	1.2+1	Expt	DOE-NDC-24	13	Apr81	BNL	Chrien+2 E RANGES.ANAL TBD.NDG.
^{235}U	$\sigma_{n,\gamma}$	NDG		Expt	DOE-NDC-24	74	Apr81	GEL	Moore+LAS,GEL,MOL RES ANAL TBD.

NEUTRON DATA REFERENCES

Element	Quantity	Energy (eV) Min	Max	Type	Documentation Ref	Page	Date	Lab	Comments
^{235}U	γ Spectra	NDG		Expt	DOE-NDC-24	17	Apr81	BNL	Chrien+NDG.LVL STRUCTURE STUDY.
^{235}U	$\sigma_{n,f}$	3.5+5	9.6+6	Expt	DOE-NDC-24	10	Apr81	ANL	Meadows.PU-240 REL U-235.TBP.NDG.
^{235}U	$\sigma_{n,f}$	Fiss		Theo	DOE-NDC-24	3	Apr81	ANL	Smith+CALC CS=0.409+-.061B.
^{235}U	$\sigma_{n,f}$	2.0+5	3.0+7	Expt	DOE-NDC-24	114	Apr81	LRL	Behrens+AM241,243 REL U-235.GRPH.
^{235}U	$\sigma_{n,f}$	1.4+7		Expt	DOE-NDC-24	102	Apr81	MHG	Mahdavi+CS MEAS TBD.NDG.
^{235}U	$\sigma_{n,f}$	1.4+7		Expt	DOE-NDC-24	104	Apr81	NBS	Wasson+CS GVN.GRPH.CFD OTH,ENDF.
^{235}U	$\sigma_{n,f}$	NDG		Expt	DOE-NDC-24	150	Apr81	RPI	Maguire+CM ISOTOPES REL U-235.NDG.
^{235}U	$\sigma_{n,f}$	3.0+5	1.5+6	Expt	DOE-NDC-24	105	Apr81	NBS	Carlson.TOF.PRELIM.TBC.NDG.
^{235}U	$\sigma_{n,f}$	NDG		Expt	DOE-NDC-24	74	Apr81	GEL	Moore+LAS,GEL,MOL RES ANAL TBD.
^{235}U	ν_p	NDG		Theo	DOE-NDC-24	82	Apr81	LAS	Madland+MULTIPLE CHANCE FISS.NDG.
^{235}U	ν_p		1.0+0	Expt	DOE-NDC-24	124	Apr81	ORL	Gwin.REL CF-252.TBD.NDG.
^{235}U	ν_d	Maxw		Theo	DOE-NDC-24	86	Apr81	LAS	England+AGGREGATE EQUILIBRIUM SPEC.
^{235}U	ν_d	0.0+0	3.0+6	Expt	DOE-NDC-24	94	Apr81	LTI	Couchell+TOF.NDG.SPEC TO BE MEAS.
^{235}U	Spect.fiss n	1.4+7		Theo	DOE-NDC-24	82	Apr81	LAS	Madland+MULTIPLE CHANCE FISS.GRPH.
^{235}U	Spect.fiss n	0.0+0	3.0+6	Expt	DOE-NDC-24	94	Apr81	LTI	Couchell+TOF.NDG.SPEC TO BE MEAS.
^{235}U	Spect.fiss n	Fiss		Eval	DOE-NDC-24	132	Apr81	ORL	Maerker+ENDF/B-V FISS SPEC UNCERT.
^{235}U	Fiss.Yield	1.7+5	7.1+6	Expt	DOE-NDC-24	10	Apr81	ANL	Glendenin+5 ES.39 PROD YLDS.NDG,TBC.
^{235}U	Fiss.Yield	Maxw		Expt	DOE-NDC-24	148	Apr81	BNW	Reeder+ISOMER YLD RATIOS.NDG.TBC.
^{235}U	Fiss.Yield	NDG		Expt	DOE-NDC-24	69	Apr81	LRL	Meyer+BR-87,I-137 YLDS.TBP PR/C.
^{235}U	Res.Params.	NDG		Expt	DOE-NDC-24	74	Apr81	GEL	Moore+LAS,GEL,MOL RES ANAL TBD.
^{238}U	σ_{tot}	NDG		Expt	DOE-NDC-24	127	Apr81	ORL	Larson+EXPT TECHNIQUE EXAMPLE.NDG.
^{238}U	$\sigma_{el}(\theta)$	6.5+6		Expt	DOE-NDC-24	56	Apr81	LRL	Hansen+LANE MDL ANAL (P,N).NDG.
^{238}U	$\sigma_{dif.inl}$	7.0+5	2.1+6	Expt	DOE-NDC-24	87	Apr81	LTI	Beghian+DIN FROM DNG CFD MEAS DIN.
^{238}U	$\sigma_{dif.inl}$	8.1+4	1.0+6	Expt	DOE-NDC-24	89	Apr81	LTI	Traegde+ RING GEOM.TOF SPEC.ANAL TBC
^{238}U	$\sigma_{dif.inl}$	8.0+5	2.5+6	Theo	DOE-NDC-24	92	Apr81	LTI	Sheldon+CALC TO BE CFD EXPT.NDG
^{238}U	$\sigma_{dif.inl}$	8.2+4		Expt	DOE-NDC-24	122	Apr81	ORL	Winters+ANGDIST.NDG.INTEG CS GVN.
^{238}U	$\sigma_{n,\gamma}$		1.0+4	Expt	DOE-NDC-24	124	Apr81	ORL	De Saussure+TBC.SELF INDIC MEAS.NDG.
^{238}U	γ Spectra	NDG		Expt	DOE-NDC-24	14	Apr81	BNL	Chrien+RES CAPT.20 NUCLIDES.NDG,TBP.
^{238}U	$\sigma_{n,n'\gamma}$	7.0+5	2.1+6	Expt	DOE-NDC-24	87	Apr81	LTI	Beghian+27 STATES.DIN FROM DNG.
^{238}U	$\sigma_{n,f}$	1.4+7		Expt	DOE-NDC-24	102	Apr81	MHG	Mahdavi+CS MEAS TBD.NDG.
^{238}U	ν_d	0.0+0	3.0+6	Expt	DOE-NDC-24	94	Apr81	LTI	Couchell+TOF.NDG.SPEC TO BE MEAS.
^{238}U	Spect.fiss n	0.0+0	3.0+6	Expt	DOE-NDC-24	94	Apr81	LTI	Couchell+TOF.NDG.SPEC TO BE MEAS.
^{238}U	Fiss.Yield	NDG		Expt	DOE-NDC-24	69	Apr81	LRL	Meyer+BR-87,I-137 YLDS.TBP PR/C.

NEUTRON DATA REFERENCES

Element	Quantity	Energy (eV) Min	Max	Type	Documentation Ref	Page	Date	Lab	Comments
^{238}U	Res.Params.	5.0+3	1.0+5	Expt	DOE-NDC-24	74	Apr81	LAS	Moore+LAS,GEL,MOL LABS ASSIGN PI.
^{237}Np	$\sigma_{n,\gamma}$	1.0-2	2.0+5	Expt	DOE-NDC-24	123	Apr81	ORL	Dabbs+CAPT CS.NDG.TBP.
^{237}Np	$\sigma_{n,f}$	1.0+0	5.0+2	Expt	DOE-NDC-24	75	Apr81	LAS	Auchampaugh+HIGH RESOL.ANAL TBC.NDG.
^{237}Np	$\sigma_{n,f}$	1.4+7		Expt	DOE-NDC-24	102	Apr81	MHG	Mahdavi+CS MEAS TBD.NDG.
^{237}Np	Fiss.Yield	2.6+5	9.6+5	Expt	DOE-NDC-24	101	Apr81	ANL	Grady+ANL,MHG LABS.TBD.NDG.
^{237}Np	Fiss.Yield	NDG		Expt	DOE-NDC-24	69	Apr81	LRL	Meyer+BR-87,I-137 YLDS.TBP PR/C.
^{237}Np	Res.Params.	1.0-2	2.0+5	Expt	DOE-NDC-24	123	Apr81	ORL	Dabbs+CAPT.RES PAR ANAL.NDG.TBP.
^{238}Pu	Fiss.Yield	NDG		Expt	DOE-NDC-24	69	Apr81	LRL	Meyer+BR-87,I-137 YLDS.TBP PR/C.
^{239}Pu	γ Spectra	2.0+3	2.4+4	Expt	DOE-NDC-24	14	Apr81	BNL	Chrien+2ES.RES AVG TECHNIQUE.NDG.
^{239}Pu	$\sigma_{n,f}$	1.4+7		Expt	DOE-NDC-24	102	Apr81	MHG	Mahdavi+CS MEAS TBD.NDG.
^{239}Pu	ν_p		1.0+0	Expt	DOE-NDC-24	124	Apr81	ORL	Gwin.REL CF-252.TBD.NDG.
^{239}Pu	ν_d	0.0+0	3.0+6	Expt	DOE-NDC-24	94	Apr81	LTI	Couchell+TOF.NDG.SPEC TO BE MEAS.
^{239}Pu	Spect.fiss n	0.0+0	3.0+6	Expt	DOE-NDC-24	94	Apr81	LTI	Couchell+TOF.NDG.SPEC TO BE MEAS.
^{239}Pu	Fiss.Prod γ	Maxw		Expt	DOE-NDC-24	124	Apr81	ORL	Dickens+NDG.SEE NSE 77 P.146 2/81.
^{239}Pu	Fiss.Yield	2.6+5	9.6+5	Expt	DOE-NDC-24	101	Apr81	ANL	Grady+ANL,MHG LABS.ANISOTROPY GVN.
^{239}Pu	Fiss.Yield	NDG		Expt	DOE-NDC-24	69	Apr81	LRL	Meyer+BR-87,I-137 YLDS.TBP PR/C.
^{239}Pu	Fiss.Yield	Maxw		Expt	DOE-NDC-24	124	Apr81	ORL	Dickens+NDG.SEE NSE 77 P.146 2/81.
^{240}Pu	σ_{tot}	3.0-4	2.5-2	Expt	DOE-NDC-24	13	Apr81	BNL	Chrien+TRNS MEAS.NDG.
^{240}Pu	σ_{tot}		3.0+1	Expt	DOE-NDC-24	122	Apr81	ORL	Weston+TRNS.NDG.EXPT TBD.
^{240}Pu	$\sigma_{n,\gamma}$	3.0-4	2.5-2	Expt	DOE-NDC-24	13	Apr81	BNL	Chrien+CAPT YLDS AT 3 TEMPS.NDG.
^{240}Pu	$\sigma_{n,f}$	3.5+5	9.6+6	Expt	DOE-NDC-24	10	Apr81	ANL	Meadows+55 ES.REL U-235.NDG,TBP.
^{240}Pu	Fiss.Yield	NDG		Expt	DOE-NDC-24	69	Apr81	LRL	Meyer+BR-87,I-137 YLDS.TBP PR/C.
^{240}Pu	Res.Params.	1.1+0		Expt	DOE-NDC-24	13	Apr81	BNL	Chrien+RES BROADENING,PARS.NDG.
^{241}Pu	Fiss.Yield	NDG		Expt	DOE-NDC-24	69	Apr81	LRL	Meyer+BR-87,I-137 YLDS.TBP PR/C.
^{242}Pu	$\sigma_{n,f}$	2.0+5	1.0+7	Expt	DOE-NDC-24	75	Apr81	GEL	Moore+REL U-235.NDG.ANAL TBC.
^{242}Pu	Fiss.Yield	NDG		Expt	DOE-NDC-24	69	Apr81	LRL	Meyer+BR-87,I-137 YLDS.TBP PR/C.
^{244}Pu	$\sigma_{n,f}$	2.0+5	1.0+7	Expt	DOE-NDC-24	75	Apr81	GEL	Moore+REL U-235.NDG.ANAL TBC.
^{244}Pu	Fiss.Yield	TR		Expt	DOE-NDC-24	75	Apr81	GEL	Moore+ANGDIST.NDG.
^{241}Am	$\sigma_{n,f}$	2.0+5	3.0+7	Expt	DOE-NDC-24	114	Apr81	LRL	Behrens+REL U-235.GRPH.TBP NSE.
^{241}Am	$\sigma_{n,f}$	NDG		Expt	DOE-NDC-24	123	Apr81	ORL	Dabbs+ANAL ALMOST DONE.NDG.
^{241}Am	Fiss.Yield	NDG		Expt	DOE-NDC-24	69	Apr81	LRL	Meyer+BR-87,I-137 YLDS.TBP PR/C.
^{242}Am	$\sigma_{n,f}$	5.0+5	2.0+7	Expt	DOE-NDC-24	58	Apr81	LAS	White+LAS AND LRL LAB WORK.NDG.
^{242}Am	$\sigma_{n,f}$	1.4+7		Expt	DOE-NDC-24	58	Apr81	LRL	White+LAS AND LRL LAB WORK.NDG.

NEUTRON DATA REFERENCES

Element	Quantity	Energy (eV) Min	Max	Type	Documentation Ref	Page	Date	Lab	Comments
^{242}Am	$\sigma_{n,f}$	NDG		Expt	DOE-NDC-24	123	Apr81	ORL	Dabbs+ANAL ALMOST DONE.NDG.
^{242}Am	ν_p	1.4+7		Expt	DOE-NDC-24	58	Apr81	LRL	Howe+REL U-235.11 PCT.NDG.
^{242}Am	Fiss.Yield	NDG		Expt	DOE-NDC-24	69	Apr81	LRL	Meyer+BR-87,I-137 YLDS.TBP PR/C.
^{243}Am	$\sigma_{n,f}$	2.0+5	3.0+7	Expt	DOE-NDC-24	114	Apr81	LRL	Behrens+REL U-235.GRPH.TBP NSE.
^{242}Cm	ν_p	NDG		Expt	DOE-NDC-24	123	Apr81	ORL	Dabbs+NDG.SEE NSE 75 P.76 1980.
^{243}Cm	Fiss.Yield	Maxw		Expt	DOE-NDC-24	124	Apr81	ORL	Dabbs+NDG.ANAL TBD.TBP.
^{244}Cm	$\sigma_{n,f}$	NDG		Expt	DOE-NDC-24	150	Apr81	RPI	Maguire+IONIZ CH.NDG.TBD.
^{245}Cm	$\sigma_{n,f}$	5.0+5	2.0+7	Expt	DOE-NDC-24	58	Apr81	LAS	White+LAS AND LRL LAB WORK.NDG.
^{245}Cm	$\sigma_{n,f}$	1.4+7		Expt	DOE-NDC-24	58	Apr81	LRL	White+LAS AND LRL LAB WORK.NDG.
^{245}Cm	ν_p	1.4+7		Expt	DOE-NDC-24	58	Apr81	LRL	Howe+REL U-235.6.7 PCT.NDG.
^{245}Cm	Fiss.Prod γ	Maxw		Expt	DOE-NDC-24	125	Apr81	ORL	Dickens+ABST.SEE PR/C 23 P.331 1/81.
^{245}Cm	Fiss.Yield	NDG		Expt	DOE-NDC-24	69	Apr81	LRL	Meyer+BR-87,I-137 YLDS.TBP PR/C.
^{245}Cm	Fiss.Yield	Maxw		Expt	DOE-NDC-24	125	Apr81	ORL	Dickens+ABST.SEE PR/C 23 P.331 1/81.
^{245}Cm	Fiss.Yield	Maxw		Expt	DOE-NDC-24	124	Apr81	ORL	Dabbs+NDG.SEE PR/C 23 P.331.
^{246}Cm	$\sigma_{n,f}$	NDG		Expt	DOE-NDC-24	150	Apr81	RPI	Maguire+IONIZ CH.NDG.TBD.
^{248}Cm	γ Spectra	Maxw		Expt	DOE-NDC-24	59	Apr81	LRL	Hoff+SPEC MEAS CFD MDL CALCS.
^{248}Cm	$\sigma_{n,f}$	2.2+0	1.0+5	Expt	DOE-NDC-24	150	Apr81	RPI	Maguire+IONIZ CH.CS GRPH.TBC.
^{249}Bk	γ Spectra	NDG		Expt	DOE-NDC-24	62	Apr81	ILL	BORNER+CAPT,CONVERSION E SPEC.TBL.
^{248}Cf	$\sigma_{n,f}$	NDG		Expt	DOE-NDC-24	123	Apr81	RPI	Dabbs+ORL,RPI EXPT.NDG.
^{249}Cf	$\sigma_{n,f}$	NDG		Expt	DOE-NDC-24	123	Apr81	ORL	Dabbs+ANAL ALMOST DONE.NDG.
^{249}Cf	Fiss.Yield	Maxw		Expt	DOE-NDC-24	10	Apr81	ANL	Gindler+40 YLDS.MASS DISTR PARS.
^{249}Cf	Fiss.Yield	NDG		Expt	DOE-NDC-24	69	Apr81	LRL	Meyer+BR-87,I-137 YLDS.TBP PR/C.
^{249}Cf	Fiss.Yield	Maxw		Expt	DOE-NDC-24	126	Apr81	ORL	Dickens+ABSOL YLDS.CFD.TBP PR/C.
^{249}Cf	Fiss.Yield	Maxw		Expt	DOE-NDC-24	124	Apr81	ORL	Dabbs+NDG.TBP.
^{250}Cf	Fiss.Yield	Spon		Expt	DOE-NDC-24	10	Apr81	ANL	Gindler+7 YLDS.MASS DISTR PARS.
^{252}Cf	ν_p	Spon		Expt	DOE-NDC-24	43	Apr81	INL	Smith+NU VAL GVN.TBP.
^{252}Cf	Spect.fiss n	Spon		Expt	DOE-NDC-24	126	Apr81	ORL	Spencer+N E SPEC MEAS TBD.NDG.
^{252}Cf	Fiss.Yield	NDG		Expt	DOE-NDC-24	69	Apr81	LRL	Meyer+I-137 YLD.TBP PR/C.CFD.

CHARGED PARTICLE REFERENCES

No.	Lab	Work Type	Reference	Date	Emin (MeV)	Emax (MeV)	Author, Comments
$^{2}H(p,n+p)^{1}H$ polarization$(E;\theta)_n$							
1	TNL	Expt	P DOE-NDC-24 175	Apr 81	1.1+0	1.5+1	Byrd+NDG.TRANSVERSE TRANSFER.0-DEG.
$^{2}H(p,elastic)^{2}H$ $\sigma(E;\theta)$							
2	LAS	Expt	P DOE-NDC-24 72	Apr 81	1.0+1		Brown+ NDG. ABS. ACCURACY = 0.8PERCENT.
$^{3}H(p,x)n$ $\sigma(E;\theta)$							
3	TNL	Expt	P DOE-NDC-24 166	Apr 81	9.8+0	1.5+1	Beyerle+CURV.0-DEG BREAK.TOF.CFD DROSG+
$^{3}H(p,n)^{3}He$ polarization$(E;\theta)$							
4	TNL	Expt	P DOE-NDC-24 176	Apr 81	2.5+0		Byrd+ CURV. CFD P + A. SUBMITTED NP/A.
$^{6}Li(p,x)$ $\sigma(E)$							
5	ANL	Expt	P DOE-NDC-24 9	Apr 81	+0	+0	Elwyn+ NDG. SUBSTANTIALLY COMPLETED.
$^{6}Li(p,x)$ $\sigma(E;\theta)$							
6	ANL	Expt	P DOE-NDC-24 9	Apr 81	+0	+0	Elwyn+ NDG. SUBSTANTIALLY COMPLETED.
$^{9}Be(p,elastic)^{9}Be$ $\sigma(E;\theta)$							
7	TNL	Expt	P DOE-NDC-24 177	Apr 81	1.1+1	1.6+1	Byrd+ CURV. TOF. SINGLE COUPLED-CHANNEL
$^{9}Be(p,elastic)^{9}Be$ polarization$(E;\theta)$							
8	TNL	Expt	P DOE-NDC-24 177	Apr 81	1.1+1	1.6+1	Byrd+ CURV. TOF. SINGLE COUPLED-CHANNEL
$^{9}Be(p,n)^{9}B$ $\sigma(E;\theta)$							
9	TNL	Expt	P DOE-NDC-24 177	Apr 81	8.0+0	1.8+1	Byrd+ NDG. NEW DATA AT 16.4-17.5MEV TBA
		Expt	P DOE-NDC-24 177	Apr 81	1.1+1	1.6+1	Byrd+ CURV. TOF. SINGLE COUPLED-CHANNEL
$^{9}Be(p,n)^{9}B$ polarization$(E;\theta)$							
10	TNL	Expt	P DOE-NDC-24 177	Apr 81	8.2+0	1.5+1	Byrd+ NDG. TOF.
		Expt	P DOE-NDC-24 177	Apr 81	1.1+1	1.5+1	Byrd+ CURV. TOF. SINGLE COUPLED-CHANNEL
$^{11}B(p,n)^{11}C$ polarization$(E;\theta)$							
11	TNL	Expt	P DOE-NDC-24 177	Apr 81	8.5+0	1.2+1	Byrd+ NDG. TOF. PRELIMINARY.
$^{11}B(p,n)^{11}C$ thick target yield$(E;\theta)$							
12	TNL	Expt	P DOE-NDC-24 177	Apr 81	1.0+1	1.6+1	Byrd+ NDG. TOF. PRELIMINARY.
$^{13}C(p,elastic)^{13}C$ $\sigma(E;\theta)$							
13	TNL	Expt	P DOE-NDC-24 177	Apr 81	1.1+1		Byrd+ CURV. SUBMITTED TO NP/A.
$^{13}C(p,elastic)^{13}C$ polarization$(E;\theta)$							
14	TNL	Expt	P DOE-NDC-24 177	Apr 81	1.1+1		Byrd+ CURV. SUBMITTED TO NP/A.
$^{13}C(p,n)^{13}N$ $\sigma(E;\theta)$							
15	TNL	Expt	P DOE-NDC-24 177	Apr 81	1.1+1		Byrd+ CURV. SUBMITTED TO NP/A.
		Expt	P DOE-NDC-24 180	Apr 81	1.2+1	1.7+1	Byrd+ NDG. LANE MODEL. MORE DATA NEEDED
		Expt	P DOE-NDC-24 180	Apr 81	1.6+1	1.7+1	Byrd+ NDG. TBA.
$^{13}C(p,n)^{13}N$ polarization$(E;\theta)$							
16	TNL	Expt	P DOE-NDC-24 177	Apr 81	1.1+1		Byrd+ CURV. SUBMITTED TO NP/A.
		Expt	P DOE-NDC-24 177	Apr 81	6.9+0	8.8+0	Byrd+ NDG. TOF. PRELIMINARY.
		Expt	P DOE-NDC-24 180	Apr 81	1.2+1	1.7+1	Byrd+ NDG. LANE MODEL. MORE DATA NEEDED
		Expt	P DOE-NDC-24 180	Apr 81	1.2+1	1.7+1	Byrd+ NDG. TBA.
$^{15}N(p,n)^{15}O$ $\sigma(E;\theta)$							
17	TNL	Expt	P DOE-NDC-24 180	Apr 81	1.2+1	1.7+1	Byrd+ NDG. LANE MODEL. MORE DATA NEEDED
		Expt	P DOE-NDC-24 180	Apr 81	1.6+1	1.7+1	Byrd+ NDG. TBA.
$^{15}N(p,n)^{15}O$ polarization$(E;\theta)$							
18	TNL	Expt	P DOE-NDC-24 180	Apr 81	1.2+1	1.7+1	Byrd+ NDG. LANE MODEL. MORE DATA NEEDED
		Expt	P DOE-NDC-24 180	Apr 81	1.2+1	1.7+1	Byrd+ NDG. TBA.

No.	Lab	Work Type	Reference	Date	Emin (MeV)	Emax (MeV)	Author, Comments
$^{15}N(p,n)^{15}O$ $\sigma(E)$							
19	TNL	Expt	P DOE-NDC-24 177	Apr 81	3.8+0	9.3+0	Byrd+ CURV. CFD OTHERS. TBP NP/A.
$^{116}Sn(p,inelastic)^{116}Sn$ partial $\sigma(E;\theta)$							
20	LRL	Expt	P DOE-NDC-24 53	Apr 81	2.5+1		Wong+ NDG. IAS. LANE MODEL ANALYSIS.
$^{116}Sn(p,n)^{116}Sb$ partial $\sigma(E;\theta)$							
21	LRL	Expt	P DOE-NDC-24 53	Apr 81	2.5+1		Wong+ NDG. IAS. LANE MODEL ANALYSIS.
$^{118}Sn(p,inelastic)^{118}Sn$ partial $\sigma(E;\theta)$							
22	LRL	Expt	P DOE-NDC-24 53	Apr 81	2.5+1		Wong+ NDG. IAS. LANE MODEL ANALYSIS.
$^{118}Sn(p,n)^{118}Sb$ partial $\sigma(E;\theta)$							
23	LRL	Expt	P DOE-NDC-24 53	Apr 81	2.5+1		Wong+ NDG. IAS. LANE MODEL ANALYSIS.
$^{120}Sn(p,inelastic)^{120}Sn$ partial $\sigma(E;\theta)$							
24	LRL	Expt	P DOE-NDC-24 53	Apr 81	2.5+1		Wong+ NDG. IAS. LANE MODEL ANALYSIS.
$^{120}Sn(p,n)^{120}Sb$ partial $\sigma(E;\theta)$							
25	LRL	Expt	P DOE-NDC-24 53	Apr 81	2.5+1		Wong+ NDG. IAS. LANE MODEL ANALYSIS.
$^{122}Sn(p,inelastic)^{122}Sn$ partial $\sigma(E;\theta)$							
26	LRL	Expt	P DOE-NDC-24 53	Apr 81	2.5+1		Wong+ NDG. IAS. LANE MODEL ANALYSIS.
$^{122}Sn(p,n)^{122}Sb$ partial $\sigma(E;\theta)$							
27	LRL	Expt	P DOE-NDC-24 53	Apr 81	2.5+1		Wong+ NDG. IAS. LANE MODEL ANALYSIS.
$^{124}Sn(p,inelastic)^{124}Sn$ partial $\sigma(E;\theta)$							
28	LRL	Expt	P DOE-NDC-24 53	Apr 81	2.5+1		Wong+ NDG. IAS. LANE MODEL ANALYSIS.
$^{124}Sn(p,n)^{124}Sb$ partial $\sigma(E;\theta)$							
29	LRL	Expt	P DOE-NDC-24 53	Apr 81	2.5+1		Wong+ NDG. IAS. LANE MODEL ANALYSIS.
$^{181}Ta(p,n)^{181}W$ partial $\sigma(E;\theta)$							
30	LRL	Expt	P DOE-NDC-24 54	Apr 81	2.5+1		Wong+ NDG. IAS. LANE MODEL ANALYSIS.
$Ir(p,x)\pi^-$ average $\sigma(E;E';\theta)$							
31	ORL	Theo	P DOE-NDC-24 130	Apr 81	+1	5.0+2	Alsmiller+ NDG. AVERAGED 45-75 DEG.
$Ir(p,x)\pi^+$ partial $\sigma(E;E';\theta)$							
32	ORL	Theo	P DOE-NDC-24 130	Apr 81	2.8+3		Alsmiller+ NDG. CFD EXPT.
$Ir(p,x)\pi^+$ average $\sigma(E;E';\theta)$							
33	ORL	Theo	P DOE-NDC-24 130	Apr 81	+1	5.0+2	Alsmiller+ NDG. AVERAGED 45-75 DEG.
$Ir(p,x)n$ average $\sigma(E;E';\theta)$							
34	ORL	Theo	P DOE-NDC-24 130	Apr 81	+1	5.0+2	Alsmiller+ NDG. AVERAGED 45-75 DEG.
$Ir(p,x)^1H$ average $\sigma(E;E';\theta)$							
35	ORL	Theo	P DOE-NDC-24 130	Apr 81	+1	5.0+2	Alsmiller+ NDG. AVERAGED 45-75 DEG.
$^{197}Au(p,n)^{197}Hg$ partial $\sigma(E;\theta)$							
36	LRL	Expt	P DOE-NDC-24 56	Apr 81	2.6+1	2.7+1	Wong+ NDG. IAR. DEDUCED NEUTRON SCATTER
$^{209}Bi(p,n)^{209}Po$ partial $\sigma(E;\theta)$							
37	LRL	Expt	P DOE-NDC-24 56	Apr 81	2.6+1	2.7+1	Wong+ NDG. IAR. DEDUCED NEUTRON SCATTER
$^{232}Th(p,n)^{232}Pa$ partial $\sigma(E;\theta)$							
38	LRL	Expt	P DOE-NDC-24 56	Apr 81	2.6+1	2.7+1	Wong+ NDG. IAR. DEDUCED NEUTRON SCATTER
$U(p,fission)$ thick target yield							
39	ORL	Theo	P DOE-NDC-24 130	Apr 81	1.0+3		Alsmiller+ NDG. HIGH-ENERGY TRANSPORT

CHARGED PARTICLE REFERENCES

No.	Lab	Work Type	Reference	Date	Emin (MeV)	Emax (MeV)	Author, Comments
$U(p,\gamma)$ thick target yield							
40	ORL	Theo	P DOE-NDC-24 130	Apr 81	1.0+3		Alsmiller+ NDG. HIGH-ENERGY TRANSPORT
$U(p,x)n$ thick target yield							
41	ORL	Theo	P DOE-NDC-24 130	Apr 81	1.5+3		Alsmiller+ NDG. NUCLEON-MESON TRANSPORT
$^{235}U(p,x)n$ ν							
42	ORL	Theo	P DOE-NDC-24 130	Apr 81	+1	+3	Alsmiller+ NDG. INTRA-NUCLEAR CASCADE.
$^{238}U(p,x)n$ partial thick target yield							
43	ORL	Theo	P DOE-NDC-24 130	Apr 81	5.4+2	1.5+3	Alsmiller+ NDG. THERMAL NEUTRONS.
$^{238}U(p,n)^{238}Np$ partial $\sigma(E;\theta)$							
44	LRL	Expt	P DOE-NDC-24 56	Apr 81	2.6+1	2.7+1	Wong+ NDG. IAR. DEDUCED NEUTRON SCATTER
systematics(p,x) $\sigma(E)$							
45	LRL	Eval	P DOE-NDC-24 70	Apr 81	NDG		Howerton+ NDG. THROUGH O-16.
systematics(p,x) $\sigma(E;\theta)$							
46	LRL	Eval	P DOE-NDC-24 70	Apr 81	NDG		Howerton+ NDG. THROUGH O-16.
systematics(p,x) $\sigma(E;E')$							
47	LRL	Eval	P DOE-NDC-24 70	Apr 81	NDG		Howerton+ NDG. THROUGH O-16.
$^{2}H(d,elastic)^{2}H$ polarization$(E;\theta)$							
48	LAS	Theo	P DOE-NDC-24 76	Apr 81	1.0+1		Hale+ CURV. COULOMB CORRECTIONS.
$^{2}H(d,p)^{3}H$ $\sigma(E;\theta)$							
49	LAS	Expt	P DOE-NDC-24 72	Apr 81	4.0-2	1.2-1	Brown+ NDG. TEST MEASUREMENTS.
$^{2}H(d,n)^{3}He$ $\sigma(E;\theta)$							
50	LAS	Expt	P DOE-NDC-24 72	Apr 81	NDG		Brown+ NDG. WORK IN PROGRESS.
$^{2}H(d,n)^{3}He$ polarization$(E;\theta)$							
51	TNL	Expt	P DOE-NDC-24 183	Apr 81	5.5+0	1.2+1	Tornow+ NDG. TBP.
		Expt	P DOE-NDC-24 183	Apr 81	8.0+0		Tornow+ NDG. EFFECTIVE POLARIZATION.
$^{6}Li(d,x)$ $\sigma(E)$							
52	ANL	Expt	P DOE-NDC-24 9	Apr 81	+0	+0	Elwyn+ NDG. SUBSTANTIALLY COMPLETED.
$^{6}Li(d,x)$ $\sigma(E;\theta)$							
53	ANL	Expt	P DOE-NDC-24 9	Apr 81	+0	+0	Elwyn+ NDG. SUBSTANTIALLY COMPLETED.
$^{7}Li(d,p)^{8}Li$ $\sigma(E)$							
54	ANL	Expt	P DOE-NDC-24 9	Apr 81	7.0-1	8.0-1	Elwyn+ NDG. CHARGED-PARTICLE TOF.
systematics(d,x) $\sigma(E)$							
55	LRL	Eval	P DOE-NDC-24 70	Apr 81	NDG		Howerton+ NDG. THROUGH O-16.
systematics(d,x) $\sigma(E;\theta)$							
56	LRL	Eval	P DOE-NDC-24 70	Apr 81	NDG		Howerton+ NDG. THROUGH O-16.
systematics(d,x) $\sigma(E;E')$							
57	LRL	Eval	P DOE-NDC-24 70	Apr 81	NDG		Howerton+ NDG. THROUGH O-16.
systematics(d,n) product yield							
58	ANL	Expt	P DOE-NDC-24 9	Apr 81	NDG		Smith+ NDG. IN COLLABORATION WITH LLNL
systematics(d,t) $\sigma(E;E')$							
59	LRL	Eval	P DOE-NDC-24 70	Apr 81	NDG		Howerton+ NDG. THROUGH O-16.
$^{2}H(t,n)^{4}He$ $\sigma(E;\theta)$							
60	LAS	Expt	P DOE-NDC-24 72	Apr 81	NDG		Brown+ NDG. WORK TO BE DONE.

No.	Lab	Work Type	Reference	Date	Emin (MeV)	Emax (MeV)	Author, Comments
systematics(t,x) $\sigma(E)$							
61	LRL	Eval	P DOE-NDC-24 70	Apr 81	NDG		Howerton+ NDG. THROUGH O-16.
systematics(t,x) $\sigma(E;\theta)$							
62	LRL	Eval	P DOE-NDC-24 70	Apr 81	NDG		Howerton+ NDG. THROUGH O-16.
$^{6}Li(^{3}He,x)$ $\sigma(E)$							
63	ANL	Expt	P DOE-NDC-24 9	Apr 81	+0	+0	Elwyn+ NDG. SUBSTANTIALLY COMPLETED.
$^{6}Li(^{3}He,x)$ $\sigma(E;\theta)$							
64	ANL	Expt	P DOE-NDC-24 9	Apr 81	+0	+0	Elwyn+ NDG. SUBSTANTIALLY COMPLETED.
$^{6}Li(^{3}He,p)^{8}Be$ *partial* $\sigma(E)$							
65	ANL	Expt	P DOE-NDC-24 9	Apr 81	5.0-1	2.0+0	Elwyn+ NDG. SEE PR/C 22, 1406(1980).
$^{6}Li(^{3}He,p)^{8}Be$ *partial* $\sigma(E;\theta)$							
66	ANL	Expt	P DOE-NDC-24 9	Apr 81	5.0-1	2.0+0	Elwyn+ NDG. SEE PR/C 22, 1406(1980).
systematics$(^{3}He,x)$ $\sigma(E)$							
67	LRL	Eval	P DOE-NDC-24 70	Apr 81	NDG		Howerton+ NDG. THROUGH O-16.
systematics$(^{3}He,x)$ $\sigma(E;\theta)$							
68	LRL	Eval	P DOE-NDC-24 70	Apr 81	NDG		Howerton+ NDG. THROUGH O-16.
systematics$(^{3}He,t)$ $\sigma(E;E')$							
69	LRL	Eval	P DOE-NDC-24 70	Apr 81	NDG		Howerton+ NDG. THROUGH O-16.
$^{9}Be(\alpha,x)n$ *thick target yield*							
70	WAU	Expt	P DOE-NDC-24 189	Apr 81	+0	1.0+1	Grant+ NDG. 20PERCENT HIGHER THAN BAIR+
$O(\alpha,x)n$ *thick target yield*							
71	WAU	Expt	P DOE-NDC-24 189	Apr 81	+0	1.0+1	Grant+ NDG. 20PERCENT HIGHER THAN BAIR+
$^{18}O(\alpha,n)^{21}Ne$ $\sigma(E)$							
72	WAU	Expt	P DOE-NDC-24 189	Apr 81	+0	1.0+1	Grant+ NDG. 20PERCENT HIGHER THAN BAIR+
$^{cmp}O(\alpha,x)n$ *thick target yield*							
73	WAU	Expt	P DOE-NDC-24 189	Apr 81	+0	1.0+1	Grant+ NDG. 20PERCENT HIGHER THAN BAIR+
$^{19}F(\alpha,x)n$ *thick target yield*							
74	WAU	Expt	P DOE-NDC-24 189	Apr 81	+0	1.0+1	Grant+ NDG. 20PERCENT HIGHER THAN BAIR+
systematics(α,x) $\sigma(E)$							
75	LRL	Eval	P DOE-NDC-24 70	Apr 81	NDG		Howerton+ NDG. THROUGH O-16.
systematics(α,x) $\sigma(E;\theta)$							
76	LRL	Eval	P DOE-NDC-24 70	Apr 81	NDG		Howerton+ NDG. THROUGH O-16.
systematics(α,t) $\sigma(E;E')$							
77	LRL	Eval	P DOE-NDC-24 70	Apr 81	NDG		Howerton+ NDG. THROUGH O-16.

ARGONNE NATIONAL LABORATORY

A. NEUTRON PHYSICS

1. Tritium Production by means of the $Li^7(n;n',t)$Reaction
(D. Smith, M. Bretscher and J. Meadows)

In view of previously reported discrepancies in this important fusion reaction,[1] a measurement program was undertaken over the incident-neutron energy range 7-9 MeV. Seven individual cross section values were obtained to accuracies of 4-6%. The tritium produced in encapsulated lithium-metal samples by fast-neutron bombardment was extracted and the activity measured using liquid-scintillation counting techniques. The neutron fluence was measured using a precision ^{238}U fission chamber that was subsequently calibrated by comparison against well established ^{235}U standard-fission deposits. Thus the fluence is essentially relative to the ^{235}U fission cross section. The results, illustrated in Fig. A-1, are insensitive to energy over the measured range and give an average cross-section value of 372 mb (±3.8%). This result is significantly lower than ENDF/B-V but larger than some recently reported experimental values for the same reaction.[1] A manuscript reporting this work has been sent to a publisher and the details of the experimental procedures, including thermal verifications, are given in the Laboratory Report, ANL/NDM-55 (1980).

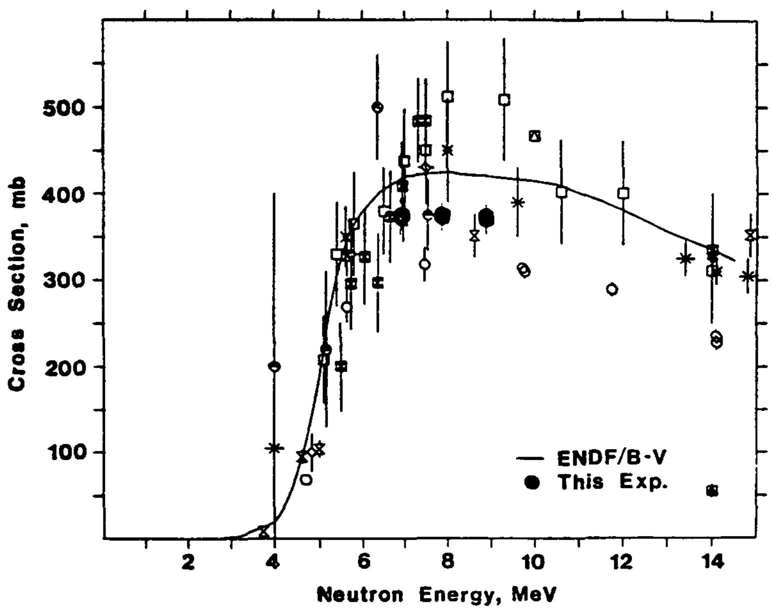

Fig. A-1. Cross section for the $^7Li(n;n',t)$ Reaction. Solid circular data points indicate averages of the results of the present measurements. Other reported data points previously reported in the literature are shown and the curve represents ENDF/B-V.

[1] M. Swinhoe and C. Uttley, NBS Special Publication 594 (1980).

2. Neutron total and scattering cross sections of ^{6}Li
(P. Guenther, A. Smith and J. Whalen)

This study, including experimental measurements and their interpretation to 4.0 MeV, has been completed and a journal manuscript has been prepared for publication.

3. Fast-neutron Total and Scattering Cross Sections of Structural Materials (P. Guenther, A. Smith, C. Budtz-Jørgensen* and J. Whalen)

a. Elemental Chromium

The work on broad resolution neutron total- and scattering-cross sections, detailed in the previous report, is now complete. The observation that the ENDF/B-V inelastic scattering cross sections are consistently smaller than those observed in this work remains valid. The results are given in the Laboratory Report ANL/NDM-57 (in press).

b. Nickel-58

As a part of a comprehensive study of the interaction of fast neutrons with nickel, neutron total and scattering cross sections of ^{58}Ni are being measured from 1 to 4.5 MeV with sufficient detail to assure reliable determination of the energy-average cross section values. The scattering measurements have been completed. The total cross section measurements are in progress. This effort compliments similar work dealing with ^{60}Ni and elemental nickel, the results of which have been published.

c. Elemental Copper

The broad-resolution neutron total- and scattering-cross sections previously reported have been extensively supplemented with additional information with emphasis on the definition of the inelastic neutron scattering processes. In all, cross sections for 13 inelastic neutron groups with scattered-neutron resolution of 0.1-0.3 MeV and excitations up to 3.0 MeV have been determined. A more detailed high-resolution study of these inelastic-scattering processes is planned using separated-isotopic targets.

4. Fission-product Nuclides

A broad program of measurement and analysis in the area of fission products has been initiated. The undertaking is in two stages; 1) the light fragment region of Z=39-52 and 2) the heavy fragment region Z=55-75. Each stage is in four elements; 1) measurement of total neutron cross sections from ≈50 keV to 5 MeV, 2) measurement of neutron scattering cross sections from a few 100 keV to 4 MeV, 3) measurement of neutron capture cross sections from approximately 20 keV, and 4) a general interpretation from which experimentally inaccessible information can be calculated. The measurements and interpretations for stage-1 (the light fragment region) are well along including all elemental materials and selected isotopic targets. Examples

*On leave from the Central Bureau for Nuclear Measurements, Geel, Belgium.

of the results are given in the subsequent paragraphs. The second stage of the work has been initiated.

a. Total Neutron Cross Section Measurements in the Light Fission Product Mass Region (W. P. Poenitz, J. F. Whalen, A. B. Smith, P. T. Guenther, and C. Budtz-Jørgensen)

Measurements of the total neutron cross section of Y, Zr, Mo, Cd, Sn, Te, Ag, Nb, Rh, Pd, In and Sb in the energy range from 50 KeV to 4.5 MeV were completed. The measurement procedure followed that used for the heavy nuclei reported earlier. Data were obtained in the 50 KeV-220 KeV energy range with pseudo-white neutron spectra and from 200 KeV to 4.5 MeV with monoenergetic neutrons. The data were corrected for resonance-self-shielding using correction factors calculated with Monte Carlo techniques. Measurements at some energies and for some samples (Nb, In, Sn, Mo, Y) with different thicknesses were used to verify these corrections. Preliminary results from the present measurements are shown in Fig. A-2. These data will be used together with scattering data (below) for establishing optical model parameters which are needed for the calculation of capture cross sections of fission product nuclei.

b. Fast-neutron Scattering Cross Sections (A. Smith, P. Guenther, and C. Budtz-Jørgensen)

The measurement program has focused upon elastic scattering in the above "stage-1" with comprehensive results obtained from Z=39 to 52 including all elemental targets and selected isotopic targets. The experimental results have been reduced to cross sections and a unified model describing the region is being developed. Illustrative experimental and model results are shown in Fig. A-3. Some of the measurements (e.g. Y and Nb) include detailed inelastic-neutron scattering results. In other instances additional inelastic-scattering measurements are planned with higher resolutions and in a few cases the isotopic complexity of the element (e.g. Sn) make inelastic-neutron studies unrewarding. In these latter instances isotopic targets are being used to the extent they are available and funded.

5. Measurement of the $^{53}Cr(n,p)^{53}V$ Cross Section below 9.4 MeV using a Sample Transport Facility (Donald L. Smith, J. W. Meadows and Frank F. Porta)

An experimental facility has been developed for short-half-life neutron activation studies whereby sample material is transported between the irradiation position and the counting position by a constant-velocity cog belt. This facility has been used to measure the $^{53}Cr(n,p)^{53}V$ cross section relative to the $^{52}Cr(n,p)^{52}V$ cross section below 9.4 MeV, using elemental chronium metal as a sample material. The measured rations and previously reported cross section information for the $^{52}Cr(n,p)^{52}V$ reaction[2]

[2] Donald L. Smith and James W. Meadows, Nucl. Sci. Eng., 76, 43(1980).

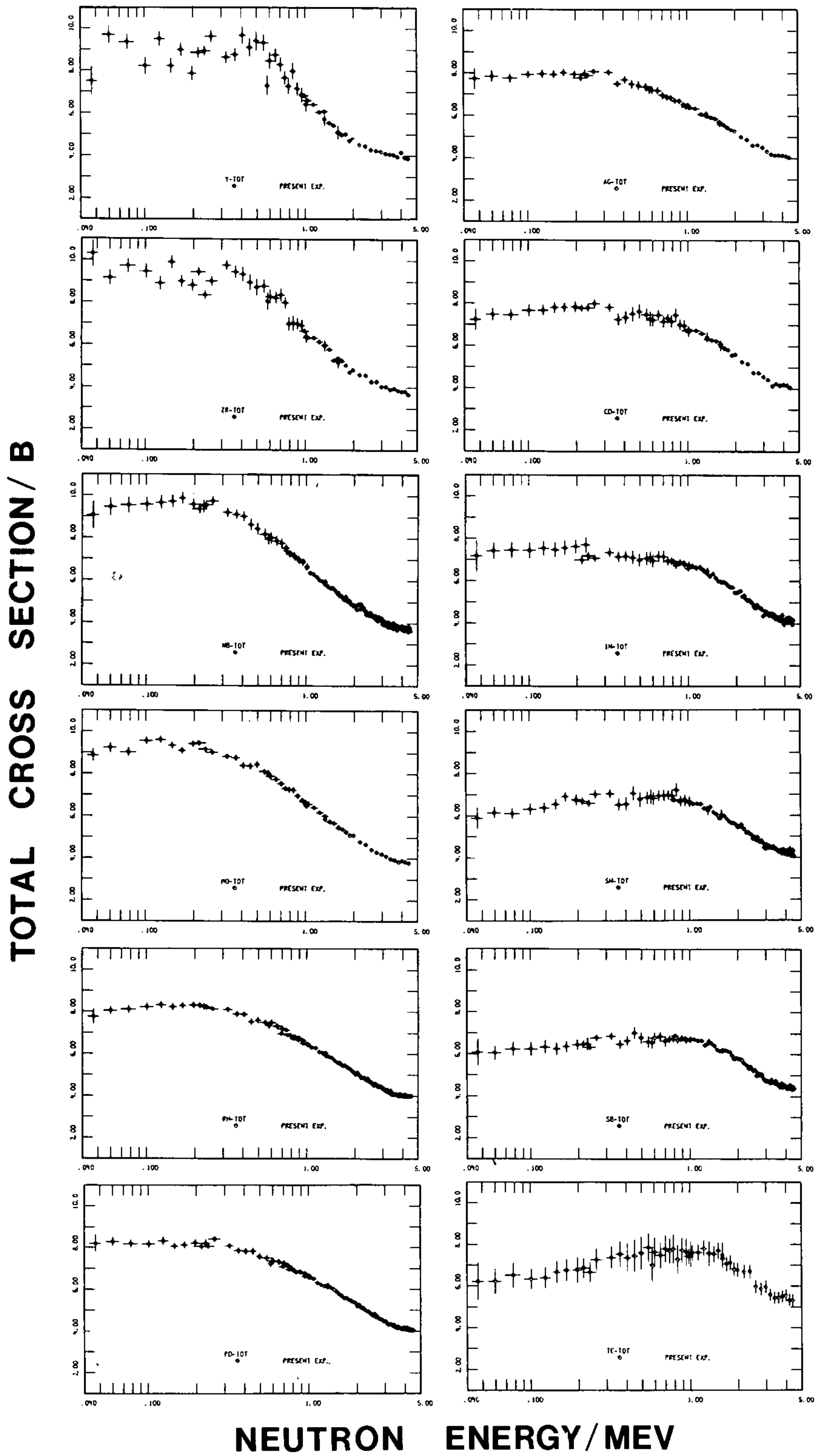

Fig. A-2. Preliminary measured neutron total cross sections in the light fission-product region.

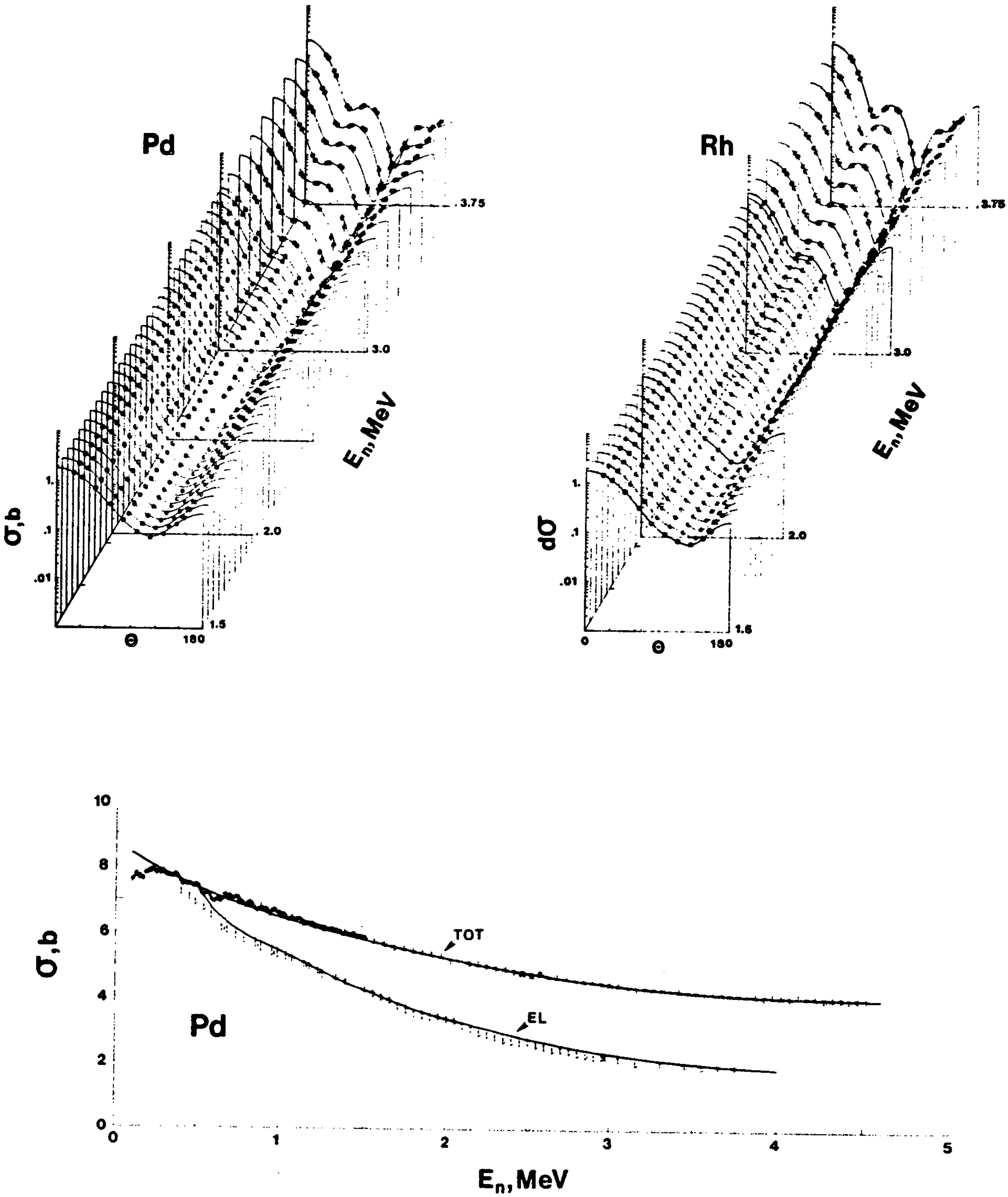

Fig. A-3. Illustrative elastic scattering results in the light fission-product region. Data points indicate measured values and curves the results obtained with a unified model.

have been used to derive the values for the $^{53}Cr(n,p)^{53}V$ cross section. The results are illustrated in Fig. A-4. The ^{235}U thermal-neutron fission spectrum average has been calculated and is 0.409 ± 0.061 mb.

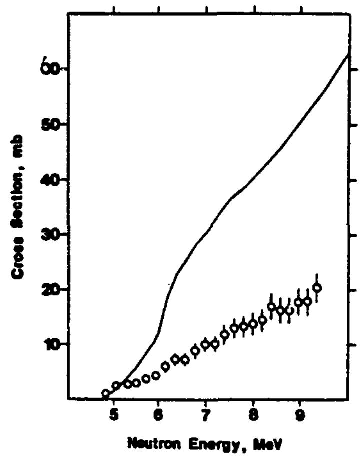

Fig. A-4. Isotopic values of the $^{53}Cr(n,p)^{53}V$ cross section from this experiment (o) and a visual fit to the $^{52}Cr(n,p)^{52}V$ cross section data of Ref. 1 (-).

6. Total Neutron Cross Sections of Hydrogen and Carbon at 0.5, 1.0 and 2.0 MeV (W. P. Poenitz and J. F. Whalen)

The total neutron cross section of hydrogen and carbon were measured at 0.509, 1.024 and 2.003 MeV using two samples each of graphite, polyethylene and polystyrene. The purpose of these measurements was to establish to what extent, if any, changes of the H(n,n) cross section given in ENDF/B-V would be required. More recent data agree reasonably well with the analysis by Hopkins and Breit[3] (used as ENDF/B-III to V) but some bias appears to exist toward lower values at higher energies ($E > 0.5$ MeV). Preliminary results from the present measurements support this trend:

E/MeV	σ/b	σ/b (ENDF/B-V)
0.509	6.049 ± 0.013	6.085
1.024	4.194 ± 0.010	4.207
2.003	2.902 ± 0.013	2.914

Lomon and Wilson[4] made an analysis of the data available in 1974 and presented a parameter set for the shape-independent effective-range approximation. This parameter set, with its uncertainties as a constraint, was used to fit data which became available since the analysis by Lomon and Wilson, including the present data. The resulting parameter set is given in Table I and describes the H(n,n) cross section below 5 MeV very well. More recent experimental data are in a ±0.25% accuracy range. ENDF/B-V agrees well with

[3] J. C. Hopkins and G. Breit, Nucl. Data A9, 137(1971).

[4] E. Lomon and R. Wilson, Phys. Rev. C9, 1329(1974).

recent measurements considering the uncertainty range of 0.5-1.0% given for ENDF/B-V, however, it is systematically higher above 0.01 MeV with differences up to 0.4%.

Table I. Parameters obtained in present fit (F)

	Triplet	Singlet
Effective Range	1.772	2.961
Scattering Length	5.428	-23.734

7. ^{238}U Neutron Capture Rate Measurement Technique (G. J. DiIorio and W. P. Poenitz)

An intercomparison of the determination of ^{238}U neutron capture rates in metallic uranium foils was made between the ANL FNG-group and the ZPR-group. An original discrepancy was resolved in subsequent extensive investigations. Four different experimental methods were employed in order to determine the effects of oblique-angle absorption and sum-coincidences. Both are important for the calibration and measurement of ^{239}Np-decay with a Ge(Li)-detector. The four methods were:

a) The measurement of the effective absorption of a uranium foil in standard measurement geometry using a transmission-type experiment.

b) The determination of the effective absorption of uranium samples which were activated in the same neutron flux by obtaining their specific activity from extrapolation to zero sample thickness.

c) The derivation of the effective absorption of a uranium sample by determining its true activity at a long distance from the Ge(Li)-detector (where sum-coincidences vanish and oblique angle absorption converges to parallel-beam absorption).

d) Determination of the effective counting efficiency based upon activation in a thermal neutron flux. The thermal cross section appears to be well known.

The present investigations resulted in a measurement capability of better than 1% uncertainty for ^{238}U capture rate determinations. Some integral $^{28}C/E$ reaction rate ratios will be revised by $\approx$3% as a result.

8. Consistent Data Set Evaluation (W. P. Poenitz)

A consistent evaluation of several energy-dependent cross sections which are of importance for practical applications remains a major concern. Many cross sections were measured relative to a set of standard cross sections or relative to one-another and thus are not independent. In other words, the experimental data base represents a multiple over-determination of the unknown cross sections with various correlations between the measured values. This requires a simultaneous evaluation of these cross sections in order to derive a consistent set. The standard mathematical procedure to do this is the derivation of the least-squares estimator as per Gauss and extended to correlated data by Aitken.

A program, GMA, has been developed to derive consistent evaluated data and their variance-covariance matrix. The procedure has been demonstrated to successfully handle rather large data systems (important reactor cross sections and standards). A detailed discussion was given at the Brookhaven workshop on evaluation methods (September 1980). The data base will be refined and extended to include ^{239}Pu(n,f) data in the near future. This will provide consistent evaluated data for ^{235}(n,f), ^{238}U(n,γ) and ^{239}Pu(n,f), their variances-covariances and the cross-covariances between the different cross sections.

9. Definition of the Neutron Reduced Width and Strength Function[5] (P. Moldauer)

Traditionally the reduced width of a resonance for emission of a neutron with orbital angular momentum ℓ is $\Gamma_n^\ell = \Gamma_n(ka/P_\ell)(1\text{e.V.}/E)^{1/2}$. If the energy dependence of the average neutron width $\langle\Gamma_n\rangle$ is that of the penetration factor P_ℓ for a hard sphere of channel radius a, then the average reduced width $\langle\Gamma_n^\ell\rangle$ is energy independent and the strength function $S_\ell = \langle g\Gamma_n^\ell\rangle/(2\ell+1)D$ can be determined by resonances at all energies. For $\ell > 0$, Γ_n^ℓ and S_ℓ still depend rather critically upon the choice of channel radius a. By using the fact that $P_\ell = (ka)^{2\ell+1}(\ell!2^\ell/(2\ell)!)^2(1-O(ka)^2)$ one can define a new reduced with

$$\tilde{\Gamma}_n^\ell = \Gamma_n P_\ell^{-1}(ka)2^{\ell+1} (\ell!2^\ell/(2\ell)!)^2 (1\text{e.V.}/E)^{\ell+1/2}$$

such that $\langle\tilde{\Gamma}_n^\ell\rangle$ and $\tilde{S}_\ell$ are still energy independent under the above assumption. But they are also independent of the choice of channel radius a up to terms of order $(ka)^2$.

[5] P. A. Moldauer, Conference on Nuclear Data Evaluation Methods and Procedures, Brookhaven National Laboratory, September 22-25, 1980.

B. CHARGED PARTICLE REACTIONS

1. Nuclear Reactions of Light Ions with ^6Li at Low Energies

(A. J. Elwyn, R. E. Holland, C. N. Davids, J. E. Monahan, F. P. Mooring, and W. Ray, Jr.)

Data analysis has been completed in the study of the $^6Li(^3He,p)$ reaction and a paper has recently appeared in the Physical Review.[6] Differential and total cross sections at incident energies between 0.5 and 2.0 MeV are presented not only for the ground and first excited states in ^8Be, but for the 16.63 and 16.92 MeV states and the underlying charged-particle continua as well. With this completed work, the ongoing research program to measure absolute cross sections for reactions of light ions with ^6Li at energies below a few MeV has been substantially concluded. The reactions studied include most of the processes (other than elastic scattering) that occur with significant probability at low energies between ^6Li and p, d, and ^3He ions. Angular distributions, total reaction cross sections, and thermonuclear reaction rate parameters were obtained for both two and three-body final states. The systematic nature of the data are relevant to the spectroscopy of light nuclear systems, reaction mechanism studies, and have proved to be of importance to the investigation of advanced fusion-fuel cycles.

2. The $^7Li(d,p)^8Li$ Reaction (A. J. Elwyn, C. N. Davids, R. E. Holland, and W. Ray, Jr.)

Because of 25% discrepancies in the most recent previous measurements,[7] an experiment to remeasure the total cross section in the $^7Li(d,p)^8Li$ reaction at incident energies of 0.7-0.8 MeV is underway. This cross section is used as normalization in the determination of the rate of the reaction $^7Be(p,\gamma)^8Be$ which, as a link in the proton-proton chain of nuclear reactions that take place in the sun, is of prime importance to the theoretical calculation of the number of solar neutrinos expected in current ^{37}Cl neutrino capture experiments. While previous studies of the $^7Li(d,p)$ reaction observed either the delayed α-particles following the ^8Li beta decay or the beta decay itself, we are using charged particle time-of-flight techniques in conjunction with Si surface barrier detectors to allow observation of the protons in the presence of a large deuteron background. It is expected that from accurate measurements of target thickness and integrated charge, total cross sections can be determined from measured yields to a precision of 10%.

---

[6] A. J. Elwyn, R. E. Holland, C. N. Davids, J. E. Monahan, F. P. Mooring, and W. Ray, Jr., Phys. Rev. C22, 1406(1980).

[7] C. R. McClenahan and R. E. Segel, Phys. Rev. C11, 370(1975); A. E. Schilling, N. F. Mangelson, K. K. Nieson, D. R. Dixon, M. W. Hill, G. L. Jensen, and V. C. Rogers, Nucl. Phys. A263, 389(1976).

3. Charged-particle Reactions for Fusion Energy (A. Smith and P. Guenther)

A measurement program in this area has been initiated in close correlation with LLL compilation and evaluation efforts. The initial measurements have focused upon (d,n) processes using targets with $A \leq 10$. Initial results are promising with the major experimental problem being excess experimental intensity at the FNG time-of-flight facility.

C. ACTINIDE FISSION

1. The Fission Cross Section of ^{240}Pu Relative to ^{235}U from 0.35 to 9.6 MeV (James W. Meadows)

The ^{240}Pu:^{235}U fission-cross-section ratio has been measured at 55 discrete energies between threshold and ≈10 MeV using the ^{7}Li(p,n)^{7}Be and D(d,n)^{3}He reactions as neutron sources. The sample masses were measured by; 1) calculated specific activities and low geometry alpha counting, 2) mass spectrographic isotopic dilution analyses, and 3) comparing the relative thermal fission rates of one of the ^{235}U samples with ^{240}Pu samples containing 9% ^{239}Pu. The results of this work have been prepared for journal publication and are available from the author upon request.

2. Product Yields from the Monoenergetic-neutron-induced Fission of ^{235}U (L. E. Glendenin, J. E. Gindler, D. J. Henderson, B. D. Wilkins and J. W. Meadows)

Yields of 39 fission products were determined for fission of ^{235}U induced by monoenergetic neutrons of energies 0.17, 1.0, 4.0, 5.5 and 7.1 MeV. Fission-product activities were measured with high resolution (Ge-Li) gamma-ray spectrometry of the neutron irradiated targets and with chemical separation of fission-product elements followed by beta counting and/or gamma-ray spectrometry. Further measurements at 0.5, 2.0, 6.3 and 8.0 MeV are planned. Yield values from the measurements to date are available from the authors. Data obtained thus far indicate that the valley fission-product yields vary with excitation energy much like those of ^{238}U. It is therefore expected that the dissipation energy in the desent from the saddle point to the scission will be similar for the fission of ^{236}U and ^{239}U.

3. Mass Distributions for Thermal-neutron Induced Fission of ^{249}Cf and Spontaneous Fission of ^{250}Cf (J. E. Gindler, L. E. Glendenin and D. J. Henderson)

The yields of forty fission products were determined for thermal-neutron-induced fission of ^{249}Cf. Cummulative yields were measured by gamma-ray spectroscopy of catcher foils and by chemical separation of some fission-product elements followed by beta counting. These yields were combined with previous literature values to give a composite mass distribution with an average mass for the light group, $\bar{A}_L$, equal to 105.9±0.2 and for the heavy group, $\bar{A}_H$, equal to 140.0±0.2. The peak to valley ratio, P/V, is approximately 26. Seven yields were determined for spontaneous fission of ^{250}Cf and combined with previous data to give mass-distribution characteristics of $\bar{A}_L$ = 105.4±0.2, $\bar{A}_H$ = 141.6±0.2, and P/V = 310.

D. FACILITIES

1. Upgrading the Energy of the Argonne Physics Division Dynamitron

(A. J. Elwyn, R. Amrein, and A. Langsdorf, Jr.*)

Primarily because of the research needs of the major atomic physics users of the Argonne Dynamitron accelerator, a project has been initiated to provide a number of modifications which it is hoped will upgrade the machine energy from near 3.7 MV to the vicinity of 5 MV. The following major changes have now been completed:

1) An additional SF_6 storage vessel has been installed, connected in parallel with the present one. This will eventually allow the insulating gas pressure in the machine to be increased from 90 to 135 psig.

2) An SF_6 on-line gas purifier was bought and installed via connecting pipes to the pressure vessel.

3) New single-piece Plexiglas supporting frame members have been bought and installed to replace the old jointed members.

4) A new toroidal induction-coil frame was purchased and the coil assembly, which provides the rf power for high-voltage generation, has been completely rebuilt.

5) A variable air-core capacitor has been installed in the high-voltage terminal which, along with a previously-installed capacitive balance plate between the top Dee and the pressure-tank wall, allows the 120-kHz rf ripple on the terminal to approach very close to a null. Subsequent measurements of the beam-energy spread, by determination of thick-target gamma-ray yields from nuclear reactions, have indicated that the energy modulation associated with the rf pickup is $\lesssim$600 eV so that at present the overall energy resolution is significantly less than 1 keV.

* Consultant to the Physics Division, Argonne National Laboratory.

Since the modifications the machine has been operating with essentially only routine maintenance problems and it is relatively spark free at energies up to about 4.4 MeV. It has not yet been possible to test the maximum energy-holding capability of the rebuilt accelerator at an SF_6 pressure above 90 psig, so that it is too early to know if other improvements (e.g. replacement and modification of the accelerator tube and/or solid-state rectifiers) will be necessary in order to accelerate particles to 5 MeV.

2. FNG Beam-handling System. (A. Smith and A. Engfer)

An isochronous beam handling system has been designed for use at the FNG time-of-flight facility. The requisite magnets are under fabrication. The objective is an improvement in overall time resolution using scattered neutron flight paths in the range 5-20 meters. The detection system is operational with ten detectors making possible the acquisition of comprehensive angular distributions in a single measurement.

The fast neutron chopper time-of-flight spectrometer shares the H-2 beam tube at the HFBR with an on-line mass separator, TRISTAN. In the last year, approximately 15% of the beam time was allocated to the chopper while 85% was allocated to TRISTAN experiments and development.

In December of 1980, the TRISTAN program of measurements was initiated and the initial results are described under section C of this report.

The beam line H-1B is used for resonance-averaged capture measurements which are used to extract information on average cross sections, on capture mechanism and photon and neutron strength functions, and for nuclear structure measurements. These are described in sections A and B. The neutron monochromator is used for resonance capture gamma-ray studies of nuclear structure, described in section B.

An active user program has been initiated with TRISTAN in the fields of delayed neutron spectroscopy, radioactivity and half-life studies, nuclear Q values, and nuclear structure studies. Participants in this effort to date include scientists from Pacific-Northwest Laboratories, Cornell University, Idaho National Engineering Laboratory, University of Maryland, Clark University, Iowa State University-Ames Laboratory, University of Oklahoma, Los Alamos National Laboratory, Lawrence Livermore National Laboratory, and staff members of the physics and chemistry departments at BNL.

A. NEUTRON CROSS SECTIONS AND CAPTURE REACTIONS

1. Neutron Capture in ^{240}Pu and the Doppler-Broadening of the 1.056 eV Resonance

The neutron capture yields of ^{240}Pu metal foil and PuO_2 were measured at 3 temperatures--293°, 77°, and 4° absolute--with the BNL HFBR fast chopper facility. The two goals of this investigation were to improve the known resonance parameters of the important 1.056 eV ^{240}Pu resonance and to study the broadening of that resonance due to Doppler effects. Because of its low energy and because of the relatively small capture width, Lamb theory suggests that this is a good case for study of the lattice binding effect on atomic thermal motion. Transmission measurements were also performed to improve knowledge of the total cross section.

2. The Total Cross Section of ^{235}U below 12 eV

Detailed analyses of ^{235}U cross sections now show that the chief uncertainties result from lack of precision in the neutron total cross sections. Transmission measurements on ^{235}U foils of thickness 1.45, 5.27, 14.22, and 28.56 gms/cm^2 were performed with the BNL HFBR fast chopper neutron spectrometer. The energy ranges covered were from 0.025 to 1.5 eV, and from 0.5 to

12 eV. The data are being analyzed with the aid of a multi-channel R-matrix code.

3. Resonance-averaged Capture in ^{239}Pu

The technique of resonance averaging through the use of tailored neutron beams at 2 and 24 keV has proved extremely successful in the study of nuclear structure. The technique, however, has heretofore been applied only to non-fissile nuclides. In ^{239}Pu, the initial states of spin $^{+}0$ and 1^{+} populate final states in the range from $0^{\pm}$ to $2^{\pm}$, and radiative capture competes with fission. The final states of ^{240}Pu populated after the capture of 2 keV neutrons show significant departures from the expected populations. Both negative and positive parity final states fail to divide into sharply defined spin-dependent bands. These effects are contrary to the usual population parameters and may reflect the competition with the fission cross section. The gamma-ray transitions closely follow an E^3 dependence, which in ^{240}Pu is quite consistent with the influence of the giant dipole resonance. A ratio of 5 is observed between E1 and M1 transitions. Absolute photon intensities have been calculated using a normalization to previous resonance capture data. (BNL/Petten/Cornell University)

4. Level Densities from Average Capture

The use of resonance-averaged capture guarantees the uniform population of all states in a given spin parity range. Experience has shown that a reliable set of level positions can be obtained up to an excitation energy of 1.5 to 2 MeV for a heavy nucleus. Accordingly the scandium tailored beam has been used to study levels by the (n,γ) technique for some 20 nuclides ranging from ^{148}Sm to ^{239}U. For each the level density has been fitted with a back-shifted Fermi gas model. The densities have been normalized to the region of the neutron binding energy. The results have been submitted for publication. (BNL/Los Alamos/Clark University)

5. A Survey of Photon Strength Functions

This work was completed and published in 1981 (Phys. Rev. C, April). Both M1 and E1 strengths have been tabulated. The results show clearly the influence of the E1 giant resonance on E1 transitions following neutron capture.

B. NUCLEAR STRUCTURE WITH THE (n,γ) REACTION

The H-1 beam tube at the HFBR provides 2 beams used almost entirely for neutron capture γ-ray studies. These include the tailored beam facility, which provides beams of thermal, 2 and 24 keV neutrons, and the neutron monochrometer, which provides energy-selected beams effective up to about 25 eV. The conversion electron spectrometer is under development and will produce experimental results at the H-3 beam port. These wide ranging beams provide a unique method of nuclear structure investigation due to the primarily non-selective character of the (n,γ) reaction. Experience has shown that a combination of the BNL filtered beams with the precise bent crystal and electron data from the Institute Laue Langevin (ILL), Grenoble is essential for the construction of reliable level schemes. These studies have led to stringent tests of the recently introduced Interacting Boson Model and its derivations. The following experiments, listed briefly, refer to various classes of tests of the IBA.

1. Studies of Odd A Transitional Nuclei

A successful interpretation of the characteristics of odd mass nuclei depends critically on a valid description of the underlying core motion. In transitional regions such as the W-Os-Pt nuclei, where the equilibrium nuclear shape is changing rapidly, the correct choice for such a description has not, until recently, been clear. However it has now been shown that, in the framework of the Interacting Boson Approximation (IBA), the changing structure of the even mass nuclei in this region can be reproduced in terms of a transition between the SU(3) and 0(6) limits predicted by the model. Thus these previous studies represent an excellent basis for an investigation of the extension of the IBA to the corresponding odd A nuclei, and a series of detailed experimental investigations of such nuclei via the (n,γ) reaction is currently in progress. These are as follows:

a. $^{186}W(n,\gamma)^{187}W$

b. $^{194}Pt(n,\gamma)^{195}Pt$

c. $^{196}Pt(n,\gamma)^{197}Pt$

d. $^{190}Os(n,\gamma)^{191}Os$

All these studies are being carried out with the help of the Institute Laue-Langevin, Grenoble.

2. The 0(6) Symmetry and the Structure of ^{136}Ba

One of the most impressive successes of the IBA model has been the prediction, and subsequent discovery, of the 0(6) symmetry in ^{196}Pt through a joint BNL-ILL (n,γ) study. It would be very interesting to find further examples, and the model indicates that this symmetry should also be apparent in the Xe, Ba nuclei at the end of N=50-82 shell. A study of the level structure of ^{136}Ba has been undertaken. Capture measurements at 2 and 24 keV neutron energy have been made at BNL, and the low energy γ-ray spectra have been studied with the GAMS spectrometers at ILL. The results of the two studies will be combined for further analysis early in 1981. (University of Manchester/ILL/BNL)

3. The Two-Phonon Quintet in Cd Isotopes

Previous studies of the even mass Cd isotopes with A=110 to 114 have shown the existence of a quintuplet of levels at the two phonon vibrational energy. Recent theoretical calculations by Heyde et al. have shown that inclusion of proton 2p-2h configurations coupled to the vibrational excitations, as well as the pure vibrations themselves, can generate a second rotational-like band structure. Indeed, the branching ratios up to and including the two phonon quintuplet are very well described. Consequently, it is of interest to know what fraction of the low lying levels can be accounted for on this basis and a comprehensive experimental study of the levels of ^{112}Cd was undertaken. Capture data at both 2 and 24 keV were obtained. The use of thermal neutron capture to study ^{112}Cd is precluded by the extremely large cross section of the neighboring ^{113}Cd isotope. However, neutron monochromator studies at BNL have led to the assignment of a previously unidentified resonance at 6.98 eV to ^{112}Cd, and hence a complete study of the low energy γ-ray spectrum was possible involving Ge(Li) singles and coincidence spectra. The analysis of these data should be completed in 1981. (BNL/Gent)

4. Consequences of Completeness in Nuclear Spectroscopy and the Levels of ^{168}Er

The unique feature of the (n,γ) reaction is its inherent non-selectivity. In appropriate cases, this non-selectivity can be exploited in novel ways to assure the observation of all states in certain spin and excitation energy ranges. This capability of identifying complete sets of states has important consequences that go beyond the immediate J,π implications of the data. In particular, the technique of spin assignment by default has been studied where the guarantee of completeness implies that states not observed must have spins not contained in the set for which completeness applies. The implications of completeness for the elucidation of rotational band structures was most extensively developed in the following study.

An extremely detailed level scheme for ^{168}Er has been developed. The scheme relies primarily on resonance-averaged capture data from BNL for the identification of complete sets of levels and on precision γ-ray and electron spectroscopy utilizing the bent crystal and conversion electron spectrometers GAMS and BILL at the ILL. The level scheme so developed is the most complete yet established for a deformed nucleus. The principal characteristics of the empirical ^{168}Er level scheme are an extensive set of bands, whose collective familial relationships are established by the observation of numerous low energy intraband transitions and the particularly thorough decay patterns established for the γ band and for the low lying excited 0^+ bands. The most remarkable feature is that, contrary to common expectation, the dominant transitions out of the lower of these 0^+ bands (the β band) are not to the ground band, but to the γ band, a decay route presumably forbidden in the simple Bohr-Mottelson picture. Such a decay pattern is rarely observed but may in fact be common. The reason is that $\beta\to\gamma$ transitions are of rather low energy and even if they proceed by substantial matrix elements will be extremely weak due to the proportionality of E2 transition rates to E^5. It is only recently, with the use of the (n,γ) reaction and the exploitation of curved crystal spectroscopy, that such decay features have been observed, notably in ^{158}Gd by Greenwood and collaborators and, here, in ^{168}Er. Such decay patterns are predicted by IBA model and arise from the basic group theoretical structure of the SU(3) limit of the IBA. (ILL/Boris Kidric Institute/University of Manchester/BNL)

5. Other Experiments

The following list includes other topics studied in 1980/81 by the Brookhaven group in collaboration with others.

a. Nuclear Structure of ^{155}Sm
(ILL/ANL/NRL/BNL)

b. High Spin States in ^{177}Lu and ^{181}Ta by (n,γ)
(ILL/Koln/BNL)

c. Tests of Odd-Mass Nuclei for the IBA: ^{103}Ru
(Purdue/BNL)

d. Study of Levels in ^{236}U
(ILL/BNL

e. Levels in ^{64}Cu and ^{66}Cu from Neutron Capture
(Petten/BNL)

f. Resonance Capture γ-ray Studies of the Se Isotopes
(Soreq/BNL)

g. Excited States of ^{192}Os by Double Neutron Capture
(ILL/BNL)

h. Study of E0 Transitions from K=0 Bands in ^{188}Os and ^{196}Pt
(ILL/BNL)

The BNL staff participating in the above experiments consists of R. E. Chrien, R. F. Casten, H. I. Liou, W. R. Kane, D. D. Warner, M. L. Stelts,† P. D. Bond, D. Horn and G. Smith.

A list of the outside collaborators in the preceding (n,γ) experiments is the following:

K. Schreckenbach--Institute Laue Langevin
H. Faust Institute Laue Langevin
H. G. Borner Institute Laue Langevin
G. Barreau Institute Laue Langevin
R. Brissot Institute Laue Langevin
S. Kerr Institute Laue Langevin
C. Hofmeyr Institute Laue Langevin
M. R. Macphail Institute Laue Langevin

†Now at Los Alamos National Laboratory.

W. F. Davidson --National Research Council, Canada
J. Simic --B. Kidric Institut
M. Stojanovic B. Kidric Institut
M. Bogdanovic B. Kidric Institut
S. Loicki B. Kidric Institut
W. Gelletly --University of Manchester
*G. B. Orr --Grinnell College
F. A. Rickey --Purdue University
P. von Brentano--University of Cologne
*K. Schiffer University of Cologne
R. Smither --Argonne National Laboratory
A. Namenson --Naval Research Laboratory
K. Heyde --Gent State University, Belgium
P. Lieb --University of Gottingen
J. Kopecky --ECN, Petten
T. R. Yeh --Cornell University
*D. Marshall --Jackson State

C. NUCLEAR SPECTROSCOPY OF FISSION PRODUCT NUCLEI

One of the most exciting and perhaps surprising developments in the last decade in nuclear physics has been the progress in our ability to explore the properties of the "exotic" nuclei, which lie off the valley of stability. This is a rich and active field as demonstrated by the large number of ISOL facilities (ISOL = isotope separator on line) situated at reactors and accelerators around the world. An examination of the nuclide chart shows that several thousand of these unstable nuclides have been identified. Some 800 or more exist as neutron-rich products of thermal neutron fission of uranium-235 or plutonium 239 alone. Thus a plethora of nuclear systems exist against which nuclear models may be tested. The ability to follow structural changes across a line of isobars, as one changes neutron or proton number, provides a stern test for such models. The ISOL facility TRISTAN at BNL started, on schedule, to produce experimental results in FY 1981.

The advantage of TRISTAN stems from the ability of the HFBR to produce a powerful neutron beam--> $10^{10}/cm^2/sec$, external to the reactor. The beam is, however, extremely well shielded. TRISTAN introduced a large and active additional user component into the nuclear physics program at the HFBR.

1. Beta-delayed Two-neutron Emission from ^{98}Rb

While multiple neutron decay of light elements such as ^{11}Li and $^{30,31,32}Na$ have been previously reported, no such phenomenon has been reported for a fission fragment. A neutron-neutron time correlation technique was employed to search for two-neutron emission in ^{98}Rb, which has an energy excess $Q_\beta - Q_{2N} \approx 1.82$ MeV. The ^{98}Rb was obtained at the isotope-separator on-line TRISTAN at BNL using a neutron detector of 40 tubes of ^3He embedded in polythene. The pulses from this detector were passed to an interval analyzer which

*Signifies student.

records the distribution of time intervals between successive events. The time distribution shows an excess near t=0 corresponding to two neutron emission with a probability $P_{2N} \approx 0.025\%$. A search for other multiple neutron emitters is being made and a similar effect is seen for ^{99}Rb.

2. Recoil Spectrometer Measurements of Beta-delayed Neutron Spectra

The use of hydrogen-filled proportional counters for neutron detection has undergone a marked improvement over the past decade. It has been shown in work at Argonne and at the INEL that measurements down to several keV are feasible with such counters, provided adequate pulse shape discrimination is provided to reject γ-ray events. Hydrogen-filled proportional counters with pressures ranging from 0.5 to 2.0 atm have been calibrated for neutron response at the HFBR tailored beam facility. Two parameter measurements of the pulse rise time and height allow optimum application of pulse shape discrimination techniques. The detectors were used to collect delayed neutron spectral distributions from ^{93}Rb, ^{94}Rb, and ^{95}Rb. The analysis of these results is in progress. (INEL/BNL)

3. Delayed Neutron Spectra by Time-of-flight

Most information relating to the spectral distribution of beta-delayed neutron emitters from fission products has been obtained from He-3 spectrometers of the Shalev-Cutler type. Such spectrometers are inadequate below about 10 keV because of resolution and thermal neutron contamination problems. The time-of-flight method promises superior performance in just this region. A TOF system employing a beta-derived start signal, and a stop signal obtained from a ^{6}Li-glass scintillator has been devised for TRISTAN. The neutron response of the detector was determined at the BNL tailored beam facility. The initial measurements with this device were made with a 0.5 meter flight path for the neutron emitter ^{95}Rb, which shows a low-lying resonance reported by Hungerford at the ILL. These data will be combined with the recoil spectrometer data obtained by the INEL group, so as to map out the low energy portion of the delayed neutron spectra. (Cornell University/BNL)

4. Precise Q-values for Neutron-rich Rb and Cs Isotopes

Beta-ray end-points for Rb and Cs fission products were determined with improved precision at the BNL TRISTAN facility with an intrinsic Ge beta detector. The beta spectra were also recorded in coincidence with gamma rays in a 20% Ge:Li detector. The well-known gamma rays of ^{90}Rb were used to calibrate the spectrum. Fermi-Kurie analysis was used to determine the end-point energies. These energies are compared to the predictions of various mass formulae and with the results of other experimenters. For the first time an endpoint energy was measured for ^{98}Rb beta decay. Together with the level scheme information a Q value for ^{48}Rb of $12{,}343 \pm 150$ keV was obtained. (Clark/Iowa State/Vanier/BNL)

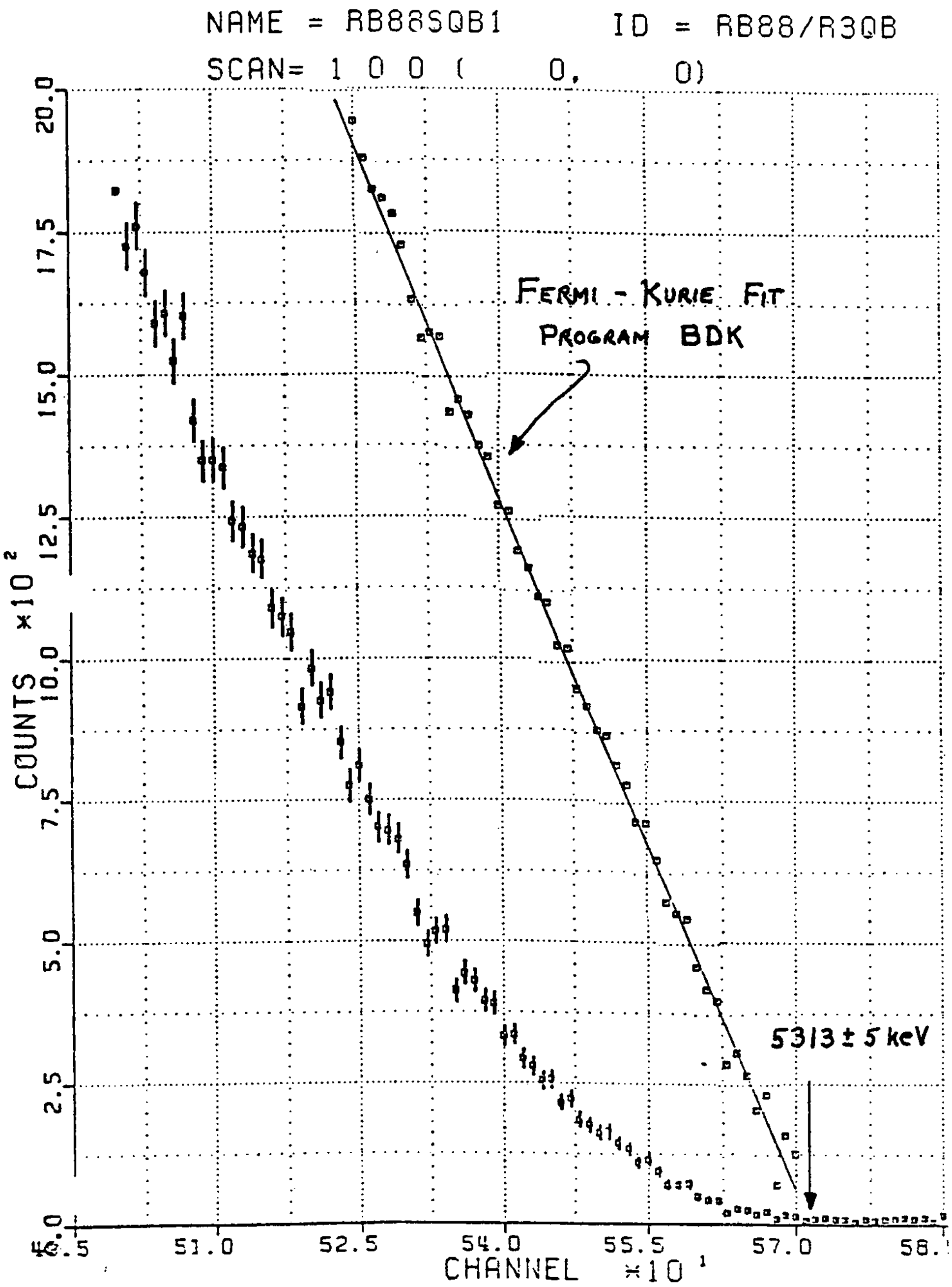

Figure C-4a. An example of a Fermi-Kurie fit to the beta spectrum of ^{88}Rb. The derived endpoint value is in excellent agreement with previous work.

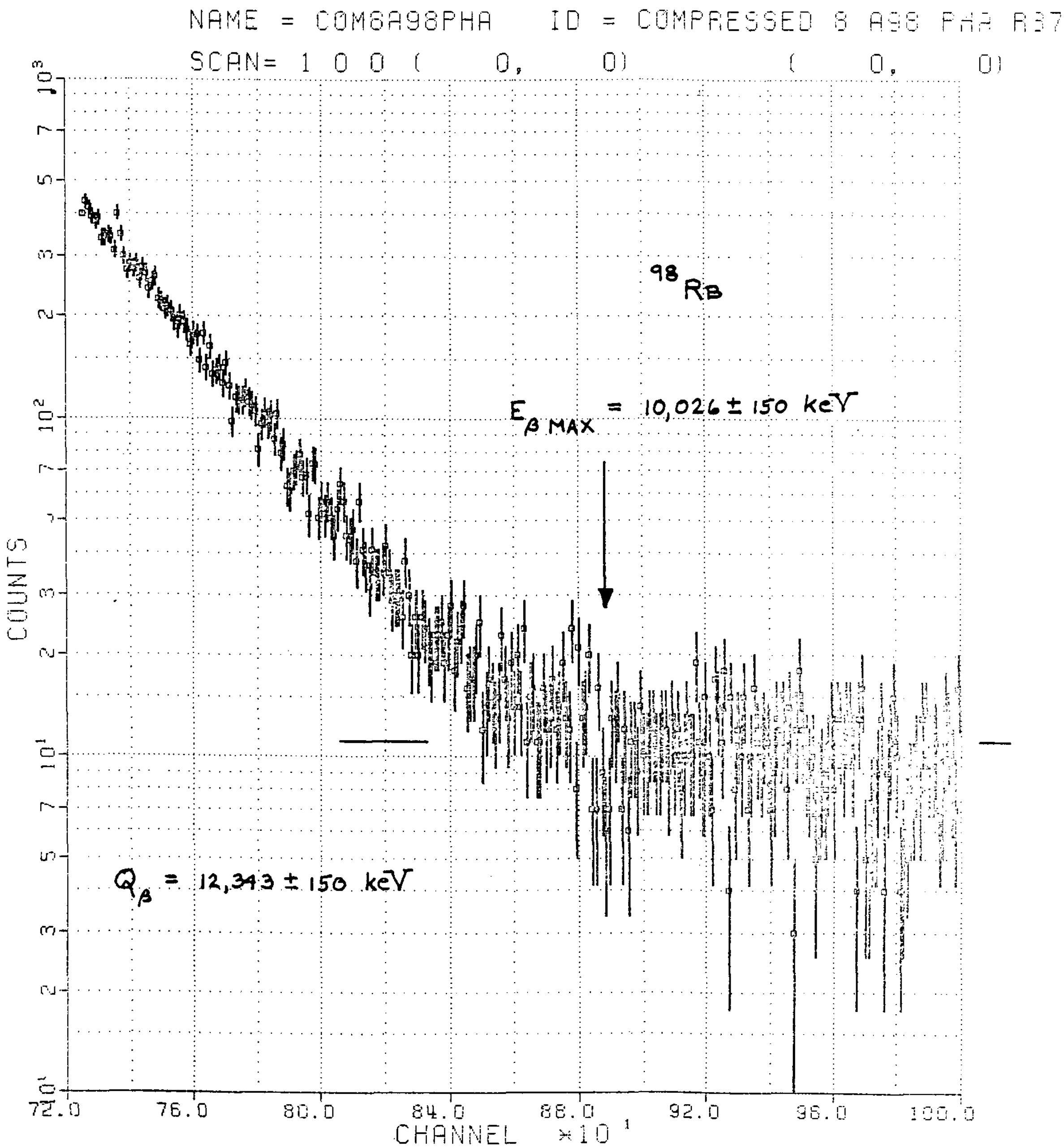

Figure C-4b. The beta spectrum for ^{98}Rb. The beta feeding is found to populate a state at 2317 keV, thus leading to a Q-value of 12,343 keV. The extremely high Q-value results in an electron range comparable to the detector size, and thus a distortion of the spectrum near the endpoint.

5. Angular Correlation Studies of the Transitional Nuclides $^{142-146}Ce$ and the Low Lying 0^+ Excited States

Gamma-gamma angular correlations have been studies for the even-A cerium isotopes from A=142 to A=146 with a multiple detector coincidence system at the on-line isotope separator TRISTAN. These studies were directed to identifying the low-lying excited 0^+ states in these nuclides and they confirm a 0^+ assignment for the previously assigned 0^+ state at 2030 keV in ^{142}Ce and establish a new 0^+ state at 1043 keV in ^{146}Ce. In ^{144}Ce extensive ($>7x10^7$ events) coincidence data on the decay of ^{144}La (spin 3^- or 4^-) were required to establish a 0^+ spin parity for the 1820 keV level. Many other new ^{144}Ce levels were also established. The systematic variation of the 0^+ states in the Ba, Ce, and Nd nuclides constitutes a severe test of nuclear models such as the IBA and initial inspection of the data tends to confirm IBA predictions. (BNL/Maryland/Clark/Iowa State/Oklahoma/Cornell/LLNL)

6. Band Structure in ^{148}Ce

The onset of nuclear deformation in the rare earth region is known to occur at N=90 for even-even nuclides with $Z>60$ (see, for example, Nd). Recent studies for the OSTIS group at the ILL of the isotopes of barium (Z=56) show that this onset tends to occur at lower neutron number for Z<60. In order to examine the intermediate situation, namely for Z=58, the neutron-rich cerium isotopes were studied through the decay of lanthanum obtained from the isotope separator on-line TRISTAN. A level scheme was established in some detail for ^{148}Ce. The decay data show levels grouped with the ground state, the β- and the γ-vibrational bands. Of special interest is evidence for a 0^+ level at 770 keV. The 0^+ to 0^+gs monopole transition has been observed with an intrinsic Ge electron detector. The results indicate an onset of deformation at a higher neutron number for the Ce isotopes than is observed for barium. (BNL/Iowa State/Clark/Oklahoma)

7. Levels of ^{146}Ce from the Decay of ^{146}La

Preliminary data on the levels of the transitional nuclide ^{146}Ce have been reported by groups at KFA, Julich and from ILL. ^{146}La is reported to decay with half-lives of 4.5 min and 8.5 sec. Recent ISOL studies at OSTIS, however, have shown that the 8.5 sec component actually consists of two components of 6 and 10 sec. An extensive study of the decay of ^{146}La was undertaken at the BNL TRISTAN mass separator to establish more firmly the level scheme of ^{146}Ce. These data include singles, gamma-gamma coincidence and angular correlations, and time-dependent spectral data (gamma-ray multiscale or GMS data). A greatly-extended knowledge of the ^{146}Ce level scheme has resulted, due to the superior beam intensities and low backgrounds available from TRISTAN. (Iowa State/Maryland/Clark/Oklahoma/BNL)

8. The Decay of Mass-separated $^{146,148}Ba$ to Levels in $^{146,148}La$

The decay of $^{146,148}Ba$ fission products to levels in the odd-odd La nuclides were studies at the on-line mass separator TRISTAN at BNL. The GMS

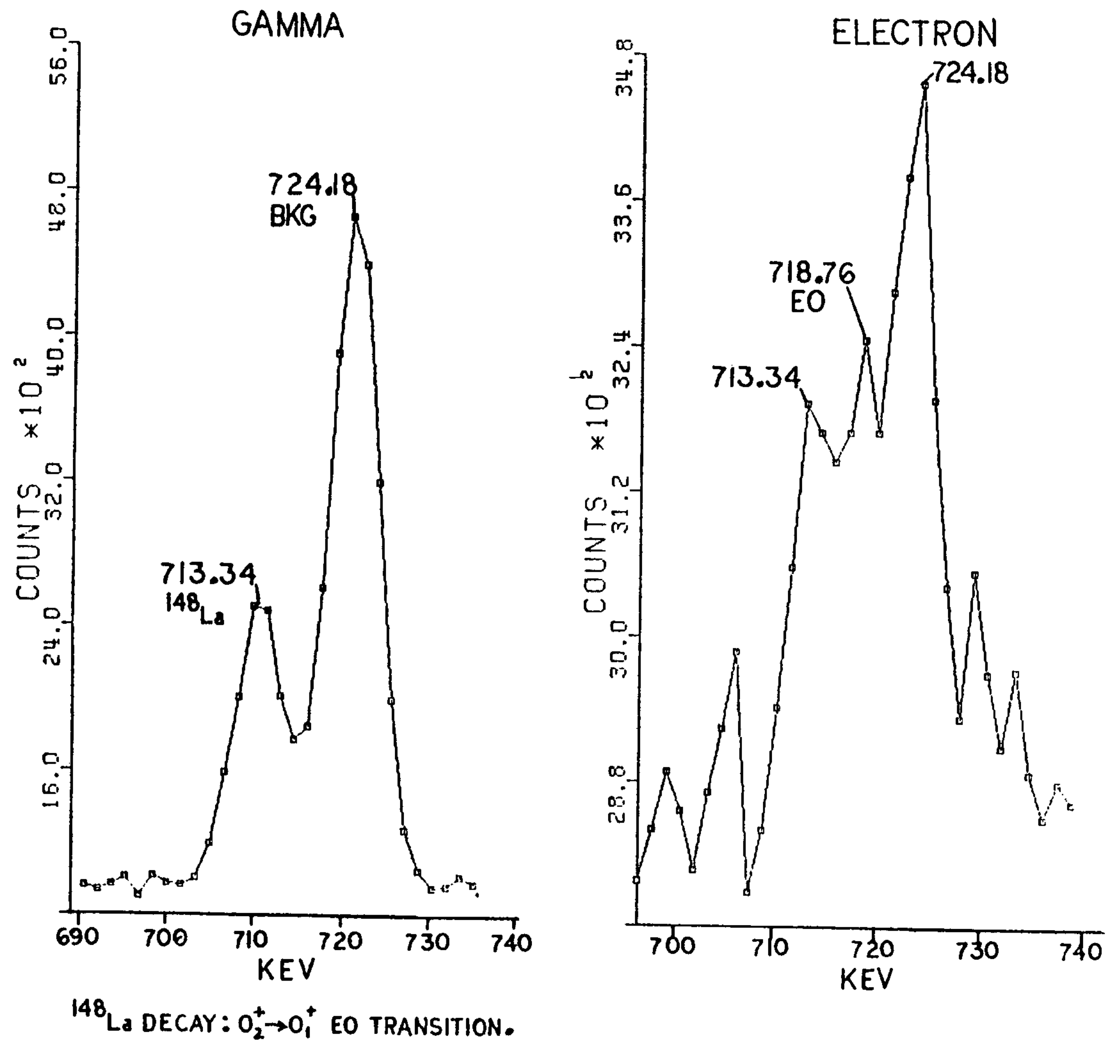

Figure C-6. A comparison of gamma and electron spectra for ^{148}La decay. The E0 transition $0_1^+ \to 0_{gs}^+$ is clearly seen and establishes definitely the 0^+ assignment for the 770 keV level in ^{148}Ce.

(gamma-ray multiscale) facility allows the collection of 32 time sequential gamma-ray spectra each with 4096 pulse height channels. The GMS allows study of growth and decay for the individual gamma-ray transitions. Some 30 gamma rays from ^{146}Ba decay were identified and a redetermination of the 1.9 sec ^{146}Ba half-life was made. In the case of ^{148}Ba, the half-life is determined to be 0.47 $\pm$ 0.08 sec. Some 37 gamma rays were also identified as due to ^{148}Ba decay. Coincidence data have established previously unknown levels at 56 and 134 keV in ^{148}La. X-rays for these nuclides were also recorded and the relative ratios of X-ray multiplet intensities allow the assignment of multipolarities to some gamma-ray transitions. (Maryland/Iowa State/BNL/Clark)

9. Study of the Decay of Low-spin ^{148}Pr to Levels of ^{148}Nd

A comparison of recent studies of the decay of ^{148}Pr from sources produced from continuous and batch process chemical separations from fission products and from fast (n,p) reactions have revealed inconsistencies in the relative intensities of a number of gamma rays. Ikeda et al. have proposed the existence of two isomers with half-lives of 2.27 $\pm$ 0.04 and 2.0 $\pm$ 0.1 minutes as the source of these disagreements. The study of mass separated ^{148}Pr, produced from the decay of ^{148}Ce at the TRISTAN facility, reveals a set of intensities in agreement with those proposed by Ikeda and which is quite different from what is observed in (n,p) studies. The level structure of ^{148}Nd is being developed with particular attention to the low-spin states populated from the ^{148}Pr decay. (BNL/LLNL/Clark/Iowa State/Oklahoma/Maryland)

10. Low-lying Levels in the N=85 Isotone ^{141}Ba

The N=85 isotones ^{149}Gd, ^{147}Sm, and ^{145}Nd are characterized by $7/2^-$ ground states and low-lying $5/2^-$ and $3/2^-$ states. ^{143}Ce has a ground state of $3/2^-$, with a $7/2^-$ state at 18.4 keV and a $5/2^-$ state at 56.2 keV. ^{141}Ba has a suggested ($3/2^-$) ground state and a proposed ($5/2^-$) state at 48.5 keV. In an effort to locate the low-lying $7/2^-$ state in ^{141}Ba, low energy gamma-ray and gamma-gamma coincidence data were obtained from the decay of mass separated ^{141}Cs at TRISTAN. A 20 nsec lifetime of the 48.5 keV level was also reconfirmed. (Iowa State/Clark/Oklahoma/BNL)

11. Levels in ^{99}Sr Resulting from the Decay of ^{99}Rb

The high temperature surface ionization source designed by Shmid, coupled with the high flux obtainable at the HFBR has made it possible to examine the decays of low yield, short-half-life isotopes such as ^{99}Rb at the BNL TRISTAN facility. The use of the GMS (gamma-ray multiscale facility, which produces a series of time-sequential gamma-ray spectra) allowed the identification of 6 previously unknown gamma rays from the decay of ^{99}Rb to levels in ^{99}Sr and 12 lines associated with the decay of ^{99}Sr. Half-lives of 70 and 250 msec have been deduced for ^{99}Rb and ^{99}Sr, respectively. The observation of these lives demonstrates the ability of the ion source to produce short-lived activities. Extensive gamma-ray coincidence data are now being taken to establish a level scheme for ^{99}Sr. (Oklahoma/Maryland/BNL)

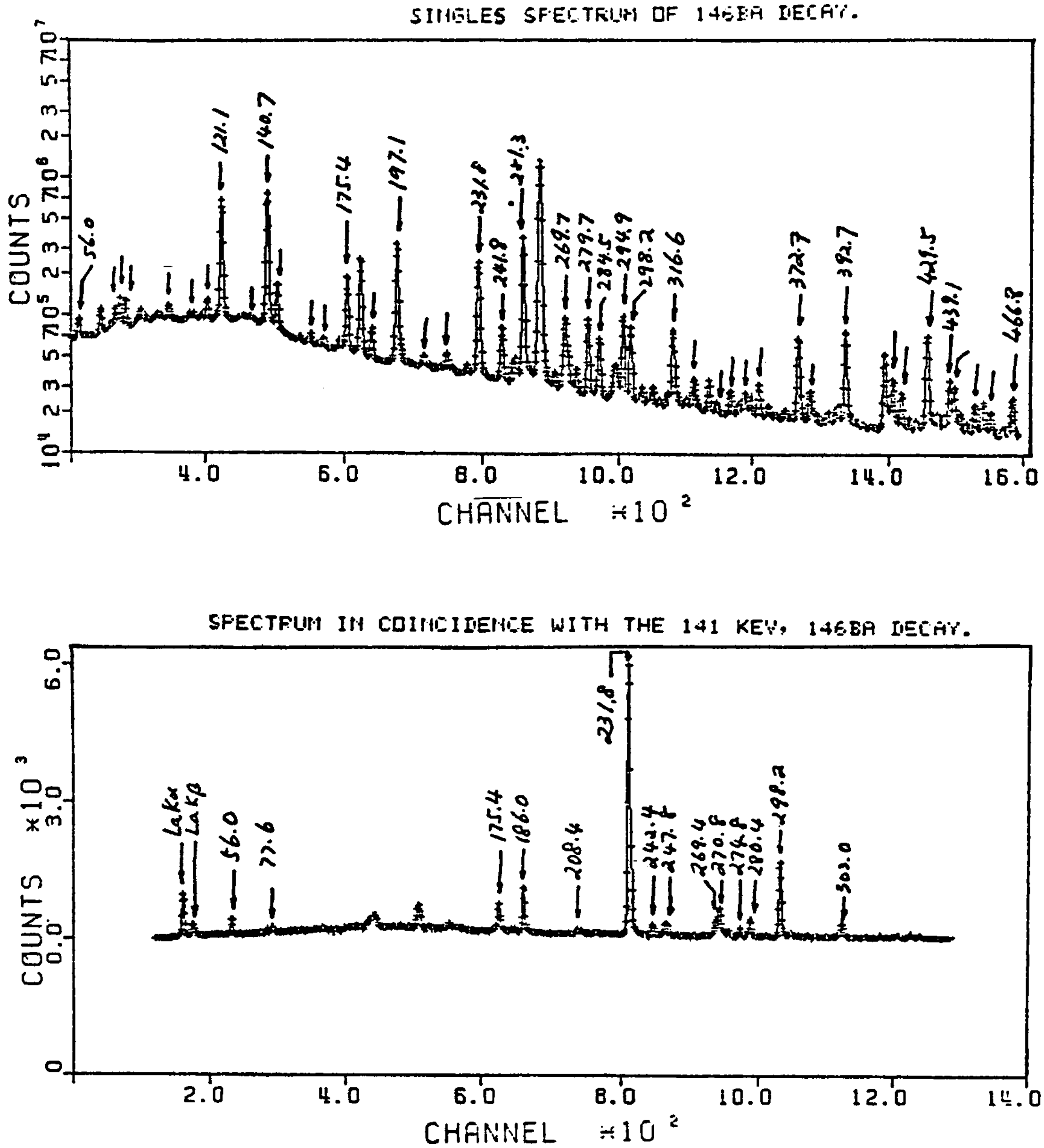

Figure C-8a. An example of singles and gamma-gamma coincidence spectra for ^{146}Ba decay.

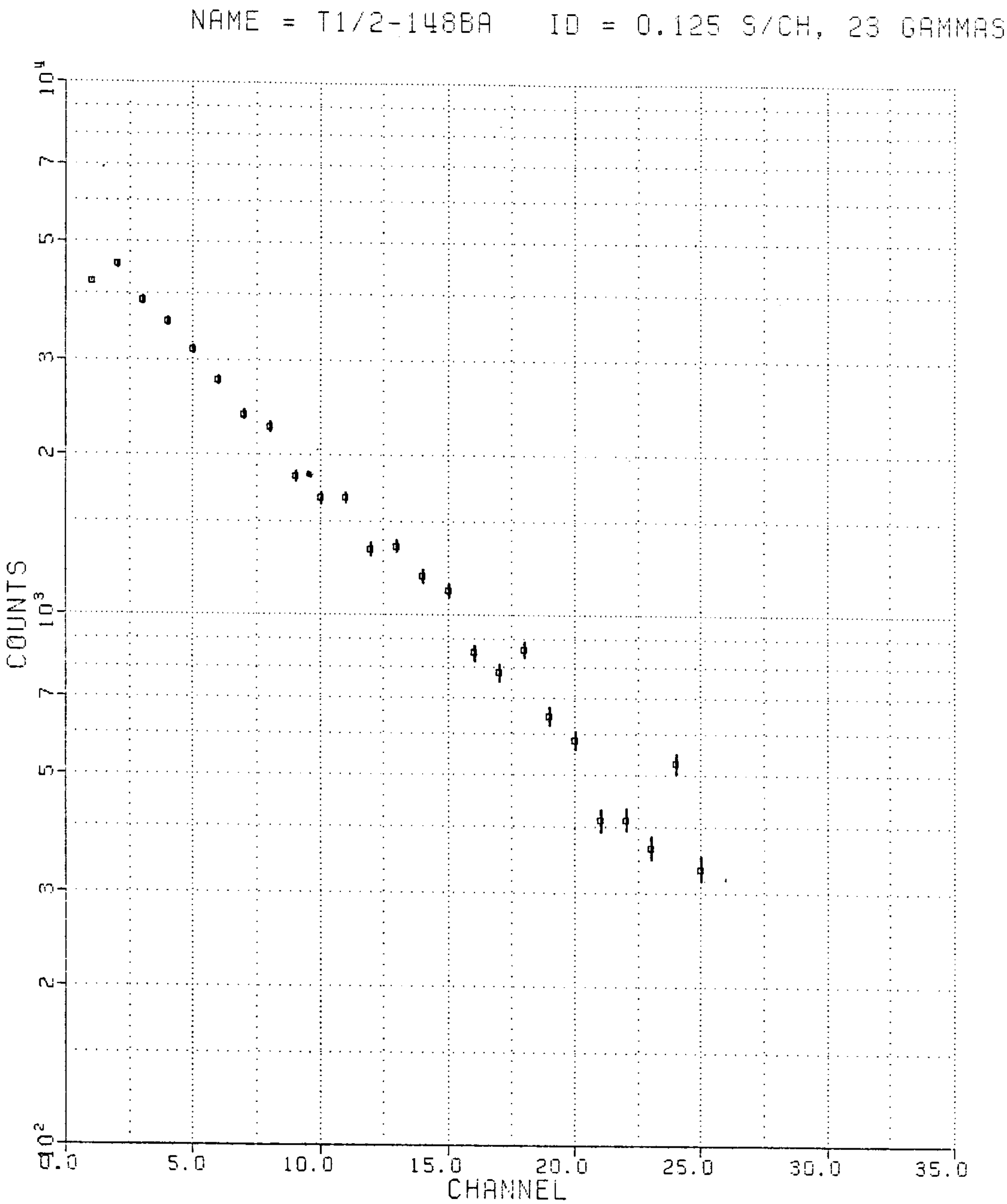

Figure C-8b. A multiscaler decay curve for ^{148}Ba. The measured half-life for ^{148}Ba is 0.64 $\pm$ 0.02 sec.

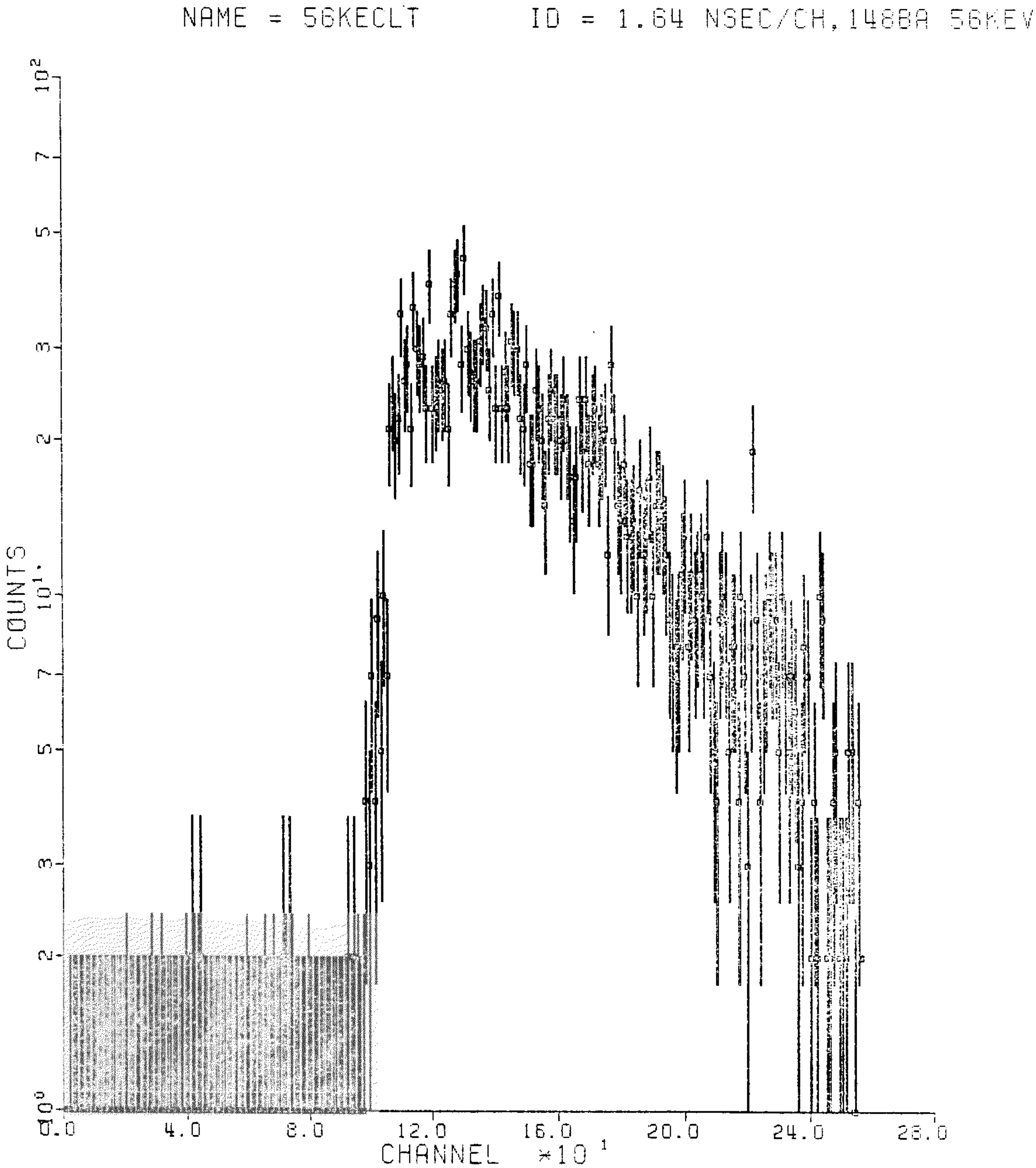

Figure C-8c. A lifetime measurement for the 56 keV level in ^{148}La populated by ^{148}Ba decay. The derived value is $T_{1/2}=90 \pm 12$ ns.

12. Studies of the Decay of ^{147}Cs and ^{147}Ba and a Reinvestigation of the Decay of ^{147}La

TRISTAN at BNL was used to study the decays of ^{147}Cs and ^{147}Ba. Singles, coincidences and multiscaling measurements were made. Half-lives were measured to improve our knowledge of lifetimes in this region. Several gamma rays previously assigned to the decay of ^{147}Cs were confirmed, and a number of ^{147}Ba gamma rays were newly established. A tentative decay scheme for ^{147}Ba is proposed. Measurements were also taken on ^{147}La decay and the deduced level scheme shows some differences from previously proposed schemes. (BNL/Oklahoma/LLNL)

At present, three graduate students are conducting research for their doctoral theses at TRISTAN and four post-doctoral fellows are broadening their training in nuclear science. Thus TRISTAN is proving to be an excellent resource for training the next generation of nuclear chemists and physicists. Additional students are expected to join our programs during the coming year.

TRISTAN users who have participated in TRISTAN experiments or development at BNL are the following:

In-house Staff: R. L. Gill, M. Shmid, H. I. Liou, M. L. Stelts, G. M. Gowdy,† and R. E. Chrien; Department of Chemistry, BNL, Y. Y. Chu.

Outside Users:

D. Brenner, M. Martel,* A. Aprahamian*	--Clark University
D. Rehfield	--McGill Univ./Vanier College
D. Clark, T. R. Yeh,† G. S. Goldhaber	--Cornell University
K. Sistemich, F. Wohn, H. Yamamoto, J. C. Hill	--Iowa State
R. Petry, H. Dejbakhsh*	--University of Oklahoma
P. Reeder, R. Warner	--Pacific Northwest Laboratory
W. Walters, C. Chung†	--University of Maryland
R. Meyer	--Lawrence Livermore National Laboratory
R. Greenwood, L. Johnson	--Idaho National Engineering Laboratory

*Signifies graduate student.
†Signifies postdoctoral fellow.

D. NATIONAL NUCLEAR DATA CENTER

1. Cross Section Evaluation Working Group (CSEWG) Activities

The report, Standard Reference and Other Important Nuclear Data, ENDF-300 (BNL-NCS-51123) was issued by the Cross Section Evaluation Working Group in December 1979. The report is a review of nuclear data of special interest intended to point out data discrepancies, recommend new measurements, and compare current versions of the Evaluated Nuclear Data File (ENDF/B) with measured data. Updates are in press for thorium-232 and uranium-238 capture, plutonium-239 decay heat, and the carbon total cross section (figure added).

A revision of the report, Data Formats and Procedures for the Evaluated Nuclear Data File, ENDF-102 (BNL-NCS-50496) dated October 1979, has been issued. This report is a manual for the data appearing in ENDF/B-V. A supplement to the report is available for users of ENDF/B-IV data.

The Committee structure of CSEWG has been revised into 3 main committees; Evaluations, Data Testing and Applications, and Evaluation Methods and Formats, that report to an Executive Committee comprised of the committee chairmen, other CSEWG members and representatives of funding agencies. Currently, the main CSEWG activities are the testing of ENDF/B-V and planning for ENDF/B-VI.

2. BNL-325, Volume I

The fourth edition of BNL-325, Volume I, Thermal Cross Sections and Resonance Parameters, has been completed for Z=1-60 and runs about 750 pages. The revised schedule calls for completing Volume I by early 1982. The work will include a simultaneous fit of the thermal cross sections of the fissile elements.

3. Nuclear Data Sheets

High priority has been given to the transfer of the responsibility for publication of Nuclear Data Sheets to NNDC. The year end cumulative issue of 1980 Recent References was prepared by NNDC. The NNDC will prepare level diagrams and decay data tables for publication starting July 1, 1981.

The U.S. is part of an international network of evaluators contributing recommended values of nuclear structure information to the Evaluated Nuclear Structure Reference File (ENSDF). Publication of Nuclear Data Sheets proceeds directly from this computerized file. In addition to the U.S., evaluations have been received or are anticipated from Germany, United Kingdom, U.S.S.R., France, Belgium, Kuwait, Sweden, and Canada. International meetings of the network evaluators are sponsored by the IAEA.

4. Meetings

A Symposium on Neutron Cross Sections from 10-50 MeV was held at BNL, May 2-14, 1980. It was attended by 96 scientists from the U.S. and abroad. The Proceedings were issued as BNL-NCS-51245.

A conference on Nuclear Data Evaluation Methods and Procedures attended by 61 scientists of which 14 were from outside the U.S. was held at BNL, September 22-25, 1980. The conference used a workshop format to critically review theoretical and semiempirical techniques used to evaluate data required by the nuclear research and the fission and fusion reactor communities. The Proceedings are in the final stage of preparation.

A two-day workshop on Thermal Reactor Benchmark Calculations, Techniques, Results, and Applications is planned at BNL for late 1981. The topics should include U-238 resonance capture, plutonium cross sections, fission products, thermal reference data, and fission spectra.

NNDC
Request Statistics
January 1, 1980 to December 31, 1980

1. Requests

a)	Number of persons requesting information	841
b)	Number of requests	4,602

2. Origin of Requests

a)	Government Agencies	203
b)	Educational Institutions	140
c)	Industry	191
d)	Foreign	307

A. NEUTRON CROSS SECTIONS

1. Total Non-elastic Cross Sections* (F.P. Brady, J.L. Romero, C.I. Zanelli, M.L. Johnson, G.A. Needham, J.L. Ullmann, P.P. Urone, and D.L. Johnson**)

We have developed a transmission technique to measure total non-elastic cross sections (σ_{non}) for neutron energies above about 15 MeV.[1] The method uses a well-collimated, nearly monoenergetic neutron beam and a neutron detector large enough to intercept both the beam and most of the neutrons elastically scattered by a thick slab of material. The latter is placed in the beam a short distance in front of the detector (fig. A-1). Optical models are used to obtain the shape of the mostly forward elastic scattering.

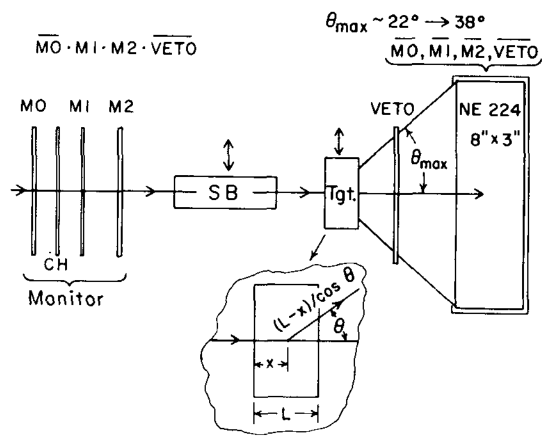

Figure A-1. Experimental setup to measure the non-elastic cross section.

---

* Supported by the National Science Foundation (Grants PHY 77-05301 and PHY 79-26282) and Department of Energy (Contract No. DE-AC 14 76FF02170)

** Westinghouse Hanford Company, Richland, WA

[1] Brady, Romero, Zanelli, Johnson, Needham, Ullmann, Urone, and Johnson, Nucl. Instr. and Meth. 178 (1980) 427

Table A-1 shows the results of measurements done at 40.3 and 50.4 MeV on C, O, Ca, and Fe. Total cross sections were measured separately.[2] [3] The method yields also a normalization factor η for the optical model elastic cross section. It is seen from Table A-1 that the results for σ_{non} are fairly insensitive to the optical model used.†

Table A-1. Values of η, σ_{el} (total elastic cross section) and σ_{non} (both in mb) determined for various OM potentials.

	σ_{tot}	OM set	η	$\eta\sigma_{el}^{OM}$	σ_{el} (weighted average)	σ_{non}
40.3 MeV						
C	1118 ± 1.3 a)	WSS	1.17 ± 0.04	764	762 ± 28	356 ± 28
		BH	0.96 ± 0.04	768		
		M	0.87 ± 0.03	754		
O	1398 ± 6.6 a)	WSS	1.36 ± 0.05	994	982 ± 35	416 ± 35
		BH	1.04 ± 0.04	972		
		M	0.97 ± 0.03	982		
Ca	2284 ± 59 b)	BG	1.08 ± 0.04	1322	1354 ± 53	930 ± 53
		M	0.97 ± 0.03	1387		
Fe	2461 ± 24 b)	BG	1.13 ± 0.03	1523	1552 ± 39	909 ± 39
		M	0.98 ± 0.02	1583		
50.4 MeV						
C	938 ± 3.0 a)	WSS	1.05 ± 0.05	582	594 ± 28	344 ± 28
		BH	0.86 ± 0.04	585		
		M	0.78 ± 0.04	619		
O	1208 ± 5.6 a)	WSS	1.25 ± 0.07	819	821 ± 45	387 ± 45
		BH	1.20 ± 0.06	832		
		M	0.91 ± 0.05	812		
Ca	2250 ± 70 b)	BG	1.08 ± 0.09	1400	1401 ± 112	849 ± 112
		M	0.99 ± 0.08	1401		
Fe	2431 ± 57 b)	BG	1.05 ± 0.03	1525	1532 ± 42	899 ± 42
		M	0.94 ± 0.02	1540		

(a) Ref. 2
(b) Ref. 3

---

[2] Auman, Brady, Jungerman, Knox, McGie, Montgomery, Phys. Rev. C5, (1972) 1.

[3] Zanelli, Brady, Romero, Castaneda, Johnson, (sec. A-2) to be published.

† See ref. 1 for the optical model sets referred to in Table A-1.

2. Total Cross Sections Measurements* (C.I. Zanelli, F.P. Brady, J.L. Romero, C.M. Castaneda and D.L. Johnson**)

Neutron total cross sections for Ca and Fe at 35.3, 40.3, and 50.4 have been measured using nearly mono-energetic neutron beams. The method used is essentially the same as that of ref. 2 except that all time-of-flight spectra were recorded for off-line analysis. The results are presented in Table A-2.

Table A-2. Experimental values for σ_{tot} in millibarns

Target	35.3 MeV	40.3 MeV	50.4 MeV
Ca	2307 ± 57	2284 ± 59	2250 ± 70
Fe	2435 ± 21	2481 ± 24	2431 ± 57

3. Kerma Values from Neutron-induced Charged Particle Measurements on C, N, and O.†† (T.S. Subramanian, J.L. Romero, F.P. Brady)

Continuum differential cross sections for neutron-induced reactions on light elements have been measured. The neutrons are produced via the $^{7}Li(p,n)$ reaction and the beam is collimated at 0° to deliver a flux of $\sim 10^5/cm^2/sec$ at the experimental area. Charged particles ranging from protons through alphas are detected with three-element charged-particle-detection telescopes.[4] The measurements were made at incident neutron energies of 27.4 MeV, 39.7 MeV, and 60.7 MeV and for wide angular range covering 15° through 150°.[4] We have integrated these cross sections over angle and particle energy to produce KERMA values for C, N, O, H, and tissue. Figure A-2 shows the results for carbon. No corrections have been included due to the (average) 4 MeV threshold for particle detection. The elastic recoil contribution to KERMA was obtained from optical model calculations. Efforts are underway to assess the missing (non-elastic) contribution due to heavier fragments using sum rules and available charge symmetric cross sections from proton-induced reactions. The measured KERMA values are compared in Fig. A-2 with various available theoretical predictions.

---

†† Supported by grant PHS CA-16261 from NCI, DHEW, and by U.S. NSF Grant PHY 71-03400, PHY 77-05301, and PHY 79-26282.

[4] T.S. Subramanian, J.L. Romero, and F.P. Brady, Nucl. Instr. and Meth. 174 (1980) 475; BNl-NCS-51245, Vol. 1, p. 331 (1980)

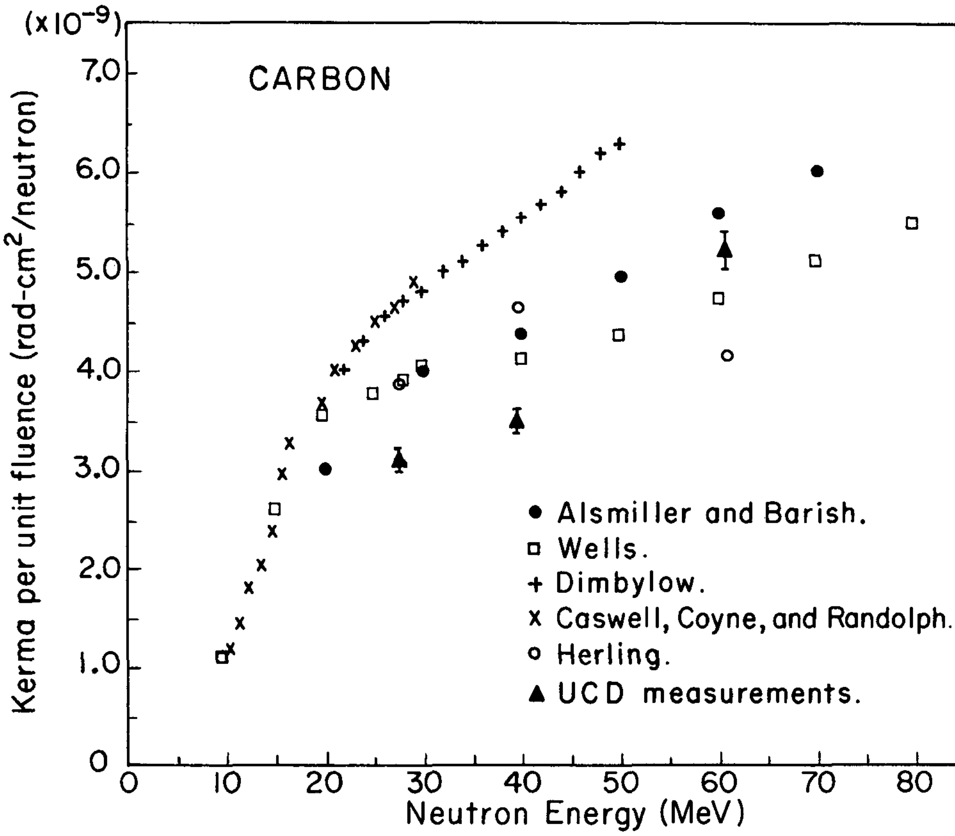

Figure A-2. Measured KERMA factors for Carbon as a function of neutron energy compared with various calculations. Our measurements do not include corrections due to detector thresholds or the effects of heavy particles.

A. NUCLEAR-STRUCTURE AND DECAY-DATA EVALUATION ACTIVITIES

1. Mass-chain Evaluation for the Nuclear Data Sheets (R. L. Bunting, M. A. Lee, C. W. Reich)

Through our participation in the International Nuclear-Structure and Decay-Data Evaluation Network, which has as its objective the establishment and maintenance of a four-year cycle time for the Nuclear Data Sheets, we have the responsibility for the ten mass chains in the region $153 \leq A \leq 162$. The work on A=158 has recently been published.[1] Mass-chain evaluations for A=157 and 153 have been completed. Work is currently in progress on the A=160 and 161 mass chains, the ones in our area of responsibility that are presently the most out of date.

2. Decay-data Evaluation for ENDF/B (C. W. Reich, R. L. Bunting)

As a part of our involvement in the work of the Cross Sections Evaluation Working Group (CSEWG), we have the primary responsibility within the U. S. for the preparation of sets of evaluated radioactive-nuclide decay data for inclusion in the Evaluated Nuclear Data File/B (ENDF/B). These evaluated decay data form a part of the nuclear data contained in the Fission-Product File, the Actinide File and the Activation File of ENDF/B, Version-V.

After the issuance of the ENDF/B-V Actinide File, containing decay-data evaluations for 60 nuclides, a request was made through CSEWG to expand the nuclide coverage of this file to include all the nuclides in the "important" actinide decay chains. This evaluation effort, which involved another 48 nuclides, is now completed. It is planned that these additional data will be issued in the form of a MOD to the ENDF/B-V Actinide File. The following list includes all the actinide and related isotopes for which ENDF/B decay-data evaluations have been done. (Isotopes underlined are to be included in the MOD to the ENDF/B-V Actinide File; revisions to the original Version-V Actinide File are indicated by a superscript 'r'.)

Hg:	$\underline{206}$
Tl:	$\underline{206}, \underline{207}, 208, \underline{209}, \underline{210}$
Pb:	$\underline{209}, \underline{210}, \underline{211}, 212, \underline{214}$
Bi:	$\underline{210}, \underline{211}, \underline{212}^{r}, \underline{213}, \underline{214}, \underline{215}$
Po:	$\underline{210}, \underline{211}, \underline{212}, \underline{213}, \underline{214}, \underline{215}, 216, \underline{218}$
At:	$\underline{215}, \underline{217}, \underline{218}, \underline{219}$
Rn:	$\underline{217}, \underline{218}, \underline{219}, 220, \underline{222}$
Fr:	$\underline{221}, \underline{223}$
Ra:	$\underline{223}, 224, \underline{225}, \underline{226}, \underline{228}$
Ac:	$\underline{225}, \underline{227}, \underline{228}$
Th:	$\underline{227}, 228, \underline{229}, 230, 231, 232, 233, \underline{234}$
Pa:	$231, 232, 233, \underline{234}, \underline{234m}$
U:	$232, 233, 234, 235, 236, 237, 238, 239, \underline{240}$
Np:	$236, 236m, 237, 238, 239, \underline{240}, \underline{240m}$
Pu:	$236, 237, 238, 239, 240, 241, 242, 243, \underline{244}^{r}, \underline{245}$
Am:	$240, 241, 242, 242m, 243, 244, 244m, \underline{245}$
Cm:	$241, 242, 243, 244, 245, 246, 247, \underline{248}^{r}, 249$
Bk:	$249, 250$
Cf:	$249, 250, 251, 252, 253$
Es:	253

[1] M. A. Lee, Nuclear Data Sheets 31, 381 (1980).

B. APPLICATIONS OF NUCLEAR-DECAY AND GAMMA-SPECTROSCOPIC DATA

1. Emission Probabilities of the Prominent Gamma-ray Transitions from the ^{240}Pu Decay (R. G. Helmer, C. W. Reich)

As a part of our laboratory involvement in the work of the IAEA Coordinated Research Program to measure and evaluate required nuclear decay data for selected transactinium isotopes, we are making precise (overall accuracy $\lesssim 1\%$) measurements of the emission probabilities (absolute intensities) of the prominent gamma-ray transitions from isotopes of U and Pu of particular importance for fission-reactor technology. As the first in this series of measurements, the emission probabilities of the three prominent gamma rays from the decay of ^{240}Pu have been measured. The gamma-ray emission rates were measured using calibrated Ge spectrometers. The decay-rate calibration was based on a measurement of the alpha-emission rate by NBS. Precise values for the gamma-ray energies were also measured. The following results were obtained: 45.244(2), 104.234(6), and 160.308(3) keV for the gamma-ray energies; and 43.9(9), 7.21(7) and 0.403(4) photons per 10^5 decays for the respective gamma-ray emission probabilities. A paper describing these measurements has been prepared for publication in the International Journal of Applied Radiation and Isotopes.

2. Gamma-ray Emission Probabilities for ^{141}La and ^{142}La (R. J. Gehrke)

Because the chain yields for masses 141 and 142 are high for the thermal neutron fission of ^{235}U (i.e., 4.82% and 5.87%, respectively), the gamma-ray emission probabilities of ^{141}La and ^{142}La are important in a number of reactor-related applications. The emission probability of the most intense gamma ray in the decay of ^{141}La (at 1354 keV) is not well established and, in fact, no direct measurement has been reported. The presently accepted value for the ^{141}La 1354-keV gamma ray, approximately 2.63 gamma rays per 100 decays,[1] is based on the β^- intensity measurements of Duffield and Langer[2] and Schuman *et al.*[3] The only direct measurement of the ^{142}La 641-keV gamma-ray emission probability is that reported by Tong *et al.*[4] This value, (52.5 ± 2.5) gamma rays per 100 decays, is the value recommended by the Nuclear Data Sheets.[5] Based on the β^- intensity measurements of Prestwich and Kennett[6]

---

[1] J. K. Tuli, Nuclear Data Sheets 23, 529 (1978).

[2] R. B. Duffield and L. M. Langer, Phys. Rev. 84, 1065 (1951).

[3] R. P. Schuman, E. H. Turk and R. L. Heath, Phys. Rev. 115, 195 (1959).

[4] S. L. Tong, W. V. Prestwich and K. Fritze, Can. J. of Phys. 49, 1179 (1971).

[5] J. K. Tuli, Nuclear Data Sheets, 25, 53 (1978).

[6] W. V. Prestwich and T. J. Kennett, Phys. Rev. 134, B485 (1964).

and the ^{141}Ce level scheme reported in Ref. 1, the 641-keV gamma-ray emission probability is deduced by the Table of Isotopes[2] to be (49$\pm$3) gamma rays per 100 decays.

In order to obtain precise values (approximately 1% uncertainty at the 1σ level) for the gamma-ray emission probabilities of ^{141}La and ^{142}La, we have undertaken to measure the emission probabilities of the 1354-keV gamma ray from ^{141}La and the 641-keV gamma ray from ^{142}La. The half-lives of these isotopes were also remeasured during this study to permit accurate decay corrections. These measurements may also be of value to those who expressed the need for more precise gamma-ray data for these fission products in a survey carried out by the International Committee for Radionuclide Metrology (ICRM).[3]

As a result of the present investigation, the emission probabilities of the 1354-keV gamma ray emitted in the decay of ^{141}La and the 641-keV gamma ray emitted in the decay of ^{142}La have been measured to be (1.643$\pm$0.021) and (47.4$\pm$0.5) gamma rays per 100 decays, respectively. The half-lives were measured to be (3.92$\pm$0.03) h for ^{141}La and (91.1$\pm$0.5) min for ^{142}La.

3. Recommended Standards for Gamma-ray Energy Calibration (1979)[4]
(R. G. Helmer, P. H. M. van Assche,[5] C. van der Leun[6])

In 1972, the Commission on Atomic Masses and Fundamental Constants of the International Union of Pure and Applied Physics appointed a committee to recommend a set of consistent and well-measured gamma-ray energies for use in the energy calibration of gamma-ray spectra, especially for Ge(Li) and Ge detectors. The committee delayed its report until new measurements of a few absolute gamma-ray wavelengths, and hence energies, were completed at the NBS. The committee report has now been published and the abstract follows.

A consistent set of gamma-ray energies, all with uncertainties of at most 10 ppm, is recommended for use in the energy calibration of gamma-ray spectra.

---

[1] J. T. Larsen, W. L. Talbert, Jr., and J. R. McConnell, Phys. Rev. C 3, 1372 (1971).

[2] C. M. Lederer and V. S. Shirley, Eds. Table of Isotopes, Seventh Edition, John Wiley and Sons, Inc., New York (1978).

[3] W. Bambynek, International Committee for Radionuclide Metrology (ICRM), Non-Neutron Nuclear Data Request List, CBNM/RN/47, June, 1979 (private communication).

[4] R. G. Helmer, P. H. M. van Assche and C. van der Leun, Atomic Data and Nuclear Data Tables 24, 39 (1979).

[5] SCK-CEN, Nuclear Energy Centre, Mol, Belgium.

[6] Fysisch Laboratorium, Rijksuniversiteit, Princetonplein 5, 3508 TA Utrecht, The Netherlands; Task group chairman.

Almost all gamma rays listed are from commercially available sources. The half-lives of the isotopes selected are generally at least 30 days. The gamma-ray energies, in the range E_γ=60-6100 keV, are all based on the value of 411 804.4$\pm$1.1 eV for the gamma-ray from the decay of ^{198}Au. The energy of the 6129-keV line in ^{16}O, which is the gamma-ray with the highest energy of the present set, has also been measured relative to another standard; the two values are consistent.

4. Analytical Functions for Fitting Peaks from Ge Semiconductor Detectors[1] (R. G. Helmer, M. A. Lee)

For the analysis of gamma-ray peaks from Ge(Li) and Ge detectors to obtain the precise intensities or to decompose multiple peaks, it would be advantageous to fit the peaks with an analytical function that includes a representation of the low-energy tail on these peaks. To aid in the determination of what function would be most useful, a comparison of the quality-of-fit to gamma-ray peaks has been made for several analytical functions. The data are for 1332-keV peaks measured on three Ge(Li) and Ge detectors with volumes of about 13, 65 and 120 cm^3. The analytical functions tested, most previously proposed, have 0, 1 or 2 additive components to represent the low-energy tailing. Since none of the functions represents the physical processes in the detection system, these analyses yield the expected result that, in general, the functions with the most parameters give the best fits. The variation of the peak areas with some of the parameters of the tailing function is investigated.

5. Delayed Neutron Spectral Measurements (R. C. Greenwood, L. O. Johnson)

A new effort has been initiated to measure the energy spectra of delayed neutrons from individual fission-product isotopes using the TRISTAN on-line mass separator at BNL. Gas-filled proton recoil detectors are being used in these experiments, with the emphasis of the measurements being on the low-energy spectral region from a few keV up to approximately 300 keV. In the first series of measurements, delayed neutron spectra were obtained for ^{93}Rb, ^{94}Rb and ^{95}Rb.

C. NUCLEAR LEVEL-SCHEMES STUDIES

1. Levels in ^{157}Gd from the Decay of ^{157}Eu (R. C. Greenwood)

Studies of the decay of 15-hr ^{157}Eu are continuing. Based on the analysis of the gamma-gamma coincidence data, some 75 gamma-ray transitions associated with this decay have been placed into a level scheme for ^{157}Gd containing 24 excited states up to an excitation energy of 1231 keV. Additional gamma-ray spectral measurements have been made using high-purity samples of ^{157}Eu. These sources were obtained by chemical and mass separation of gross fission-

[1] R. G. Helmer and M. A. Lee, Nucl. Instr. and Meth. 178, 499 (1980).

product samples obtained by direct collection following gas-jet transport from our two recently acquired "open" 300-μg ^{252}Cf spontaneous-fission sources.

2. The Neutron Separation Energy for ^{153}Gd (R. C. Greenwood)

For some time now there has been unresolved a discrepancy in the mass systematics in the region of ^{153}Gd and ^{154}Gd. This involves the measured Q values for the $^{152}Gd(d,p)^{153}Gd$ and $^{154}Gd(d,t)^{153}Gd$ reactions and the decay energy derived for the EC decay of ^{153}Gd from measurement of the K-capture probability.[1,2] The magnitude of this discrepancy is such that the $S_n(^{153}Gd)$ value derived from the reaction and electron-capture decay differ by 242±5 keV. In recent work using the Sc filtered beam at HFBR we have measured the spectrum of prompt gamma rays resulting from 2-keV neutron capture in ^{152}Gd and have deduced the value $S_n(^{153}Gd) = 6247.0 \pm 0.7$ keV. This value confirms that it is the reaction-energy values which are correct, since it is in good agreement with the earlier value of $S_n(^{153}Gd) = 6240 \pm 10$ keV derived from the $^{152}Gd(d,p)$ reaction. This also confirms the choice, adopted in Ref. 2, of the reaction data over the decay data as the source of the Q value for the EC decay of ^{153}Gd.

3. Level Structure of ^{174}Yb from the $^{173}Yb(n,\gamma)$ Reaction[3] (R. C. Greenwood, C. W. Reich)

The level structure of ^{174}Yb has been studied using the $^{173}Yb(n,\gamma)$ reaction with both thermal and 2-keV neutrons. Measurements of gamma-ray energies and intensities were made using Ge(Li) detectors. From these data a neutron separation energy of 7464.8±0.5 keV has been determined for ^{174}Yb. A level scheme is proposed for ^{174}Yb which containes 47 excited states, with identified de-excitation modes, below 2.35 MeV. Features of the proposed level scheme include: the $K^\pi=2^-$, 0^- and 3^- octupole-vibrational bands with band-head energies of 1318, 1710 and 1851 keV, respectively; the gamma-vibrational band at 1634 keV; three excited $K^\pi=0^+$ bands with band-head energies of 1487, 1885 and 2100 keV; and, several two-quasiparticle bands with band-head energies in keV (and K^π assignments) of $1606(3^+)$, $1624(1^+)$, $2016(3^+)$ and $2049(3^-)$. Configuration assignments for these two-quasiparticle bands are discussed. The available data for the $K^\pi= 3^+$ band at 1606 keV are not inconsistent with the assumption that it has collective character; and it is suggested that it, together with the lowest-lying 3^+ band in ^{172}Yb (at 1172 keV), might represent, in the framework of the Interacting Boson Approximation model, examples of g-boson excitations.

D. SHORT-LIVED FISSION-PRODUCT STUDIES UTILIZING He-JET TRANSPORT AND ^{252}Cf SOURCES

---

[1] A. H. Wapstra and K. Bos, At. Data and Nucl. Data Tables 20, 1 (1977).

[2] L. A. Kroger and C. W. Reich, Nuclear Data Sheets 10, 429 (1973).

[3] R. C. Greenwood and C. W. Reich, Physical Review C 23, 153 (1981).

1. Rapid Separation of Individual Rare-Earth Elements from Fission Products[1] (J. D. Baker, D. H. Meikrantz, R. J. Gehrke, R. C. Greenwood)

The rare-earth isotopes far from beta stability are presently of particular interest in the study of nuclear structure. For the most part the only neutron-rich rare-earth isotopes presently identified for $Z \geq 60$ are those which are only 2-3 mass units greater than the highest stable isotope of each element. To permit the identification and study of additional higher-mass isotopes of each element, we have developed a microprocessor-controlled radiochemical separation system to rapidly separate rare-earth elements from mixed fission products. The system is composed of two high performance liquid chromatography columns coupled in series by a stream-splitting injection valve. The first column separates the rare-earth group by extraction chromatography using dihexyldiethylcarbamylmethylenephosphonate (DHDECMP) adsorbed on Vydac C_8 resin. The second column isolates the individual rare-earth elements by cation exchange using Aminex A-9 resin with α-hydroxyisobutyric acid (α-HIBA) as the eluent. With this system, fission-product rare-earth isotopes with half-lives as short as approximately three minutes have been studied.

2. He-Jet Coupled On-Line Mass Separator (R. C. Greenwood, R. A. Anderl, V. J. Novick)

A significant effort has been made to test and optimize the production of fission-product ion beams for a Sidenius hollow-cathode ion source coupled to the He-gas jet transport system by means of a double flat-plate skimmer arrangement. A 7-μg ^{252}Cf source was used as the source of fission products in these tests. Gamma-ray spectral measurements with a Ge(Li) detector of the activity deposited on an ion-beam collector relative to that deposited on a pre-skimmer collector were used to obtain estimates of the ion-beam separation efficiencies for the different fission-product elemental species. Typical ion-source separation efficiencies, using NaCl transport aerosols, are shown in Table D-1. The use of CCl_4 as a support gas resulted in significant enhancement of the alkaline-earth and rare-earth ion-source separation efficiencies, as illustrated in Table D-2. The current emphasis of this work is on the coupling of the present He-jet coupled Sidenius ion source onto the INEL mass separator.

E. INTEGRAL REACTION-RATE AND CROSS-SECTION MEASUREMENTS

1. Capture and Fission Cross Sections for Actinides (R. A. Anderl)

In progress are measurements of the integral cross sections important to the production and depletion of plutonium, americium and curium in advanced

[1] J. D. Baker, R. J. Gehrke, R. C. Greenwood and D. H. Meikrantz, to be published in Radiochimica Acta, Vol. 28.

Table D-1. Absolute elemental separation efficiencies for He-jet-coupled ion source operated with Ta and Mo anodes, Ar and CCl_4 support gas and NaCl aerosols.

Element Separated	Ta Anode Ar[a]	Ta Anode CCl_4[b]	Mo Anode Ar-1[c]	Mo Anode Ar-2[d]	Mo Anode CCl_4[e]
Sr	0.5	0.8	0.1	0.6	0.3
Sr/Y	0.9	1.4	---	---	1.0
Mo/Tc	0.4	0.3	0.2	0.4	0.2
Te	0.6	1.0	0.5	0.5	1.2
Cs	4.0	3.0	2.5	2.5	1.5
Ba	0.9	1.9	0.3	0.6	1.7
Ce	0.5	1.5	0.2	0.4	1.2
Ce/Pr	0.5	1.6	0.2	0.5	1.4
Pr	0.9	1.0	0.1	0.2	0.9
Nd	0.5	1.1	0.2	0.6	1.6
Sm	0.8	1.9	---	---	1.5

[a]Arc power of 150 watts

[b]Arc power of 130 watts

[c]Arc power of 60 watts

[d]Arc power of 170 watts

[e]Arc power of 70 watts

Table D-2. Chemical enhancement of the He-jet-coupled ion source separation efficiencies by use of CCl_4 support gas as compared to use of Ar support gas.

Element Separated	Enhancement factor - CCl_4:Ar Ta Anode[a]	Enhancement factor - CCl_4:Ar Mo Anode[b]
Sr	>1	3
Te	2	2
Ba	2	6
Ce	3	6
Ce/Pr	3	7
Pr	>1	9
Nd	2	8
Sm	2	>5

[a]Arc power of 125-150 watts

[b]Arc power of 60-70 watts

reactor systems. Measurements are made for samples irradiated in the fast neutron field of the Coupled Fast Reactivity Measurements Facility (CFRMF) operated at a power level of 100 kW and an integral flux of 8.7×10^{11} n/cm^2-sec. These measurements are used primarily for integral testing of the capture and fission cross-section data in ENDF/B.

In FY-1980, the experimental work was completed for the determination of the production cross sections of ^{242}Cm and ^{244}Cm from neutron capture in ^{241}Am and ^{243}Am, respectively. The work required extensive quantitative chemical separations and isotope dilution alpha spectrometry. The analysis of these experiments is in progress. Partial cross sections and isomer ratios will be obtained by combining the results of those experiments with earlier radiometric experiments based on gamma spectrometry.

To be initiated in FY-1981 are fission chamber measurements for ^{241}Am, ^{243}Am and ^{242}Pu irradiated in the fast neutron field of the CFRMF. The results of these experiments, combined with earlier radiometric experiments which employed gamma spectrometry, will permit the determination of fast fission yields for important long-lived fission products produced by fast fission in ^{241}Am, ^{243}Am and ^{242}Pu.

2. <u>Capture Cross Sections for Fission Products</u> (R. A. Anderl, Y. D. Harker)

Our program to provide integral cross sections of interest to the development of fast reactor systems has included measurements in the CFRMF and in EBR-II. These data are used primarily for integral testing of the capture and fission cross sections in ENDF/B.

Integral testing of the capture cross sections for approximately 40 fission-product isotopes in ENDF/B-V was initiated in FY-1980 and is nearing completion. Based on preliminary results of these analyses and on the recommendations of the NEANDC Specialist's Meeting on Neutron Cross Sections of Fission-Product Nuclei (1979), experiments are planned for remeasuring the integral cross sections in CFRMF for ^{99}Tc, ^{103}Rh, ^{104}Ru, ^{109}Ag, ^{127}I, and ^{147}Pm.

3. <u>Dosimetry Cross Sections for Fusion Applications</u> (F. Y. Tsang, Y. D. Harker, V. J. Novick)

A program is underway to evaluate the use of passive neutron dosimetry for characterizing the neutron fields inside fusion-blanket assemblies. This effort entails the measurement of integral reaction rates for selected dosimetry materials irradiated in a lead assembly placed around the target region of a 14-MeV neutron generator. To date, measurements have been made for ^{27}Al(n,α), ^{59}Co(n,α), ^{197}Au(n,γ), ^{48}Ti(n,p), ^{56}Fe(n,p), ^{58}Ni(n,2n), ^{115}In(n,n'), ^{115}In(n,γ), ^{55}Mn(n,γ), ^{64}Zn(n,p), and ^{24}Mg(n,p). Integral tests of the cross sections and spectrum-unfolding analyses are then made to evaluate both the adequacy of the cross sections and their use as passive dosimeters. Preliminary results of this work have been reported.[1]

F. THE ^{252}Cf $\bar{\nu}$ PROBLEM

1. Determination of $\bar{\nu}$ for ^{252}Cf (J. R. Smith, S. D. Reeder (ENICO), R. J. Gehrke)

The manganese bath measurement of the average number of neutrons per fission ($\bar{\nu}$) for ^{252}Cf has been completed. A value of 3.764 ± 0.014 neutrons per fission was reported at the ANS Annual Meeting at Washington, D. C., November 17-21, 1980. The traditional capture cross section for sulfur, 0.52 ± 0.03 b, was used in the analysis of the manganese bath data. The sulfur cross section value continues to represent the largest single uncertainty associated with the measurement. A detailed report on this work is being prepared for publication.

[1] F. Y. Tsang, Y. D. Harker, D. W. Nigg, R. C. Greenwood, J W Rogers, V. J. Novick, "Low-Neutron-Fluence Fusion-Blanket Dosimetry Experiment", paper presented at the Fourth ANS Topical Meeting on the Technology of Controlled Fusion, Oct. 14-17, 1980, King of Prussia, PA.

A. DECAY STUDIES OF GASEOUS FISSION PRODUCTS WITH TRISTAN I

The TRISTAN I on-line mass separator facility at the Ames Laboratory was used until mid 1976 to study gaseous fission products and their daughters. Most of this work has been published and presented in past contributions to the Nuclear Data Committee.

1. Decays of Mass-Separated ^{139}Xe and ^{139}Cs (M. A. Lee and W. L. Talbert, Jr.)

For the ^{139}Xe decay, 230 γ rays were observed, of which 213 were placed in a ^{139}Cs level scheme with 55 levels. For the ^{139}Cs decay, 179 γ rays were observed, of which 167 were placed in a ^{139}Ba level scheme with 59 levels. Q_β values, determined from β-γ coincidences, have been reported previously.[1] Ground-state β branches of 21±9% and 83±7% for the decays of ^{139}Xe and ^{139}Cs, respectively, were determined from equilibrium γ spectra of ^{139}Xe, ^{139}Cs, and ^{139}Ba. Absolute γ intensities, β branches and log ft values were deduced for all β and γ transitions in the decays of ^{139}Xe and ^{139}Cs. This work, which has been published,[2] updates the preliminary results reported in the 1974 revision[3] of the A=139 mass chain.

2. Decay of ^{90}Rb^g and ^{90}Rb^m (W. L. Talbert, Jr., F. K. Wohn, L. J. Alquist, and C. L. Duke)

Decay schemes for ^{90}Rb^g and ^{90}Rb^m to levels in ^{90}Sr have been deduced from γ spectroscopic studies. (Q_β values were previously reported.[1]) Of the 161 γ rays observed, all but 12 were placed in the two decay schemes, with 83 γ rays placed in 33 levels for the ^{90}Rb^g decay and 108 γ rays placed in 43 levels for the ^{90}Rb^m decay. (42 γ rays are common to both decays.) A ground-state β branch of 53±5% was deduced for the decay of 0^- ^{90}Rb^g. This study indicates that 13.8±0.8% of ^{90}Kr decays populate ^{90}Rb^m, in excellent agreement with the 13.0±0.9% result[4] from our ^{90}Kr decay study.

---

[1] F. K. Wohn and W. L. Talbert, Jr., Phys. Rev. C18, 2328 (1978).

[2] Lee and Talbert, Phys. Rev. C21, 328 (1980).

[3] L. R. Greenwood, Nucl. Data Sheets 12, 139 (1974).

[4] Duke, Talbert, Wohn, Halbig, and Nielsen, Phys. Rev. C19, 2322 (1979).

3. Structures of Neutron-Rich Even-Even Cd Nuclei II-Decay of $^{120}Ag^g$ and $^{120}Ag^m$ (T. K. Li, J. C. Hill, and C. M. McCullagh

The decays of $^{120}Ag^g$ and $^{120}Ag^m$ were studied by γ spectroscopy. Half-lives of 1.36±0.04 s for $^{120}Ag^g$ and 0.32±0.02 s for $^{120}Ag^m$ were determined by γ spectrum multiscaling. 50 of the 58 observed γ rays were placed in a ^{120}Cd level scheme involving 19 levels. J^π values of 3^+ and 6^- were tentatively deduced for $^{120}Ag^g$ and $^{120}Ag^m$, respectively, which implies a zero ground state β branch for both decays. Since Q_β has not been measured, an assumed value of 8.35 MeV from the Garvey-Kelson relations was used in calculating log ft values. Absolute γ intensities, β branches, and log ft values were deduced for both the $^{120}Ag^g$ and $^{120}Ag^m$ decays. This work has been submitted to Phys. Rev. C.

C. DECAY STUDIES OF NON-GASEOUS FISSION PRODUCTS WITH TRISTAN (BNL)

The TRISTAN facility became operational at the High Flux Beam Reactor at BNL in 1980. Using an integral target and surface-ionization source, the first experiments were done in late 1980 on Rb, Sr, Cs, and Ba fission products and their daughters. These initial experiments were done by varior teams of TRISTAN users from BNL(6), Ames Laboratory (4), PNL(2), LLL(1), Clark U.(1), U. of Maryland(2), U. of Oklahoma(1), and Cornell U.(2). (The numbers in parentheses are the number of scientists involved at each institution.) Members of the Ames Laboratory group (Hill, Wohn, K. Sistemich and H. Yamamoto) participated in data accumulation and/or data analysis of decay studies of the following Cs, Ba and daughter isotopes: ^{141}Cs, ^{146}Ba, ^{148}Ba, ^{142}La, ^{144}La, ^{146}La, ^{148}La, ^{148}Pr. We have concentrated in particular on the decays of ^{148}La, ^{146}La, and ^{141}Cs.

The initial measurements in late 1980 consisted of γ singles, γ spectrum multiscaling, β multiscaling, γ-γ coincidences, and γ-γ angular correlations (for 0-2-0 cascades). Additional measurements of these types were also made in January and February 1981. Although much new information has been gained to date on the decay properties and level structure of these nuclei (only scanty data, if any, existed prior to our studies for some), further measurements may be needed to complete these studies. Thus it would be premature in the present report to the Nuclear Data Committee to present tabular data. We anticipate providing more detailed information in the next report.

In addition to the γ spectroscopic studies mentioned above, Dr. Wohn is working with Dr. D. S. Brenner of Clark University on a project to measure Q_β values. A Ge(Hp) detector with a thin window and with known β response function is used either in singles or in coincidence with a Ge γ detector to measure β end-point energies with a precision of better than 0.1 MeV. In late 1980 data were obtained and analyzed for well-known cases such as ^{88}Rb and ^{141}Cs as test cases. Data for more neutron-rich Rb and Cs nuclides has been taken and is currently being analyzed.

Absolute γ intensities, β branches, and log ft values were deduced for all β and γ transitions in the decays of $^{90}Rb^{g}$ and $^{90}Rb^{m}$. This work, which has been accepted for publication in Phys. Rev. C, updates the preliminary results reported in the 1975 revision[5] of the A=90 mass chain.

B. DECAY STUDIES OF NON-GASEOUS FISSION PRODUCTS WITH TRISTAN II (AMES).

The TRISTAN II facility,[6] with a new integrated target and ion source, became operational in late 1976 and made available 14 fission-product elements. It was used to study neutron-rich isotopes of Zn, Ga, Ag, Cd, and In until the Ames Laboratory Research Reactor was shut down at the end of 1977. Decay studies of ^{122}Ag, ^{126}Cd, $^{126}In^{g}$, and $^{126}In^{m}$ have been reported to the Nuclear Data Committee. Studies on ^{78}Zn, ^{78}Ga, $^{120}Ag^{g}$, and $^{120}Ag^{m}$ are summarized below.

1. Decay of Mass-Separated ^{78}Zn (F. K. Wohn, J. C. Hill, and D. A. Lewis)

The half-life of ^{78}Zn was determined to be 1.47±0.15 s by γ spectrum multiscaling. 57 γ rays were placed in a level scheme for ^{78}Ga with 19 levels up to 3.5 MeV. This work is the first detailed study of levels in odd-odd ^{78}Ga, for which we tentatively assign a 3^+ ground state. Absolute γ intensities, β branches and log ft values were deduced. This work has been published.[7]

2. Decay of Mass-Separated ^{78}Ga to Levels in Even-Even ^{78}Ge (D. A. Lewis, J. C. Hill, F. K. Wohn, and M. L. Gartner)

The half-life of ^{78}Ga was determined to be 5.49±0.25 s by γ multiscaling. 45 γ rays were placed in a ^{78}Ge level scheme including 19 levels up to 5.1 MeV. Using our level scheme and the β-γ coincidence measurements of Aleklett et al.,[8] a Q_β value of 7.89±0.16 MeV was deduced. Absolute γ intensities, β branches and log ft values were deduced. This work has been published.[9]

---

[5] D. C. Kocher, Nucl. Data Sheets 16, 55 (1975).

[6] Talbert, Wohn, Hill, Landin, Cullison, and Gill, Nucl. Instrum. Meth. 161, 431 (1979).

[7] Wohn, Hill, and Lewis, Phys. Rev. C. 22, 2547 (1980).

[8] Aleklett, Lund, Nyman, and Rudstam, Nucl. Phys. A285, 1 (1977).

[9] Lewis, Hill, Wohn, and Gartner, Phys. Rev. C22, 2178 (1980).

LAWRENCE BERKELEY LABORATORY

A. ISOTOPES PROJECT (E. Browne, J.M. Dairiki, R.B. Firestone, C.M. Lederer, and V.S. Shirley)

The Isotopes Project compiles and evaluates nuclear structure and decay data and develops compilation methodology. The evaluation efforts are coordinated with those of other data centers via national and international networks. The Project has responsibility for 39 mass chains in the regions A = 146-152 and A = 163-194. All evaluated data are entered into the international Evaluated Nuclear Structure Data File (ENSDF) and are published in Nuclear Data Sheets.

During the past year mass-chain evaluations for A = 163 and A = 191 have been published. The A = 193 and A = 188 evaluations have been reviewed and are ready for publication. Three additional mass-chain evaluations (A = 185, 189, and 190) have been completed and submitted for review. Presently being evaluated are data on the A = 169, 181, 187 and 192 mass chains.

In addition to the evaluation effort, the Isotopes Project will produce, on behalf of the U.S. Nuclear Data Network (NDN), a Radioactivity Handbook for applied users. The purpose of the Handbook is to provide a compilation of recommended decay data that is detailed enough for use in sophisticated applications but that is organized clearly so as to be usable in simple routine applications. Recommended decay data will be taken from the current version of ENSDF, with no further updating. Additional calculations and evaluation will be done to provide recommended data on atomic radiations and conversion electrons. Each mass chain will be referenced to the most recent evaluation in Nuclear Data Sheets, as the source for further details and references to the original papers.

Nearly 5000 copies of a Handbook sample and a survey requesting specific comments and feedback were distributed to members of professional societies and other data centers. The 800 surveys completed, in general, indicate satisfaction with the planned Handbook.

The computer codes needed to produce the Handbook from ENSDF are being developed. As a first step, a program to establish the parent-daughter links and to check the data for completeness and consistency has been completed. Work is progressing on the next step which involves modification of the data in ENSDF so that each decay set will contain the "best" values for γ-ray and level properties, independent of the decay parent. At the same time work is proceeding on the program to output the data in publication formats. The existing level-scheme graphics program (used for the Table of Isotopes) is being modified to handle data in ENSDF formats. Subroutines and tables (e.g., conversion coefficients and binding energies) required for the tabular data listings are being assembled.

B. THE SuperHILAC ON-LINE ISOTOPE SEPARATOR (J.M. Nitschke)

In the interaction of two heavy ions, many different elements and dozens of isotopes can be produced simultaneously. To study the decay properties of individual species, therefore, some form of separation is necessary. The study of short-lived isotopes, in particular, favors the choice of an electromagnetic separator over traditional chemical separation methods. For this reason an on-line isotope separator system has been constructed and tested at the SuperHILAC.

The separator consists of an ion source to ionize the reaction products after they are stopped in hot Ta (2600° C), an extraction and focusing system, and a 180°, $n = 1/2$ analyzing magnet. Thus far, two different types of ion sources have been employed, a surface ionization and a plasma source. The former source works very well in the actinide region since ionization efficiencies for rare earth and actinide elements can be as high as 10% at the source operating temperature. In on-line tests using ^{20}Ne beams on targets of Ce, Pr, Nd, Ir, Pt and Au, observed overall efficiencies (target to focal plane) for various products were: Fr (12%), Ac (3%) and rare earths (∿2%). The plasma ion source is of more recent design and has been used to separate Se and As isotopes. Cross contamination from adjacent masses is negligible in the separator since a mass resolution $M/\Delta M$ of about 2000 has been achieved.

From present results it can be extrapolated that more than 80% of all elements of the periodic table can be investigated with the on-line isotope separator. Thus, this instrument is a universal tool for the study of nuclear properties far from the line of beta stability.

C. ISOTOPES* (C.M. Lederer)

Ordinary matter consists of the 286 isotopes of 83 elements that are stable or long-lived compared to the age of the earth. For most polyisotopic elements, the relative abundances of the isotopes are remarkably constant. Isotopes are usually assayed by mass spectrometry.

Of many isotope-separation methods that have been developed, two (electromagnetic and thermal diffusion) are used commonly to produce small quantities of many isotopes for research purposes, and two others (the GS chemical-exchange process for hydrogen, gaseous diffusion for uranium) are used on an industrial scale. The large-scale use of gas centrifuges for uranium is imminent, and laser separation methods appear promising for uranium, deuterium, and expanded-scale production of research materials.

---

* Abstract of a review article to be published in Encyclopedia of Chemical Technology, 3rd ed., edited by David Eckroth, John Wiley and Sons, New York (1981). The article includes 6 tables, 5 figures, and 95 references. A longer version, from which the published article was condensed, is contained in LBL-10124.

In addition to the applications of ^{235}U and deuterium in nuclear energy, separated isotopes serve as chemical tracers and as targets or beam particles in radioisotope production and nuclear research. Isotope effects on chemical equilibria and reaction rates are well understood; kinetic effects provide a useful tool for the study of reaction mechanisms. Isotopic substitution in living systems has yielded new knowledge in the biological sciences, as has the study of natural isotopic abundance variations in the geosciences.

D. BETA ENDPOINT MEASUREMENTS OF ^{105}In AND ^{103}In (J. Wouters, J. Aysto,† M. Cable, P. Haustein,†† R. Parry and J. Cerny)

In a continuing series of experiments[1] to determine beta endpoints we have now measured the beta endpoint of ^{105}In and ^{103}In. The ^{105}In beta endpoint of 3.8 ± 0.2 MeV is a new measurement while that of ^{103}In, 4.1 ± 0.2 MeV is a corroboration of a previous measurement by G. Lhersonneau et al.[2] Comparison of these measurements with the various mass formula predictions enables the observation of any effects on the mass surface due to the nearby double shell closure.

The beta endpoint measurements were conducted using the RAMA mass separator system together with standard β^{+}-γ coincidence techniques for data collection. Preliminary results, including a detailed description of the techniques used, were reported at the 6th International Conference on Atomic Masses and Fundamental Constants.[3] We have since repeated the experiments with the following refinements. The beta-telescope was calibrated with the endpoints of the strongest allowed decay branches of ^{123}Cs (3.410 ± 0.122 MeV) and ^{124}Cs (4.574 ± 0.150 MeV) produced in ^{14}N on Cd at 110 MeV, and ^{80}Rb (4.069 ± 0.025 MeV), ^{79}Rb (1.837 ± 0.041 MeV), and ^{78}Rb (3.41 ± 0.37 MeV) produced in ^{14}N on Zn at 150 MeV. ^{105}In and ^{103}In were produced by bombarding 1 mg/cm^2 natural Mo and separated ^{92}Mo targets, respectively, with 110 MeV ^{14}N ions. The data were collected using hardwire coincidences between the beta-telescope detectors and the gamma detector and analyzed using software gates on known γ rays of the daughter nucleus to project out a single component beta spectrum.

The resulting beta spectra were analyzed two ways. The spectra were plotted in Fermi-Kurie form using a computer code that also corrects for the response function of the beta detector. Linear least squares fits of the resulting spectrum determined the endpoints (see Fig. D-1). Second, the spectra were analyzed using the shape function fitting technique of Davids et al.[4]

---

† Permanent address: University of Jyvaskyla, Finland.

††Permanent address: Brookhaven National Laboratory, Upton, NY.

1 Nuclear Science Division Annual Report for 1978-1979, LBL-9711, p. 21.

2 Lhersonneau, Dumont, Cornelis, Huyse, and Verplancke, Phys. Rev. C18, 2688 (1978).

3 J. Cerny et al., Lawrence Berkeley Laboratory preprint LBL-9876.

4 Davids, Guliardi, Murphy, and Norman, Phys. Rev. C19, 1463 (1979).

A summary of our measurements and the mass excesses of ^{105}In and ^{103}In are presented in Table D-1. Deviations of the experimental values from a semiempirical shell model formula by Liran and Zeldes and from a Garvey-Kelson transverse equation are given[5] for comparison. In the main, these predicted masses agree fairly well with the experimental measurements. An interesting disagreement of -1.0 MeV of the ^{103}In mass excess from the Liran-Zeldes calculations is inconsistent with the good agreement of their approach in predicting the other experimentally known In mass excesses. Further systematic studies are required to understand both this behavior and whether it might have any possible relationship with the nearby double shell closure.

Table D-1. Summary of Q_{EC} determinations and comparison to different mass predictions.

Nuclide	Decay Energy [MeV] This work	Decay Energy [MeV] Literature	Mass excess [MeV]	Δ=Me(Exp) - Me(theory)[5] L-Z [MeV]	G-K
^{103}In	5.31±0.20	5.8±0.5[2]	-75.31±0.20	-1.00	-0.61
^{105}In	4.95±0.20		-79.39±0.20	0.24	0.55

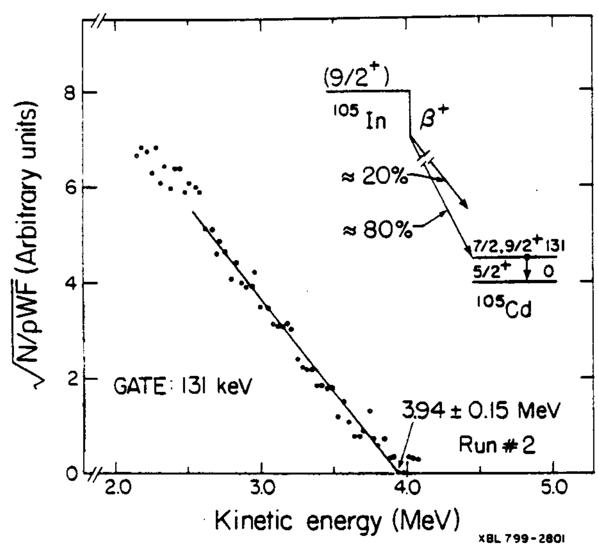

Fig. D-1. Fermi-Kurie plot and partial decay scheme for ^{105}In. Beta-branching ratios were determined from the γ spectrum in coincidence with positrons. (XBL 799-2801)

[5] S. Liran and N. Zeldes, At. Data and Nucl. Data Tables 17, 431 (1976); J. Janecki, ibid., 17, 455 (1976).

A. NUCLEAR DATA APPLICATIONS - MEASUREMENTS

1. Studies of (n, charged particle) Reaction with 14-15 MeV Neutrons (Haight, Grimes, Johnson*, Barschall**)

In fusion reactors, materials bombarded by fusion neutrons will be altered by nuclear transmutations that produce hydrogen and helium. To assess the potential performance of specific materials for fusion reactor application, cross section data are required by the fusion community and the Office of Fusion Energy. Under the sponsorship of the DOE Office of Basic Energy Sciences, we measure these quantities by detecting the charged particles emitted by materials under bombardment by neutrons of 14 to 15 MeV. By also measuring the energy and angular distributions of the charged particles, we are able to test nuclear reaction theories through model calculations and to deduce KERMA factors for energy deposition by the neutrons.

In the past year we have measured cross sections for charged-particle emission from targets of ^{9}Be, N, O, and Si bombarded with 14.1 MeV neutrons. The alpha-particle spectrum from ^{9}Be is shown in Fig. A-1. In addition to the continuum of alpha-particle energies, peaks corresponding to the ground and first excited states of ^{6}He are easily discerned. For these light nuclei, the (n,α) differential cross sections to resolved final states are observed to vary strongly with reaction angle.

2. Photoneutron Cross Sections for ^{15}N (Berman, Jury***, McNeill^{+}, Pywell^{++}, Thompson^{+++}, Woodworth)

We have measured the photoneutron (γ,n) and $(\gamma,2n)$ cross sections for ^{15}N from threshold to 40 MeV at the LLNL Linac, using a gaseous sample and monoenergetic photons from the annihilation in flight of fast positrons with photon resolution between 1 and 2% with an experimental accuracy of 10%. Similar measurements on ^{13}C, ^{17}O and ^{18}O have been reported and published previously. Data for the nuclei ^{29}Si and ^{30}Si were also taken and are being analyzed.

---

* Present address: Center for Radiation Research, National Bureau of Standards, Washington, D. C. 20234

** University of Wisconsin, Madison, WI 53706

*** Trent University, Peterborough, Ontario, Canada

\+ University of Toronto, Toronto, Ontario, Canada

++ University of Saskatchewan, Saskatoon, Canada

+++ University of Melbourne, Parkville, Victoria, Australia

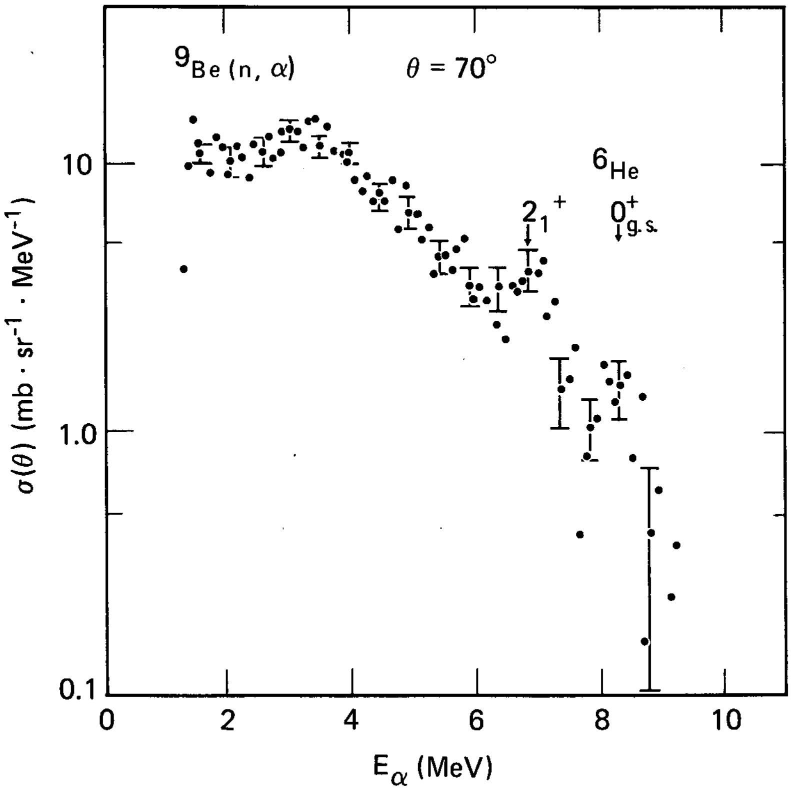

Figure A-1. Cross section for alpha-particle emission at 70° for ^{9}Be under bombardment by 14.1 MeV neutrons.

Table A-1. Lane-model parameters for E_p = 24.5 MeV and E_n = 11 MeV.

	^{116}Sn	^{118}Sn	^{120}Sn	^{122}Sn	^{124}Sn
V_0	49.9	49.8	50.1	49.8	49.9
W_0	9.22	9.15	9.44	9.38	9.54
V_1	71.8	67.6	69.0	75.5	71.2
W_1	69.4	68.3	63.0	59.0	71.4
$\sqrt{V_1^2+W_1^2}$	99.9	96.1	93.4	95.8	100.8

$$\left.\begin{aligned} V &= Vo \pm \frac{V_1}{4} \frac{(N-Z)}{A} \\ W &= Wo \pm \frac{W_1}{4} \frac{(N-Z)}{A} \end{aligned}\right\} \begin{aligned} &+ \text{ protons} \\ &- \text{ neutrons} \end{aligned}$$

3. Neutron Radiative Captive (Sullivan, Becker, Stelts*, Browne**)

Neutron-capture reactions are of both basic and applied interest in testing nuclear reaction models. For nuclei near closed shells such as in the mass-90 region, the reaction-model parameters are generally more uncertain than they are away from closed shells. To validate these calculations we wish to compare predictions with measurements of the detailed shape of the gamma-ray spectrum following neutron capture.

Measurements were made of the shape of the gamma-ray spectrum from neutron capture by ^{87}Sr at three neutron energies: E_n = thermal, 2 keV, and 24 keV. The measured gamma-ray yields were corrected for detector efficiency and normalized to an intensity of 0.95 per capture for the transition from the 2^+ first excited state to the ground state. Averaged over 100-keV intervals, the gamma-ray intensities are shown in Fig. A-2; they are also available in tabular form for comparisons with calculations. The measured spectra set limits on alternative descriptions of the gamma-ray strength function and perhaps on other parameters.

4. Lane-Model Analysis of (p,p) and (n,n) Scattering on the Even Tin Isotopes (Wong, Grimes, Finlay+)

We have applied the Lane model to analyze (p,p), (p,n) and (n,n) scattering on the even isotopes of $^{116,118,120,122,124}Sn$. The (p,n) measurements were taken at E_p= 24.5 MeV, the appropriate energy at which to compare with (p,p) measurements[1] at 24.5-MeV and (n,n) measurements[2] at 11 MeV. The Lane-model Code (LOKI 74) was employed to simultaneously calculate (p,p) and (p,n) scattering. Starting with Set A of the global Ohio University potentials[3] and assuming the full coulomb correction in the real and imaginary potentials, a four-parameter search was instituted on the isoscalar and isovector strengths to best fit the (p,p) and (p,n) data. The final searched isoscalar strengths (V_0, W_0) and isovector strengths (V_1, W_1) are listed in Table A-1. It is gratifying to observe that the (p,p) and (p,n) data on the Sn isotopes are explicable in terms of a relatively constant "total" isovector ($\sqrt{V_1^2 + W_1^2}$) and isoscalar strengths. The resulting potential parameters were then used to calculate (n,n) scattering on the ten isotopes with the optical

---

* Brookhaven National Laboratory, Upton, NY 11973
**Present address: Los Alamos National Laboratory, Los Alamos, NM 87545.
+ Ohio University, Athens, OH 45701.

1 O. Beer et al., Nucl. Phys. A147, 326 (1970).
2 J. Rapaport et al., Nucl. Phys. A341, 56 (1980).
3 J. Rapaport, V. Kulkarni and R. W. Finlay, Nucl. Phys. A330, 15 (1979).

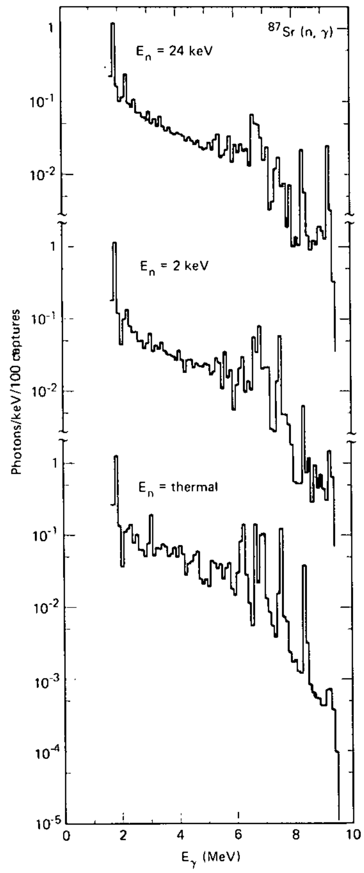

Figure A-2. Gamma-ray spectra from neutron capture on ^{87}Sr at E_n = 24 keV, 2 keV, and thermal.

model code LOKI 3-D. Fig. A-3 shows a typical fit to the (n,n) data for ^{120}Sn; Fig. A-4 shows the corresponding (p,p) and (p,n) fits. Equally good fits to (p,p), (p,n), and (n,n) were observed for the other isotopes. The near constancy of the "total" isovector strengths implies either that the effect of 2^+ channel coupling is small or that it is relatively constant over these isotopes. These conclusions are not unexpected since the β_2 values are $\sim$0.1 and vary by less than 15%. In summary, the Lane model can simultaneously describe (p,p), (p,n) and (n,n) scattering on the even Sn isotopes. In addition, rigorous isospin conservation requires the full coulomb correction in the real and imaginary potentials.

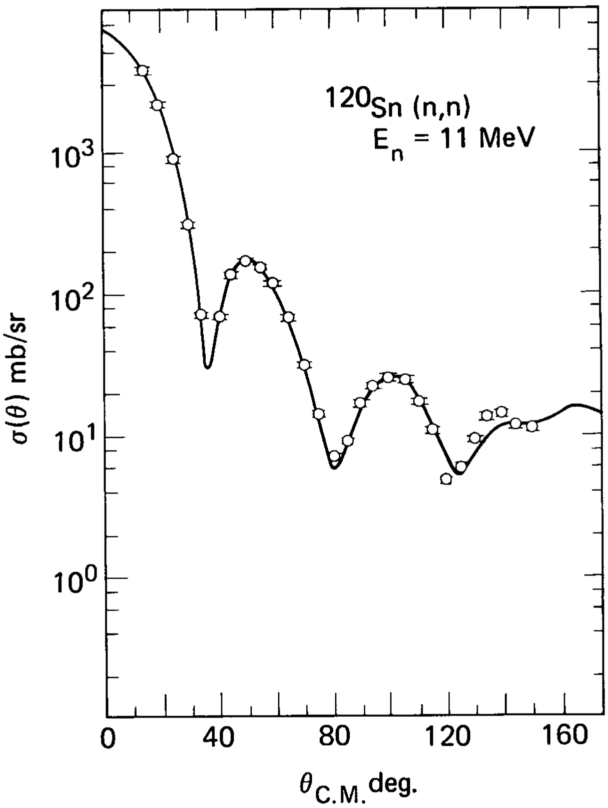

Figure A-3. Elastic scattering of 11-MeV neutrons by ^{120}Sn. The data are from Ref. 2. The calculations are from an optical model deduced from the results of Figure A-4.

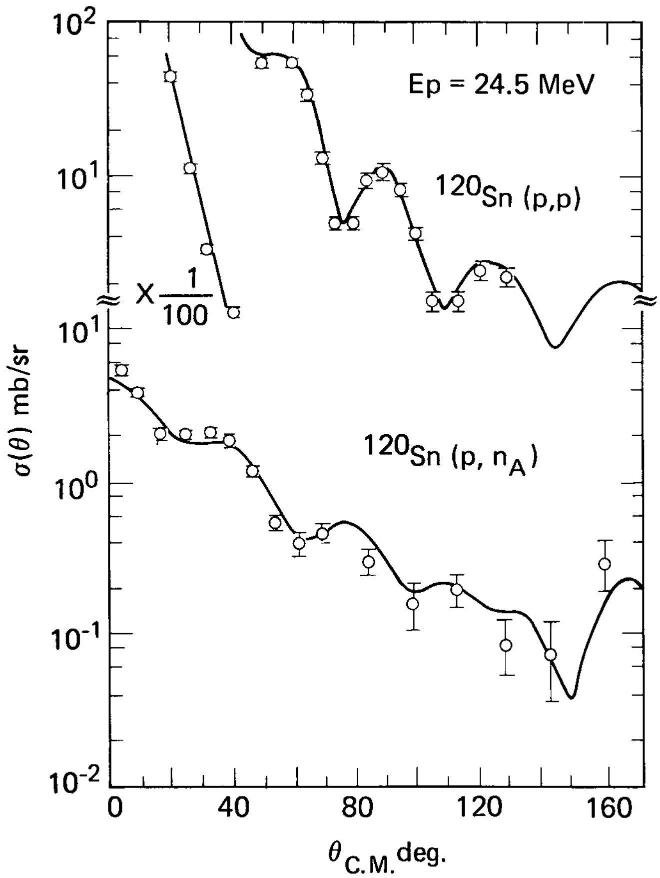

Figure A-4. Interactions of 24.5-MeV protons with ^{120}Sn: Top - elastic proton scattering. Bottom - (p,n) reaction to the isobaric analog state of ^{120}Sn. The data are experimental results from LLNL. The curves are optical model calculations consistent with the Lane model.

5. Neutron Scattering Cross Sections for ^{181}Ta, ^{197}Au, ^{209}Bi, ^{232}Th and ^{238}U Inferred from Proton Scattering and Charge-Exchange Cross Sections. (Hansen, Grimes, Pohl, Poppe, Wong)

Differential cross sections for the (p,n) reactions to the isobaric analog states (IAS) of ^{181}Ta, ^{197}Au, ^{209}Bi, ^{232}Th and ^{238}U have been measured at 26 and 27 MeV.[4] For ^{232}Th and ^{238}U, (p,p) data at 26 MeV are also available[5]. Coupled-channel calculations have been carried out in both proton and neutron channels and optical potential parameters for 6-8 MeV neutrons were inferred from a Lane model-consistent analysis of the data.

---

[4] Status Report to DOE Nuclear Data Committee UCID-18577 (1980).
[5] R. Batchelor, Nucl. Phys. 65, 236 (1965).

Generally good agreement has been obtained between the calculations and the (p,p) and (p,n) data. The neutron differential elastic-scattering cross sections obtained from these calculations using the optical parameters from the proton elastic channel, as prescribed by the Lane model ("proton potentials") have been compared with measurements available in the literature in the energy region of 6-8 MeV and with calculations obtained using neutron parameters from global sets[6] reported at these energies. (See Fig. A-5.) The comparisons for ^{181}Ta, ^{197}Au, and ^{209}Bi show that these neutron scattering cross sections can be predicted as well by the Lane-model approach as by neutron global parameter sets. Similar agreement was found for the neutron elastic scattering from ^{232}Th and ^{238}U at 6.5 MeV. These results support the theoretical assumption that the isospin symmetry of the Lane-model potential works as well for heavy nuclei as it does for nuclei with A $\leq$ 50.

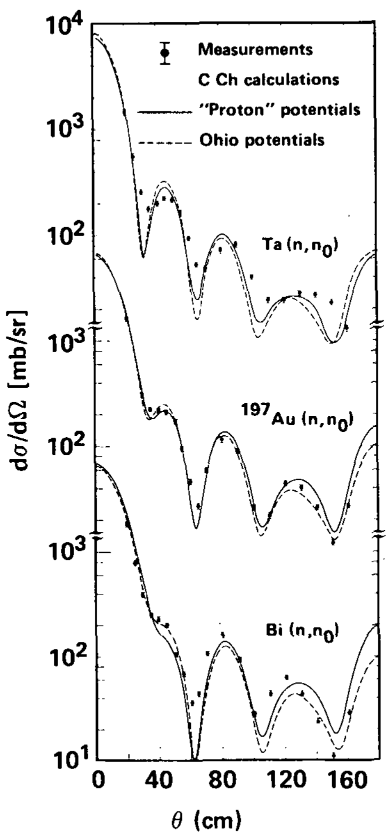

Figure A-5. Neutron differential elastic scattering cross sections for ^{181}Ta, ^{197}Au, and ^{209}Bi at $E_n \approx 8$ MeV. The data are from Ref. 6. The curves are optical model calculations described in the text.

---

[6] J. Rapaport et al., Nucl. Phys. A330, 15 (1979).

6. Neutron-induced Fission Cross Sections of ^{245}Cm and ^{242}Am. (White, Howe, Browne*, Auchampaugh*, Lisowski*)

Our neutron-induced fission cross section measurements in the transplutonium mass region have continued this year with remeasurement of both the $^{245}Cm(n,f)$ and $^{242m}Am(n,f)$ cross sections in the 500 keV to 20 MeV region at the WNR facility at Los Alamos. Preliminary values for the $^{242m}Am(n,f)$ cross section are in good agreement with previous LLNL linac data. Final mass assays for the ^{245}Cm samples (two each approximately 200 μg) have been completed and good agreement between the WNR and LLNL linac measurements have been obtained for this cross section.

Further, an independent high energy point at 14.1 MeV was measured for both ^{245}Cm (n,f) and ^{242m}Am (n,f) cross sections at the Livermore ICT facility (RTNS-I). Preliminary results are in excellent agreement with data obtained at both the LLNL linac and WNR for both isotopes. Final data for both isotopes will be published this year.

7. Fission Neutron Multiplicities for ^{245}Cm and ^{242m}Am (n,f) Reactions. (Howe, White, Browne**, Dupzyk, Landrum, Dougan).

Additional measurements of fission neutron multiplicities, $\bar{\nu}$, have been conducted recently for 14.1 MeV neutrons incident on ^{245}Cm and ^{242m}Am. Both numbers were measured relative to that of ^{235}U using a monoenergetic neutron source. Uncertainties were about 6.7% for ^{245}Cm and 11% for ^{242m}Am. In each case these results agree wih previous measurements performed with a white spectrum from the LLNL 100 MeV electron linac. This result was especially interesting for ^{245}Cm where the measured increase of $\bar{\nu}$ with incident neutron energy is significantly less than that for many other fissioning systems.

Curves of $\bar{\nu}$ as a function of fragment mass, A, typically show a sharp drop near A $\sim$ 120. If the ^{245}Cm+n system were to undergo symmetric fission, it is quite likely that both fragments would have these exceptionally low $\bar{\nu}$ values. While the thermal energy $\bar{\nu}$ value, 3.7, is not indicative of a symmetric breakup, the rate of increase in $\bar{\nu}$ with E_n might indicate a growing symmetric component. All of this suggests a change in the fission fragment mass distribution and/or kinetic energy distribution with excitation energy. Thus it is possible that our observed $\bar{\nu}$ (E_n) may be an indication of a fission barrier surface whose probable paths to scission change as a function of system excitation energy.

---

* Los Alamos collaboration - WNR experiment.
** Present address: Los Alamos National Laboratory, Los Alamos, NM 87545.

8. The Transport of 14 MeV Neutrons through Heavy Materials $150 \leq A < 208$ (Hansen, Komoto, Pohl, Wong)

The neutron emission spectra from Ho (0.8 mean-free-path (mfp)), Ta (1 and 3 mfp), Au (1.9 mfp) and Pb (1.0 mfp) have been measured using the sphere transmission and time-of-flight (TOF) techniques for 14-MeV incident neutrons from the Livermore Insulated-Core-Transformer (ICT) accelerator. The spectra were measured for the energy interval of 1 to 15 MeV using a stilbene scintillator (5.08 cm-diam x 5.08 cm-long) positioned at 26°, pulse-shaped discrimination, and flight paths of about 10m. The calculations have been carried out with TARTNP, a coupled neutron-photon Monte Carlo transport code, with the ENDL neutron and photon cross section library. For gold and lead, calculations also have been carried out with the ENDF/B-V library which has independent evaluations of the cross sections for these two materials. (The tantalum evaluation is from the ENDL library and no evaluation is available for holmium.) To compare the calculations with the measurements, the efficiency of the stilbene detector as a function of neutron energy and the time resolution of the system have been folded into the calculations. The descripion of the 14-MeV neutron source (the ^{3}H (d,n) ^{4}He reaction using the ICT 400 keV D^{+} beam) with its variations of energy and intensity as functions of angle has also been included.

The measured integrals are given in Table A-2 for the energy intervals 1.0 to 5.0, 5.0 to 10 and 10 to 15 MeV. The tabulation of the ratios of the calculated-to-measured integrals show that there is very good agreement (differences <10%) between measurements and calculations with the ENDL library, with the exception of the Ho and Ta low-energy neutron production. In the 1.0 to 5.0 MeV interval, the calculations are greater than the measurements by more than 15% for Ho and Ta. These discrepancies point to an overly large (n,2n) cross section for these materials. Furthermore, the decrease in the calculated integrals for the 10 to 15 MeV energy interval between 1 and 3 mfp of Ta indicates that the ENDL evaluated non-elastic cross section, to which the (n,2n) value is the main contributor, is too large.

9. ^{249}Cm Energy Levels from Measurement of Thermal Neutron Capture Gamma Rays (Hoff, Davidson*, Warner*, Schreckenbach*, Börner*, von Egidy*)

The excited levels of ^{249}Cm have been determined by use of neutron-capture gamma-ray spectroscopy. Gamma-ray measurements were made with curved-crystal spectrometers of focal lengths 5.8 and 24 m, and a pair spectrometer. These experimental data represent the first measurement of gamma transitions depopulating the levels of ^{249}Cm. The

*Institut Laue-Langevin, Grenoble, France.

Table A-2. Measured Integrals and Ratios of Calculated-to-Measured Integrals for Holmium, Tantalum, Gold and Lead for the ENDL Library

Material	mfp	$\rho \cdot r$ (g/cm^2)	E (MeV)	Experiment[a] ±5%	R ENDL ±5%
Ho	0.8	40.5	1.0-5.0	0.251	1.163
			5.0-10	0.023	0.913
			10-15	0.742	0.966
Ta	1.0	56.4	1.0-5.0	0.256	1.184
			5.0-10	0.025	1.000
			10-15	0.618	1.060
Ta	3.0	169.3	1.0-5.0	0.323	1.173
			5.0-10	0.028	0.929
			10-15	0.283	0.834
Au	1.9	119.8	1.0-5.0	0.485	0.940
			5.0-10	0.344	1.029
			10-15	0.406	0.980
Pb	1.0	63.5	1.0-5.0	0.530	0.917
			5.0-10	0.338	0.944
			10-15	0.660	0.976

a.) In units of neutron counts (sphere in) divided by the total number of 14-MeV source counts (sphere out).

---

neutron binding energy was determined to be 4713.7 ± 0.3 keV. We find evidence for the population of 23 levels in ^{249}Cm up to 1300-keV excitation. From an interpretation of our data, we make the following new configuration assignments (listed with the corresponding bandhead energies): $5/2^+$[622], 529.58 keV; $3/2^-$[752], 772.74 keV; $1/2^-$[501], 917.49 keV. In comparing the experimental results with various model calculations, we find best agreement with the calculations of Gareev et al.[7] which involve use of a Woods-Saxon potential form and take into account the interaction of quasiparticles with phonons.

Some of the configurations appear experimentally at energies much below those calculated, most notably the $5/2^+$[622], $3/2^-$[752], and $1/2^-$[501] bands. Much of this energy decrease appears to be due to

[7] F. A. Gareev et al. Nucl. Phys. A171, 134 (1971).

mixing of the quasiparticle state with vibrational components. A particularly outstanding difference between two types of calculations is found for the excitation energy of the 1/2[501] configuration. In the calculations of Gareev *et al.*,[7] this state is found at 920 keV; its primary single particle configuration is 65% of the wave function with most of the remainder described as gamma vibrational components built on the 1/2[761] and 3/2[752] configurations. A modified oscillator potential calculation puts this band at extremely high energy, 2500 keV. We find three levels whose characteristics are appropriate for assignment to the 1/2[501] band; the bandhead energy is 917 keV.

From our results, one can conclude that the calculations made by Soloviev's group[7] for level structure in actinide nuclei agree quite well with the experiment and are the preferred calculations for comparison with other experimental studies in this deformed region.

10. ^{231}Th Energy Levels from Neutron Capture Gamma Ray and Conversion Electron Spectroscopy (White*, Hoff, Lougheed, Lougheed, Barreau**, Börner**, Davidson**, von Egidy**, Jeuch**, Schreckenbach**, Warner**, Casten+, Kane+, Stelts+)

The excited levels in ^{231}Th have been studied by use of thermal and resonance neutron capture gamma-ray spectroscopy. The curved-crystal spectrometers, GAMS 1 and GAMS 2/3, installed at the High-Flux Reactor in Grenoble[8], have been used to make precise measurements of secondary gamma rays from a 30-mg ^{230}Th target in the energy range, $30 < E_\gamma < 1200$ keV. The same target was viewed by a Ge(Li)-pair spectrometer in order to measure primary gamma rays in the range, 3.6-5.2 MeV. Absolute intensities of the secondary gamma rays were obtained from comparison with ^{231}Th decay lines[9]. The BILL spectrometer[10] at Grenoble was used to measure conversion electrons in the energy range $70 < E_e < 900$ keV following thermal capture in a 6-mg target. At the Brookhaven research reactor, HFBR, the following complementary measurements have been made: primary gamma rays from neutron capture in the 1.427 eV resonance (75-mg target)[11], high-low energy coincidences for 10 primary transitions (75-mg target), and primary gamma rays from 2-keV average resonance capture (18-gm target).

---

* Oregon College, Monmouth, OR 97361.
** Institut Laue-Langevin, Grenoble, France.
+ Brookhaven National Laboratory, Upton, NY 11973.

[8] H. R. Koch *et al.*, Nucl. Instr. Meth. 175, 401 (1980).
[9] P. Hornshoj *et al.*, Nucl. Phys. A248, 406 (1975).
[10] W. Mampe *et al.*, Nucl. Instr. Meth. 154, 127 (1978).
[11] W. R. Kane *et al.*, Proc. Int'l. Symp. on Neutron Cpature Gamma-Ray Spectroscopy and Related Topics (IAEA, Vienna), p. 105 (1969).

After data reduction and analysis, the results of these measurements are being interpreted, along with information from single-particle transfer reactions, in terms of the "unified model" of Bohr and Mottelson[12]. From these neutron capture studies, we have constructed a scheme involving 55 energy levels, of which 42 have configuration assignments. These levels are grouped into 20 rotational bands. Of particular interest is the evidence for configuration mixing between single-particle and vibrational excitations. This interpretation involves analysis of multipolarities and relative strengths of transitions connecting related configurations along with single-particle configuration strengths from theoretical analysis of transfer reaction data.

One of the more distinct features of this analysis has been the observation of appreciable E0 components in certain transitions. For example, we observe the first two excited levels of three distinct K = 1/2 rotational bands with bandhead energies of 687.6, 793.0, and 820.5 keV. The deexcitation spectrum of each of these levels includes a transition with appreciable E0 strength leading to the I = 1/2 or 3/2 level of the $1/2^{+}[631]$ configuration at 247.6 and 272.2 keV. The strong E0 component is interpreted to indicate a component of beta vibrational motion coupled to the $1/2^{+}[631]$ configuration in each of the three higher rotational bands. Theoretical calculations by Soloviev's group[13] which include the interaction of quasiparticles with one-phonon quadrupole and octupole vibrational motion do not reflect this experimental observation. These calculations predict in the energy range 300-1000 keV just one K = 1/2 band whose predominant configurational components are 1/2[640], 50%, and 1/2[640]Q, (20), 30%, the latter being their notation for a quadrupole, K = 0, vibration ("beta") coupled to that single-particle configuration. It will require further study to understand what aspects of the theoretical treatment require modification in order to more closely fit experimental data.

11. New Measurements of Conversion Electron Binding Energies in Berkelium and Californium (Borner*, Barreau*, Davidson*, von Egidy*, Hoff, Lougheed, Schreckenbach*)

The subject of this report is a new determination of electron binding energies in Bk and Cf which have been obtained when studying excited levels in ^{250}Bk by use of the (n,γ) and (n,γe) reactions at

---

* Institut Laue-Langevin, Grenoble, France.

12 A. Bohr and B. R. Mottleson, Nuclear Structure, Vols. I and II, W. A. Benjamin, Inc., Reading, Mass. (1975, 1979).

13 S. P. Ivanova et al., Izv. Akad. Nauk SSSR, ser. fiz., 39, 1612 (1975).

the High-Flux Reactor in Grenoble. We have reported previously on measured energies, intensities, and natural widths of K x-ray lines for several actinides[14].

Starting with a ^{249}Bk target, neutron capture leads mainly to the build-up of ^{250}Bk, ^{250}Cf, and ^{251}Cf through the following reaction sequence: $^{249}Bk(n,\gamma)^{250}Bk \; \beta^- \; ^{250}Cf(n,\gamma)^{251}Cf$.

The curved-crystal spectrometers GAMS 1, 2/3[8] have been used to measure secondary gamma rays in the region $30 \leq E\gamma \leq 1600$ keV with a 0.5-mg ^{249}Bk target in a neutron flux of 5.5×10^{14} n cm^{-2}s^{-1}. The BILL-beta spectrometer[10] was used to measure conversion electrons in the energy range $17 \leq E_e \leq 830$ keV with a different 0.5-mg ^{249}Bk target in a neutron flux of 3×10^{14} n cm^{-2}s^{-1}. Gamma-ray energies were calibrated by use of fission-product lines (from accompanying fission of ^{250}Bk and ^{250}Cf) whose energies are accurately known from other GAMS measurements[15]. Along with secondary gamma rays, K x-ray energies for Bk and Cf have been derived from GAMS measurements (Table A-3). A comparison with the x-ray energies listed in the Table of Isotopes[16] shows there is reasonable agreement for Bk (a mean deviation of 20 eV) whereas there is a 1-keV discrepancy for Cf.

Using our Bk x-ray energies and a value of 19.452 keV[17] as a reference for the LIII-electron binding energy in Bk, we derive E = 131.582 $\pm$ 0.003 keV and E = 24.401 $\pm$ 0.007 keV for the K and LII binding energies, respectively, again in good agreement with reference[16]. These binding energies together with gamma-ray energies in Bk have been used for calibration of the corresponding conversion electron transitions. The other electron shell binding energies for Bk listed in Table A-4 were obtained from relative energy differences, $E\gamma^{Bk}-E_e^{Bk}$.

In a similar manner the binding energies for Cf have been obtained by the use of the energy differences $E\gamma^{Cf}-E_e^{Cf}$, with the results listed in Table A-5.

---

14 G. Barreau et al., proceedings of the Third International Symposium on Neutron Capture Gamma-Ray Spectroscopy and Related Topics, edited by R. E. Chrien and W. R. Kane, pp. 552-554, Plenum Press, New York (1979).

15 H. G. Börner et al., Nucl. Instr. Methods 164, 579 (1979).

16 Table of Isotopes, Seventh Edition, edited by Lederer et al., pp. 8-12 Appendices, Wiley-Interscience, New York (1978).

17 J. M. Hollander et al., Arkiv Fysik 28, 375 (1965).

Table A-3. K x-ray energies in berkelium and californium.

	Bk		Cf	
	E [keV]	ΔE [keV]	E [keV]	ΔE [keV]
K LII	107.181	0.006	109.831	0.015
K LIII	112.130	0.003	115.030	0.012

Table A-4. Electron binding energies in berkelium. The errors are statistical; all energies are based on E = 19.452 keV [6] for the Bk-LIII shell.

Shell	E [keV]	ΔE [keV]	E [keV] Ref. 16	E [keV] Ref. 18
K	131.582	0.003	131.590	131.570
LI	25.278	0.010	25.275	25.266
LII	24.401	0.007	24.385	24.372
LIII	19.452	--	19.452	19.439
MI	6.560	0.005	6.556	6.545
MII	6.156	0.008	6.147	6.142
MIII	4.991	0.010	4.977	4.983
NI	1.768	0.005	1.755	1.750
NII	1.572	0.009	1.554	1.562

Table A-5. Electron binding energies in californium. The errors are statistical; all energies are based on E = 19.452 keV [6] for the Bk-LIII shell.

Shell	E [keV]	ΔE [keV]	E [keV] Ref. 16	E [keV] Ref. 18
K	134.972	0.010	135.960	134.952
LI	26.050	0.010	26.110	26.015
LII	25.121	0.002	25.250	25.104
LIII	19.931	0.005	19.930	19.905
MII	6.370	0.002	6.359	6.347
MIII	5.140	0.003	5.109	5.118
NII	1.652	0.003	1.616	1.617
NIII	1.310	0.003	1.279	1.289
OII	0.332	0.006	--	0.338
OIII	0.246	0.004	--	--
PII/III	0.056	0.010	--	--

[18] T. A. Carlson and C. W. Nestor, Jr., At. Data Nucl. Data Tables 19, 153 (1977).

When the tabulated values for K and L shell binding energies[16] of the elements Pu (Z = 94) to Lr (Z = 103) are plotted against atomic number, a break in continuity can be observed at around Z = 97. Inclusion of our new values for Bk and Cf along with measured data for Pu, Am, and Cm demonstrates an essentially linear behavior within this range of atomic numbers. Extrapolation of the linear trends yields estimated K and LII binding energies for transcalifornium elements that are considerably lower than the calculated values listed in Ref. 16.

B. NUCLEAR DATA APPLICATIONS - CALCULATIONS

1. Nuclear Level Densities. (S. Grimes, S. Bloom)

During the past year modifications to our shell model code have been made which allow calculation of Hamiltonian moments as high as $\langle H^4 \rangle$. These in turn may be used with the theory of spectral distributions to calculate the level density of a nucleus with complete inclusion of two-body effects[19]. Related parameters such as the spin-cutoff factor and the positive-parity negative-parity ratio as functions of energy may also be calculated.

We are applying this new approach to ^{28}Si. Recently, spin-cutoff factors and level-density parameters have been determined for this nucleus[20]. Earlier efforts to apply the theory of spectral distributions to ^{28}Si were hampered by the limitation to two moments of the Hamiltonian. We find significant improvement when $\langle H^3 \rangle$ is included in the calculation but find some residual descrepancies. Our fourth moment calculation will be ready shortly. We will then be able to evaluate whether the present code is adequate for spectral distribution calculations of nuclear level densities. Additional studies of results with various sets of two-body matrix elements will be necessary before the code can be used routinely for calculating level densities.

2. Relative Importance of Statistical vs Valence Neutron Capture in the Mass-90 Region. (D. G. Gardner)

It has often been reported[21] that, in certain mass regions corresponding to peaks in the neutron strength function, nonstatistical mechanisms contribute a significant or even major portion of the radiation width in the resolved resonance region. Such effects are sensitive

---

19 J. B. French and K. F. Ratcliff, Phys. Rev. C 3, 97 (1971).

20 S. M. Grimes, et al. Phys. Rev. C 18, 1100 (1978).

21 B. J. Allen and A. R. de L. Musgrove, Advances in Nuclear Physics (M. Baranger and E. Vogt, editors), Vol. 10, p. 129 (1979).

to the single-particle character of the final states, which might severely limit our ability to calculate low-energy neutron capture cross sections for nuclei where experimental data are lacking. The mass-90 region corresponds to a peak in the p-wave neutron strength function, and the study of several target nuclei in this region is now underway. These targets include ^{89}Y and ^{98}Mo, the latter often being cited as a classic example of valence neutron capture effects. Preliminary statistical model calculations indicate that the s-wave and p-wave radiation widths, as well as the total capture cross section for neutrons from 1 keV to several MeV, may be well represented without recourse to valence capture mechanisms. Furthermore, the calculated intensities of the primary gamma-ray transitions from p-wave states to the first eight levels in ^{99}Mo compare well with recent measurements[22], when the data from several resonances are averaged. We conclude that, for targets ^{89}Y and ^{98}Mo at least, all nonstatistical effects rapidly disappear when even a small number of resonances are averaged. For neutron energies in the overlapping resonance region and higher, no direct-type capture mechanism need be invoked until incident energies of perhaps 5-10 MeV are reached.

C. NUCLEAR DATA FOR REACTOR SAFETY

1. Determination of Properties of Short-Lived Fission Products (Meyer, Henry, Lien, Massey, Lin, Rengan)

Decay data on short-lived fission products are required to resolve a number of problems associated with the design and operation of both thermal and fast reactors. Existing reactors cannot exceed power levels which are determined by the amount of heat generated in the core following a loss-of-coolant accident. This decay heat is produced by fission products and can be measured on a case-by-case basis or calculated using summation. These calculations depend on existing data bases. In a program supported by DOE/BES we are measuring the decay properties of critical short-lived fission products in order to upgrade the ENDF/B data base. Existing nuclear power plants must also carefully monitor effluents and the production of poisons (neutron absorbers) in the reactor core; these procedures too depend on an accurate fission product data base. Our program is directed toward the measurement of the gamma-ray spectra, total decay energies, and the determination of average beta- and gamma-energy releases from these isotopes. Isolation of individual elements is performed with rapid automated radiochemical

---

22 R. E. Chrien *et al.*, Phys. Rev. C 13, 578 (1976).

separation procedures because our technique yields elements not available with the purely physical separation systems currently being used[23-25].

We have completed analysis, interpretation, and reporting of several fission product nuclei in the ^{132}Sn region. In Table C-1 we give the absolute abundance of major gamma rays in $^{132}Sb^{g}$ and $^{132}Sb^{m}$, an isotope which is of importance in decay-heat calculations. A second isotope of some yield is ^{130}Sb (6.5 m). The information on this decay scheme, thought to be known well enough, was found to be incorrect. Our experiments on antimony fission products also gave detailed results for ^{130}Sb (6.5 m) decay. We give the major gamma rays of this decay in Table C-2.

Equally important are predictive capabilities for the structure and properties of the nuclei in the ^{132}Sn region. In order to perform microscopic shell-model calculations, we have used the Lanczos method which tridiagonalizes in an iterative fashion large sparse matrices in such a way that the lowest eigenvalues converge fastest. Original calculations of Whitehead[26] and Hausman[27] have been extended to the ^{132}Sn region. A stringent test is how well the calculations agree with the detailed nature of the electromagnetic deexcitations. We have tested predictions of our large-scale shell-model calculations by comparing them with our experimental data for ^{130}Sb, ^{131}Sb, ^{132}Sb, ^{133}Te, ^{134}Te, ^{134}I, ^{135}I, ^{135}Xe, and ^{136}Xe nuclei[28-35] In addition, we have discussed modifications to the tensor M1 operator[35] in order to explain particular M1 transitions in ^{134}Te.

---

23 O. G. Lien, III, *et al.*, UCRL-84371 (Nucl. Instr. Methods, in press, 1981).
24 R. A. Meyer, Energy and Technology Review, UCRL-52000-80-5, p. 8 (May 1980).
25 R. A. Meyer and E. A. Henry, in Nuclear Spectroscopy of Fission Products, The Institute of Physics, Bristol, England (1980).
26 R. R. Whitehead, Nucl. Phys. A182, 290 (1972).
27 R. F. Hausman, Ph.D. Thesis, Univ. of California, Davis (1978).
28 S. M. Lane, *et al.*, UCRL-84492 (submitted to Phys. Rev. C, 1981).
29 S. M. Lane, *et al.*, UCRL-85219 (submitted to Phys. Rev. C, 1980).
30 R. P. Yaffe *et al.*, UCRL-85263 (submitted to Phys. Rev. C, 1981).
31 R. A. Meyer, *et al.*, UCRL-85262 (submitted to Phys. Rev. C, 1981).
32 H. Hicks, *et al.*, UCRL-84372 (submitted to Phys. Rev. C. 1980).
33 E. A. Henry, *et al.*, UCRL-84372 (submitted to Phys. Rev. C, 1981).
34 W. B. Walters, *et al.*, UCRL-85265 (submitted to Phys. Rev. C, 1981).
35 K. Heyde, *et al.*, UCRL-85170 (submitted to Phys. Rev. C, 1980).

Table C-1. Energy and intensity values for gamma rays of the ^{132}Sb isomers with abundance greater than 5% (n.b. complete lists of all 245 gamma rays of 132 g and all 106 of 132 m are in UCRL-85262).

2.8 min ^{132}Sb

E (ΔE)	I (ΔI) (per 100 decays)
103.6(2)	36(3)
635.90(2)	11(1)
697.02(5)	82(7)
816.8(3)	16(1)
974.29(3)	100(7)
989.64(9)	16(1)
1133.70(7)	5.7(2)

4.2 min ^{132}Sb

E (ΔE)		I (ΔI) (per 100 decays)
103.6(2)		92(3)
382.64(9)		19.4(1.2)
496.99(9)		8.2(7)
697.08(5)		100(5)
1042.1(1)		15.0(6)
1128.39(8)		6.0(5)
1166.43(9)		8.8(7)
1170(1)	4.8(5)	3.5(3)
1170.5(2)		1.3(2)

Table C-2. Decay of 6.5-min ^{130}Sb (all gamma rays above one percent are given).

E (ΔE)	I (ΔI) (per 100 decays)	E (ΔE)	I (ΔI) (per 100 decays)
182.35(8)	35(1)	920.9(2)	3.6(3)
348.5(2)	5.3(3)	942.2(2)	2.8(3)
369.9(2)	2.5(3)	950.3(2)	1.6(3)
405(1)	1.0(6)	1017.78(4)	27(1)
462.02(6)	4.7(5)	1046.5(4)	2.8(5)
481.4(5)	2.4(6)	1071.7(4)	2.2(5)
503.6(6)	1.3(5)	1102(1)	1.9(3)
513.7(5)	3(1)	1141.82(6)	4.9(5)
647.7(4)	5.8(9)	1177.2(3)	1.9(3)
696.0(5)	4.1(5)	1200.0(2)	3.3(3)
748.7(2)	4.5(3)	1232.3(2)	1.7(5)
793.51(8)	86(4)	1489.5(5)	1.3(6)
816(1)	11.6(5)	1597.9(2)	2.7(4)
839.49(7)	100(4)	1897.0(2)	1.7(3)

In order to obtain absolute gamma-ray intensities for the decay of ^{86}Se and ^{87}Se we had to first measure the amount of ground state to ground state(GS/GS) beta decay in the ^{86}Se to ^{86}Br and ^{87}Se to ^{87}Br decay. Until now it has not been possible to obtain an accurate measure of the GS/GS branching of Se isotopes. We have successfully used a saturation/stop flow technique to measure the GS/GS branching. This technique allows the collection of Se until saturation of the activity occurs followed by stopping the flow of activity and measurement of the growth and decay of known daughter activities (saturation/stop flow). Since we measure the growth of known Br daughter decay products to determine the GS/GS branching of the Se isotope's decay, the main obstacle that had to be overcome was prior removal of fission-produced bromine. To remove the fission-produced bromine, we inserted an oven in the flow line after a primary globular trap. This oven, when operated at 940°C, cracks all the gases present to atomic form. By use of a selective cold trap all halogens (Br and I) are removed. The remaining Se is caught in a carbon trap at the detector site. By using this modification of our gas-phase, rapid-chemistry system, we have measured ground-state beta-decay branchings for $^{86,87}Se$ to $^{86,87}Br$ to be 12% and 30%, respectively[36].

2. <u>Fission Yield of ^{87}Br and ^{137}I from 15 Nuclei Ranging from ^{232}Th to ^{249}Cf</u> (Meyer, Waldo,* Karam,** Henry, Kusnezov+)

We have used our time-dependent beta-delayed neutron measurements from a ^{3}He ionization chamber in a computer-controlled rapid rabbit transit system and known P_n values to determine the fission yield of ^{87}Br and ^{137}I in 15 different nuclei[37]. The results are compared, where possible, to other works in Table C-3. Also, we are adapting our fission yield model[37] to operate on an ECLIPSE computer[38]. We note that nuclides such as ^{232}Th and ^{238}U were supposed to have large even-odd effects and seem instead to have very small effects. Estimates of the size of the even-odd effect have been made for a large variety of nuclides[39].

---

* Present address: So. Calif. Edison, San Onofre, CA 91170.
** Present address: Dept. of Nuc. Eng., Georgia Tech., Atlanta, GA.
\+ Associated Western Universities Fellow to LLNL.

36 J. Lin, *et al.*, UCRL-85397 (submitted to JINC, 1981).
37 R. Waldo, *et al.*, Phys. Rev. *C* (in press).
38 D. Kusnezov, Nuclear Chemistry Division Internal Report (1980).
39 B. F. Rider and M. E. Meek, "Compilation of Fission Product Yields," NEDO-121-54-2(e), General Electric Co., Vallecitos, CA (1978).

Table C-3. Cumulative fission yield for ^{87}Br and ^{137}I.

Fissioning nuclide	^{87}Br fission yield (%) This Work[a]	Rider and Meek[b]	^{137}I fission yield (%) This Work[a]	Direct I isolation	Rider and Meek[b]
^{232}Th	7.61(39)	<7.15(20)	4.1(1.4)	5.15(82)	5.39(59)
^{232}U	2.81(18)		0.48(34)		
^{233}U	2.31(19)	2.20(13)	1.4(7)	1.67(10)	1.65(7)
^{235}U	2.35(09)	2.27(14)	3.0(6)	3.46(21)	3.22(19)
^{238}U	2.02(18)	1.36(44)	6.0(1.0)	5.31(85)	
^{237}Np	1.51(14)	<1.73(7)	2.4(5)		2.90(67)
^{238}Pu	0.84(13)		1.5(4)		
^{239}Pu	0.80(5)	0.73(4)	2.0(3)	2.57(21)	2.43(14)
^{240}Pu	0.92(13)	<1.01(16)	2.7(4)		2.58(59)
^{241}Pu	0.76(5)	0.61(5)	3.9(5)	3.86(23)	4.13(25)
^{242}Pu	0.80(13)	<0.86(14)	3.5(1.6)		3.70(85)
^{241}Am	0.76(9)		1.8(3)		
^{242m}Am	0.71(5)		2.4(3)		
^{245}Cm	0.51(4)		2.2(3)		
^{249}Cf	0.30(3)		1.25(17)		
^{252}Cf			3.0(3)		2.29(73)

[a] Number in parenthesis is error x 10^3, e.g. 7.61(39) = 7.61 $\pm$ 0.39.

[b] Taken from Ref. 39.

D. DATA EVALUATION AND COMPILATION

1. Evaluation of Charged Particle Data for the ECPL Library (Howerton, MacGregor, Perkins)

The interactions of five light charged particles (p, d, t, ^3He, ^4He) with each other and with heavier nuclei through ^{16}O, are being evaluated. The evaluations will include cross sections, energy distributions, angular distributions and average energy deposits. The energy and angular distributions will be for the five charged particles (both as secondary particles and as residual nuclei) and for neutrons.

2. Evaluation of Secondary Charged Particle Energy and Angular Distributions for ENDL (Howerton, MacGregor, Perkins)

Work is progressing in providing explicit energy and/or angular distributions for secondary charged particles (p, d, t, ^3He, ^4He) resulting from neutron-induced reactions in the ENDL library. These data are included both for the charged particles as reaction products and as residual nuclei. When this work is complete, new total and local energy deposits will take the place of those currently in ENDL. The new energy deposits will reflect the fact that secondary-light-charged-particle average energies can be obtained explicitly from the new distributions.

3. Evaluated Nuclear Structure Libraries Derived from the Table of Isotopes (R. J. Howerton)

Two new libraries, ENSL and CDRL, of evaluated nuclear structure data have been created. The data are based on the recent edition of the Table of Isotopes with modifications, as needed, to insure completeness. The modifications are described in the documentatiuon (currently in press) which will be issued as Vol. 23 of UCRL-50400.

LOS ALAMOS NATIONAL LABORATORY

A. NUCLEAR DATA MEASUREMENT

1. Low-Energy Fusion Cross Sections (Brown, Jarmie, Hardekopf)

The goal of this project is to measure cross sections for interactions between hydrogen isotopes in the bombarding energy range 10-120 keV. Such cross sections are fundamental to the operation of future controlled fusion systems.

A series of test measurements on the D(d,p)T reaction (6 angular distributions from 40 to 118 keV) yielded information that allowed us to redesign the inner region of the cryogenic target. Initial studies have been carried out on the laser-photodetachment, time-of-flight technique for beam-energy measurement, with very encouraging results. In a separate experiment, we measured to an absolute accuracy of ±0.8% the p+d elastic differential cross section at 10.04-MeV proton bombarding energy at the five angles (45°, 75°, 90°, 120°, and 150°) needed to calibrate the target density for the low-energy experiment. We plan to begin measurements on the D(t,α)n reaction as soon as our tritium handling system is complete; meanwhile, we will continue to work on the D(d,p)T andD(d,^{3}He)n reactions.

2. Cross Sections for Neutron-Induced, Neutron-Producing Reactions in ^{6}Li and ^{7}Li at 14.1 MeV (Drake)

We have measured the spectra and angular distributions of neutrons emitted from 14 MeV neutron induced reactions on ^{6}Li and ^{7}Li. Our preliminary results, shown in table A-1 as partial angle integrated cross sections, seem to be in reasonable agreement with previous measurements.

Table A-1. Angle Integrated Cross Sections (mb)

	^{6}Li	^{7}Li
Elastic	910 ± 70	1100 ± 80
Inelastic	128 ± 13 (2.18 MeV State)	170 ± 20 (4.63 MeV State)
Continuum	464 ± 111	217 ± 43

3. Sulfur Neutron Capture Cross Sections (Jurney; S. Raman, ORNL)

We have measured the thermal (n,γ) cross sections of ^{32}S by summing the unfolded capture gamma spectrum taken with a carefully calibrated NaI spectrometer and of ^{33}S, ^{34}S, and ^{36}S by summing the gamma intensities observed with a Ge(Li) spectrometer. The thermal neutron capture cross section of H (332 mb) was used as a standard for all the measurements.

The importance of the S absorption cross section to corrections required in the manganese bath technique for measurement of $\bar{\nu}$ has been reviewed by Smith.[1]

Our preliminary values for σ_γ are given in Table A-2.

Table A-2. σ_γ for the Sulfur Isotopes

Isotope	σ_γ (b)
32	0.518 ± .015
33	0.454 ± .050
34	0.294 ± .020
36	0.152 ± .010

By combining the values of σ_γ for the four isotopes in their natural abundances, we arrive at σ_γ = 0.508 ± 0.015 b for S.

4. Decay of 5.1-m ^{37}S (Bunker, Starner)

The β^- decay of 5.1-m ^{37}S to levels of ^{37}Cl has been reinvestigated, using sources prepared by thermal neutron activation of natural sulfur (0.017% ^{36}S) and isotopically enriched sulfur (∿80% ^{36}S). In addition to the four gamma-rays previously reported (906.3, 3103.6, 3741.3, 4010.4 keV),[2] we observe three additional low-intensity transitions of energy 1169.1, 3086.3, and 4396.3 keV. The 3086.3- and 4396.3-keV gamma-rays are presumed to be ground-state transitions since levels of these approximate energies are known from charged-particle reaction data. Through 2-parameter Ge(Li)-Ge(Li) coincidence measurements, we have established that the very weak (0.034%) 1169.1-keV gamma ray populates the known 3103.6-keV level, establishing a new level in ^{37}Cl at 4272.7 keV, of spin $7/2^-$ or $9/2^-$. These measurements also confirm that the previously observed 906.3-keV γ-ray feeds the 3103.6-keV level (see Fig. A-1).

Several large-scale shell-model calculations have been made for ^{37}Cl, the most recent and most successful being that of Hasper,[3] which utilized the Oak Ridge-Rochester shell-model code. The latter calculations predict a $7/2^-$ state of energy 4.1 MeV, which probably corresponds to the level we have established at 4.272 MeV.

---

[1] J. R. Smith, Proc. Intl. Conf. on Nuclear Cross Sections for Technology, Knoxville, NBS Special Publication 594, p. 738 (1980).

[2] J. C. Hill, Phys. Rev. C 9, 1453 (1974).

[3] H. Hasper, Phys. Rev. C 19, 1482 (1979).

5. Neutron Capture by $^{182,183,184,186}W$ and ^{87}Sr (Drake)

In collaboration with R. L. Macklin of ORNL we have collected data which will enable us to deduce neutron capture cross sections for ^{87}Sr and four isotopes of tungsten for neutron energies from 2.6 to 2000 keV.

6. Intermediate Structure in $^{238}U(n,\gamma)$ and $^{235}U(n,f)$ [Moore; F. Corvi, L. Mewissen, and F. Poortman (BCMN, Geel, and SCK/CEN, Mol)]

Evidence for intermediate structure in $^{238}U(n,\gamma)$ was reported by Perez et al.[1] who attributed the structure to a $p^{3/2}$ neutron channel doorway state. Some years ago, a method was devised by Corvi et al.[2] to assign the parity of neutron resonances in certain actinide and fission-product nuclei. Noting that all the lowest lying low-spin levels in ^{239}U have even parity, Corvi suggested that the relative intensity of primary gamma transitions to these low-lying states in neutron capture could be used as a signature of the parity of the capturing resonance. We used Corvi's method to assign the parity of the intermediate-structure fluctuations observed by Perez et al., between 5 and 100 keV neutron energy. While all the structure above 50 keV is consistent with p-wave neutron capture, as postulated by Perez et al., we found that the strongest intermediate-structure fluctuations below 50 keV do not show the characteristic p-wave signature of enhanced high-energy primary transitions. The obvious interpretation is that these fluctuations are due to s-wave neutron interactions. However, statistical model calculations show that the capture cross section is relatively insensitive to variations in the average s-wave neutron width, because the neutron width is so much larger than the radiation width. The only way we can calculate fluctuations in s-wave neutron capture of the size of those observed is to assume neutron- and radiation-width correlations.

Intermediate structure in the neutron-induced fission cross section of ^{235}U below 50 keV appears to be well established, and the average parameters obtained by Moore et al.[3] suggested that width correlations may exist here also. New measurements of the capture and fission cross sections of ^{235}U with substantially improved statistical accuracy have just been completed by Corvi et al., and it is planned that we shall carry out an analysis of these data to obtain average parameters for a width correlation study.

---

[1] R. B. Perez, et al., Phys. Rev. C<u>20</u> 528 (1979).

[2] F. Corvi, et al., NBS Spec. Pub. 425, Vol. I, p. 733 (1975).

[3] M. S. Moore, et al., Phys. Rev. C<u>18</u>, 1328 (1978).

7. ^{237}Np Fission Cross Section Measurement at WNR [Auchampaugh, Extermann, Moore, Moses, Olsen; Hill (ORNL)]

High-resolution measurements of the neutron-induced fission cross section of neptunium-237 were performed at WNR in the range from 1 to 500 eV. At these energies, the largest contribution to the observed resonance widths is that from the thermal motion of target nuclei. This effect can be reduced by cooling the sample. Solid-state theory indicates that 95% of the ultimate improvement corresponding to zero sample temperature can already be achieved at liquid nitrogen temperature. Having shown that fast and efficient ionization chambers can be operated in this temperature range with better discrimination against alpha pile-up than other fission fragment detectors normally used at low temperatures, we decided to design such a chamber for use in a pulsed neutron beam for fission cross-section measurements. The resulting instrument is capable of maintaining samples at a temperature of 83.9 $\pm$ 0.1 K over the extended period needed for good statistics.

Data reduction of the neptunium-237 fission data is nearly complete. The $^{6}Li(n,\alpha)$ signal obtained at the same time as the ^{237}Np data was analyzed to give an analytical representation of the flux shape from 1 eV to 5 keV. The energy scale was adjusted to give agreement with the Cd resonance structure as recommended by Mughabghab and Garber, BNL-325, Third Edition, Volume I (1973). As a further check the cross-section shape of $^{235}U(n,f)$ was calculated with the same procedure as that used for $^{237}Np(n,f)$ and compared with recommended integrals from ENDF/B-V; agreement was obtained within the statistical accuracy of the data.

8. Fission Cross Sections of ^{242}Pu and ^{244}Pu and Angular Distribution of Fragments from (^{244}Pu + n) [Moore, Olsen; J. Wartena and H. Weigmann (CBNM, Geel)]

As part of a program at the Central Bureau for Nuclear Measurements for studying the systematics of near-barrier fission in the even plutonium isotopes, we have carried out a measurement of the neutron-induced fission cross sections of ^{242}Pu and ^{244}Pu from 200 keV to 10 MeV using neutron-induced fission of ^{235}U as a flux monitor, and of the fragment angular distribution from (^{244}Pu + n) over the threshold region and above. Reduction of the cross-section data is essentially complete; the final normalization of the data remains to be done after an independent assay of the alpha and spontaneous-fission rates of the foil material used. A second measurement of the fission cross section of ^{242}Pu will be carried out with improved material purity.

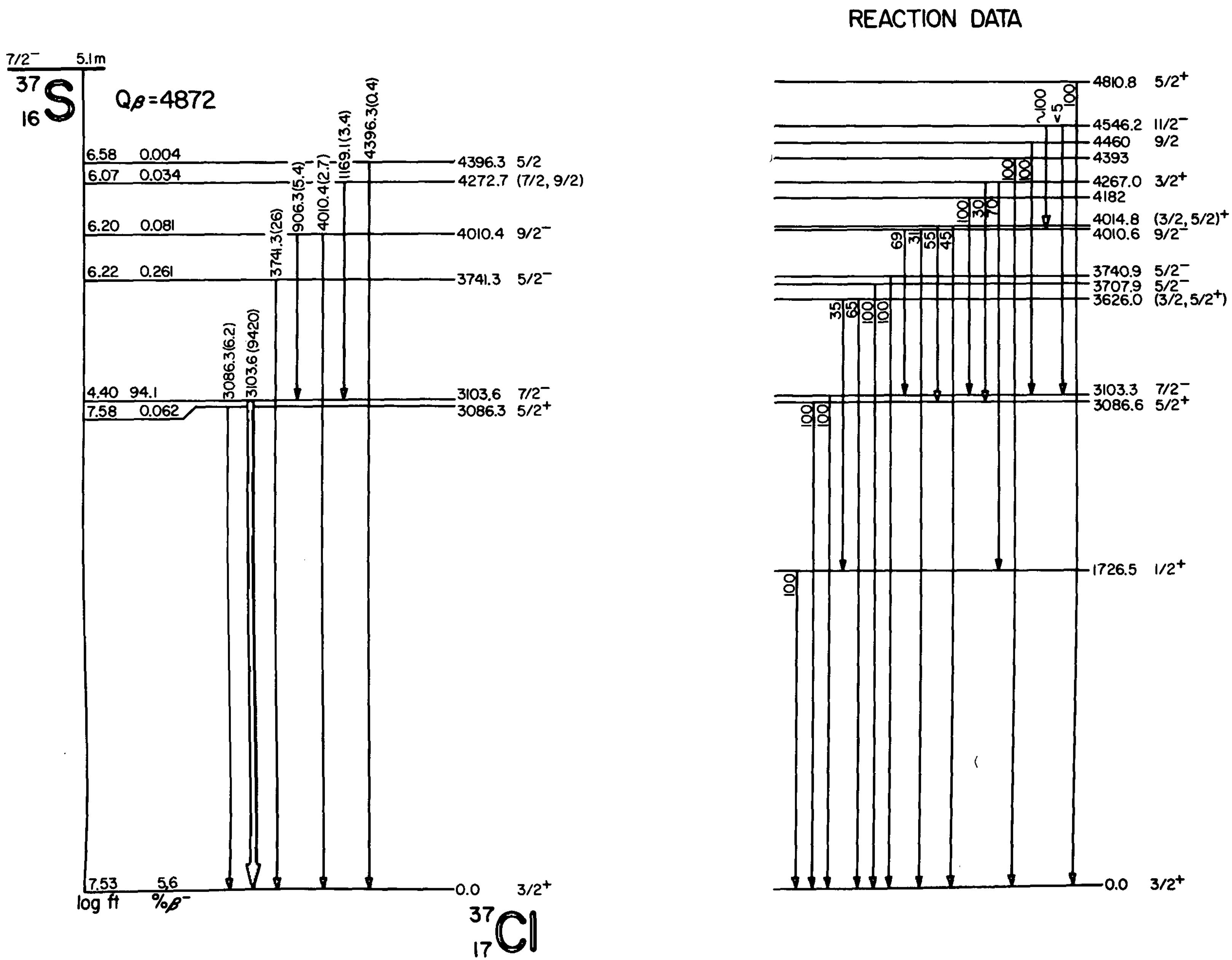

Fig. A-1. Decay scheme of ^{37}S. Levels of ^{37}Cl known from reaction data are shown at the right.

B. NUCLEAR DATA EVALUATION

1. Coulomb Corrections in the Three Nucleon System (Hale, H. Zankel)

In several instances where large differences in data for mirror reactions among light elements have been observed, the inevitable question is raised," are these differences compatible with charge-symmetric nuclear forces?" Our charge-independent R-matrix studies[1] indicate that generally they are, but these studies have used quite simple corrections for internal Coulomb effects in light nuclei. Another approach developed recently by Zankel and his collaborators[2,3] involves using an approximation to the two-potential integral equations for the transition operator in order to make Coulomb corrections in light nuclei, assuming the nuclear forces are charge-symmetric. We have applied this method to nucleon-deuteron scattering,[4] where such corrections are of great interest, since all the theoretical calculations are for n-d and most of the measurements are for p-d.

A sample of these calculations is shown in Fig. B-1 for the deuteron tensor analyzing power T_{20} at E_d = 10 MeV (E_N = 5 MeV). The solid curve is calculated from p-d phase shifts[5] that represent the measurements well at this energy. The dashed curve is calculated from the same phase shifts, omitting contributions from the Coulomb amplitude and asymptotic Coulomb phase shifts. This is the type of correction normally made to relate the n-d calculations and p-d measurements. It can be seen to give in this case a small difference, except at forward angles. The dash-dot curve is our prediction for n-d, which includes in addition to the asymptotic Coulomb effects an approximate correction for the Coulomb distortion of the "nuclear" T matrix. This calculation differs markedly from the p-d curve in the minimum at θ_{cm} = 105 degrees and corresponds more closely to the differences seen in n-d calculations and p-d measurements.

Our calculations indicate that this approximate Coulomb correction is an improvement over the simple one normally used. It can be used to correct n-d calculations for comparisons with p-d data (or vice versa) and to guide experimentalists in judging what sort of differences between p-d and n-d measurements are consistent with charge-symmetric nuclear forces.

---

[1] D. C. Dodder and G. M. Hale, in Proc. Int. Conf. on Neutron Physics and Nuclear Data, p. 490 (1978).

[2] J. Frolich et al., J. Phys. G6, 841 (1980).

[3] J. Frolich, L. Steit, and H. Zankel, Phys. Lett 92B, 8 (1980).

[4] H. Zankel and G. M. Hale, "An Approximate Coulomb Correction to Elastic N-d Scattering," submitted to Phys. Rev. C (1981).

[5] P. A. Schmelzbach et al., Nucl. Phys. A197, 273 (1972).

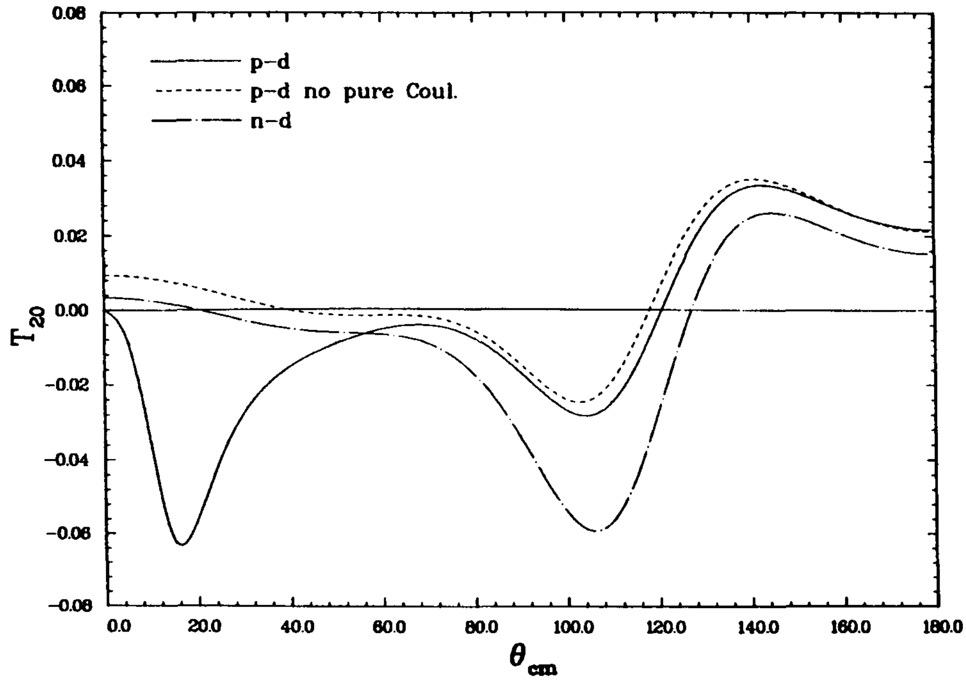

Fig. B-1. Calculations of the tensor analyzing power T_{20} for deuteron-nucleon scattering at 10 MeV.

2. <u>Neutron and Gamma-Ray Production by Cosmic-Ray Bombardments of Thick Objects</u> (Reedy)

The energetic nuclei in the galactic cosmic rays interact with matter to produce a variety of products, including neutrons and gamma rays. These neutrons induce nuclear reactions and produce nuclides (e.g., ^{21}Ne, ^{60}Co) which can be used to study the exposure history of the object. Cross sections for producing neutrons are being compiled and will be used to calculate neutron production rates in the moon and meteorites. Outputs from neutron-transport calculations made with these neutron source terms will be used to predict nuclide production rates.

Gamma-ray lines escaping from many planetary bodies (e.g., the moon and Mars) can be used to determine chemical compositions.[1] Cosmic-ray interactions will be simulated by the bombardment of thick targets with ≈ 1 GeV/nucleon particles, and the escaping gamma rays will be measured (in collaboration with others from JPL and UCSD). External beams at Berkeley and/or Los Alamos will be used; thick targets will include Mg, Al, Si, Fe, and $CaCO_3$, and will be mounted inside a large steel or iron sleeve. Foil packets inside the targets will be used to monitor particle fluxes. The measured gamma-ray fluxes will be compared with those calculated for the cosmic-ray bombardment of the moon.[1]

---

[1]R. C. Reedy et al., J. Geophys. Res. 78, 5847-5866 (1973).

3. Calculation of Neutron Induced Reactions on ^{59}Co Between 3 and 50 MeV (Arthur, W. Matthes, Young)

Several neutron reactions on ^{59}Co have been suggested as leading candidates to fulfill dosimetry needs for the Fusion Materials Irradiation Test Facility (FMIT). Since cross sections are needed to 50 MeV but available measurements extend only to 24 MeV, we performed nuclear-model calculations to provide the desired (n,xn) and (n,p) data. Our technique was similar to that used in our calculations[1] of the neutron reactions on $^{54,56}Fe$ between 3 and 40 MeV. We used a combination of multistep Hauser-Feshbach, preequilibrium, and direct-reaction models along with consistent input parameters determined or verified through the analysis of varied types of independent data. The calculated (n,xn) cross sections are compared to data in Fig. B-2 where good agreement was obtained. Calculations of the ^{59}Co(n,p) reaction on the other hand indicated possible inconsistencies between newer measurements from threshold to 10 MeV and older 14 MeV data. In particular, we were unable to adjust our calculation to agree both with the 14-MeV results and with the threshold data below 10 MeV.

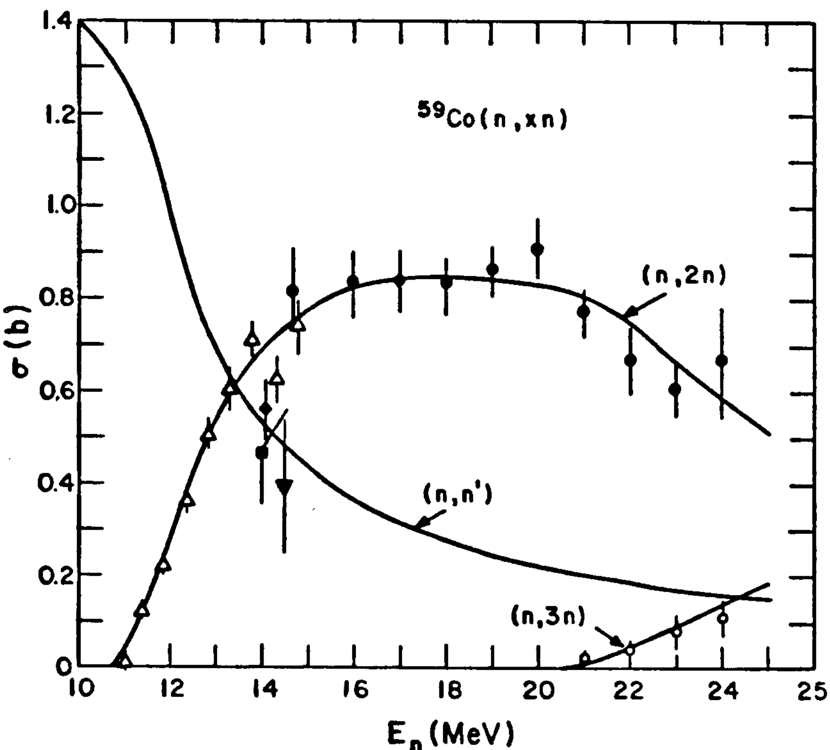

Fig. B-2. Calculated and experimental ^{59}Co(n,xn) data. All symbols refer to (n,2n) and (n,3n) experimental data with the exception of the solid diamond, square, and triangle, which represent (n,n') data measured around 14 MeV.

---

[1] E. D. Arthur and P. G. Young, "Evaluated Neutron-Induced Cross Sections for $^{54,56}Fe$ to 40 MeV," Los Alamos Scientific Laboratory report LA-8626-MS (ENDF-304) (1980).

4. Calculation of Proton Emission Spectra Induced by 15-MeV Neutrons in the Mass 90 Region (Arthur)

Recently, new measurements[1] have been made of proton emission spectra induced by 15-MeV neutrons on target nuclei where the proton binding energy lies substantially below that of the neutron. In these cases, "proton windows" exist where only proton and gamma-ray emissions compete with each other in the decay of the compound system. Thus calculations of (n,np) cross sections for such nuclei are sensitive to the behavior of sub-Coulomb barrier proton emission. We calculated proton emission spectra induced by 15-MeV neutrons for several nuclei (^{89}Y, ^{90}Zr, and ^{92}Mo) having such proton windows to compare to the results of Ref. 1. The techniques of the calculations (multistep Hauser-Feshbach with preequilibrium corrections) are described in Ref. 2, and include calculation of sub-Coulomb barrier (p,n) reactions on ^{88}Sr, ^{89}Y, and ^{93}Nb to confirm the low-energy behavior of our proton optical model parameters.

The calculated spectra are compared to data in Fig. B-3. With the exception of some disagreement for secondary proton energies below 2 MeV, the calculations reproduce well the portion of the spectra resulting from (n,np) and (n,pn) reactions. However, there is a consistent underprediction of the calculations at higher energies where (n,p) reactions dominate. This disagreement may indicate the presence of direct reaction contributions to the (n,p) cross section not included in the present calculations.

5. ^{182,183,184,186}W Evaluations (Arthur, Young, Smith, C. Philis)

New evaluations for the tungsten isotopes have been completed in the energy range from 0.1 to 20 MeV. These results were combined with ENDF/B-V data below 0.1 MeV to produce evaluated data files applicable over the energy range 10^{-5} eV to 20 MeV. These new evaluations combine recent experimental results with nuclear theory calculations and correct many of the deficiencies of the previous ENDF/B evaluations, particularly with regard to energy balance and the spectra of emitted neutrons. The nuclear models that were used (coupled-channel deformed optical, Hauser-Feshbach statistical, and preequilibrium) were optimized to the experimental data and used to produce most of the desired cross sections and spectra.

Several significant discrepancies in data were found, both among experimental results and between the older ENDF/B-V evaluations and our new results. For example, Smith's[3] new total cross-section measurements differ significantly from older measurements by Martin[4] for ^{184}W between 1-2 MeV.

---

[1]R. C. Haight et al, Phys. Rev. C 23, 700 (1981).

[2]E. D. Arthur, Nucl. Sci. Eng. 76, 137 (1980).

[3]A. B. Smith, Argonne National Laboratory, personal communication (1980).

[4]R. C. Martin et al., Bull. Am. Phys. Soc. 12, 106 (1967).

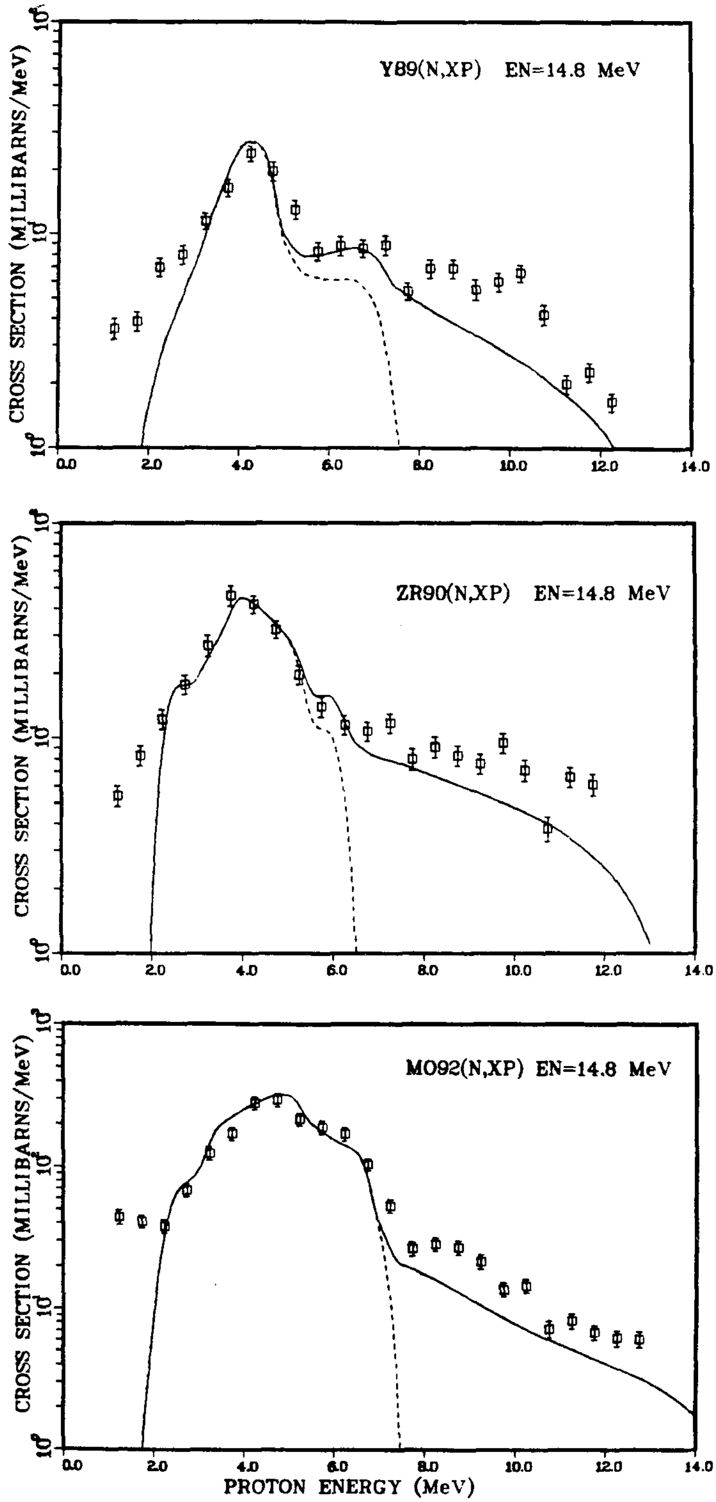

Fig. B-3. Calculated and experimental proton emission spectra induced by 15-MeV neutrons on ^{89}Y, ^{90}Zr, and ^{92}Mo. The area below the dashed curve represents the sum of (n,np + n,pn) contributions as determined from the calculation.

Likewise, a serious discrepancy was found to exist between the gamma-ray emission measurements of Dickens et al,[1] which were used for ENDF/B-V, and older measurements by Drake[2] and Savin.[3] As seen in Fig. B-4, our new calculations support the latter measurements. Since the parameters used in the calculations were determined independently from these measurements, we chose to incorporate the calculated data in the evaluations.

6. Calculation of Prompt Fission Neutron Spectra and $\bar{\nu}_p$ (Madland, Nix)

Our main effort has been in the theoretical calculation of prompt fission neutron spectra N(E) and average prompt neutron multiplicities $\bar{\nu}_p$. The purpose is to predict N(E) and $\bar{\nu}_p$ as functions of the fissioning nucleus and its excitation energy (incident neutron energy in the case of neutron-induced fission). This work has been completed for spontaneous fission and for neutron-induced fission up to the threshold for multiple-chance fission.[4-7] More recently we have extended our calculations up through the region of third-chance fission, that is, first-chance, second-chance, and third-chance fission processes have been included.[6,7] For example, Fig. B-5 illustrates N(E) calculated for the fission of ^{235}U induced by 14-MeV neutrons. Each multiple-chance fission spectrum component and the total spectrum are shown. Similarly, the capability to calculate the dependence of $\bar{\nu}_p$ on incident neutron energy including multiple-chance fission has also been implemented.

---

[1] J. K. Dickens et al, Oak Ridge National Laboratory report ORNL-4847 (1973).

[2] D. M. Drake et al, Nucl. Sci. Eng. 40, 294 (1970).

[3] M. B. Savin et al, Proc. 4th All Union Conf. Neutron Physics, Kiev, Vol. 2, p. 103 (1978).

[4] D. G. Madland and J. R. Nix, Trans. Am. Nucl. Soc. 32, 726 (1979).

[5] D. G. Madland and J. R. Nix, Proc. Int. Conf. on Nuclear Cross Sections for Technology, NBS Spec. Pub. 594, p. 788 (1980).

[6] D. G. Madland and J. R. Nix, "Calculation of Neutron Spectra and Average Neutron Multiplicities from Fission," Proc. Int. Conf. on Nuclear Physics, Berkeley, CA, August 24-30, 1980 (to be published).

[7] D. G. Madland, "Prompt Fission Neutron Spectra and $\bar{\nu}_p$," Proc. Workshop on Evaluation Methods and Procedures, Brookhaven National Laboratory, September 22-24, 1980 (to be published).

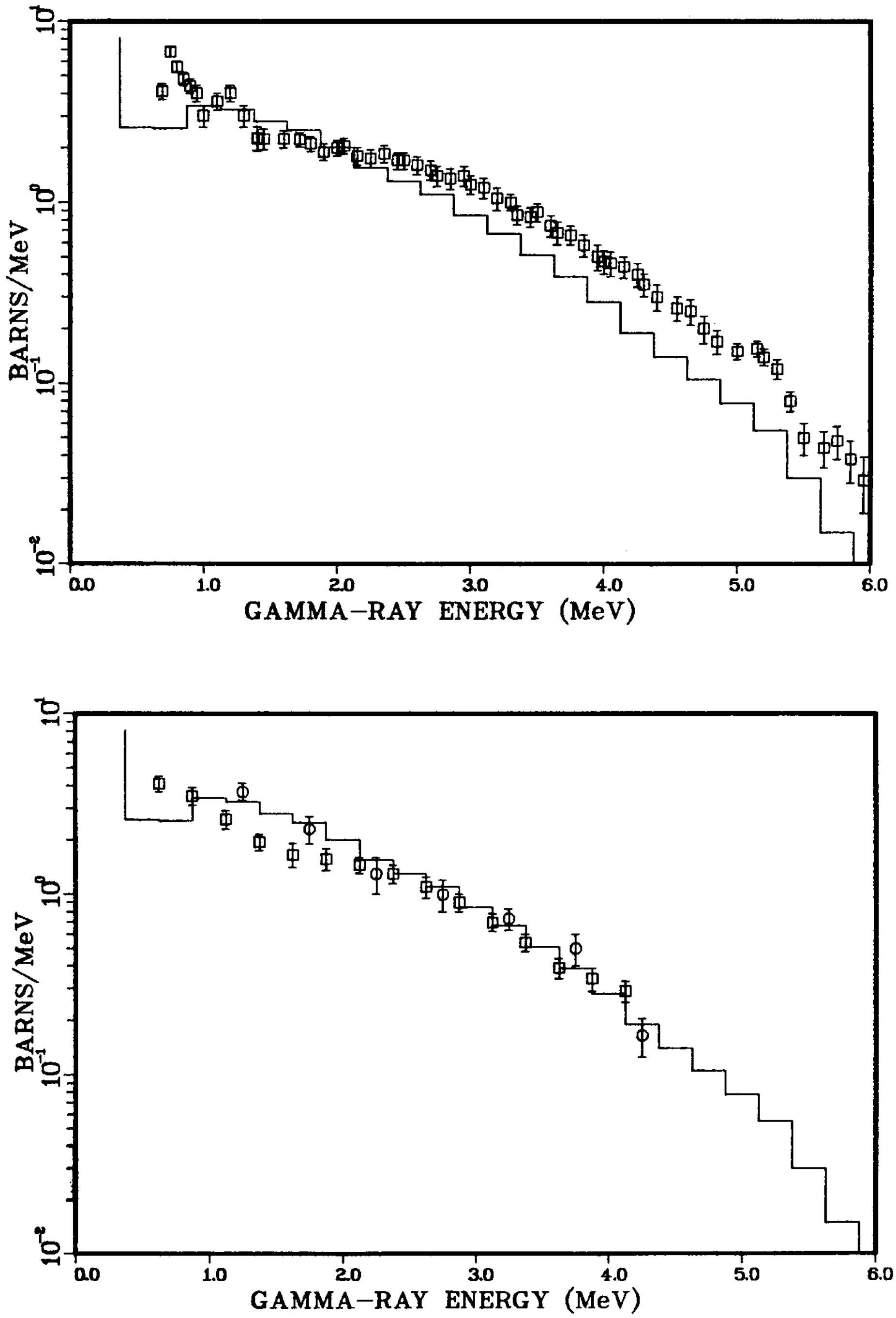

Fig. B-4. Calculated gamma-ray production spectrum for 6.25-MeV neutrons on tungsten compared to the Dickens et al. measurement (upper figure) and to the Drake and Savin data (lower figure).

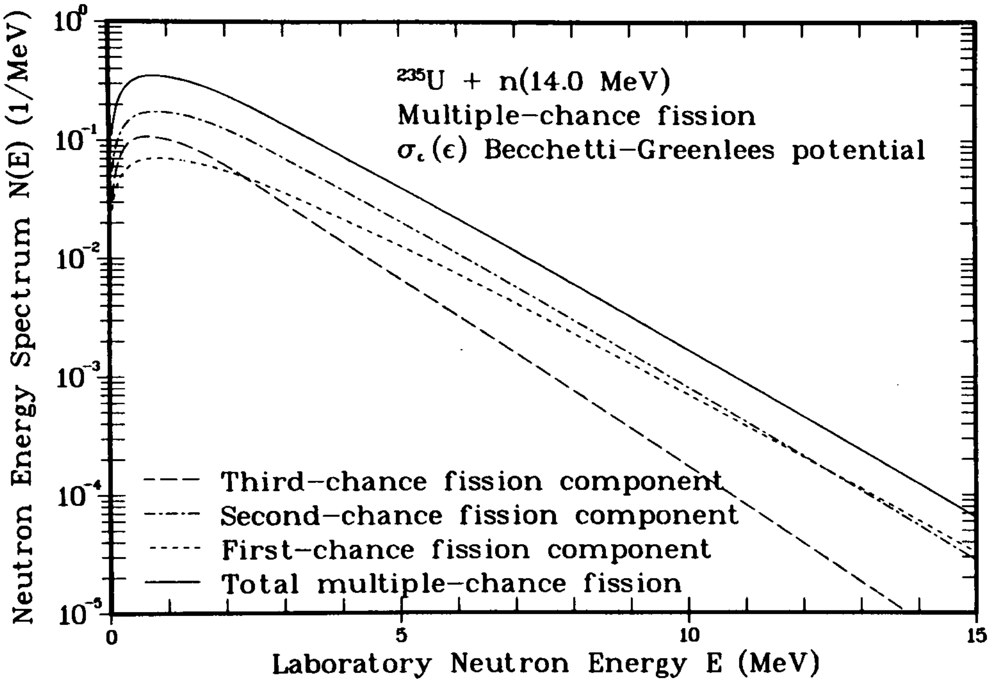

Fig. B-5. Prompt fission neutron spectrum for the fission of ^{235}U induced by 14-MeV neutrons. The contributions to the total spectrum due to third-, second-, and first-chance fission are shown. Energy-dependent compound-nucleus formation cross sections have been used.

7. <u>ENDF/B-V Decay and Cross-Section Data</u> (England, Wilson, LaBauve)

All ENDF/B-V yield data and cross-section data have been processed into CINDER-10 and general purpose multigroup libraries. Decay spectra for $\beta^{\pm}$, γ, α, neutrino, and antineutrino are in 158 groups for each nuclide in units of energy and particles per energy group. These are data for 877 fission products and 60 actinides, of which some 237 have cross-section data processed into 154 neutron energy groups. The actinide data have been augmented with decay data for an additional 84 nuclides (not in ENDF/B-V format).

Extensive microscopic tests have been made and current testing of integral data is in progress. Figure B-6 shows a comparison of ENDF/B-V and the 1978 ANS/ANSI 5.1 Decay Power Standard. The new results are believed to be too small in the gamma energy component and too large in the beta energy. A comparison with the Los Alamos decay-heat experiment[1] based on a 2×10^4 s irradiation is given in Fig. B-7.

---

[1]J. Yarnell and P. Bendt, Los Alamos Scientific Laboratory report LA-7452-MS (1978)

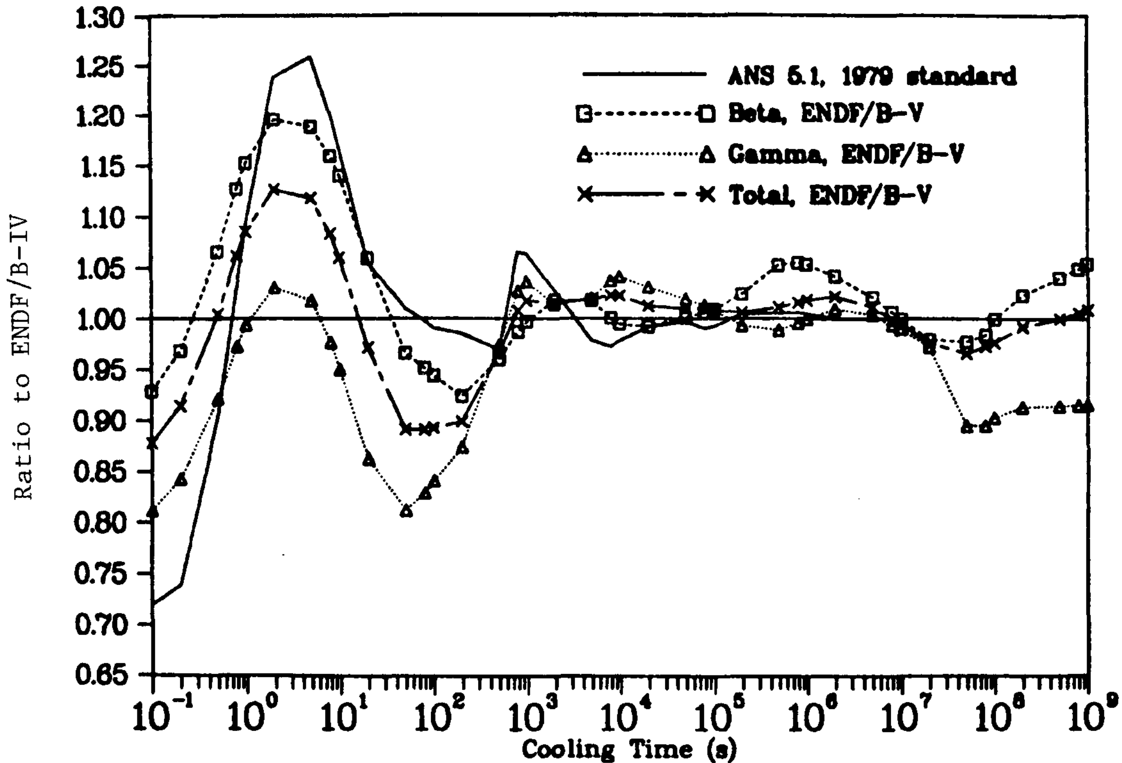

Fig. B-6. ^{235}U thermal fission pulse comparison of ANS 5.1 and calculated ENDF/B-V fission-product decay powers as ratios to ENDF/B-IV.

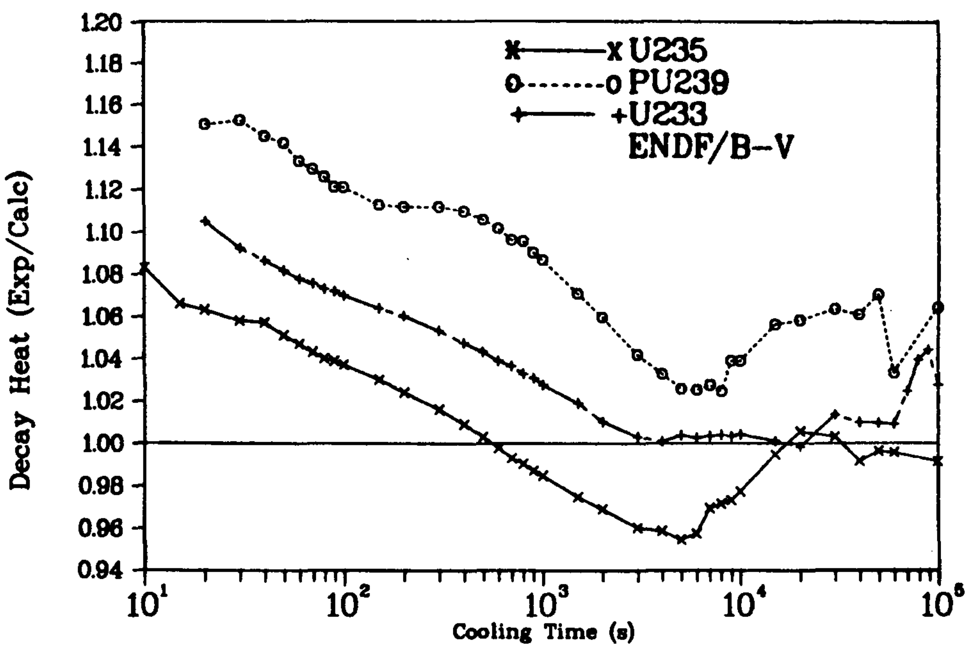

Fig. B-7. Ratio of experimental to calculated decay heat for a 2×10^4 s irradiation at constant flux.

8. Delayed Neutrons (England, R. Schenter, F. Schmittroth)

Extensive measurements of delayed neutron branching fractions (Pn) have become available along with delayed neutron energy spectra for individual precursors. A set of Pn values is given in Ref. 1 including values computed at Los Alamos based on systematics for those emitters having no measured values (105 precursors). For 24 important precursors, Rudstam[2] has supplied his measured spectral shapes. These precursors account for ≈ 80% of the total number of delayed neutrons per fission. Using the new Pn values and the ENDF/B-V fission yields, the aggregate equilibrium spectra has been calculated. A comparison with the ENDF/B-V evaluation is given in Fig. B-8.

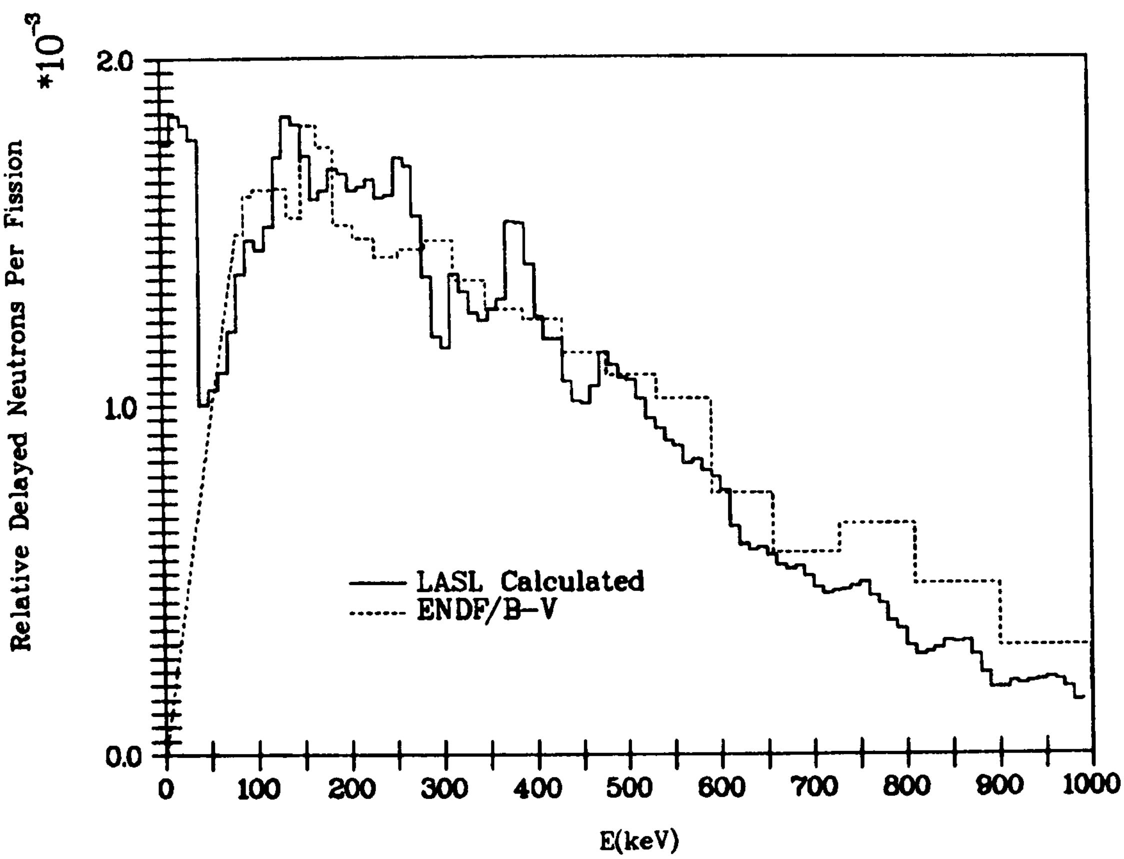

Fig. B-8. Comparison of calculated and ENDF/B-V evaluated delayed neutron spectra from ^{235}U thermal fission.

---

[1]T. R. England, R. E. Schenter, and F. Schmittroth, Proc. Int. Conf. on Nuclear Cross Sections for Technology, NBS Special Publication 594, p. 800 (1980).

[2]G. Rusdstam, personal communication (1979).

UNIVERSITY OF LOWELL

A. NEUTRON CROSS SECTIONS

1. Neutron Inelastic Scattering Cross Sections For ^{232}Th and ^{238}U for States above 600 keV in Excitation.

(L.E. Beghian, G.H.R. Kegel, G.P. Couchell, J.J. Egan, A. Mittler, D.J. Pullen, W.A. Schier, J.H. Dave (Menachery)*, J.H. Chang, C. Ciarcia and J. Shao).

The analysis of the data from (n, n'γ) measurements on ^{232}Th and ^{238}U has been completed, yielding neutron level cross sections for 46 states in ^{232}Th ranging in excitation energy from 714 keV to 1834 keV, and 27 states in ^{238}U from 680 keV to 1516 keV, at neutron bombarding energies in the range 0.7-2.1 MeV. These inferred cross-sections have been supplemented by neutron data obtained from (n,n') measurements using disk scatterers. Our time-of-flight spectrometer, optimized for detection of 250-400 keV neutrons, has achieved an overall energy resolution of 15 keV. We have investigated the incident energy range 0.7-2.1 MeV, in 50-keV steps following each neutron group corresponding to the states observed in the (n,n'γ) work, for an energy interval of 250-400 keV above the threshold of the level. This gives us cross section measurements at three or four energies for each state. Such direct measurements are useful in determining whether any of the cross section values inferred from (n,n'γ) are lower than those obtained from (n,n') due to strong E0 transitions as suggested by McMurray *et al.*[1] Some preliminary results for ^{222}Th are shown in Figure A-1. The analysis of this (n,n') data for outgoing neutrons in the energy range 200-400keV is in progress.

The next stage of our (n,n') program for ^{232}Th and ^{238}U will be measurements for incident neutron energies of 1.1-2.1 MeV with resolution optimized for outgoing neutrons in the range 400-900 keV. These measurements will correspond to regions of the (n,n'γ) excitation functions where feeding from higher levels may be significant and any discrepancy between the two sets of results may be attributed to unobserved feeding gamma-ray transitions.

---

*Current address, Triangle Universities Nuclear Laboratory.

[1] McMurray, van Heerden, Barnard and Jones, Southern Universities Nuclear Institute Annual Research Report, SUNI-45,5(1976).

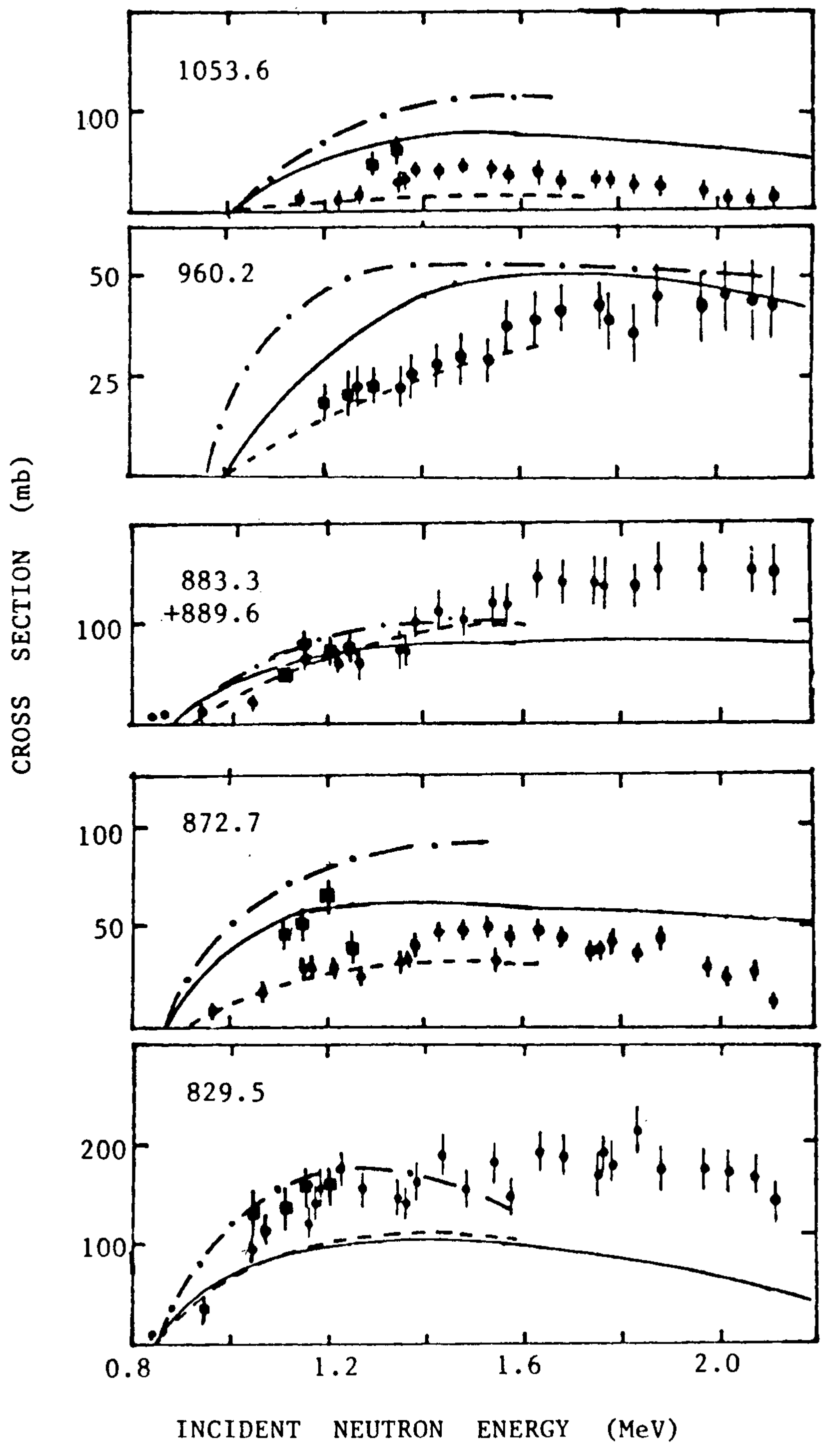

Fig. A-1. Cross sections for levels from 829.5-1053.6 keV in ^{232}Th obtained from (n,n',γ) (dots) and (n,n') (squares) measurements. Dashed lines represent the (n,n',γ) (---) and (n,n') (-·-) data of McMurray et al. [1] and the solid lines represent the theoretical compound nucleus calculations.

2. Near-Threshold $^{238}U(n,n')\ ^{238}U^*(45keV)$ Measurements (K. Traegde, W.A. Schier, G.P. Couchell and G.H.R. Kegel).

Inelastic neutron scattering from the first excited state of ^{238}U at 45keV has been measured at incident energies as low as 36 keV above its threshold. The measurements (see Figure A-2) were made in a ring geometry at flight paths of 50 cm. Corrections for neutron attenuation and multiple scattering, neutron detection efficiency and the inelastic angular distribution shape will soon be completed resulting in absolute cross section values at incident neutron energies of 81, 99 and 122 keV. These measurements will be extended to span the incident energy range from near-threshold up to 1 MeV. Similar measurements will be made for ^{232}Th.

3. Unfolding of Neutron Time-of-Flight (TOF) Spectra. (G.P. Couchell, G.H.R. Kegel, C.A. Ciarcia, S.F. LeBrun).

The spectra obtained in our $^{238}U(n,n')$ work reveal considerable complexity, especially in the 1000 to 1200-keV excitation energy region. The frequent occurrence of overlapping peaks requires the use of an unfolding code to obtain reliable yield data. This code approximates, in a weighted least-squares fashion, the measured neutron TOF spectrum by a linear combination of standard response functions. These response functions depend on the geometry of the experiment, the type of scatterer used, the timing performance of accelerator and detector, and on neutron target thickness and kinematics. We have developed several procedures to obtain response functions. Two codes which use our response functions in the unfolding of neutron TOF spectra are under development. Both codes will be used concurrently to obtain a basis for their evaluation.

4. Multiple Scattering Corrections (G.H.R. Kegel)

We have continued our investigation of neutron multiple scattering. The following procedure may be used to obtain an estimate for the ratio of multiple to single scattering,

$$\xi = \frac{\text{Multiple Scattering Probability}}{\text{Single Scattering Probability}}$$

and we assume isotropic scattering.

Kinney[2] has noted the commonly accepted approximation that the ratio γ of (n+1)-fold scattering probabil-

---

[2] W.E. Kinney, Nucl. Intr. Meth. 83, 15(1970)

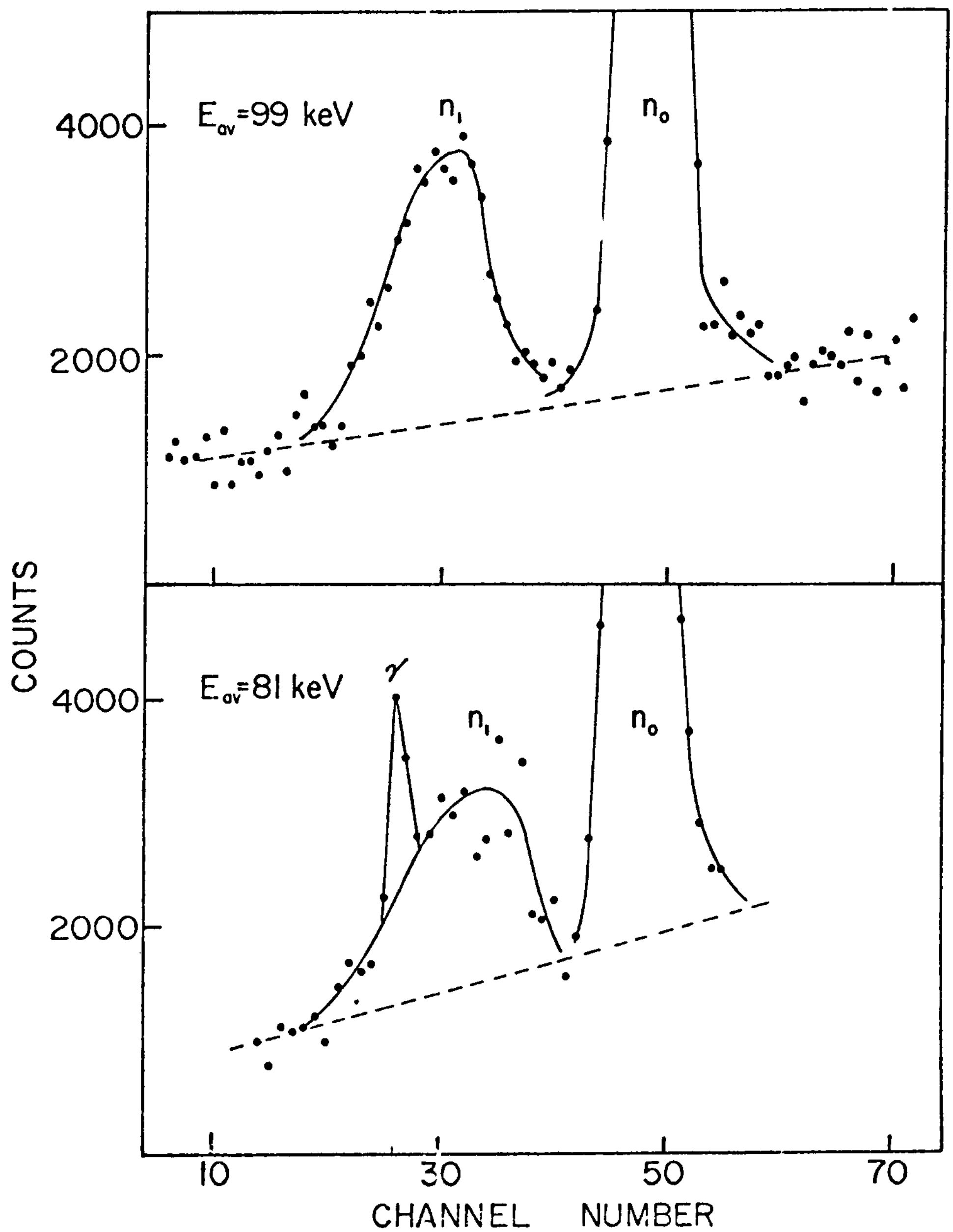

Fig. A-2. Neutron time-of-flight spectra for incident neutron energies of 81 and 99 keV.

ity, $P^{(n+1)}$, to n-fold scattering probability, $P^{(n)}$, is independent of n. This ratio is expected to be proportional to the average differential scattering cross section, $(d\sigma/d\Omega)_{av} = \sigma/4\pi$, to the concentration of scattering nuclei, C, and to a geometrical factor, D, which measures the average inverse square separation between two volume elements $d\tau_1$, and $d\tau_2$:

$$D = \frac{1}{V}\iint \frac{d\tau_1 d\tau_2}{R^2_{12}}.$$

For a spherical scatterer D = $2\pi R$, where R is the scatterer radius. The relation should also hold for a compact, nonspherical scatterer, R then being the radius of the equivalent sphere with volume equal to that of the scatterer. It follows that:

$$\frac{P^{(n+1)}}{P^{(n)}} = \gamma = \frac{\sigma CR}{2}.$$

We introduce the total scattering probability, P, and the multiple scattering probability $P^{(>1)}$ and obtain:

$$P = \sum_{n=1}^{\infty} P^{(n)} = P^{(1)}\sum_{n=0}^{\infty} \gamma^n = P^{(1)}\frac{1}{1-\gamma}$$

$$P^{(>1)} = P - P^{(1)} = P^{(1)}\frac{\gamma}{1-\gamma}$$

so that

$$\xi = \frac{P^{(>1)}}{P^{(1)}} = \frac{\gamma}{1-\gamma} = \frac{\sigma CR}{2-\sigma CR}.$$

We can now use our simple model to obtain an upper bound for γ. If we require $\xi < 1/2$, then $\gamma < 1/3$ so that the scatterer radius, or its equivalent, should be consistent with:

$$R < \frac{2}{3}\frac{1}{\sigma C}.$$

The implicit energy dependence of R should be noted; a scatterer, which is quite adequate for 1-MeV work where the neutron cross section is small, may be too large when used with 100-keV neutrons because σ is larger.

5. Theoretical Investigations

a. Theoretical Calculations of Neutron Inelastic Scattering Cross Sections for ^{232}Th and ^{238}U (E. Sheldon and D. Chan).

Further progress has been made in the computation of inelastic scattering cross sections for fast neutrons on ^{232}Th and ^{238}U over the incident energy range 0.8-2.5 MeV for comparison with experimental data acquired for most of the first twenty excited levels in both nuclei. The Compound-nucleus contribution was calculated using the code "CINDY", including the effect of competing levels but not making allowance for width-fluctuation corrections of the Moldauer type, and the direct-interaction contribution as obtained from the coupled-equations program "JUPITOR" in a modification of the Karlsruhe version. For the latter, estimated values of the respective coupling strengths were employed for each of the coupled levels, based upon a surmised rotation-vibrational collective-band scheme. The incoherent sum of these contributions provided only a fair overall fit to the data: the match to experimental data was particularly poor in the case of higher levels of low nuclear spin. A sample of these preliminary results are reproduced in Figure A-3; they were presented in Poster Sessions at the Polish Summer School in Nuclear Physics, held in September, 1980 in Mikolajki, Poland, but have not been published, pending further investigations which are now underway. In these subsequent studies, the values of the coupling strengths have been varied to derive an optimal fit, and additional levels have been included in the analyses. The program "KARJUP" has been recomplied. Improving its accuracy into a more expeditious version. The optical-model potential due to Haout has been employed throughout; the calculations are currently approaching completion and will be prepared for publication.

At the same time, work has continued on the assembly of a computer program to undertake the calculation of these cross sections as a function of energy and coupling strength in the "unified CN/DI" formalism due to Tepel, Hofmann, Weidenmuller, and others. In this S-matrix approach, allowance is made for fluctuations and all channels are coupled within a comprehensive formalism that employes the entire (extended) S-matrix element array. It is anticipated that the current version will be completed by this summer, and that its results will offer a further improvement in the fit to experimental data. Arrangements have been made to obtain a running version of the coupled-channels program "ECIS" as a basis for comparison with the data so obtained.

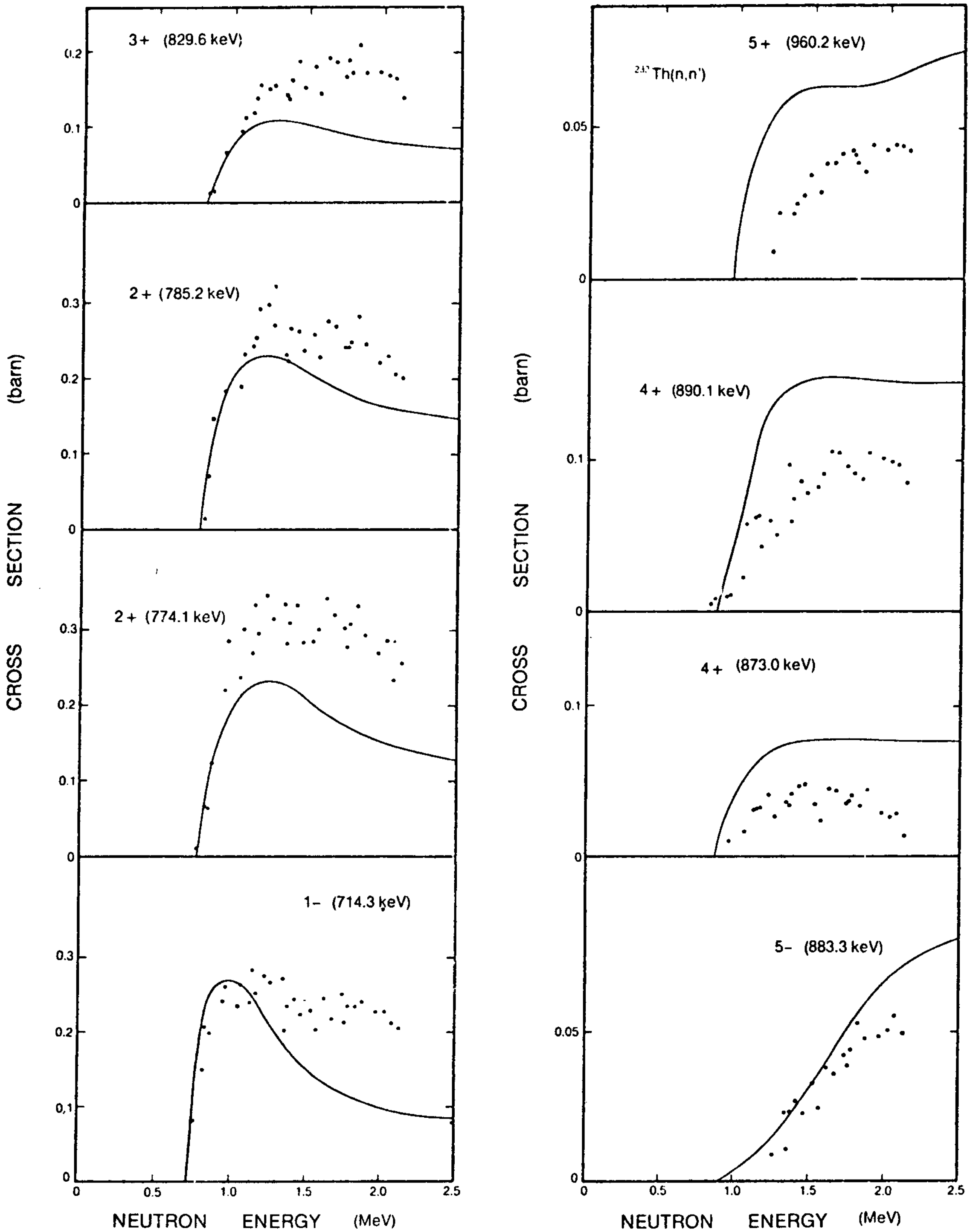

Fig. A-3. Excitation functions for eight levels in ^{232}Th, in which the measured cross sections inferred from (n,n',γ) data are compared with theoretical curves obtained from an incoherent combination of computed magnitudes for CN and DI mechanisms, using strong coupling for the latter.

b. Magnetic Substate Population Characteristics (E. Sheldon).

Further investigations into the character of the population of nuclear magnetic substates in the course of scattering and other reactions have been pursued, and reported at a Europhysics Study Conferrence, held in October 1979 at Hvar, Yugoslavia.[3] A review of the entire body of data for nuclei of integer and half-integer spin has been compiled, and presented at the Polish Summer School in Nuclear Physics, held in September, 1980 at Mikolajki.[4]

B. DELAYED-NEUTRON ENERGY SPECTRA OF FISSIONABLE ISOTOPES (G.P. Couchell, W.A. Schier, J.J. Egan, G.H.R. Kegel, A. Mittler, D.J. Pullen, C. French, and N. Sampas)

We plan to study the distribution in energy and time of delayed neutrons following neutron-induced fission of a number of reactor fuel materials. Neutrons will be generated by the $^{7}Li(p,n)^{7}Be$ reaction using the University of Lowell 5.5-MV Van de Graaff Accelerator. Initially we shall employ a rather thick lithium target to produce neutrons spanning a broad energy band from 0 to 3.6 MeV. If intensity conditions prove favorable we shall supplement these measurements with others utilizing a narrower incident energy range, e.g., $\Delta E_n = 0.5$ MeV, and study delayed-neutron emission as a function of incident energy. These studies will be supplemented by measurements performed with the University of Lowell 1-MW swimming-pool reactor which will provide various reactor-type neutron spectra. The thermal column is a source of thermal neutrons; with proper combination of full plates and thermal neutron absorbers it can also generate a Watt prompt-fission spectrum. Neutron spectra of intermediate hardness are available in the reactor beam ports.

---

[3] E. Sheldon, Fizika 1979, 11, (suppl. 2), 65-70; Proceedings of the Adriatic Europhysics Study Conference on Statistical Properties of Nuclei, Hvar, Yugoslavia, Oct. 1-5, 1979 "Statistical and Non-Statistical Behaviour in the Population of Nuclear Magnetic Substates".

[4] E. Sheldon, Invited Talk at the XIII. Polish Summer School in Nuclear Physics, Mikolajki, Masuria, Poland, Sept. 1-12, 1980; to be published in Nukleonika (1980/1) "Nuclear Magnetic Substate Populations".

Accelerator-produced or reactor-produced neutrons will be incident on thin foils of fissionable material. Our initial study will concentrate on ^{235}U and ^{239}Pu because of their importance for fast-reactor kinetics calculations. Once the experimental procedure has been optimized we propose to extend our investigations to include ^{233}U, ^{238}U and ^{232}Th.

One of the main difficulties besetting delayed-neutron measurements is caused by the intense background of incident and promopt fission neutrons and gamma-rays. Typically 10^9 s^{-1} incident neutrons may produce 10^5 s^{-1} prompt fission neutrons and gammas and 10^3 s^{-1} delayed neutrons. A helium jet gas transport system will be used to rapidly transfer recoiling fission fragments to a low background counting room outside the target area or reactor environment. The fragments will be swept by a helium gas stream at nearly sonic speeds, allowing transfer times of less than 50 ms over distances as large as 10 m. At the exit of the jet transfer system the fragments are imbedded into a moving tape of a tape transport system. Each segment of the moving tape thus contains fission fragments generated during a well defined earlier time interval. The contribution of each delayed-neutron Group (the accepted six-group time parameters will be assumed) can be enhanced in a particular spectrum by proper choice of tape segment for investigation.

Delayed neutrons will be detected by a specially designed neutron spectrometer utilizing four ^{6}Li-loaded glass scintillators 4-1/2" diameter by 1/4" thick. The spectrometer is designed with special emphasis placed on the study of the low-energy-region, 10 keV $\leq E_n \leq$ 200 keV, of the spectrum where present data show large discrepancies. Neutron energies will be determined by the neutron time-of-flight technique using beta particle-delayed neutron correlations for timing purposes. The spectrometer has a high overall neutron detection efficiency (.05-.10%) with a smooth energy response and excellent energy resolution ($\Delta E/E$ = 10%) for 10 keV $\leq E_n \leq$ 250 keV. Four Pilot U plastic scintillators will be used to measure the high-energy-region, $E_n >$ 200 keV, of each delayed-neutron spectrum.

The moving tape containing fission fragments passes between two closely spaced beta-particle detectors which define the section of the tape to be investigated. The beta detectors are shielded from beta particles emitted from neighboring segments. Even though the spectrometer is sensitive to thermal neutrons (inevitably there are moderated neutrons included in any spectral measurement), the time-of-flight technique which requires neutron-beta correlation for processing a signal allows rejection of all but 1-2% of those thermal neutrons that interact with the detector. Thermal neutron pulses that are processed correspond to events that accidentally fall within 400 ns of a beta pulse and so form a constant background throughout the time-of-flight spectrum. This rather innocuous thermal neutron background contrasts sharply with the situation for measurements involving ^3He spectrometers, where thermal neutrons interfere seriously with the low-energy portion of delayed-neutron spectra. ^6Li-Loaded detectors are also less sensitive to background gamma-rays than ^3He detectors. In addition the time-of-flight technique permits rejection of most randomly occurring gamma-rays and segregates those gammas correlated with beta emission to the prompt gamma-ray peak, which in no way interferes with the neutron portion of the time-of-flight spectrum.

A typical spectrum is expected to require approximately twenty-four-hours acquisition time. A significant gain in counting efficiency and improved relative normalization among different spectra will be achieved by simultaneously measuring the spectra of three different tape segments with each segment having an enhanced contribution from a particular delayed-neutron Group. Relative normalization of each spectrum to a common fission-fragment yield can be achieved by having each series of measurements contain at least one tape segment in common with another series. Simultaneous acquisition of spectra will require three sets of beta detectors and accompanying electronic logic for proper routing of spectrometer events. Furthermore pulses must be rejected if two or more beta detectors record events during a time interval, e.g. 400 ns, selected as the range of the time-of-flight spectrum or if a second beta particle is detected in one detector within the 400 ns interval.

Studies of the characteristics of the helium jet and tape transport systems are now under way using a ^{252}Cf spontaneous fission source. The neutron spectrometer will be assembled and tested during the summer of 1981. Preliminary measurements with fission foils are expected to begin by the end of the year.

THE UNIVERSITY OF MICHIGAN
Department of Nuclear Engineering

I. OVERVIEW

Over the past year, our efforts in The University of Michigan cross section project have been directed toward two general objectives: continuing measurements using our photoneutron facilities, and the development of equipment and a new laboratory to extend our capabilities into the 14 MeV neutron energy range.

The work in our photoneutron laboratory has concentrated on measurements of the capture cross sections in In-115 and Th-232. These measurements are nearly completed, and we do not now anticipate the start of any new photoneutron measurements in the near future. Nonetheless, we will continue to devote enough attention to maintain these facilities because of their valuable and unique nature. In particular, we will continue to maintain our maganese bath source calibration facility because of the excellent documentation on its efficiency that we have accumulated over nine years of operation.

Our emphasis for the future has shifted to the 14 MeV measurements. Over the past year we have successfully refurbished and operated a 150 keV neutron generator in a well-shielded and low-scatter laboratory. Many aspects of the associated electronics and detection apparatus also have been designed and fabricated. Our initial measurements are aimed at fission cross sections of the common uranium and plutonium isotopes.

II. MEASUREMENTS WITH PHOTONEUTRON SOURCES (D. J. Grady, Grady, G. T. Baldwin, and G. F. Knoll)

A. In^{115} Capture Cross Section Measurements

The In^{115} capture cross section is being measured at the four following photoneutron energies: 23, 265, 770 and 964 keV. The reactions of interest are the following:

$$In^{115}\ (n, \gamma)\ In^{116m2}$$

$$In^{115}\ (n, \gamma)\ In^{116m1}$$

The measurements have involved the use of several different techniques and components. As in our previous fission cross section work, we have made use of the photoneutron sources, the mananese bath calibration system and the VES Monte Carlo computer program for the modelling of the photoneutron sources. In addition, we have developed a $4\pi\beta$ gas flow proportional counter beta-gamma coincidence counting, and an indium foil holder which allows for both the accurate placement of the foil during the irradiation and the precise determination of the source-foil separation. All experimental measurements have been completed, and we are now in the final stages of data analysis.

Indium Target Foils and Activation

A set of eight, 3/4" diameter indium foils with a thickness of 0.006 cm were prepared from 99.999% pure indium ribbon. Foil masses of about 0.14 gm were measure to an accuracy of $\pm$ 20 micrograms. Three precision machined foil holder assemblies were constructed with adjustable stainless steel spacers to allow the activation of indium foils at spacings ranging from 0.4 cm to 9.0 cm between the foil and the source surface. These assemblies were attached to the removable source well bottom plate that supports the source, centered over the foil and fixed by a positioning ring within the source well. This design facilitated the precise measurement of the source surface-to-indium foil spacing. The activations took place for between one and three hours and at several different spacings. The different spacings were required in order to obtain the room return contribution to the indium activity.

Absolute Activity Determination and the Beta Detector Efficiency

Once activated, the indium foil absolute disintegration rate must be determined. This was done in two steps. The foils were first counted in the $4\pi\beta$ gas flow proportional counter. The second and much more difficult step was the determination of the beta detector efficiency for the decay of the In^{116m1}. This step was accomplished using a combination of $4\pi\beta$-γ coincidence counting and beta detector efficiency variation. The experimental technique involved the detemination of the apparent beta efficiency for a series of modifications in this efficiency created by the use of aluminium absorbers covering the indium foils. Graphical analysis of these data gave rise to a spectrum or "K" correction factor which accounts for the extremely complicated interaction of In^{116m1} decay scheme components with the beta detector. Further experiments were performed to determine possible effects on the efficiency due to variation in foil thickness or non-uniformity in the activity across the foil caused by variations in the flux profile.

Neutron Source Strength and Correction Factors

As in all of the past cross section meaurements, we rely on the manganese bath for our neutron source strength deteminations. Uncertainties in the source strength of about $\pm$ 0.7% are limited by the uncertainties in our local standard, a Cf^{252} neutron source. Plans are underway to indirectly recalibrate this local standard against NBS-I using an intermediate standard Cf source shipped from the National Bureau of Standards.

Several correction factors will also be required for this measurement series. Neutron scattering from the experimental package and containment is handled with a discrete element approximation that accounts for neutron scattering anisotropies. Scattering from the target foil backing is handled by a Monte Carlo path length procedure due to the extremely close proximity of the scatterer and target.

The contribution of competing neutron-induced reactions in indium to the In^{116m1} activity must also be accounted for. Inelastic scattering reactions in In^{113} and In^{115} give rise to metastable states whose decay may be detected in the proportional counter. Beta detector efficiencies of 0.2% and 30.7% for these two isotopes (In^{113m} and In^{115m} respectively) have been determined using absolute gamma counting techniques.

Additional corections for the contribution of room return activity to the total indium activity and neutron energy spectrum effects are also being determined in the capture cross section measurements.

B. Absolute Measurement of the ^{232}Th (n, γ) Cross Section at 24 keV

Overview of Method

This experiment is based on neutrons from a spherical Sb-Be photoneutron source. A relatively large cylindrical target of natural thorium is irradiated for approximately two weeks. The flux is calculated by Monte Carlo modeling. The source strength is calibrated against a Cf-252 standard as in previous measurements using a manganese sulfate bath system. Neutron captures in thorium initiate the sequence:

$$^{232}Th(n,\gamma)^{233}Th \xrightarrow[t_{1/2}=22min]{\beta^-} {}^{233}Pa \xrightarrow[t_{1/2}=27\ day]{\beta^-} {}^{233}U$$

The cross section is obtained from a determination of the absolute amount of ^{233}Pa produced. A Ge(Li) detector is used to count the 312 keV gamma line in ^{233}Pa decay, for which the branching ratio is well known. To improve the geometry of the counting and isolate the low-level ^{233}Pa activity from high natural thorium background, the protactinium is first separated from the target chemically. A solvent extraction is performed with diisobutylcarbinol, with another isotope (^{232} Pa) employed as a tracer to measure protactinium recover. Experimental work is nearly complete, and analysis will provide a cross section value within the next several months.

Thorium Target and Irradiation

Three targets of natural thorium metal have been obtained from the Isotope Target Laboratory at the Oak Ridge National Laboratory. Each target is a flat sheet 0.05cm (0.020") thick, which is rolled into cylindrical shape (12 cm. high x 4 cm. radius) and clamped in place on a supporting framework. This framework consists of a 5 cm. O.D. brass source well with the 8 cm. I.D. target mounted concentrically. Two aluminum rings top and bottom hold the target to the source well in this geometry. The source is supported in the well at the midpoint of the target by an aluminum crosspiece insert. Much of the wall of the brass source well was machined away to reduce the scattering perturbation.

A computer code was written to model neutron transport specifically for the source-target geometry used in this measurement. A spherical source of finite extent emits neutrons uniformly but distributed in polar angle according to the description provided by the VES code. Neutron histories are traced to the enclosing thorium cylinger, where their path lengths through the target are summed. This sum, appropriately normalized, gives the average scalar flux at the target.

The cylindrical target geometry has an advantage of being relatively insensitive to error in source position. A quantitative analysis was made to determine the deviation of the average scalar flux seen by the target as a function axial and radial source position offsets from center. This study was performed for a variety of target dimensions before selecting the present configuration.

Chemical Separation

A carrier-free solvent extraction scheme to chemically separate protactinium from thorium has been developed and demonstrated using reactor activated thorium. Excellent radiochemical purity has been achieved, and recovery yields on the order of 70% have been accomplished with approximately 2μCi of ^{233}Pa in 100 grams of thorium.

The quantitative yield from this extraction is measured by using a tracer amount of ^{232}Pa. A solution of this isotope is sampled volumetrically by micropipette: one aliquot is used to spike the dissolved neutron-activated thorium target; one or more other are used as control samples (do not go through the separation). After separation, the liquid volumes are made equal and the samples counted in the same geometry. The ratio of the counts in the prominent 969 keV gamma peak gives the yield directly.

Absolute ^{233}Pa Activity Measurement

The ^{232}Pa tracer isotope has only a 1.3 day half-life, and therefore quickly decays to reduce the Compton continuum background that underlies the 312 keV peak of the 27 day half-life ^{233}Pa (equal volume, same geometry) used as a reference. The reference sample in turn is produced in advance of the activity measurement by equal-volume sampling of a ^{233}Pa stock solution (from a chemical separation of reactor activated throium) both into the liquid counting container and onto a planchet which is dried. The evaporated deposit is then standardized by absolute Ge(Li) counting. The Ge(Li) detector efficiency is calibrated using a mixed radionuclide standard obtained from Amersham-Searle and traceable to NBS.

C. Angular Distribution of Fission Fragments (with J. Meadows, ANL)

Accurate knowledge of the fission fragment angular distribution is needed for the various neutron energies at which our fission cross section measurements have been made. The need arises from the fact that we utilize limited solid angle counting to determine fission rates. These measurements have been made using the Tandem Dynamitron Neutron facilities at ANL.

Work on the Pu^{239} fission fragment anisotropy has been completed. In the analysis of the data, corrections were made for solid angle effects, neutron scattering, lower energy neutron groups and smearing effects caused by the finite angular resolution. The data were fitted to the expression

$$W(\theta) = 1 + A\cos^2(\theta)$$

where "W(θ)" is the normalized angular distribution, "θ" is the center-of-mass angle between the incident direction and the fission fragment direction and "A" is the anisotropy coefficient. Our results are tabulated below:

ENERGY	ANISOTROPY
265 keV	$.035 \pm .012$
770 keV	$.076 \pm .011$
964 keV	$.106 \pm .020$

Similar data have also been completed for U^{233} and Np^{237}. Analysis is near completion and these results should be available shortly.

D. Fast Fission Cross Section for U^{233}

We have completed a series of measurements with five photoneutron sources ranging from 23 to 964 keV on U^{233}. Techniques were similar to those described for our previous fission cross section measurements. Final cross section values will be published upon completion of the angular distribution results described above.

III. FACILITY DEVELOPMENT AND PRELIMINARY MEASUREMENTS AT 14 MeV (M. Mahdavi, K. Zasadny, and G. Knoll)

A new laboratory has been developed and equipped to carry out cross section measurements at 14 MeV. A 150 kV Cockroft-Walton accelerator has been installed on a low-mass flor situated near the midpoint of a large well-shielded experiment roon. Auxillary equipment has been developed and tested to provide monitoring of the neutron yield from tritium targets, neutron energy measurement, and tritium discharge level. Efforts have concentrated on establishing a stable and well-aligned deuteron beam to provide a suitable neutron source cross section measurements and other physics experiments.

During the coming year, we will begin to carry out a series of absolute cross section measurements that will extend the experience gained at lower energies in our photoneutron program. Elements common to both will include a common set of target foils, a $4\pi\beta$ counter for activity determination, and a number of experimental techniques. For the fission measurements, these techniques include limited solid angle product detection and the use of track etch films for fission fragment counting.

The 14 MeV measurements will concentrate initially on a series of fission cross sections for U-235, Pu-239, U-233, and Np-237. Additionally, a target foil of U-238 will be obtained in order to add this isotope to the series. As this measurement program matures, we plan to investigate a series of other cross sections of importance in fast neutron dosimetry and in transmutation processes.

This program is being carried out in collaboration with Professor Craig Robertson of the University of New Mexico.

A. NEUTRON PHYSICS

1. Measurement of the ^{235}U(n,f) Cross Section at 14.1 MeV

(O. A. Wasson, A. D. Carlson, K. C. Duvall)

The absolute ^{235}U(n,f) cross section was measured at the 3 MV Positive Ion Van de Graaff Laboratory. The 14.1 MeV neutron fluence was measured using the time-correlated associated-particle technique with the ^{3}H(d,n)^{4}He reaction. The measured cross section of (2.080±0.03)b is consistent with the ENDF/B-V evaluation and agrees within 1% with the results of Cancé and Grenier[1] and Adamov et al.[2] The present status of all measurements using this technique is shown in Fig. A-1. These measurements, which were done in four separate countries and were based on three independent mass scales, are consistent within the approximately 1.5% uncertainties and indicate that the ^{235}U cross section is known to an ∿ 1% uncertainty in the 14 MeV region.

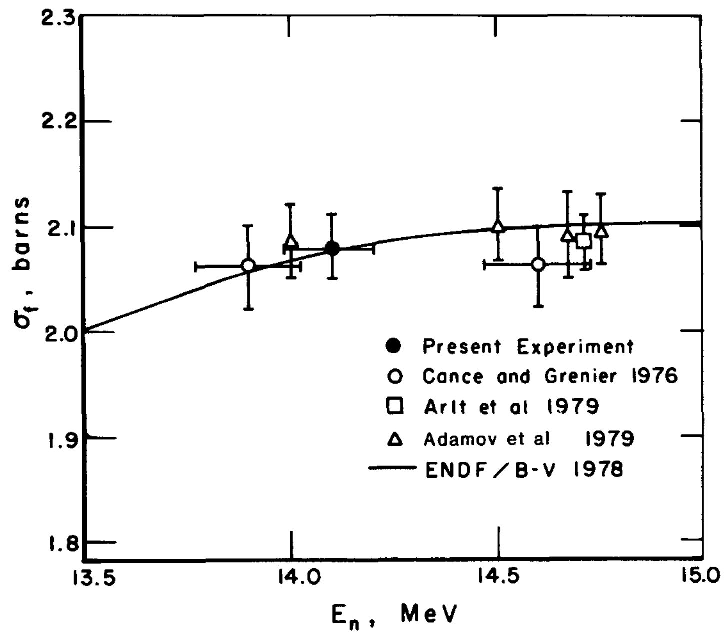

Fig. A-1. The ^{235}U(n,f) cross section measured with the time-correlated associated-particle technique.

1 M. Cancé and G. Grenier, Nucl. Sci. Eng. 68, 197 (1978).

2 V. M. Adamov et al., NBS Special Publication 594, p. 995 (1980).

2. Measurement of the ^{235}U Areal Density of ^{235}U Fission Deposits (A. D. Carlson, O. A. Wasson)

The total ^{235}U mass and areal density of the deposits used in the 14 MeV cross section measurement were measured relative to the standard Los Alamos Spare Number 1 using thermal neutron induced fission counting at the thermal column of the NBS Reactor. The areal density of Los Alamos Spare Number 1 was determined to be uniform within 1% using both optical techniques and thermal neutron fission counting. We obtained an areal density of $(500.8 \pm 1.3) \mu g/cm^2$ for the reference deposit and a value of $(1042 \pm 4) \mu g/cm^2$ for the two deposits used in the cross section measurements. The total ^{235}U mass was determined by both thermal neutron induced fission and by the alpha-particle decay rate.

3. An Absolute Measurement of the ^{235}U(n,f) Cross Section from $\sim$ 300-1500 keV Neutron Energy (A. D. Carlson)

Diagnostic work pertinent to this measurement has been completed. Preliminary data have been obtained and final data taking will begin soon. The measurements are being made at the NBS Neutron Time-of-Flight Facility. The determination of the neutron flux is being made with a large plastic scintillator (black detector) of known absolute efficiency located 200 m from the neutron target. On the same beam line at 68 m from the target, a well-characterized ^{235}U thin film fission chamber is being used to measure the reaction rate. This absolute measurement will be compared with earlier relative measurements[3] on the NBS linac and absolute measurements[4] recently completed at the NBS Van de Graaff facility.

4. An Investigation of Structure in the (n,α) Cross Section of ^{6}Li Glass in the eV Energy Region (A. D. Carlson, J. W. Behrens)

Recent NBS measurements[5] indicate structure at $\sim$ 10 eV in the ratio of the (n,α) cross sections of $^{10}BF_3$ and ^{6}Li glass. Comparisons[6,7] of the (n,α) cross section of $^{10}BF_3$ with the (n,p) cross section of ^{3}He and the (n,α) cross section of solid ^{10}B suggest that the structure is in the ^{6}Li glass response.

---

[3] O. A. Wasson, Proc. of the NEANDC/NEACRP Specialists Meeting on Fast Neutron Fission Cross Sections, Argonne National Laboratory, ANL-76-90 and Supplement (1976).

[4] M. M. Meier, O. A. Wasson, and K. C. Duvall, Proc. International Conf. on Nuclear Cross Sections for Technology, U. of Tenn., NBS Special Publication 594, p. 966 (1980).

[5] J. B. Czirr and A. D. Carlson, Proc. of the Int. Conf. on Nuclear Cross Sections for Technology, U. of Tenn., NBS Sp. Publication 594, p. 84 (1980).

[6] Bowman, Behrens, Gwin, and Todd, same Conf. as Ref. 4, p. 97.

[7] Carlson, Bowman, Behrens, Johnson, and Todd, same Conf. as Ref. 4., p. 89.

Two experiments are proposed to test the results[5] obtained previously. The first experiment is a transmission measurement of a thick piece of enriched ^{6}Li glass. The second requires measuring the ^{10}B to ^{6}Li glass responses as was done previously. However, an enriched ^{6}Li glass scintillator will replace the natural abundance glass. The first measurement is now in progress and the second will be started when the enriched ^{6}Li glass has been obtained.

5. Inelastic Scattering of eV Neutrons from Molecules (R. G. Johnson, C. D. Bowman, A. D. Carlson)

The NBS linac has been used for the first measurements to our knowledge of the inelastic scattering of eV neutrons. The scattering of eV neutrons should excite high lying vibrational states and electronic states, and may lead to the ejection of an atom from a nucleus. None of these excitations are accessible with reactor neutrons.

The experiments were conducted at the 21 meter flight path of the NBS 100-MeV electron linac. A 0.625-cm thick sample of benzene was placed in the neutron beam which was collimated to a vertical slit 2.5 cm wide by 12.5 cm high. Scattered neutrons were captured in the 1.45 eV resonance of a rhodium foil located just outside of the collimated neutron beam. The rhodium capture events were recorded using a deuterated-benzene liquid scintillator to detect capture γ-rays. The energy of an incoming neutron was determined by the neutron time-of-flight along the 21 meter flight path using the γ-ray detection as the timing signal. The final neutron energy is always the energy of the resonance in the absorber. The energy difference is the energy taken up by the molecule. By doing measurements at different angles and also with different resonance absorbers, the momentum transfer in the interaction can be varied.

Fig. A-2 shows a spectrum measured using the Rh foil placed to accept neutrons scattered at an angle of $30^\circ\pm10^\circ$ from benzene. The incoming neutron energy in eV is shown on the lower abscissa; the momentum transfer in units of inverse angstroms is shown on the upper abscissa. The spectrum shows a sudden rise at 1.45 eV corresponding to elastic scattering and a decreasing trend of inelastic scattering at higher energies. Some structure is seen with decreasing definition as the energy increases. The vertical arrows show the center of several such possible structures. Note that the spacing between these arrows appears not to be uniform hinting at the possibility of detection of a sequence of vibrational structures exhibiting anharmonity. The relationship between levels is given by $E_\nu = A\nu - E\nu^2$ where ν is the order of the vibration, A is the spacing between levels for a harmonic oscillator and B is the anharmonic coefficient. An analysis of the structure shown indicates the values $A = 328+6$ meV and $B = -10.2\pm.2$ meV. The spacing of 328 meV does not correspond to any of the fundamental modes of benzene but appears to be a combination of hydrogen bend, and ring stretch or deformation normal modes. Why there should be a sequence of states involving a combination of normal modes is not clear. Definitive assignments must await measurements with a deuterated benzene sample.

Other spectra taken at higher values of momentum transfer show evidence for the excitation of electronic transitions and for measurements of the disassociation energy for both hydrogen and carbon.

This method is potentially a new source of information on molecular dynamics with implications for molecular physics and with applications in neutron dosimetry, neutron damage to materials and living tissue, and neutron moderation at low energy. If the deexcitation modes of these molecular excitations can be measured, these studies might lead to new or improved detectors for neutrons.

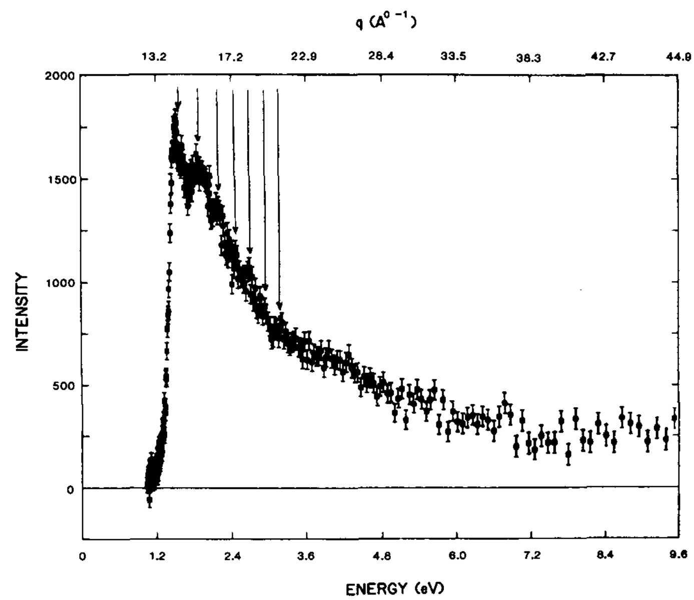

Fig. A-2. The inelastic scattering of eV neutrons from benzene. Incoming neutron energy is shown on the lower abscissa and momentum transfer on the upper abscissa. The vertical arrows are positioned over possible structures which may represent an anharmonic vibrational spectrum of benzene.

6. Powder Diffraction Studies by Neutron Time-of-Flight (R. G. Johnson, C. D. Bowman, A. D. Carlson, R. A. Schrack)

Recently we have recognized some distinct advantages in studying powder diffraction of neutrons in transmission geometry as opposed to the usual scattering geometry. The principal advantage is that in transmission geometry, which is effectively a measure of the scattering at 180°, there is no resolution broadening from angular dispersion. Consequently, the only contribution to the resolution of diffraction edges is the energy resolution of the time-of-flight system. For example, using a 60-m flight path the energy resolution is 0.2% at 0.01 eV and 0.08% at 0.3 eV. This should be compared to a resolution of 0.3% for the best powder diffractometers.

Preliminary results of a powder diffraction measurement using an iron sample are shown in Fig. A-3. Although these results were obtained using a 20-m flight path, similar measurements have been performed at 60 m and are presently being analyzed.

The primary use of high resolution powder diffraction will probably be in studying strain in materials. For that use the present technique has several attractive advantages: (1) Transmission geometry preserves the spatial distribution of the neutron beam. Thus the distribution of strains as a function of position in the sample can be measured. (2) The method is volume sensitive rather than surface sensitive and therefore provides information not obtainable by other common methods. (3) The pulsed character of the source can be exploited by examining the strains in a dynamic system (e.g., flywheel, reciprocating engine, etc.) synchronized to the source.

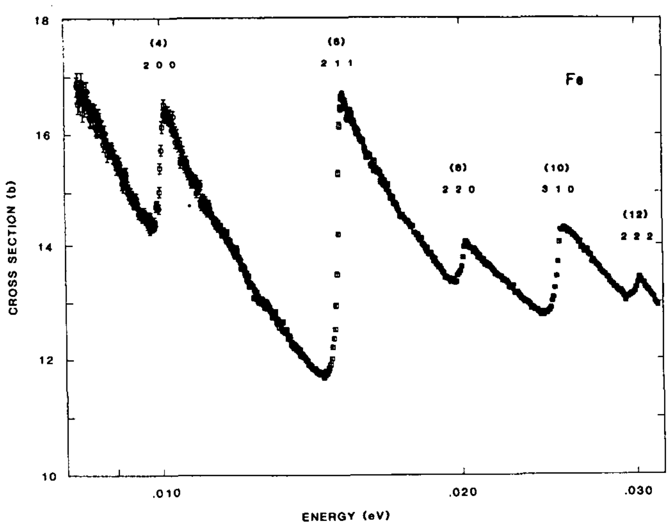

Fig. A-3. Neutron total cross section for Fe. Note the suppressed zero on the cross-section scale. The numbers above the diffraction edges are the indices of the plane producing that diffraction. The number in parentheses is the sum of the squares of the indices. --continued

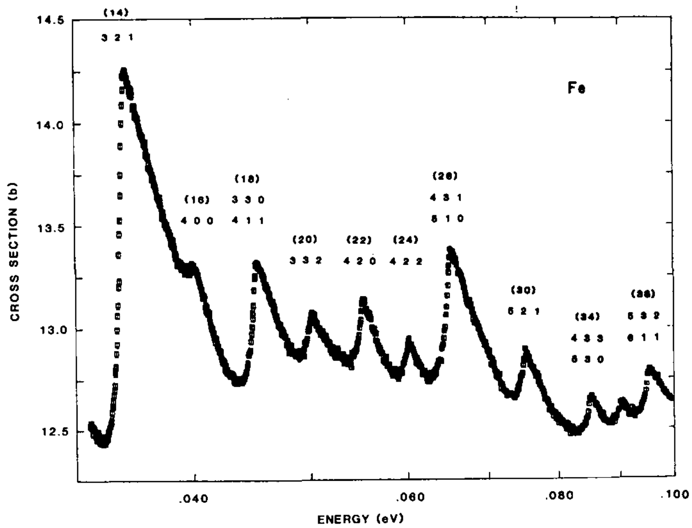

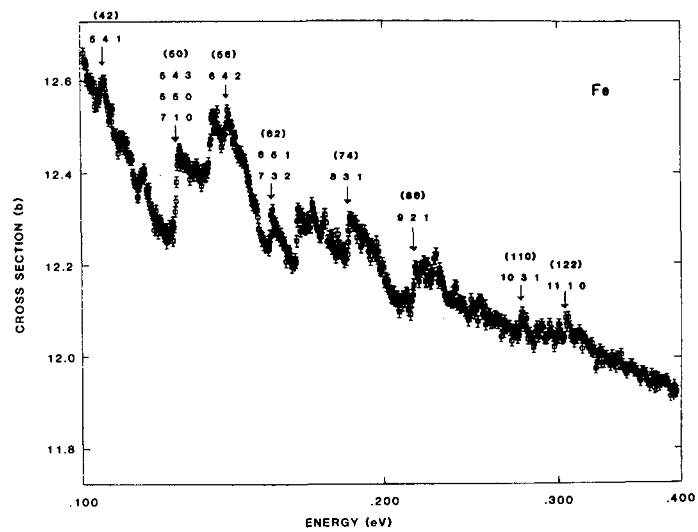

Fig. A-3.—continued— Neutron total cross section for Fe. Note the suppressed zero on the cross-section scale. The numbers above the diffraction edges are the indices of the plane producing that diffraction. The number in parentheses is the sum of the squares of the indices.

7. Spent Fuel Assay (J. W. Behrens, R. G. Johnson, R. A. Schrack)

A set of neutron transmission measurements has been made for samples of high burnup commercial power reactor fuel. Two samples were used, one was cut from the center of the fuel rod and one cut from an end. The pieces are approximately 2.5 cm thick and 1 cm in diameter. The measured gamma activity of the surface of the samples is about 5-10 rad. The transmission of the samples was measured from about 0.6 eV to about 50 eV on the 20 m flight path of the Linac facility. Figure A-4 shows the data with curve A being the end cut and B the center cut. Absorption lines for 16 isotopes have been identified.

The data consists of 8000 values for each sample so that a full non-linear search for 16 parameter values is not possible. Where possible a line shape fit for isolated resonances has been made and some preliminary results obtained that indicate the relative abundance of the major isotopes. Preliminary results of the analysis are given in Table 1 where both the absolute thickness in atoms per barn and the abundance relative to ^{238}U are given. Useful measurements were made on four isotopes of uranium, five isotopes of plutonium, two isotopes of americium, and five fission products. A comparison of the two transmission curves clearly shows the effect of higher burn-up on the center cut (curve B), compared to the end cut (curve A); ^{240}Pu at 1.05 eV, ^{242}Pu at 2.67 eV, and ^{235}U at 8.78.

The method opens up new possibilities for burn-up measurements or spent fuel assay. Since essentially all heavy actinides are measured, the comparison with the fresh fuel composition gives directly the fraction of fresh heavy isotope which underwent fission. Moreover this fraction can be cross checked by the absolute measurement of the fission products.

Studies at NBS also indicate that the method can be implemented with intact fuel assemblies in the field using a commercial accelerator sold for heavy section steel radiography. The accelerator is no more complex or expensive than a high quality mass spectrometer. It appears that data of the quality of that in Fig. A-4 could be obtained on a spent fuel assembly in only twenty minutes of running time with the radiographic accelerator used as a neutron source.

8. Assay of Nonhomogeneous Samples (R. A. Schrack)

The determination of sample thickness by a measurement of neutron transmission of a known resonance line is straightforward when the sample is homogeneous over the area being measured. In any unknown sample the relative homogeneity will usually increase as the area being measured (pixel) is decreased. The loss of counting rate and consequent loss of statistical precision limit the amount of reduction of pixel size that is practical for neutron radiography measurements. It is, therefore, of great interest to see what the dependence of analysis accuracy is on sample homogeneity and how it can be overcome.

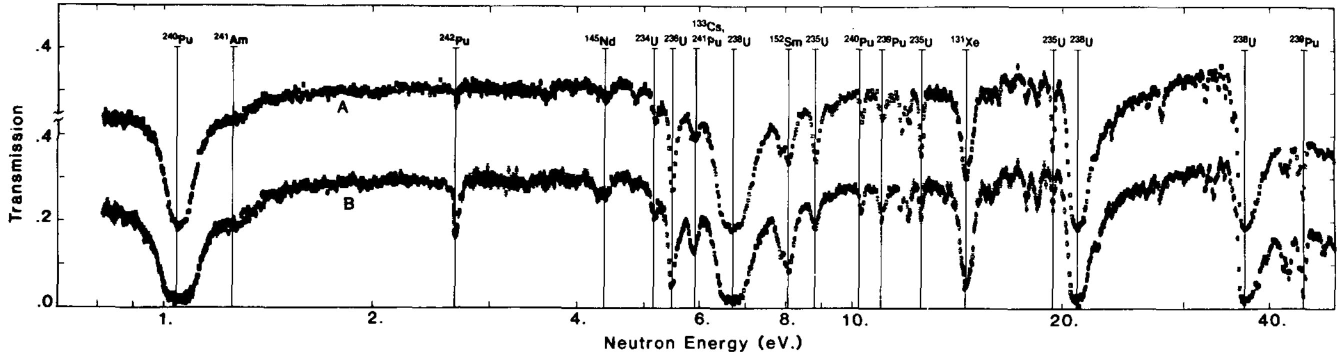

Fig. A-4. Neutron transmission through spent fuel.

Table A-1. Current Analysis Results for Center Cut 2.5 cm Sample

Isotope	E_o (eV)	Atoms/Barn	Current Precision	Relative Abundance
^{234}U	5.19	1.E-5	*	2.E-4
^{235}U	8.78	(4.36±0.15)E-4	3.%	9.4E-3
^{236}U	5.45	1.E-4	*	2.E-3
^{238}U	6.6	.0465±.0004	1%	1.
^{238}Pu	18.6	3.E-5	*	6.E-4
^{239}Pu	10.93	(2.60±.11)E-4	4%	5.6E-3
^{240}Pu	1.05	(1.11±.02)E-4	2%	2.4E-3
^{241}Pu	13.4	8.5E-5	*	1.8E-3
^{242}Pu	2.67	(1.40±.04)E-5	3%	3.0E-4
^{131}Xe	15.	(3.26±.05)E-5	2%	7.0E-4
^{133}Cs	5.8	8.E-5	*	1.7E-3
^{241}Am	1.27	6.E-5	*	1.3E-3
^{243}Am	1.36	8.E-6	*	1.7E-4
^{152}Sm	8.1	(7.27±.14)E-6	2%	1.6E-4
^{145}Nd	4.35	2.E-5	*	4.E-4
^{99}Tc	5.6		*	4.E-4

*Visual fit only, probably good to 10%.

If area analysis techniques were used there would be no way of knowing that the transmission measurement was made of a nonhomogeneous sample. However, using shape analysis techniques one can easily obtain a measure of the sample nonhomogeneity if all transmission measurements are of Doppler-broadened Breit-Wigner line shapes. It has been found that a code that uses non-linear least squares fitting procedures to obtain the best fit to a model and which assumes the sample to be composed of only two areas of different thickness can be used to fit nonhomogeneous samples with very little error. In samples with a linear variation of a factor of two in thickness over the area measured, the error using the two component model is less than 0.1% for $n\sigma<10$. Without the two component model the error would be as high as 3%. If one allows for variation of a factor of ten in thickness over the sample area, the two component model error is only 2%. Thus shape analysis of transmission data can yield assay results that have high accuracy even when samples are quite nonhomogeneous. The implication for neutron radiographic assay techniques is that pixel size can be quite large, usually covering the whole sample. This means that higher statistical precision is possible with limited measurement times and that high resolution position sensitive detectors are not required for accurate assay measurements.

9. Multichannel Plate Neutron Detector (R. A. Schrack, R. G. Johnson)

The need for two-dimensional position-sensitive neutron detectors for neutron measurements has stimulated the development of a detector system using a multichannel plate (MCP) detector. Instead of a scintillator screen output, a resistive anode was used to provide x and y position signals for the centroid of the current pulse. (Fig. A-5) The photocathode is 2.5 cm in diameter on the back surface of an optical fiber input window. The position resolution for optical photons is 1% and the current gain is about 10^6 with about 2200 volts across the MCP. Thin enriched Li glass scintillators 1. mm and about 0.5 mm thick have been used for neutron detection. Tests indicate a position resolution slightly better than 1 mm.

10. Development of High Spatial Resolution Position-Sensitive Proportional Counters (J. W. Behrens, M. K. Kopp*)

Two-dimensional position-sensitive proportional counters (PSPCs) were built for use in development of resonance neutron radiography[8] and for use in development of neutron pinhole camera imaging techniques.[9] The desired spatial resolution of 1.0x1.0 mm^2 for a sensitive area 50x50 mm^2 has been achieved in each of two "area" PSPCs built. A paper[10] has been submitted for publication which describes the PSPC development in more detail.

---

* Oak Ridge National Laboratory, Instrumentation and Controls Division, Oak Ridge, TN.

8 J. W. Behrens, R. A. Schrack, and C. D. Bowman, Nucl. Technol. 51, 78 (1980).

9 R. G. Johnson, J. W. Behrens, and C. D. Bowman, "Source Imaging Using Neutron Pinhole Cameras Based on Position-Sensitive Proportional Counters," submitted to Nucl. Technol.

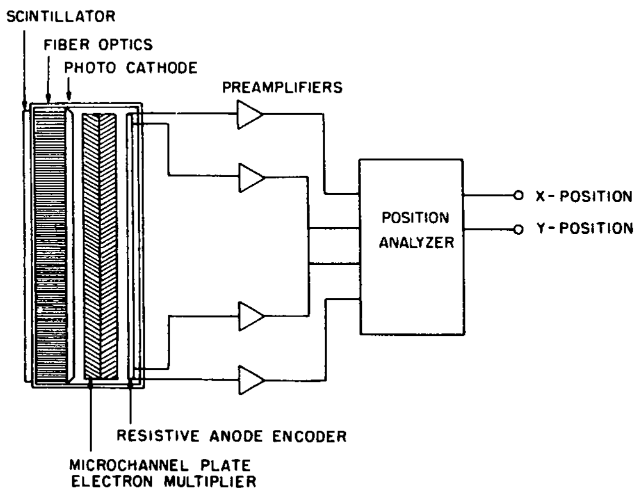

Fig. A-5. Multichannel plate neutron detector.

11. ^{241}Am:^{235}U and ^{243}Am:^{235}U Fission Cross Section Ratio Measurements in the MeV Energy Region (J. W. Behrens, J. C. Browne**)

Final results are published[11] on the fission cross-section ratios for ^{241}Am and ^{243}Am relative to ^{235}U in the neutron energy range from 0.2 to 30 MeV (see Fig. A-6). These measurements were conducted at the Lawrence Livermore National Laboratory 100 MeV electron linac. Our measurements provide fission cross section ratios for these two americium-isotopes that fill gaps in the MeV range where past experimental data were lacking.

** Los Alamos Scientific Laboratory, Los Alamos, NM.

10 M. K. Kopp, J. W. Behrens, M. A. Meacham, and J. A. Williams, "Development of Proportional Counter Cameras for Neutron Imaging with 1-mm Resolution," submitted to Rev. Sci. Instrum.

11 J. W. Behrens and J. C. Browne, to be published in Nucl. Sci, Eng. (April 1981).

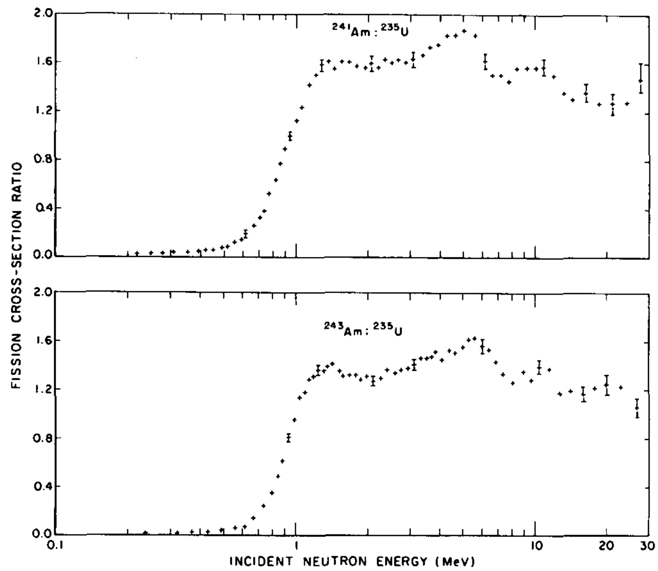

Fig. A-6. Measurements of the (a) ^{241}Am:^{235}U and (b) ^{243}Am:^{235}U fission cross-section ratios over the energy range from 0.2 to 30 MeV.

12. Neutron-Source Imaging Using Position-Sensitive Proportional Counters (R. G. Johnson, J. W. Behrens, C. D. Bowman)

The Neutron Measurements and Research Group has an interest in developing and using neutron detectors which can provide position sensitivity with a 1-2 mm resolution. In other sections of this report the latest developments of such detectors is described. In this section measurements using such detectors for imaging neutron sources are summarized. Two experiments of this type have been performed.

In the first experiment the variation in neutron-emission intensity over the area of the neutron-producing target of the NBS electron linac has been measured. Low-energy neutrons (E_n<0.3 eV) were imaged using a pinhole camera technique. A linear position-sensitive proportional counter (PSPC) with an active length of 50 mm and a resolution of 1.2 mm was used in this case. The experimental arrangement is shown in Fig. A-7a where the moderator has a height of 18 cm and the pinhole is in a 1.6-mm thick Cd sheet. To obtain information in the vertical direction the detector could be remotely positioned in that direction. The results of the measurement are shown in Fig. A-7b. A total of eleven vertical steps were used to produce this image.

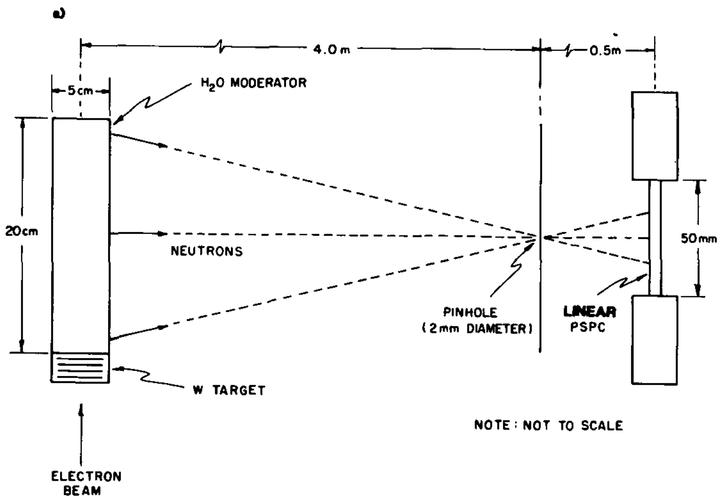

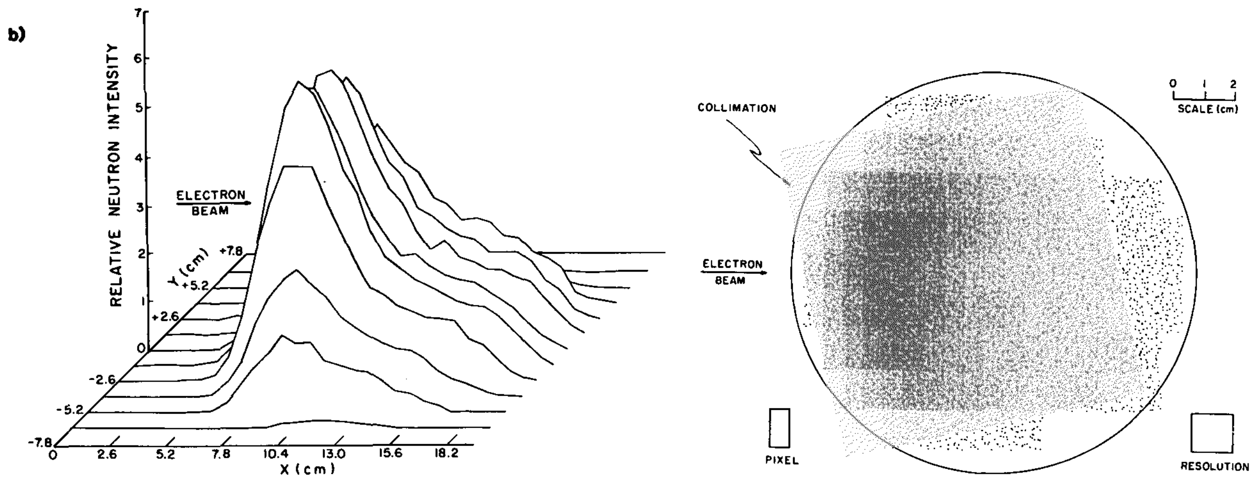

Fig. A-7(a) Experimental arrangement for imaging the neutron emission from the neutron-producing target of the NBS Electron Linac. (The height of the target is 18 cm.)

(b) Image obtained from the pinhole camera shown in (a). Both a three-dimensional representation and a grey-scale representation are shown. The circle represents the limits imposed by the flight-path collimation.

In the second experiment the 14-MeV neutrons from the (d,t) reaction were imaged. A neutron cone was defined by the associated-particle technique and the neutrons were detected by a two-dimensional PSPC. The experimental details for this measurement are shown in Fig. A-8a. The results of the measurement are shown in Fig. A-8b. The neutron cone of the associated-particle system is readily apparent.

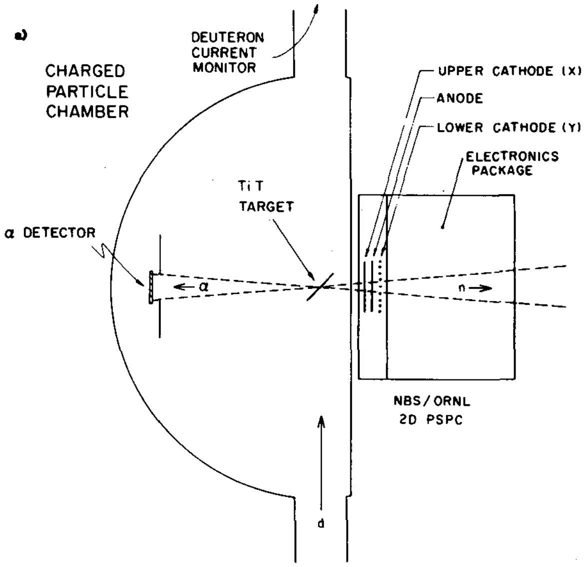

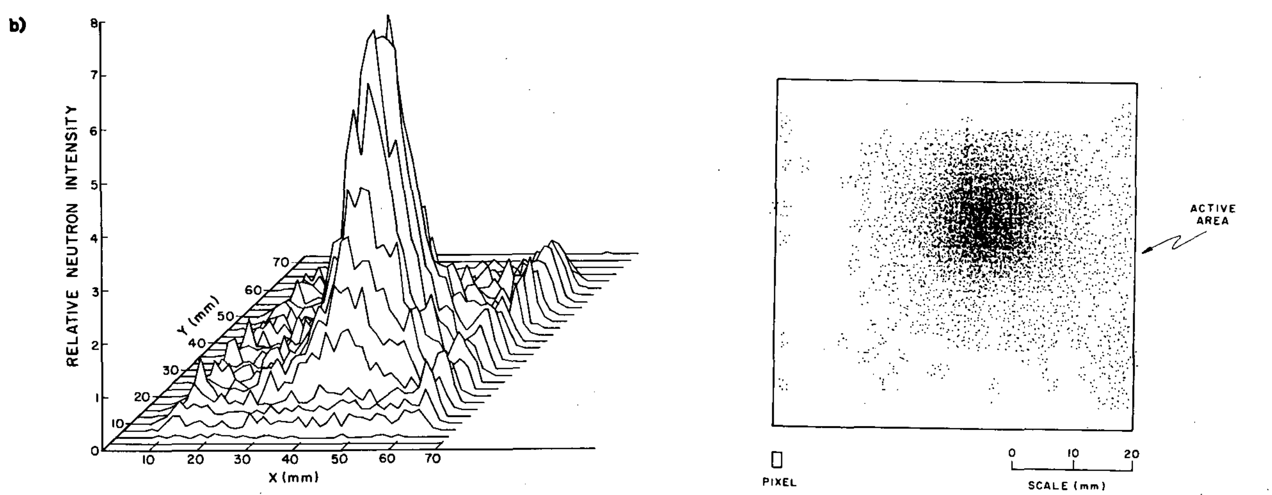

Fig. A-8 (a) Schematic diagram of the imaging system using the associated-particle technique and a two-dimensional PSPC.

(b) Image of the neutron cone from the (d,t) reaction. Both a three-dimensional representation and a grey-scale representation are shown.

Further details for these measurements may be found in Ref. 12. The concept of active neutron imaging and dosimetry for both low- and high-energy neutrons has been demonstrated in these measurements. Further measurements combining the pinhole camera technique and the two-dimensional position-sensitive neutron detector are planned to fully demonstrate the concept.

13. Development of ^{235}U Fission Chambers as Neutron Flux Monitors at Breeder Reactors (K. Valentine†, M. K. Kopp†, J. W. Behrens)

A painting technique[13] for fabricating actinide fission foils is being evaluated at ORNL in an attempt to determine the most economical way to mass-produce thick, i.e., 2000 μg/cm^2, ^{235}U fission foils for use in fission chambers designed as exvessel flux monitors for breeder reactors. At the October 1980 meeting of the International Nuclear Target Development Society held in Gatlinburg, Tennessee, a paper[14] was given which emphasized that the painting technique is a relatively inexpensive method by which thick actinide deposits, having excellent adhesion and nonuniformities of less than ±10%, could be produced.

Thick fission foils produced by painting, electroplating, and vacuum evaporation techniques are presently being compared at ORNL on the basis of adhesion, uniformity, general performance in a fission chamber geometry, and cost.

B. FACILITIES

1. The 3 MV Positive Ion Van de Graaff Facility (O. A. Wasson, K. C. Duvall, L. J. Goodman)

The turbomolecular vacuum pumps used for the main accelerator and beam lines operated routinely during the past year. A new charging belt was installed in October of 1980. The 0.2-1.2 MeV neutron beam line is maintained for standard measurements. The 14 MeV neutron facility using the associated particle technique with the $^3H(d,n)^4He$ reaction was developed to measure the $^{235}U(n,f)$ cross section and is being studied for activation measurements and calibrations. The 10^8 n/sec source strength is limited by the TiT target cooling. A new beam line is being developed to provide a more intense neutron source in the heavily shielded room for neutron dosimetry standards.

---

† Oak Ridge National Laboratory, Instrumentation and Controls Division, Oak Ridge, TN.

12 R. G. Johnson, J. W. Behrens, and C. D. Bowman, "Source Imaging for FMIT Using a Neutron Pinhole Camera," Proceedings of the Symposium on Neutron Cross Sections from 10 to 50 MeV, eds. M. R. Bhat and S. Pearlstein, BNL-NCS-51245 Vol. II of II, 629 (1980).

13 J. W. Behrens, Lawrence Livermore National Lab. Report UCRL-51476 (Nov. 1973).

14 J. W. Behrens, Proc. to be published in Nucl. Instrum. Methods.

2. Development of the 14-MeV Neutron Flux Facility for the Absolute Measurement of Neutron Induced γ-ray Activity (K. C. Duvall, O. A. Wasson)

The $T(d,n)^4He$ source reaction, combined with associated particle detection, is being developed for absolute measurement of neutron induced γ-ray activity. Currently, the neutron-source is being studied to determine background radiation components. A 500-keV D_2^+ beam, pulsed at 1 μsec intervals is used along with time-of-flight techniques to assess backgrounds in 14-MeV neutron flux measurements. This method is compared with the time-correlated coincidence method for background elimination. Two parameter spectra can be collected using the on-line computer for simplifying the application of these techniques for background measurement. The 14 MeV neutron flux facility will be used beginning May 1981 to measure the $^{113}In(n,n')^{113}In^m$ neutron induced activation as part of the NBS participation in the International Intercomparison sponsored by BIPM.

C. DATA COMPILATION

1. X-Ray and Ionizing Radiation Data Center (J. H. Hubbell)

The previously-mentioned high-energy photon cross section compilation, co-authored with Gimm (Mainz) and Øverbø (Trondheim) was published with several revisions in the final version.[15] In addition, this Data Center in 1980 responded to a total of 245 requests for data or information, of which 113 were in basic research subject areas (standards, metrology, atomic and nuclear physics, astrophysics, etc.), 72 were in health physics areas (medical therapy and diagnosis, dosimetry, shielding, etc.), 50 were in industrial/agricultural/mining areas (radiation gauging, control, processing, well-logging, etc.) and the remaining 10 were in civil defense/weapons (U.S. military) areas.

---

[15] J. H. Hubbell, H. A. Gimm, and I. Øverbø, "Pair, Triplet and Total Atomic Cross Sections (and Mass Attenuation Coefficients) for 1 MeV-100 GeV Photons in Elements Z=1 to 100," J. Phys. Chem. Ref. Data 9, 1023-1148 (1980).

A. CROSS SECTION MEASUREMENTS

1. Capture Cross Sections

a. Current (2/81) Fission Product and other Capture Cross Section Measurements (R. L. Macklin)

Samples of ^{99}Tc, ^{109}Ag (and ^{107}Ag) have been requested to fulfill data needs. We hope to obtain and measure ^{131}Xe and ^{136}Xe as we have already successfully taken data for ^{86}Kr. Outside the fission product mass range we have a sample of ^{22}Ne and have measured $^{182,183,184,186}W$ samples (courtesy of D. Drake, LANL) up to $\sim$2 MeV.

b. Stable Isotope Capture Cross Sections from ORELA (R. L. Macklin and R. R. Winters*)

A computer coding error in data processed prior to December 1979 led to percentage errors in several published cross sections. Palladium isotope data were severely changed (up to $\sim$40%), thorium, sulfur, holmium and ^{186}osmium in the 10-15% range and others were unaffected or in the 2-7% range. Corrected data for the most severe cases have been reprocessed to average microscopic capture cross sections and to resonance parameters.

c. Neutron Capture Cross Section in ^{64}Zn** (J. B. Garg,† V. K. Tikku,† J. Halperin, and R. Macklin)

Total neutron capture cross section measurements of the separated isotope $^{64}_{30}Zn$ have been made in the energy interval of 2.5-900 keV. These were made using time-of-flight techniques and a total energy γ-ray detector system with a nominal resolution of about 0.12 ns/m. Resonance energies and capture areas were determined for 191 resonances up to 131 keV. Values of the radiation widths and neutron widths for many resonances have been determined making use of the results available from transmission measurements. From these results mean values of $\langle\Gamma_\gamma\rangle$ = (726±60) meV for s-wave and $\langle\Gamma_\gamma\rangle$ = (272±30) meV for p-wave resonances have been determined. A value for the p-wave strength function $S_1 = (0.75\pm0.08) \times 10^{-4}\ eV^{-1/2}$ was obtained for neutron energy up to 130 keV. Bayes' theorem for conditional probability was used to identify d-wave levels and from these resonances a lower limiting value for d-wave strength function $S_2 = (0.78\pm0.12) \times 10^{-4}\ eV^{-1/2}$ was obtained. The values for the p-wave mean level spacing for all resonances observed up to 130 keV and after elimination of d-wave resonances, were found to be (0.68±0.04) and (1.10±0.07) keV, respectively. An analysis of the linear correlation coefficient (ρ) between Γ_n^0 and Γ_γ gave a value of (0.47±0.08) at a confidence level of 99.7%.

---

*Denison University, Granville, Ohio.

**Phys. Rev. C 23, 683 (1981).

†State University of New York, Albany, New York 12222.

d. $^{186,187,188}Os(n,\gamma)$ Cross Sections and Galactic Nucleosynthesis*
(R. R. Winters, R. L. Macklin, and J. Halperin)

The $^{186,187,188}Os(n,\gamma)$ cross sections were measured over the incident neutron energy range 2.6-800 keV. Optimized statistical model fits to the average cross sections were made employing estimates of the ^{186}Os, ^{187}Os, and ^{188}Os p-wave strength functions 0.29×10^{-4}, 0.45×10^{-4}, and 0.33×10^{-4}, respectively, d-wave strength functions 1.3×10^{-4}, 4.0×10^{-4}, and 1.5×10^{-4}, respectively, and gamma ray strength functions ($\bar{\Gamma}_\gamma/D_0$) 26.8×10^{-4}, 176×10^{-4}, and 20.8×10^{-4}, respectively. A lower bound for the ^{187}Os neutron inelastic cross section is estimated as 0.25(20) b at 30 keV. The Maxwellian-averaged capture cross sections are presented as a function of temperature. The ratio of 30 keV Maxwellian-averaged cross sections $\langle\sigma_\gamma(186)\rangle/\langle\sigma_\gamma(187)\rangle = 0.504(17)$ is reported and the lack of agreement with earlier measurements of this ratio is discussed. The use of this cross section ratio in estimating, via the ^{187}Re-^{187}Os beta decay, the duration of galactic nucleosynthesis is discussed. The cross section ratio from this work yields an estimate of $10.4(25) \times 10^9$ yr for the duration of galactic nucleosynthesis, a result higher than but still consistent with the estimate $7(2) \times 10^9$ yr derived from U/Th decay.

e. Thorium Resonance Neutron Capture (2.6-10 keV) (R. L. Macklin)

Individual resonance parameters are fitted to thorium neutron capture data up to 10 keV. The ENDF/B-V parameters (given up to 4 keV) do not describe the data well. An average radiation width $\Gamma_\gamma = 25.5 \pm 1.2$ meV is derived together with fitted strength functions $10^4 S_1 = (1.47 \pm 0.07)$ $eV^{-1/2}$, $10^4 S_2 = (1.13 \pm 0.06)$ $eV^{-1/2}$ and $10^4 \Gamma_\gamma/D_{\ell=0} = 14.6 \pm 0.4$.

2. Total Cross Sections

a. ORELA Measurements to Meet Fusion Energy Neutron Cross Section Data Needs** (D. C. Larson)

Major neutron cross section measurements that have been made at the Oak Ridge Electron Linear Accelerator (ORELA) and are useful to the fusion energy program will be reviewed. Cross sections for production of gamma rays with energies $0.3 < E_\gamma < 10.5$ MeV have been measured as a function of neutron energy over the range $0.1 < E_n < 20.0$ MeV for Li, C, N, O, F, Na, Mg, Al, Si, Ca, Ti, V, Cr, Mn, Fe, Ni, Cu, Zn, Nb, Mo, Ag, Sn, Ta, W, Au, Pb and Th. Neutron emission cross sections have been measured for ^7Li, Al, Ti, Cu and Nb for $1 < E_n < 20$ MeV. Results of recent neutron total cross section measurements from 2-80 MeV for eleven materials of interest (C, O, Al, Si, Ca, Cr, Fe, Ni, Cu, Au and Pb) to the FMIT project will be presented. Finally, future directions of the ORELA program will be outlined.

*Phys. Rev. C 21, 563 (1980).
**Abstract of paper presented at the Symposium on Neutron Cross Sections from 10-50 MeV, BNL, May 12-14, 1980; Proc. BNL-NCS-51245, Vol. I, p. 277 (1980).

b. Precise Measurement and Analysis of Neutron Transmission through ^{232}Th* (D. K. Olsen, R. W. Ingle, and J. L. Portney**)

Three sets of transmission time spectra through up to eight samples of ^{232}Th have been measured for neutron energies from 6.0 meV to 0.1 MeV using a flight-time technique over 22- and 40-m path lengths, the ORELA pulsed neutron source, and a 1-mm thick lithium glass detector. The resulting total cross section from 0.1 to 20.0 eV seems to be smaller than that contained in the ENDF/B-V evaluation. Least-squares analysis of the transmissions from 9 to 440 eV using a multilevel Breit-Wigner formalism results in neutron widths consistent with those previously reported. An average radiation width of 25.2 meV is obtained for 19 low-energy s-wave resonances. Higher resolution measurements are planned for next year.

c. ^{240}Pu Total Cross Section (L. W. Weston and R. R. Spencer)

Preparation has begun for measurements of the transmission of ^{240}Pu up to a few eV, concentrating on the large resonance at 1 eV.

3. Scattering and Reactions

a. ^{56}Fe Inelastic Scattering (J. K. Dickens and D. C. Larson)

Measurements are being prepared to observe the excitation function of the cross section for inelastic scattering to the first 2^+ level of ^{56}Fe (846 keV) over a broad region of neutron energies.

b. $^{187}Os(n,n')$ Cross Section (Winters, Käppeler,† Beer,† Berman,‡ Hershberger,¶ McEllistrem,¶ Macklin, and Hill)

The very difficult measurement of the cross section for inelastic neutron scattering to the 9.8 keV state has been pursued first at Van de Graaff accelerators. In the Karlsruhe measurement an upper limit of 0.4 barns was found at 30 keV. Collaborative measurements at the University of Kentucky are getting under way (30 keV and 65 keV). Some planning has been done for a possible 34 keV measurement at ORELA using an anisotropic Fe-Al filter.

c. ^{238}U Inelastic Neutron Scattering at 82 keV§ (Winters, Hill, Macklin, Harvey, Olsen, and Morgan◊)

Using a thick iron filter to produce an 82 keV group of nearly monoenergetic pulsed neutrons from the Oak Ridge Electron Linear Accelerator white neutron source, the differential and integrated neutron inelastic scattering cross sections from the first excited state of ^{238}U have been measured.

---

*Proc. ANS Topical Meeting, Sun Valley, Idaho, Sept. 14-17, 1980, p. 743.
**ORAU 1980 Summer Student, permanent address 2617 Pinetree, Flint, Michigan.
†Kernforschungszentrum Karlsruhe.
‡Lawrence Livermore Laboratory.
¶University of Kentucky
§Nucl. Sci. Eng. (in press).
◊Los Alamos National Laboratory, Los Alamos, New Mexico 87545.

We find that the angular distribution is forward-peaked and we obtain estimates of the Legendre coefficients P_0, P_1, and P_2. The measured integrated inelastic cross section is 381 ± 21 mb, in good agreement with the ENDF/B-V evaluation and with other statistical and optical model calculations.

4. Actinides

a. Actinide Neutron Cross Sections Program (Dabbs, Johnson, Weston, Todd, Williams, Harvey, Carter, Dickens, Raman, Bemis, Halperin, Macklin, and Hill)

Fission - Conversions of measured data to cross sections for ^{241}Am(n,f), ^{242m}Am(n,f), and ^{249}Cf(n,f) have been brought near to completion. Useful new techniques for handling complex background analyses were developed in the course of these conversions. A first measurement at RPI Pb Spectrometer on ^{248}Cf(n,f) was completed; continuation measurements on lighter even isotopes of Cm await sample preparations now in progress at LLL. A precise value of $\bar{\nu}_p$ for ^{242}Cm was published.[1]

Capture - A paper entitled "Neutron Capture Cross Section of Neptunium-237" has passed the review process and is ready for publication. The measurement covers the neutron energy region from 0.01 eV to 200 keV. Both resolved and unresolved resonance parameters were derived. These data in conjunction with previously reported total cross sections yield a 2200 m/s cross section which is 6.4% higher than that in ENDF/B-V.

Total - Measurements of the total cross section for ^{231}Pa were carried out over the range 0.01 eV-10 keV on two sample thicknesses at the 18 m and 80 m flight paths of ORELA. Liquid nitrogen cooling was used. The data were analyzed; a total of 137 resonances were characterized, and the s-wave strength function below 70 eV was determined. A paper has been submitted for publication.

Integral Experiments - The measurement program for analyzing 12 in-core and 2 in-blanket actinide samples irradiated for 4 years in EBR-II h-s been completed. For samples located near the core center, ORIGEN calculations show good agreement with experiment. A final report is in preparation. Encapsulation of 21 actinides (between ^{230}Th at the low mass end and ^{248}Cm at the high) for extended irradiations at the Dounreay PFR has also been completed.

Calculation and Analysis - During FY'81, the remaining irradiated EBR-2 samples were calculated and results compared with the experimentally determined compositions. For most samples agreement was quite good; however, for the ^{238}U and Th samples, which were located near the axial blankets of EBR-2, significant discrepancies were observed.

Although some results showed considerable improvement as a consequence of these studies, the calculated Pu concentration in the ^{238}U

---

[1] Nucl. Sci. Eng. 75, 56 (1980).

sample was still 20-30% lower than the measured value. A comprehensive final report on the EBR-2 actinide irradiation experiment is currently in preparation.

Concurrent with the above study was one that attempted to determine the effects of recent ORELA cross section measurements on the nuclear industry, as manifested by improvements in reactor calculations, fuel cycle costs, etc. The difference in the version IV and V results is an indication of the effect of recent cross section improvements. A report on this study has begun.

Fission-Product Yields - Measurements of thermal-neutron induced fission-product yields utilizing gamma-ray assay have been completed for ^{243}Cm. Data reduction is expected to be initiated soon and completed within a year. These measurements will yield the first fission-product yield data for ^{243}Cm. Data reduction to obtain fission-product yields for ^{229}Th(n,f) is in progress. Results of previous work on ^{245}Cm fission product yields were published[1] and on ^{249}Cf yields have been submitted for publication.

Actinide Newsletter - The fourth issue, edited by S. Raman, will appear in early 1981 and has 72 contributions from 24 laboratories in 11 countries. The IAEA Advisory Group on Transactinium Isotope Nuclear Data at its second meeting in Cadarache, France, in May 1979, made a strong recommendation for the continuation of the Actinide Newsletter and for persons working in this field all over the world to make contributions to it. The publication schedule is expected to be one issue per year in the future.

b. $\bar{\nu}_p$ of ^{233}U (R. Gwin)

The energy dependence of the average number of prompt neutrons emitted on fission $\bar{\nu}_p(E)$ has been measured relative to the $\bar{\nu}_p$ for ^{252}Cf. The results are higher than currently accepted values above the resonance region up to a few hundred keV. It is planned to measure simultaneously below 1 eV the ratio of $\bar{\nu}_p$ of ^{233}U, ^{235}U, and ^{239}Pu to the Cf standard.

c. ^{238}U Neutron Capture (de Saussure, Perez, Mukhopadhyay, and Yang)

Careful remeasurements of ^{238}U neutron capture up to $\sim$10 keV have been initiated, and are to be supplemented with self-indication measurements planned to enable deduction of self-shielded cross sections.

d. Yields of Short-Lived Fission Products Produced by Thermal-Neutron Fission of Plutonium-239* (J. K. Dickens, J. W. McConnell, and K. J. Northcutt)

The absolute yields of 28 fission products representing 23 different mass chains produced by thermal-neutron fission of ^{239}Pu and having half-lives between 30 and 1100 s have been determined using Ge(Li) spectroscopy

[1]Phys. Rev. C 23, 331 (1981).
*Nucl. Sci. Eng. 77, 146 (1981).

methods. Spectra of 30 gamma rays emitted in the decay of the fission products between 35 and 1950 s after a 5-s irradiation were obtained. Gamma rays were assigned to the responsible fission products by matching gamma-ray energies and half-lives. Fission-product yields were then obtained from the data by first determining the appropriate gamma-ray activity as of the end of the irradiation, correcting for detector efficiency and gamma-ray branching ratio, and, finally, dividing by the number of fissions created in the sample. The number of fissions was determined by direct comparison of gamma rays emanating from fission products created during a careful irradiation of a well-calibrated ^{239}Pu-loaded fission chamber.

The resulting fission-product yields are compared with previous measurements and with recommended yields given in two recent (and independent) evaluations. Uncertainties assigned to the present results range between 6 and 45%, and are smaller than or comparable to uncertainties assigned to previous experimental or evaluated yields for six mass chains.

e. Yields of Fission Products Produced by Thermal-Neutron Fission of ^{245}Cm* (J. K. Dickens and J. W. McConnell)

Absolute yields have been determined for 105 gamma rays emitted in the decay of 95 fission products representing 54 mass chains created during thermal-neutron fission of ^{245}Cm. These results include 17 mass chains for which no prior yield data exist. Using a Ge(Li) detector, spectra were obtained of gamma rays between 30 sec and 0.3 yr after very short irradiations of thermal neutrons on a 1 μg sample of ^{245}Cm. On the basis of measured gamma-ray yields and known nuclear data, total chain mass yields and relative uncertainties were obtained for 51 masses between 84 and 156. The absolute overall normalization uncertainty is <8%. The measured A-chain cumulative yields make up 81% of the total light mass ($A \leq 121$) yield and 92% of the total heavy mass yield. The results are compared with fission-product yields previously measured with generally good agreement. The mass-yield data have been compared with those for thermal-neutron fission of ^{239}Pu and for ^{252}Cf(s.f.); the influences of the closed shells Z=50, N=82 are not as marked as for thermal-neutron fission of ^{239}Pu but much more apparent than for ^{252}Cf(s.f.). Information on the charge distribution along several isobaric mass chains was obtained by determining fractional yields for 12 fission products. The charge distribution width parameter, based upon data for the heavy masses, A=128 to 140, is independent of mass to within the uncertainties of the measurements. Gamma-ray assignments were made for decay of short-lived fission products for which absolute gamma-ray transition probabilities are either not known or in doubt. Absolute gamma-ray transition probabilities were determined as (51±8)% for the 374-keV gamma ray from decay of ^{110}Rh, (35±7)% for the 1096-keV gamma ray from decay of ^{133}Sb, and (21.2±1.2)% for the 255-keV gamma ray from decay of ^{142}Ba.

*Phys. Rev. C 23, 331 (1981).

f. Gamma Rays Following Alpha Decay of ^{245}Cm and the Level Structure of ^{241}Pu* (J. K. Dickens and J. W. McConnell)

Relative intensities for K x rays and gamma rays emanating from ^{245}Cm have been measured using several Ge photon detectors. The absolute intensity for the dominant 175-keV gamma ray in ^{241}Pu was determined to be 9.5 photons per 100 ^{245}Cm alpha decays with an uncertainty of ±7%. Eleven gamma rays have been placed as transitions among levels in ^{241}Pu.

g. Yields of Fission Products Produced by Thermal-Neutron Fission of ^{249}Cf** (J. K. Dickens and J. W. McConnell)

Absolute yields have been determined for 107 gamma rays emitted in the decay of 97 fission products representing 54 mass chains created during thermal-neutron fission of ^{249}Cf. These results include 14 mass chains for which no prior yield data exist. Using a Ge(Li) detector, spectra were obtained of gamma rays between 45 sec and 0.4 yr after very short irradiations of thermal neutrons on a 0.4 μg sample of ^{249}Cf. On the basis of measured gamma-ray yields and known nuclear data, total chain mass yields and relative uncertainties were obtained for 51 masses between 89 and 156. The absolute overall normalization uncertainty is ∿8%. The measured A-chain cumulative yields make up 77% of the total light mass ($A \leq 123$) yield and 79% of the total heavy mass yield.

The results are compared with fission-product yields previously measured, with generally good agreement. Information on the charge distribution along several isobaric mass chains was obtained by determining fractional yields for 11 fission products and combining these results with other measurements. The charge distribution width parameter for the heavy masses, A = 128 to 140, is independent of mass to within the uncertainties of the measurements. For the light masses, A = 89 to 112, the charge distribution parameter is also independent of mass but is smaller than for the heavy masses. Total chain yields are in fair agreement with the current evaluation for ^{249}Cf.

h. ^{252}Cf Spontaneous Fission Neutron Spectrum (R. R. Spencer and D. K. Olsen)

A careful remeasurement of the ^{252}Cf spontaneous fission neutron energy spectrum has been initiated. Recognized pitfalls in all previous measurements and a conflict of many of the experimental measurements with a recent theoretical prediction have made this work necessary. The importance of accurate knowledge of the ^{252}Cf neutron spectrum lies in its use as a reference in a variety of measurements and in its effect on determinations of $\bar{\nu}$, the average number of neutrons emitted in fission, for this isotope.

*Phys. Rev. C 22, 1344 (1980).
**Submitted for publication in Physical Review C.

5. Experimental Techniques

a. Preliminary Study of Pseudorandom Binary Sequence Pulsing of ORELA* (N. M. Larson and D. K. Olsen)

It has been suggested that pseudorandom binary sequence (PRBS) pulsing might enhance the performance of the Oak Ridge Electron Linear Accelerator (ORELA) for neutron-induced, time-of-flight (TOF) cross-section measurements. In this technical memorandum, equations are developed for expected count rates, statistical variances, and backgrounds for a pulsing scheme in which a PRBS is superimposed on the periodic equal-intensity ORELA bursts. Introduction of the PRBS modification permits neutrons of different energies originating from different bursts to reach the detector simultaneously, and the signal corresponding to a unique flight time to be extracted mathematically. Relative advantages and disadvantages of measurements from conventional and PRBS pulsing modes are discussed in terms of counting statistics and backgrounds. Computer models of TOF spectra are generated for both pulsing modes, using as examples a 20-meter ^{233}U fission-chamber measurement and a 155-meter ^{238}U sample-in transmission measurement. Detailed comparisons of PRBS vs conventional results are presented. This study indicates that although PRBS pulsing could enhance ORELA performance for selected measurements, for general ORELA operation the disadvantages from PRBS pulsing probably outweigh the advantages.

b. User's Guide for SAMMY: A Computer Model for Multilevel R-Matrix Fits to Neutron Data Using Bayes' Equations** (N. M. Larson and F. G. Perey)

In this report we describe a method for determining the parameters of a model from experimental data based upon the utilization of Bayes' theorem. This method has several advantages over the least-squares method as it is commonly used; one important advantage is that the assumptions under which the parameter values have been determined are more clearly evident than in many results based upon least squares. Bayes' method has been used to develop a computer code which can be utilized to analyze neutron cross-section data by means of the R-matrix theory. The required formulae from the R-matrix theory are presented, and the computer implementation of both Bayes' equations and R-matrix theory is described. Results of our analysis of Ni^{60} transmission data from ORELA and of several artificial data sets, and a comparison of our results with those of an earlier multilevel R-matrix code, are also presented. Finally, details about the computer code and complete input/output information are given.

---

*Abstract of ORNL/TM-6632, ENDF-290 (March 1980).
**Abstract of ORNL/TM-7485, ENDF-297 (November 1980).

c. Liquid Argon as an Electron/Photon Detector in the Energy Range of 50 MeV to 2 GeV: A Monte Carlo Investigation* (Goodman,** Denis,** Hall,** Karpovsky,** Wilson,** Gabriel, and Bishop)

Monte Carlo techniques have been used to study the characteristics of a proposed electron/photon detector based on the total absorption of electromagnetic showers in liquid argon. The energy range studied was 50 MeV to 2 GeV. Results are presented on the energy and angular resolution predicted for the device, along with the detailed predictions of the transverse and longitudinal shower distributions. Comparisons are made with other photon detectors, and possible applications are discussed.

d. A Monte Carlo Simulation of an Actual Segmented Calorimeter: A Study of Calorimeter Performance at High Energies† (Gabriel, Bishop, Goodman,** Sessoms,** Eisenstein,‡ Wright,¶ and Kephart§)

The calculated responses including energy resolution, angular resolution, and spatial energy deposition of a segmented iron and liquid-argon calorimeter to incident pions in the energy range of 10- to 250-GeV are presented. Experimental data for this calorimeter have been obtained in the 10- to 40-GeV energy range and these results compare favorably with the calculated data. The energy and angular resolutions including experimental and calculated data can be summarized by the following expressions:

$$\sigma(E)/E = (5.07 + 33.4/\sqrt{E})\% \quad ,$$

and

$$\sigma_\theta(E) = 15.7 + 458./E \quad (\text{mrad}) \quad ,$$

respectively, where E is in GeV.

B. DATA ANALYSES

1. Theoretical Calculations

a. Calculation of the ^{23}Na(n,2n) Cross Section◊ (D. C. Larson)

The ^{23}Na(n,2n) reaction produces the radioactive product ^{22}Na, which has a half-life of 2.61 years. For sodium-containing systems this reaction can result in a radioactive contamination problem. Currently available experimental cross sections for this reaction are in strong conflict.

*Abstract of ORNL/TM-7556 (December 1980).
**Harvard University.
†Abstract of ORNL/TM-7123 (January 1981).
‡University of Illinois, Urbana.
¶Enrico Fermi Institute, University of Chicago.
§Fermi National Accelerator Laboratory.
◊Abstract of paper presented at ANS Meeting, Minneapolis, October 9-11, 1980.

Extensive multi-step Hauser-Feshbach calculations have been done for neutron-induced reactions on sodium and will be presented. These consistent calculations reproduce data for the (n,n'), (n,p), ($n,\alpha\gamma$) reactions, a neutron emission measurement and a gamma-ray production measurement. The resulting cross sections for the (n,2n) reaction are found to be in good agreement with one of the experimental data sets.[1]

b. Development and Applications of Multi-Step Hauser-Feshbach/Pre-Equilibrium Model Theory* (C. Y. Fu)

A recently developed model that combines compound and precompound reactions with conservation of angular momentum is discussed. This model allows a consistent description of intermediate excitations from which tertiary reaction cross sections can be calculated for transitions to the continuum as well as to the discrete residual levels with known spins and parities. Predicted neutron, proton, and alpha-particle production cross sections and emission spectra from 14-MeV neutron-induced reactions are compared favorably with angle-integrated experimental data for 12 nuclides. The model is further developed to include angular distributions of outgoing particles. The random phase approximation used for the compound stage is partially removed for the precompound stages, allowing off-diagonal terms of the collision matrix to produce both odd and even terms in the Legendre polynomial expansion for the angular distribution. Calculated double differential cross sections for the 14.6-MeV $^{23}Na(n,n'x)$ reaction are compared with experimental data.

c. Evaluation of Photon Production Data from Neutron-Induced Reactions** (C. Y. Fu)

The evaluation methods and procedures used for generating the photon production data in the current Evaluated Nuclear Data File (ENDF/B, Version V) are reviewed. There are 42 materials in the General Purpose File of ENDF/B-V that contain data for prompt photon production. Almost all evaluations had substantial experimental data bases, but less than half of them employed any of the available evaluation methods. Only a few used theoretical techniques that are sophisticated enough to ensure internal consistency with other particle production data. Comments are made on four evaluation methods: the empirical formalism of Howerton *et al.*, the Troubetzkoy model, the multiparticle Hauser-Feshbach/Precompound model, and the Yost method. Critiques are also made on three procedures used for conserving photon energies in neutron capture reactions. The presence of photon production data in the file is necessary for studying energy balance, since photon production generally accounts for a dominant portion of the reaction energy output. Problems found in energy balance checks are discussed.

[1]H. Liskien and A. Paulsen, Nucl. Phys. 63, 393 (1965).
*Proc. BNL-NCS-51245, Vol. 2, p. 675 (July 1980).
**Presented at Workshop on Evaluation Methods and Procedures, BNL, Sept. 1980.

d. Neutron Production by Medium-Energy ($\lesssim$1.5 GeV) Protons in Thick Uranium Targets* (R. G. Alsmiller, Jr., T. A. Gabriel, J. Barish, and F. S. Alsmiller)

A model, that includes fission, for predicting particle production spectra from medium-energy nucleon and pion collisions with uranium nuclei has been incorporated into the nucleon-meson transport code HETC. A variety of calculated results obtained with this revised code for protons incident on uranium targets have been obtained and are compared with experimental data and with the calculations of other investigators. For incident proton energies $\lesssim$1 GeV the calculated results are in good agreement with several, but not all, of the available experiments.

e. A Phenomenological Model for Particle Production from the Collision of Nucleons at Medium Energies with Fissile Elements** (F. S. Alsmiller, R. G. Alsmiller, Jr., T. A. Gabriel, R. A. Lillie, and J. Barish)

A phenomenological model for particle production from the collision of nucleons at medium energies ($\lesssim$3 GeV) with fissile elements is presented. Calculated neutron multiplicities are compared with experimental data and agreement is found to be within the statistical errors expected from the Monte Carlo nature of the calculations.

f. Thermal Neutron Flux Generation by High-Energy Protons in Thick Uranium Targets† (R. G. Alsmiller, Jr., T. A. Gabriel, J. Barish, and F. S. Alsmiller)

For several applications, e.g., in designing facilities to produce an intense source of low-energy neutrons by using medium-energy protons and for studies of the feasibility of converting fertile-to-fissile material using medium-energy protons, it is necessary to carry out calculations of the transport of medium- and low-energy nucleons and pions through fissionable material. The high-energy transport code HETC[1] has often been used to carry out such transport calculations, but because this code did not take into account high-energy fission, the results were very approximate. Recently, a fission channel has been added to the intranuclear-cascade-evaporation model of nuclear reactions and this revised cross-section model has now been incorporated into the transport code, HETC, so that medium-energy nucleon and pion transport calculations in fissionable material may be carried out.

To test the validity of the revised code, calculations have been carried out and compared with the experimental data of Fraser *et al.*[2] At the proton energies of 540 and 960 MeV the calculated and experimental results are in very good agreement, but for incident protons of 1470 MeV the calculated results are larger than the experimental data. Comparisons similar to these with a variety of other experimental data will also be presented.

*Abstract of ORNL/TM-7527 (January 1981).
**Proc. ANS 35, 475 (1980).
†Proc. ANS 35, 477 (1980).
[1]T. W. Armstrong and K. C. Chandler, ORNL-4744 (1972).
[2]J. S. Fraser *et al.*, Phys. Canada 21, 17 (1965).

g. Calculated Differential π^+ Production Spectra at Large Angles from 28 GeV Protons on a Thick Iridium Target and Comparisons with Experimental Data* (R. G. Alsmiller, Jr., T. A. Gabriel, and B. L. Bishop)

Calculated results of the low-energy (<100 MeV) π^+ production spectra from 28 GeV protons incident on a thick iridium target are presented and compared with experimental data. Experimental results are available at angles of 66°, 90°, and 133° with respect to the incident proton beam and comparisons with calculations are given at each of these angles. The calculated and experimental results are in moderately good agreement (factor of 2 to 4) over the energy range considered. Calculated results of the neutron, proton, π^+ and π^- energy spectra, averaged over the angular interval 45° to 75°, are also presented for energies $\lesssim$500 MeV.

2. ENDF/B Related Evaluations

a. Logical Inference and Evaluation** (F. G. Perey)

Most methodologies of evaluation currently used are based upon the theory of statistical inference. It is generally perceived that this theory is not capable of dealing satisfactorily with what are called systematic errors. Theories of logical inference should be capable of treating all of the information available, including that not involving frequency data. A theory of logical inference as an extension of deductive logic via the concept of plausibility and the application of group theory is presented. Some conclusions, based upon the application of this theory to evaluation of data, are also given.

b. An Evaluation of Cross Sections for Neutron-Induced Reactions in Sodium† (D. C. Larson)

An evaluation of the neutron-induced cross sections of ^{23}Na has been done for the energy range from 10^{-5} eV to 20 MeV. All significant cross sections are given, including differential cross sections for production of gamma rays. The recommended values are based on experimental data where available and use results of a consistent model code analysis of available data to predict cross sections where there are no experimental data. This report describes the evaluation that was submitted to the Cross Section Evaluation Working Group (CSEWG) for consideration as a part of the Evaluated Nuclear Data File, Version V, and subsequently issued as MAT 1311.

c. Evaluation of Resonance Parameters for Neutron Interaction with Iron Isotopes for Energies up to 400 keV‡ (C. M. Perey and F. G. Perey)

This report documents the evaluation of the resolved resonance parameters of iron isotopes 54, 56 and 57 in the neutron energy region below

*Abstract of ORNL/TM-7647 (January 1981).
**Presented at Workshop on Evaluation Methods and Procedures, BNL, Sept. 1980.
†Abstract of ORNL-5662, ENDF-299 (September 1980).
‡Abstract of ORNL/TM-6405, ENDF-298 (September 1980).

400 keV. Estimates of the uncertainties in the resonance parameters and correlation between the partial widths Γ_n and Γ_γ are given when significant. Some details about the procedures used to evaluate the resonance parameters, their uncertainties and correlations are reported. This evaluation was performed for the general purpose file of the Evaluated Nuclear Data File (ENDF/B-V MAT 1326).

d. Estimation of the Uncertainties in the ENDF/B-V ^{235}U Fission Spectrum* (R. E. Maerker, J. H. Marable, and J. J. Wagschal)

The uncertainty of the fission spectrum is necessary for calculating uncertainties of reactor performance parameters, for the adjustment of cross sections, and for applications using the dosimetry unfolding technique. However, the ENDF/B-V evaluation of χ^{25} does not include any uncertainties.

Assuming a Watt formulation for χ^{25}, the uncertainty in χ^{25} will be determined by the standard deviations in the Watt parameters a and b and by the correlation in the uncertainties of a and b.

From estimates[1] of the standard deviations in a and b and estimates[2] of the standard deviation of $\bar{E}$, the average energy, the covariance between a and b can be deduced and the uncertainties in the spectrum calculated. Typical standard deviations are 3% below 0.5 MeV and 10% at 10 MeV.

e. Evaluation of Neutron Cross Sections for Fissile and Fertile Nuclides in the keV Range** (L. W. Weston)

Procedures for evaluation of radiative capture, elastic and inelastic processes, and fission in the keV region of neutron energies are described. The use of theoretical tools along with the available ENDF utility codes allows the evaluator to extend and expand upon the experimental data which are often sparse or discrepant. A few problems with the utility codes are noted and suggestions made for improvement and extension. Some ENDF/B-V cross sections for important nuclei are plotted in detail and show significant need for improvement in the shape of the individual partial cross sections to be consistent with theoretical predictions within the constraints of the experimental data. In particular, uranium and plutonium isotopic evaluations, which are of critical importance to fast reactors, deserve careful attention using improved methodology.

*Proc. ANS 35, 555 (1980).
[1]P. I. Johansson and B. Holmqvist, Nucl. Sci. Eng. 62, 695 (1977).
[2]J. L. Lucius and J. H. Marable, Trans. Am. Nucl. Soc. 32, 731 (1979).
**Presented at Workshop on Evaluation Methods and Procedures, BNL, Sept. 1980.

f. GLUCS: A Generalized Least-Squares Program for Updating Cross Section Evaluations with Correlated Data Sets* (D. M. Hetrick and C. Y. Fu)

The PDP-10 FORTRAN IV computer programs INPUT.F4, GLUCS.F4, and OUTPUT.F4, which employ Bayes' theorem (or generalized least-squares) for simultaneous evaluation of reaction cross sections, are described. Evaluations of cross sections and covariances are used as input for incorporating correlated data sets, particularly ratios. These data are read from Evaluated Nuclear Data File (ENDF/B-V) formatted files. Measured data sets, including ratios and absolute and relative cross section data, are read and combined with the input evaluations via the least-squares technique. The resulting output evaluations have not only updated cross sections and covariances, but also cross-reaction covariances. These output data are written into ENDF/B-V format.

3. Validation of ENDF/B Evaluations Through Integral Measurements

a. ORNL Fusion Reactor Shielding Integral Experiments** (Santoro, Alsmiller, Barnes, and Chapman)

Integral experiments that measure the neutron and gamma-ray energy spectra resulting from the attenuation of $\sim$14 MeV T(d,n) ^{4}He reaction neutrons in laminated slabs of stainless steel type 304, borated polyethylene, and a tungsten alloy (Hevimet) and from neutrons streaming through a 30-cm-diameter iron duct (L/D = 3) imbedded in a concrete shield have been performed at ORNL. The facility, the NE-213 liquid scintillator detector system, and the experimental techniques used to obtain the measured data are described. The two-dimensional discrete ordinates radiation transport codes, calculational models, and nuclear data used in the analysis of the experiments are reviewed. The measured and calculated neutron energy spectra (>850 keV) obtained for the attenuation experiments are in excellent agreement ($\sim$10%) for shield compositions and thicknesses up to 412 g/cm^2 thick. The calculated gamma-ray spectra (>750 keV) agree with the measured data to within 15% for the slabs containing stainless steel and borated polyethylene and within a factor of 5 when Hevimet is included in the shield composition. The calculated neutron spectra obtained for the streaming experiments are in good agreement ($\sim$10-15%) with the measured data for the on-axis detector position. For the off-axis detector locations, the calculations overestimate the measurements by as much as a factor of 5 depending on detector location. Current evidence suggests that the angular distributions for elastic and inelastic neutron scattering are not properly represented in the discrete ordinates analysis and more accurate methods are required. The calculated and measured gamma-ray spectra agree within $\sim$30%.

*Abstract of ORNL/TM-7341, ENDF-303 (October 1980).
**Invited paper at ANS Topical Meeting, King of Prussia, PA, October 1980.

b. The Adjustment of Cross Sections Based on Integral Experiments in Fast Benchmark Assemblies* (J. H. Marable)

The adjustment of multigroup cross sections using fast benchmark integral experiments is reviewed. The question of whether such adjustments lead to actual improvements in differential data or only to the determination of parameters in an artificial mathematical model is discussed. Data bases required for adjustment are also discussed, and the concept of calculated-response correctors (calculational biases) based on modeling and calculational approximations is presented. Linear and nonlinear adjustments are illustrated graphically. The need for careful examination of both input and output data, application of the χ^2-test, and confrontation with evaluators and experimentalists for feedback if emphasized. Applications based on ENDF/B-IV and ENDF/B-V are discussed. It is pointed out that in addition to being a practical tool for creating libraries incorporating integral experiment information, and in addition to the possibility of leading to improved nuclear data, least squares adjustment is required for the understanding of the complex of differential nuclear data, integral data, reactor modeling, cross section processing, analysis and calculational methods.

c. Calculation of Neutron and Gamma Ray Energy Spectra for Fusion Reactor Shield Design: Comparison with Experiment** (Santoro, Alsmiller, Barnes, and Chapman)

Integral experiments that measure the transport of $\sim$14 MeV D-T neutrons through laminated slabs of proposed fusion reactor shield materials have been carried out at ORNL. Measured and calculated neutron and gamma ray energy spectra are compared as a function of the thickness and composition of stainless steel type 304, borated polyethylene, and Hevimet (a tungsten alloy), and as a function of detector position behind these materials. The measured data were obtained using a NE-213 liquid scintillator using pulse-shape discrimination methods to resolve neutron and gamma ray pulse height data and spectral unfolding methods to convert these data to energy spectra. The calculated data were obtained using two-dimensional discrete ordinates radiation transport methods in a complex calculational network that takes into account the energy-angle dependence of the D-T neutrons and the nonphysical anomalies of the S_n method. The transport calculations incorporate ENDF/B-IV cross section data from the VITAMIN C data library. The measured and calculated neutron energy spectra are in good agreement behind slab configurations of stainless steel type 304 and borated polyethylene ($\sim$10% for all neutron energies above 850 keV). When 5 cm of Hevimet is added to a 45-cm-thick SS-304 plus borated polyethylene slab assembly, the agreement is less favorable. The agreement among the measured and calculated gamma ray spectra for energies above 750 keV ranges from $\sim$25% to a factor of $\sim$5 depending on the slab composition.

*Presented at Workshop on Evaluation Methods and Procedures, BNL, Sept. 1980.
**Abstract of ORNL/TM-7360 (August 1980).

C. NUCLEAR DATA PROJECT ACTIVITIES - 1980 (S. J. Ball,* Y. A. Ellis, W. B. Ewbank, B. Harmatz, F. W. Hurley,* M. J. Martin,** M. R. McGinnis,* J. T. Miller,* S. Ramavataram,** C. D. Savin,* and M. R. Schmorak)

1. Data Evaluation

As part of the international network, for nuclear structure data evaluation, the Nuclear Data Project has continuing responsibility for mass chains in the region A $\geq$ 195. Revised nuclear data sheets for 11 mass chains were prepared during 1980. In addition to its evaluation responsibility, NDP is committed to maintaining uniform, high standards for ENSDF (and consequently for Nuclear Data Sheets) by providing a thorough review of the first few mass chains prepared by each new evaluator. The Nuclear Data Project provided a thorough review for 11 such mass chains during 1980. NDP staff members have also organized training seminars for new data evaluators in order to introduce them to NDP evaluation techniques, analysis programs, and conventions used in ENSDF and Nuclear Data Sheets.

2. Evaluated Nuclear Structure Data File

The Evaluated Nuclear Structure Data File (ENSDF), developed and implemented by the NDP, contains a documented summary of the current status of nuclear measurements. The ENSDF now contains 7792 distinct sets of evaluated nuclear information. This includes:

1965 sets of adopted level properties (41,000 nuclear levels)
2139 decay schemes
3688 nuclear reaction data collections.

All decay scheme information in ENSDF is now at least as complete as the most recent Nuclear Data Sheets. Normalization information is included wherever available, and details of electron capture and internal conversion have been added systematically, so that complete tables of atomic and nuclear radiations can be assembled for more than 1600 decay schemes.

The ENSDF computer format has been adopted as an international standard for the systematic storage and exchange of nuclear structure data. At six-month intervals NDP has prepared complete copies of ENSDF on magnetic tape for distribution through an international network of data centers.

3. Nuclear Structure References

Nuclear Data Project's Nuclear Structure References (NSR) file contains about 70,000 entries. Approximately 5000 indexed new research works are added each year. About half of the additions are journal publications; the other half consists of reports, conference abstracts, preprints, etc. Each month an SDI (selective dissemination of information) service is provided from new entries to the NSR file. An index to the new literature is published three times per year as "Recent References," which includes both isotope and reaction indexes for both journal and nonjournal literature.

*Technical support staff.
**Part-time assignment to Nuclear Data Project.

The NSR file is being used as an international standard for the systematic exchange of indexed reference information. Copies of the complete indexed file have been distributed to the international network of data evaluation centers.

4. Publications

The Nuclear Data Project is the editorial and publications office for the journal Nuclear Data Sheets. The NDP prepares camera-ready copy which is sent to Academic Press for publication and distribution. Manuscripts are now being received from several data evaluation centers other than NDP. Thirty percent of the new evaluations published during 1979 were prepared by non-NDP evaluators.

OHIO UNIVERSITY

A. NEUTRON SCATTERING MEASUREMENTS

1. ^{6}Li+n (Knox, Koehler, Resler, Lane)

Neutron differential elastic and inelastic (Q = -2.18 MeV) scattering cross sections for ^{6}Li have been measured at four energies between 4.5 and 6.4 MeV incident neutron energy. At each energy cross sections were measured at nine equally spaced angles between 20° and 160°. The flight path was 2.5 m and the scattering sample was 16.5 gms of highly enriched (98.7%) ^{6}Li. Analysis of these data is currently underway. These measurements will be extended upwards in energy to $E_n \approx 8$ MeV this year and up to $\sim$ 11 MeV later. As these inelastic scattering data become available, they will be included in a comprehensive R-matrix analysis of the ^{7}Li system described in Section C of this report.

2. ^{11}B+n (Koehler, Resler, Lane, Knox)

Elastic and inelastic (2.12, 4.45 and 5.02 MeV levels) differential cross sections for neutrons scattered from an enriched sample of ^{11}B have been measured at incident energies of 5.25, 5.75 and 6.40 MeV. These data, together with measurements reported the last two years,[1,2] complete our survey of the differential inelastic cross sections for this nucleus at a total of 13 incident energies. These data are now fully corrected for multiple scattering effects. At 7.5 MeV these data disagree in part with the results of Hopkins and Drake,[3] and at 4.8 MeV they disagree completely with earlier results of Porter et al.[4] Very good agreement with the previous elastic data of White et al.[5] was obtained. R-matrix calculations for elastic and inelastic scattering have been made to extract some of the salient features of this region of high density[5,6] of states in ^{12}B. The

---

1. Reports to the DOE Nuclear Data Committee, BNL-NCS-27800, pg. 145

2. Reports to the DOE Nuclear Data Committee, BNL-NCS-26133, pg. 184

3. J.C. Hopkins and D.M. Drake, Nucl. Sci. and Eng. 36, 275 (1969)

4. Porter, Coles and Wyld, AWRE Report No. 045/70, U.K.A.E.A., A.W.R.E., Aldermaston, England, unpublished (1970)

5. White, Lane, Knox and Cox, Nucl. Phys. A340, 13 (1980)

6. Auchampaugh, Plattard, Extermann and Ragan III, Proc. of the Int. Conf. on the Interactions of Neutrons with Nuclei, Lowell, Mass., July 1976, E.R.D.A. CONF-760715, pg. 1389; Los Alamos Scientific Laboratory Report LA-6761, June, 1977

results are not inconsistent with those of White et al.[5] and will be compared to the shell model calculations of J. Millener[7] of BNL.

3. ^{13}C (Resler, Koehler, Lane, Knox)

Measurements of the differential elastic and inelastic (3.09 MeV level) cross sections for ^{13}C+n were made at six incident neutron energies (4.55, 4.68, 4.74, 4.79, 4.84 and 4.89 MeV). In this energy range the total cross section and the integrated elastic cross section show a resonance. However, the integrated first inelastic cross section did not show any resonant behavior although the angular distributions did change with energy. The R-matrix analysis of previous elastic data (described below) indicate an assignment of $J^{\pi} = 2^-$ or 3^- at an excitation of 12.61 MeV in ^{14}C. The present data would be consistent with a 3^- assignment because the 3^- could not inelastically decay to the $1/2^+$ first excited state of ^{13}C except by $\ell_{n'} \geq 3$ which is very unlikely at the low energy ($E_{n'} \sim 1.5$ MeV) of the inelastic neutrons.

Final analysis of these data will be carried out in the near future. Also more measurements are planned using the new TOF tunnel. A long flight path will allow better resolution of the second and third inelastic at higher energies. An R-matrix analysis including the elastic and inelastic data should provide further information on the level structure of ^{14}C at energies above the current analysis.

4. ^{18}O+n (Koehler, Resler, Lane, Knox)

Elastic and inelastic (1.98, 3.92 and 4.45 MeV levels) differential cross sections for neutrons scattered from an enriched water sample of ^{18}O have been measured at incident energies of 6.0, 6.1, 6.2, 6.3 and 6.4 MeV. This energy region corresponds to an apparent broad resonance structure in the total cross section. At present, the measurements have not been corrected for the presence of hydrogen in the sample or for multiple scattering. Angular distributions were obtained at nine angles at the above-mentioned energies for the elastic group and for the 1.98-, 3.92- and 4.45-MeV levels, but the 3.55 and 3.63 MeV levels were not resolved from each other. No previous elastic or inelastic measurements have been reported on ^{18}O in this energy region. Analysis of these data is presently underway.

5. ^{54}Fe and ^{12}C at 24 MeV* (Mellema, Soleimani, Kurup, Tailor, Rapaport)

Preliminary studies of the differential elastic and inelastic scattering of 24 MeV neutrons have been carried out on the nuclei ^{54}Fe and ^{12}C. The angular range of the measurements extended from 15° to 150° for the elastic scattering and from 15° to about 110° for the inelastic data. For ^{12}C the first 2^+ state at 4.43 MeV was easily resolved. For ^{54}Fe

* Supported in part by the National Science Foundation

7. J. Millener (private communication, 1981)

preliminary data for five excited states was obtained. The elastic scattering cross section data were used in the search code GENOA to obtain optical model parameters which were used to calculate inelastic cross sections and deformation parameters using the code DWUCK for ^{54}Fe and DWUCK and ECIS for ^{12}C. Energy resolution and counting statistics were marginal for the inelastic scattering work on ^{54}Fe. Both experiments were performed with the conventional time-of-flight spectrometer. The new beam swinger spectrometer will be used to repeat and extend both sets of measurements.

6. ^{26}Mg (n,n) at 24 MeV** (Tailor, Rapaport, Kulkarni, Randers-Pehrson)

An enriched ^{26}Mg sample (20.287 g) was used to study the elastic and inelastic scattering of 24 MeV neutrons. Standard pulsed-beam time of flight methods were employed. Data were taken at angles between 15° and 150° every 5°. The time of flight events were biased at electron energies of 5 MeV (E_n = 8.8 MeV) and 7 MeV (E_n = 11.3 MeV). This "low" and "high-bias" technique allows a check on the relative detector efficiency, which was desired because of the kinematic shift of the neutron energy with change of angle.

We have obtained angular distributions for the g.s. transition and for the excitation of the first 2_1^+ (1.81 MeV) state and second 2_2^+ (2.94 MeV) state in ^{26}Mg. States up to 7 MeV in excitation were seen, but too weakly to extract meaningful information. Optical model potential parameters have been extracted from the elastic scattering and deformation parameters obtained for the 2_1^+ and 2_2^+ states. Coupled channel calculations are being performed and will be compared with similar calculations reported[8] from the scattering of 24 MeV protons from ^{26}Mg to extract neutron and proton matrix elements.

B. NEUTRON INDUCED CHARGED PARTICLE REACTION MEASUREMENTS

1. $^{58}Ni(n,z)$ (Randers-Pehrson, Finlay, Rapaport, Kulkarni, Brient)

We are studying the $^{58}Ni(n,z)$ reactions at 11 MeV which is just about the opening of the n,n'p reaction channel. This region is interesting because the proton and alpha particle separation energies in ^{58}Ni are smaller than that for neutrons, thus permitting the emission of lower energy charged particles than usually observed.

Measurements have been made for the charge particles emitted from $^{58}Ni(n,z)$. The experiment employed an electron emitting foil coupled to a channel plate

---

** Supported by the National Science Foundation

8. Alons, Blok and van Heinen, Phys. Lett. 83B, 34 (1979)

as the first element of a detector telescope.[9] Using this device we have observed protons of energy as low as 300 keV. A second challenge in this experiment is the presence of n,p reaction products arising from the d(d,np) continuum. A double gas cell arrangement was used to address this problem.[10] The first cell contained the deuterium source gas while the second cell was filled with ^{3}He to provide a breakup continuum but no monoenergetic peak.

The data are in too early a stage of analysis to draw any conclusions yet except to observe that the protons produced by the continuum seem to be forward peaked.

2. The $^{12}C(n,\alpha_0)^9Be$ and $^{12}C(n,n')3\alpha_n$ Reactions† (Finlay, Randers-Pehrson, Rapaport, Kulkarni, Grabmayr, Graham)

Double differential cross sections $d\sigma/d\Omega dE$ have been measured at 0° for neutron energies of 9.5, 10.5 and 24 MeV for the important dosimetric reactions $^{12}C(n,\alpha_0)^9Be$ and $^{12}C(n,n')3\alpha$. At E_n = 9.5 MeV, the bombarding energy is too low to populate the 3^- level at 9.63 MeV in ^{12}C and 3α decay, although allowed energetically, is not observed. An incident energy of 10.5 is barely sufficient to populate the 3^- state, and a large increase in the production of low energy alpha particles is observed (see Figs. 1 and 2).

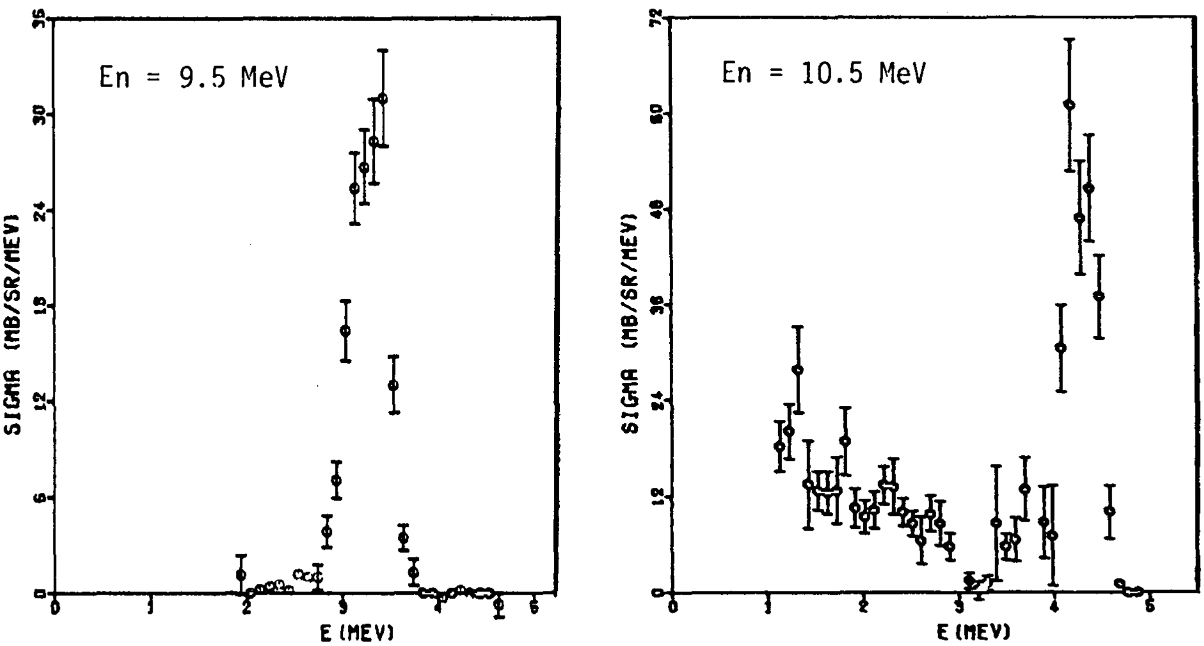

Fig. 1 (left) and Fig. 2 (right). Double differential cross sections for alpha particles produced at zero degrees from neutron bombardment of carbon.

† Supported by the National Cancer Institute

9. "Neutron Induced Charged Particle Reaction Studies at Ohio University," G. Randers-Pehrson et al., Symposium on Neutron Cross Sections from 10 to 50 MeV, BNL-NCS-51245, Pg. 389 (1980)

10. "A Study of Neutron Source Reactions," P. Grabmayr et al., Proc. Int. Conf. on Cross Sections for Tech., Knoxville (1979) NBS Spec. Pub., pg. 594

At E_n = 24 MeV, the discrete alpha particle group from the $^{12}C(n,\alpha_0)^9Be$ reaction is very weak at 0° compared with the continuum from the 3α reaction.

For medical applications it would be important to extend the measurement of the alpha particle spectrum to below 1 MeV. These measurements were performed on the magnetic quadrupole triplet spectrometer which uses pulsed-beam time-of-flight information to improve the mass identification in the spectrometer. At an alpha particle energy of 1 MeV the flight time of the alpha particle exceeds the time interval between beam bursts at a repetition frequency of 2.5 MHz. In principle it should be possible to extend the measurement of the alpha particle spectrum to well below 1 MeV by operating the accelerator at one-fourth of the master oscillator frequency (i.e. at 1.25 MHz) with a considerable increase in the required beam time.

All of these measurements were taken in order to test the development of the spectrometer system and to determine the feasibility of the measuring program. Present plans call for the measurement of the energy and angular distribution of alpha particles from these reactions at 24 MeV in 1981.

C. R-MATRIX ANALYSIS

1. ^{6}Li+n (Knox, Lane)

A comprehensive R-matrix analysis of the ^{7}Li system is currently underway. The neutron elastic, inelastic (Q = −2.18 MeV) and (n,α) channels are included in this analysis. Preliminary results for E_n < 2 MeV were given in Progress Report DOE/ER/02490-1. A series of measurements of the $^6Li(n,\alpha)t$ reaction cross section for $E_n \geq 2$ MeV are to be carried out on the triplet quadrupole spectrometer at this laboratory beginning this spring. These data, as well as new inelastic neutron scattering data (Section A.1) will be included in the analysis as they become available.

2. ^{7}Li+n (Knox, Lane)

An R-matrix analysis of all available ^{7}Li+n differential elastic, differential inelastic (Q = −0.478 MeV and Q = −4.63 MeV) and $^7Li(n,n'\gamma)^7Li$ (Q = −0.478 MeV) data up to 8 MeV incident neutron energy has been completed. A paper describing this work entitled "States in ^{8}Li from an R-Matrix Analysis of $^7Li(n,n)^7Li$, and $^7Li(n,n')^7Li^*$ (0.478, 4.63) Measurements," H.D. Knox and R.O. Lane has been accepted for publication in Nuclear Physics.

3. ^{12}C+n (Knox, Lane)

An earlier R-matrix analysis[11] of the ^{13}C system for $E_n \lesssim 4.5$ MeV has been extended upwards in neutron energy to $E_n \gtrsim 8.5$ MeV. This new

11. Knox, Cox, Finlay and Lane, Nucl. Phys. A217, 611 (1973)

analysis is the first R-matrix study of ^{12}C+n scattering above the threshold for inelastic scattering. Included in the analysis are ^{12}C+n total, differential elastic and inelastic (Q = -4.44 MeV) scattering cross section data as well as available $^{12}C(n,\alpha)^{9}Be$ differential cross section data. Spins and parities of several levels in ^{13}C have been determined through this analysis. A report describing this work is currently being prepared.

4. ^{13}C+n (Lane, Knox, Hoffmann-Pinther, White, Auchampaugh)

An analysis of neutron elastic scattering cross section data for E_n < 6.5 MeV has been completed. A paper describing these results entitled "States in ^{14}C from σ_T and $\sigma_{el}(\theta)$ for ^{13}C+n; Measurement, R-Matrix Analysis and Model Calculations," R.O. Lane, H.D. Knox, P. Hoffmann-Pinther, R.M. White and G.F. Auchampaugh has been accepted for publication in Phys. Rev. C.

D. THE OHIO UNIVERSITY BEAM SWINGER FACILITY†† (Finlay, Brient, Rapaport, Randers-Pehrson, Marcinkowski)

It has been clear to us for some time that the original time-of-flight spectrometer had important limitations, the most obvious of which was that the maximum available flight path at which an entire angular distribution could be measured was only 6.6 m long. At that flight path, it has been difficult to obtain an energy resolution better than 800 keV for 26 MeV neutrons (300 keV for 11 MeV neutrons). Because of these limitations, we have focused attention on the study of inelastic scattering from closed-shell nuclei with widely separated final states. Even with this restriction, some experiments--such as the study of isospin effects in the excitation of low-lying octupole states--have had ambiguous results because of the competition from unresolved levels.

A next-generation time-of-flight spectrometer is being installed. The new spectrometer will provide a dramatic improvement in performance over our present system in the following parameters: pulsed beam quality, resolution, background reduction, signal-to-noise ratio and flexibility of operation. The system consists of three essential components: the beam-swinger magnet, the time-of-flight tunnel, and new, large-area neutron detectors.

The beam-swinger magnet was designed by Aaron Galonsky and has been in service at the Michigan State Cyclotron Laboratory for the last 3-4 years. The magnet rigidity of the beam-swinger was well matched to the MSU K = 50 cyclotron but will not be useful for the beams from the new superconducting cyclotrons. Michigan State University has transferred the magnet to Ohio University.

The principal advantage of a beam swinger magnet is that an angular distribution may be measured by varying the direction of the incident beam.

---

†† Also supported by the National Science Foundation and Ohio University

The outgoing-particle direction is fixed in space. This is particularly important for reactions involving outgoing fast neutrons since it is often necessary to use long flight paths to obtain adequate energy resolution. A long flight path in one direction is much more reasonable architectually than is a long flight path in all directions. Accordingly, we have constructed a long underground flight path adajacent to our accelerator building (see Fig. 3). The underground tunnel has been built from precast concrete pipe (7 ft. inside diameter x 88 ft long).

The tunnel is separated from the accelerator vault and beam swinger by a thick concrete wall. Scattered neutrons are admitted to the counting tunnel through a long (2 m) tapered collimator pipe. This "pin-hole camera" approach to neutron time-of-flight measurements promises to provide advantages in signal-to-noise ratio and general flexibility compared with our present semi-open geometry.

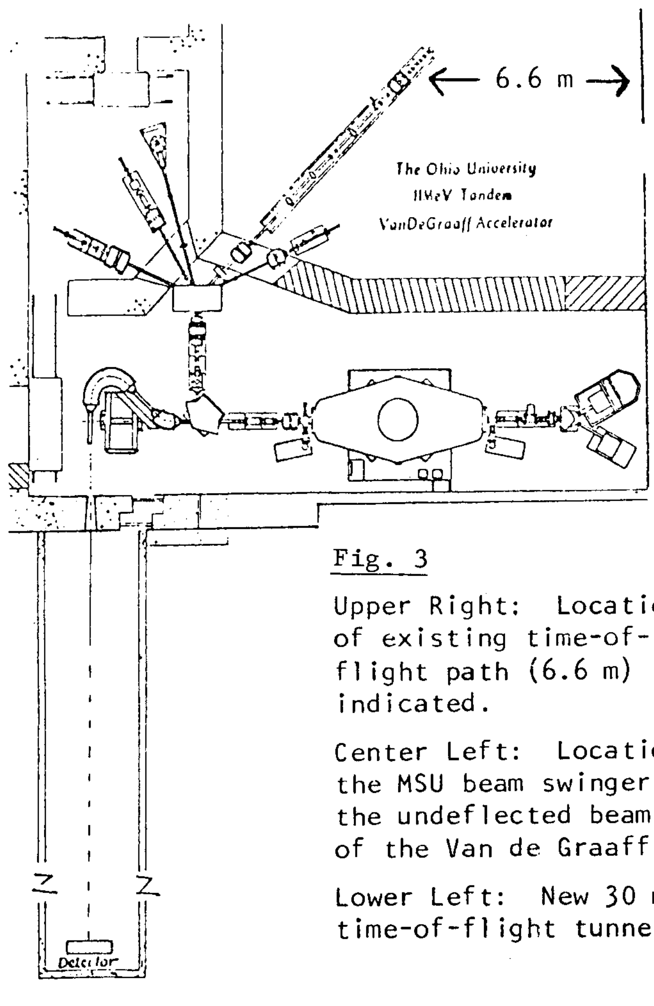

Fig. 3

Upper Right: Location of existing time-of-flight path (6.6 m) indicated.

Center Left: Location of the MSU beam swinger along the undeflected beam line of the Van de Graaff.

Lower Left: New 30 m time-of-flight tunnel.

At this writing the tunnel construction has been completed, the swinger magnet has been installed and aligned, the cryogenic vacuum pump has evacuated the beam swinger to about 10^{-7} torr and a 10 μA (dc) deuteron beam has been delivered to a gas cell at the target location. Pulsed beams with burst duration of < 600 picoseconds have been obtained on target.

Present activity is centered about detector development. While the availability of long flight paths make greatly improved energy resolution possible, it would be intolerable to obtain this resolution at a cost of $(\frac{1}{r^2})$ losses in counting rate. The challenge to the experimenter is to develop highly efficient, fast, large-area neutron detectors. The experience we have recently gained in this area[12,13] has been helpful in approaching this task. We are presently developing detectors which we estimate will provide a factor-of-two improvement in energy resolution for 25 MeV neutrons simultaneous with a factor of 6-8 improvement in data rate over our present system. At a later date we will investigate the ultimate energy resolution which will be available with reasonable counting rates at the full flight path.

---

12. Carlson, Finlay and Bainum, Nucl. Inst. and Meth. 147, 353 (1977)

13. Goodman, Bainum, Rapaport and Brient, Nucl. Inst. and Meth. 151, 125 (1978)

A. DELAYED NEUTRON STUDIES

1. Delayed Neutron Emission Probabilities (P_n)
(P. L. Reeder and R. A. Warner)

The final results on our 1978 measurements of Rb and Cs P_n values are now available.[1] Both the ion counting and beta counting techniques were used in an effort to minimize any systematic errors. Our results are compared to world averages computed before and after inclusion of our latest results in Table 1.

About 50 delayed neutron precursors should be available from the new TRISTAN isotope separator facility at Brookhaven National Laboratory. We plan to measure P_n values for all available precursors using the beta counting technique.

2. Delayed Neutron Average Energies ($\bar{E}$)
(P. L. Reeder and R. A. Warner)

The final results on our 1978 measurements of the average energies of neutrons from Rb and Cs precursors are now available.[2] We have also compiled average energies of all fission product precursors to obtain "best values" for 34 precursors. These average energies were then weighted by the corresponding fission yields from ENDF/B-V and the P_n values to give average energies of group and equilibrium delayed neutron spectra. These calculations have been submitted for publication.[3]

Average energy measurements will be performed along with the P_n measurements at the TRISTAN facility. The ring ratio technique will be slightly modified for mass chains containing more than one precursor. Simultaneous neutron decay curves will be measured for all three counter rings. After decay curve analysis the ratio of initial activities of each component will

---

[1] P. L. Reeder and R. A. Warner, "Delayed Neutron Emission Probabilities of Rb and Cs Precursors," PNL-SA-8766, submitted to Phys. Rev. C.

[2] P. L. Reeder and R. A. Warner, "Measurement of Average Neutron Energies by a Counting Rate Ratio Technique," PNL-SA-7536 REV, Nucl. Instrum. Methods (to be published).

[3] P. L. Reeder and R. A. Warner, "Average Energy of Delayed Neutrons from Individual Precursors and Estimation of Equilibrium Spectra," PNL-SA-9071, submitted to Nucl. Sci. Eng.

TABLE 1. P_n VALUES (IN %) FROM THIS WORK AND WORLD AVERAGE VALUES

Precursors	This Work	World Average[a]	Revised World Average
^{87}Br	2.1 ±0.4	2.38 ± .11	2.48 ± .11
^{88}Br	6.1 ±0.7	6.7 ± .3	6.6 ± .3
^{89}Br	13.9 ±2.0	13.5 ±1.3	13.0 ± .8
^{92}Rb	.0098± .0010	0.0116± .0006	.0108± .0007
^{93}Rb	1.36 ± .14	1.39 ± .08	1.31 ± .06
^{94}Rb	10.1 ±1.0	10.4 ± .6	9.9 ± .3
^{95}Rb	8.7 ±0.9	8.8 ± .4	8.5 ± .3
^{96}Rb	14.5 ±1.5	14.2 ± .8	13.3 ± .5
^{97}Rb	27.9 ±3.1	28. ±2.5	25.1 ±1.3
^{98}Rb	12.8 ±2.0	16.0 ±1.0	15.1 ±1.2
^{137}I	7.6 ±1.1	6.6 ± .4	6.5 ± .3
^{138}I	5.1 ±3.0	5.3 ± .4	5.3 ± .4
^{141}Cs	.034 ± .005	0.036 ± .005	.037 ± .007
^{142}Cs	.105 ± .012	0.091 ± .004	.093 ± .006
^{143}Cs	1.61 ± .17	1.68 ± .10	1.61 ± .08
^{144}Cs	3.1 ± .3	3.0 ± .3	3.1 ± .3
^{145}Cs	13.3 ±1.4	13.3 ± .9	13.6 ±1.0

[a]G. Rudstam, in Proceedings of the Consultants' Meeting on Delayed Neutron Properties, Vienna, 26-30, March 1979. International Atomic Energy Agency, INDC(NDS)-107/G + Special.

be obtained. The technique has been demonstrated at mass 147 where the ring ratio for ^{147}Ba is dramatically lower than the ring ratio for ^{147}Cs.

3. Delayed Neutron Spectra
(P. L. Reeder and R. A. Warner)

We have investigated the possibility of approximating delayed neutron spectra by the Maxwellian function

$$N(E) \sim E^{\frac{1}{2}} \exp(-E/T)$$

where N(E) = the number of neutrons per unit energy interval
E = neutron energy
T = "temperature" parameter = $2\,\bar{E}/3$

This function does not reproduce the peak structure in spectra of individual precursors. However, when individual spectra are weighted by fission yields and P_n values and combined into group and equilibrium spectra, the peak structure is much less important. The overall shape of the equilibrium spectra generated by summing the individual precursor spectra from Kratz, et al.[4] is reasonably approximated by a Maxwellian curve. This is not true for equilibrium spectra measured directly by other workers.[5,6,7] These comparisons are presented in Ref. 3.

4. Delayed Neutron Half-Lives
(P. L. Reeder and R. A. Warner)

We are currently measuring half-lives of delayed neutron precursors produced at the TRISTAN facility. The emphasis is on those precursors for which limited data are available such as the Sr, Y, Ba and La precursors. Measurements have been performed as masses 97,98,99,146,147 and 148.

---

[4] K. L. Kratz, Proc.Consultants' Mtg. Delayed Neutron Properties, Vienna, March 26-30, 1979, INDC(NDS)-107/G + Special, p. 103, International Atomic Energy Agency (1979).

[5] W. R. Sloan and G. L. Woodruff, Nucl. Sci. Eng. 55, 28 (1974). G. W. Eccleston and G. L. Woodruff, Nucl. Sci. Eng. 62, 636 (1977).

[6] A. E. Evans and M. S. Krick, Nucl. Sci. Eng. 62, 652 (1977).

[7] D. R. Weaver, J. G. Owen and J. Walker, Proc. Consultants' Mtg. Delayed Neutron Properties, Vienna, March 26-30, 1979, INDC(NDS)-107/G + Spécial, p. 207, International Atomic Energy Agency (1979)

5. Beta-Delayed Two-Neutron Emission
(P. L. Reeder and R. A. Warner)

We have searched for beta-delayed two-neutron emission from ^{98}Rb and ^{99}Rb by use of the time correlation technique of Azuma, et al.[8] Positive results have been obtained for ^{98}Rb while the results for ^{99}Rb are presently inconclusive. Other candidates such as ^{83}Ga, ^{84}Ga, ^{92}Br, ^{142}I and ^{148}Cs will be investigated whenever these ion beams become available at the TRISTAN facility. In addition to the P_{2n} value, we hope to measure average energies of the two-neutron emission by means of the ring ratio technique.

B. ISOMER YIELDS (P. L. Reeder and R. A. Warner)

Experiments are currently in progress to measure independent isomer yield ratios for thermal neutron induced fission of ^{235}U. Fission products from a neutron pulse from a TRIGA reactor are mass analyzed by the SOLAR on-line mass spectrometer. The first cases being studied are ^{90}Rb and ^{138}Cs. The half-lives of these isomers are long enough so that samples will be collected on a catcher foil and counted off-line to determine the yield ratios. Future experiments will include measurements on In, Br and I isomers.

C. GAS SCINTILLATION PROPORTIONAL COUNTER FOR NEUTRON SPECTROMETERY (P. L. Reeder and H. E. Palmer)

A high efficiency, high resolution neutron spectrometer based on the gas scintillation proportional counter principle is currently under development. Neutrons will be captured in a high pressure, large volume cell of ^{3}He plus a small amount of Xe. Scintillation light from the Xe will be detected by a photoionization counter containing Tetrakis-(dimethylamino)-ethylene (TMAE). This detector will be used for a variety of neutron spectrometry experiments including coincidence measurements on delayed neutron precursors.

[8] Azuma, Carraz, Hansen, Jonson, Kratz, Mattsson, Nyman, Ohm, Ravn, Schröder and Ziegert, Phys. Rev. Letters 43, 1652 (1979).

UNIVERSITY OF PENNSYLVANIA

A. COMPLETED WORK

1. "Energy levels of light Nuclei: A = 11-12"

This paper has been published in Nuclear Physics A336 (1980) p. 1-154.

F. Ajzenberg-Selove and C. L. Busch

2. "Energy levels of light Nuclei: A = 13-15"

The proofs for this paper have been corrected. This 185 page paper will appear in "Nuclear Physics" in about two months.

F. Ajzenberg-Selove

B. WORK IN PROGRESS

A review paper on A = 16-17 is being prepared, to be submitted for publication in September 1981. The first preprint, a preliminary review of A = 16, will be sent out for comments in March 1981. Our work is proceeding on schedule.

F. Ajzenberg-Selove (and G. C. Marshall)

RENSSELAER POLYTECHNIC INSTITUTE

A. NUCLEAR DATA

1. Fission Cross Section Measurement of ^{248}Cm

(H. T. Maguire, Jr., C. Stopa, D. R. Harris, R. C. Block, R. E. Slovacek (KAPL), R. W. Hoff (LLL) and J. W. T. Dabbs (ORNL))

The even isotopes of curium have large spontaneous fission decay rates, requiring a large neutron intensity to measure the fission cross section in the presence of a strong spontaneous fission background. The RINS (Rensselaer Intense Neutron Spectrometer) system, consisting of a 75-ton lead slowing-down spectrometer coupled to the RPI Gaerttner Laboratory electron linac [1], produces a very intense neutron flux of broad resolution in the 1 to 100,000 eV energy range, and this system has been used to measure the fission cross section of ^{248}Cm.

Following the method developed by Bicknell et al.[2], the measurement was made with a gaseous fission ionization chamber located inside the lead spectrometer. Hemispherical electrodes [3] and fast electronics designed and constructed at ORNL were used for this measurement. An aluminum chamber was built to contain up to five pairs of these electrodes, with each pair connected to a separate set of electronics. A 27-μg deposit of highly-enriched $^{248}Cm[(3.2 \times 10^{-4})^{245}Cm$ and $(1.6 \times 10^{-4})^{247}Cm]$ was placed on a 4-mm-dia spot at the center of the inner electrode. Two other pairs of electrodes, containing respectively ^{252}Cf and ^{235}U deposits, were also placed inside the chamber. All pairs of electrodes were operated at a bias of 300 volts and the chamber was filled with 3 atmospheres of pure methane. The linac was operated for ~2 hr at 200 pps repetition rate and with ~0.7 kw of electron beam power on the photoneutron target.

The counting data were corrected for spontaneous fission background, and the relative fission cross section was obtained by dividing the neutron-induced fission counts in each slowing-down time interval by the relative number of neutrons incident upon the ^{248}Cm. The relative spectrum of neutrons in RINS was determined in a previous measurement.[1] The fission cross section is shown in Fig. A-1 over the energy range from 2.2 eV to 100 keV. The error bars are for counting statistics (1σ) only. This cross section curve was provisionally normalized by integrating the area under the low-energy half of the data for the 76-eV resonance and then setting this integral equal to the half area calculated from the reported resonance parameters.[4]

The statistical accuracy of these data is quite good, especially considering the rather short (~2 hr) time over which the data were taken. The signal-to-background ratio was better than 3:1 near the peak of the 76-eV resonance, and this ratio did not fall below 1:2 from 72 eV to 100 keV. Thus, the RINS method provides sufficient neutron intensity to measure the fission cross section in a nucleus like ^{248}Cm which has a large spontaneous fission background. The data from the ^{252}Cf chamber indicated that this system does not suffer from the linac gamma flash at energies below ∿100 keV, so the data in Fig. A-1 are free from electronic artifacts.

Figure A-1 shows the resolved resonances at 7.3 and 27 eV, the resolved low-energy half of the 76 eV resonance, and "bulges" in the curve caused by partially resolved resonances near 100, 240 and 700 eV. There is also a "bulge" near 13 keV which suggests the possibility of intermediate structure, but this interpretation is considered preliminary at this time.

The data above ~20 eV provide an independent measurement of the fission cross section, to which the results of an earlier nuclear explosion measurement can be compared. Below ~20 eV there exist no measurements of the fission cross section, except at thermal, so these results represent the only measured data in this energy range.

The RINS method has been successfully applied to measure the fission cross section of ^{248}Cm from a few eV to 100 keV with broad neutron energy resolution. This technique provided the first measurement of the ^{248}Cm fission cross section in the energy range from a few eV to ~20 eV, a range not covered in nuclear explosion measurements. The RINS method will be used to measure simultaneously the important fission cross sections of ^{244}Cm as well as those of ^{248}Cm and ^{235}U in order that all three even curium isotopes be measured in the same neutron flux and resolution and be directly normalized to the ^{235}U fission cross section.

---

[1] R. E. Slovacek, D. S. Cramer, E. B. Bean, J. R. Valentine, R. W. Hockenbury and R. C. Block, Nucl. Sci. and Eng., 62, 445 (1977).

[2] P. A. Bicknell, R. C. Block, G. Krycuk and Y. Nakagome, Nucl. Instr. and Methods, 178, 221 (1980).

[3] J. W. T. Dabbs, N. W. Hill, C. E. Bemis and B. Raman, Nuclear Cross Sections and Technology, Vol. 1, p 81, NBS Spec. Publ. 425 (1975).

[4] S. F. Mughabghab and D. I. Garber, BNL 325, Third Ed., Vol. 1, Resonance Parameters (1973).

[5] M. S. Moore and G. A. Keyworth, Phys. Rev. C, 3, 1656 (1971).

2. Neutron Capture and Total Cross Section Measurements of ^{232}Th from 0.006 eV to 18 eV
(R. C. Little, R. C. Block, D. R. Harris, R. E. Slovacek (KAPL) and O. N. Carlson (Ames)

The neutron total cross section and the shape of the neutron capture cross section of ^{232}Th have been measured in the energy range from 0.006 eV to 18 eV at the RPI Gaerttner Linac Laboratory. The neutron total cross

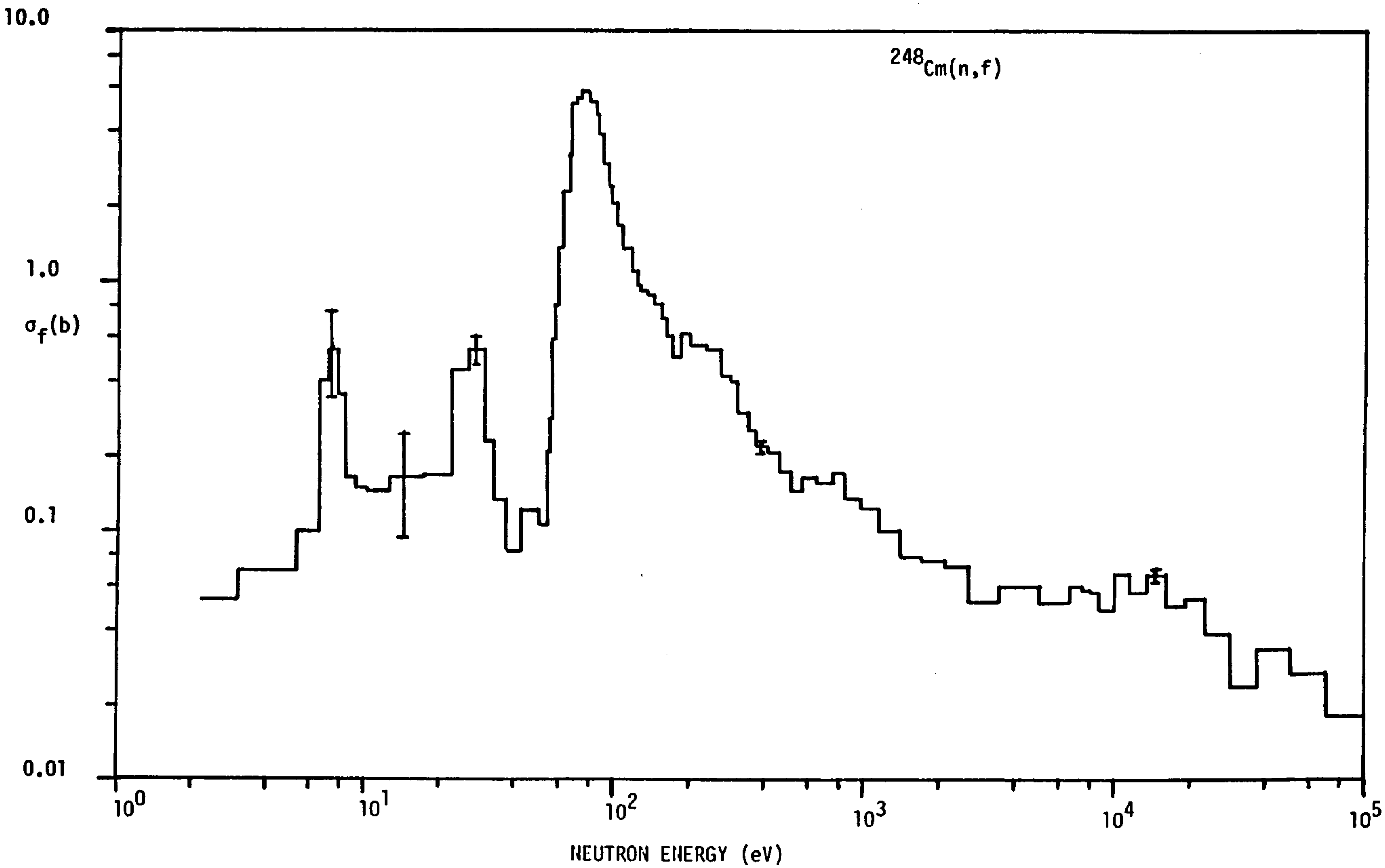

10.0
1.0
0.1
0.01
σ_f(b)
^{248}Cm(n,f)
10^0
10^1
10^2
10^3
10^4
10^5
NEUTRON ENERGY (eV)

Figure A-1

section was obtained from transmission measurements using metallic ^{232}Th samples and a ^{6}Li-glass neutron detector. The total cross section above 0.1 eV is in good agreement with the ENDF/B-V evaluation. Below 0.1 eV, where Bragg scattering is important, the measured total cross section is significantly lower than the evaluated total cross section. The shape of the neutron capture cross section was obtained from 0.009 eV to 18 eV using a ThO_2 sample and a 1.25-m-dia. liquid scintillator detector. The shape of the measured capture cross section above 0.1 eV is in good agreement with a recent shape measurement at Brookhaven National Laboratory. The neutron capture cross section below 0.1 eV is found to increase less rapidly than 1/v with decreasing neutron energy.

B. INTEGRAL MEASUREMENTS

1. Neutron Spectra Measurements Upon a Spherical Assembly of Thoria

[R.C. Block, M. Becker, D.R. Harris, P.S. Feigenbaum and S.A. Hayashi, S. Yamamoto (KUR)]

Calculations with DTF-IV were carried out at both RPI and Kyoto University (KUR) for a double-Maxwellian source inside the o.6-m-diam. spherical ThO_2 assembly to confirm that both laboratories were obtaining the same calculated leakage spectrum. Calculations were then carried out with the source spectrum measured at RPI and with both ENDF/B-IV and ENDF/B-V data. The calculated spectrum was slightly softer in the high-energy (~ 2 to 10 MeV) region for the ENDF/B-V data than for the ENDF/B-IV data. The measured spectrum seemed to agree more closely with the ENDF/B-IV calculation; however, this is considered preliminary at this stage until the effects of mean emission time and the efficiency of the proton recoil detector are re-examined.

C. SAFEGUARDS AND FISSILE ASSAY

1. The Applicability of the Lead Slowing Down Spectrometer For Non-Destructive Assay of Commercial-Size Fuel Elements

[F.W. Bornt, Jr., D.R. Harris and R. C. Block]

As the use of nuclear power increases, so will the amounts of fissionable material (^{235}U and ^{239}Pu in particular). This will require improved non-destructive assay (NDA) methods for both fresh and spent fuel which must be able to determine accurately how much and what kind of fissionable material is in the pin or assembly, and which must also be relatively tamper-proof. The Lead Slowing Down Spectrometer (LSDS), able to meet these conditions, has been used in the past to assay single fresh fuel pins[1], but no one has ever, to our knowledge, used it for spent fuel assemblies.

At the RPI Gaerttner LINAC Laboratory there is a 75-ton LSDS which was built as part of a program to develop a system that can assay single spent fuel pins from the Shippingport LWR breeder experiments. Used with a 100-MeV electron linear accelerator, this system produces ~ 10^{12}n/sec in 60-nsec bursts at a repetition rate of 400 pps. Based on experiments with breeder mock-up (BMU) single fuel pins, assay accuracies of better than 0.5% are obtained for 50 pins/day and (with appropriate sampling) 0.2% for the E.O.L. core inventory

We are trying to determine what effects a full size, 17 x 17 commercial PWR fuel assembly will have on the LSDS assay system. Among these effects is the shielding of the inner pins by the outer pins. To study these effects, preliminary measurements were begun using a 10-cm-(4 in.)-diameter-by-61-cm-(24 in.)-long aluminum cylinder filled with depleted U_3O_8 (~ 0.2 w/o ^{235}U). The U_3O_8 in this cylinder is approximately equivalent to a one eighth section of a 17 x 17 fuel assembly. We have been looking at the detection system's relative sensitivity to a fission event at the center compared to a fission event at the surface, and we plan to measure the interrogation flux depression across the cylinder.

Relative sensitivity measurements were carried out by surrounding the U_3O_8-filled cylinder with ~ 10cm of lead, and a ^{238}U fission chamber was placed near the U_3O_8 cylinder with a variable thickness of lead placed between the chamber and the U_3O_8. A 3.6-Ci PuBe neutron source was placed in a small hole in the center of the U_3O_8 cylinder, and then the PuBe source was moved across the surface of the U_3O_8 cylinder. The ratio of the average ^{238}U chamber counting rate with the source in the center of the U_3O_8 to the source distributed along the surface varied from 0.67 to 0.85 as the lead thickness between the U_3O_8 and the chamber was varied from 0 to 5cm. Thus, the relative sensitivity for fission neutron detection in this approximate one eighth section of a fuel element is the order of 0.8 with a few cm of lead between the U_3O_8 and the ^{238}U fission chamber.

The assembly will be placed in the LSDS to determine the interrogation flux depression and then to make "assay" measurements with enriched uranium foils placed at the assembly center and on its surface.

---

[1]H. Krinninger, E. Ruppert, and M. Siefkes, Nucl. Instr. and Meth. 117, (1974)

A. NEUTRON PHYSICS

1. Helium Generation Cross Sections for 14.8-MeV Neutrons
(D. W. Kneff, B. M. Oliver, M. M. Nakata, and Harry Farrar IV)

Neutron-induced helium generation is a major consideration in the development of materials for fusion reactor components. Rockwell International is engaged in two programs to measure total helium generation cross sections for fast neutrons. The Department of Energy's Office of Basic Energy Sciences is sponsoring the measurement of the cross sections of a large range of separated isotopes and their associated pure elements for ~14.8-MeV neutrons from the T(d,n) reaction. The Office of Fusion Energy is supporting cross section measurements of other fusion-related materials in this neutron field, plus helium generation cross section measurements in the broad energy spectrum of the Be(d,n) neutron environment.

These cross section measurements are made by irradiating small (~10-20 mg) samples of a wide range of materials in the neutron environment of interest. The amount of helium generated in each sample is subsequently measured by high-sensitivity gas mass spectrometry. The neutron environment for the irradiation is characterized in detail using a comprehensive set of radiometric and helium accumulation neutron dosimeters.[1] The dosimetry results are used to unfold a neutron fluence/energy spectrum map of the irradiation volume of interest. The helium generation measurements are then combined with this map to deduce cross sections. Irradiations performed to date have utilized the T(d,n) Rotating Target Neutron Sources-I and -II (RTNS-I,II) at the Lawrence Livermore National Laboratory, and a ~0-32 MeV Be(d,n) neutron field produced with 30-MeV deuterons at the Crocker Nuclear Laboratory of the University of California at Davis.

The measured total helium generation cross sections of several pure elements and separated isotopes for ~14.8-MeV neutrons were reported at the Symposium on Neutron Cross Sections from 10 to 50 MeV at Brookhaven National Laboratory in May 1980,[1] and summarized in our previous Report to the DOE Nuclear Data Committee.[2] Since that time we have performed a third T(d,n) irradiation, at RTNS-II, and have determined the cross sections of a number of additional materials irradiated at RTNS-I. The cross section results from RTNS-I, encompassing 62 samples of Fe, Mo, and their separated isotopes, are given in Table A-1. They correspond to an average neutron energy of 14.8 ± 0.1 MeV and a spectrum full-width-at-half-maximum of ~0.6 MeV.

---

[1] Kneff, Oliver, Nakata, and Farrar, BNL-NCS-51245, Vol. I, p. 289 (1980).

[2] Kneff, Oliver, Nakata, and Farrar, BNL-NCS-27800, p. 181 (1980).

TABLE A-1

Preliminary Total Helium Generation Cross Sections for ~14.8-MeV Neutrons

Material	Cross Section (mb)	Material	Cross Section (mb)
Fe (natural)	48 ± 3	Mo (natural)	15 ± 2
^{54}Fe	88 ± 6	^{92}Mo	31 ± 2
^{56}Fe	45 ± 4	^{94}Mo	22 ± 2
^{57}Fe	-	^{95}Mo	17 ± 2
^{58}Fe	20 ± 2	^{96}Mo	11 ± 1
		^{97}Mo	10 ± 1
		^{98}Mo [a]	23 ± 2
		^{100}Mo	3.8 ± 0.5

[a] See text.

The results presented in Table A-1 are preliminary in that the data from additional samples irradiated in RTNS-II have not yet been included. The results from the multiple sample analyses of the RTNS-I materials are in excellent agreement, having an average helium analysis reproducibility of 1%. The final results in Table A-1 include the additional uncertainties associated with the neutron fluence. We believe that there is some basis for questioning the value obtained for ^{98}Mo (a value also obtained in preliminary RTNS-II results). The ^{98}Mo isotopic material had a different appearance and released more non-helium gases during the analysis procedure than the other separated molybdenum isotopes. Its unexpectedly high value could also explain the difference between the measured natural molybdenum cross section (15 ± 2 mb) and that derived from a weighted average of the measured isotopic cross sections (18 ± 1 mb). Chemical analyses conducted so far on the ^{98}Mo isotopic material do not indicate sufficient chemical impurity concentrations to generate significant helium. Other isotopes present in each separated isotope material were corrected for by solving a matrix of equations using the ORNL-supplied isotopic abundances.

The materials listed in Table A-1 were also included in both the Be(d,n) and RTNS-II irradiations, and most of the helium analyses of those samples are complete. Those cross section results (including ^{57}Fe from RTNS-II) will be reported later when the fluence mapping and dosimetry correlations have been completed. The helium analyses of natural zirconium samples irradiated in the RTNS-I, RTNS-II, and Be(d,n) neutron environments are also nearly complete, and analyses will begin shortly on natural V and Nb. Other materials that have now been irradiated in RTNS-II for helium cross section measurements include Be, O, F, Si, Mn, Co, Sn, W, Pb, and most of the separated isotopes of Ti, Cr, Sn, W, and Pb.

TRIANGLE UNIVERSITIES NUCLEAR LABORATORY

A. NEUTRON CROSS SECTION EXPERIMENTS

1. Neutron Cross Section Studies - An Overview

(A. Beyerle, J. Dave, S. G. Glendinning,* C. R. Gould, C. Howell, Sadiq El Kadi, C. E. Nelson,** R. Pedroni, F. O. Purser, L. W. Seagondollar, P. Thambidurai, R. L. Walter, G. Tungate)

TUNL has been involved in a major program of neutron elastic and inelastic scattering cross section measurements since 1975. The work was initiated to support the high-priority and long-range nuclear data needs of the U.S. fusion energy program and the main thrust of the program has been directed towards satisfying these needs. The information gained is also of basic interest, however, and is relevant to optical model parametrizations of nucleon scattering, studies of isospin dependence in nucleon scattering, nuclear level density parameters and pre-equilibrium emission processes.

The focus of the early work was on measurements of elastic and inelastic scattering cross sections for 1-p shell nuclei. More recently the emphasis has shifted to heavier nuclei, and the program now concentrates on neutron emission spectra measurements in addition to the continuing elastic scattering studies.

The status of the TUNL neutron scattering program has been reviewed at two recent conferences, namely, the Symposium on Neutron Cross Sections from 10 to 50 MeV at Brookhaven, [1] and the Conference on the Application of Accelerators in Research and Industry at Denton, Texas. [2]

---

* Now at General Electric Co., Wilmington, N. C.

** Now at Department of Radiology, Duke University Medical Center

1. R. L. Walter and C. R. Gould, BNL-NCS-51245 (July 1980) 259
2. C. R. Gould, IEEE Trans. on Nucl. Sci. (March, 1981)

2. Summary of Recent Facility Changes

Improvements have been made in the electro-mechanical system that is used to position our scattering samples remotely so that the vibrations have been eliminated almost completely. Also, we have changed the method of coupling sample "modules" into the cable system so that fabrication of couplings is easier and fumbling problems are virtually eliminated. For our "stop" signal on the time-of-flight electronics, we use a pulse from a capacitive pickoff. A more reliable signal was obtained by replacement of the old preamplifier by two Hewlett Packard 108555A preamplifiers connected directly to the pickoff.

There is great desire to increase our ability to measure at scattering angles as far forward and backward as possible, with the two carts or detectors simultaneously at equal angles. By remodelling some support systems we now can locate both detectors at scattering angles of 22° or 155° simultaneously. Additional modifications are planned that will permit us to reduce the most forward angles to 16° and the maximum angle to 163°, simultaneous positions.

The silicon pressure transducer system that was developed to measure gas pressure in our tritium gas target worked beautifully for several months (see TUNL XVIII, 1979). Two problems have recently developed. The first is that hydrogen apparently diffuses through the barrier across which the transducer measures a pressure differential. The second problem is that the calibration of two such transducers has changed drastically under long term use. At present we do not know the reason; the convenience and added security of the transducer system is sufficient, however, that the reason for the difficulties is being pursued.

3. Studies in The 1p Shell Between 7 and 15 MeV

Elastic and inelastic scattering studies on light nuclei were among the first experiments carried out with the TUNL neutron time-of-flight system. Data for 6Li, 7Li, 9Be and 12C have been reported in the literature [1, 2, 3] and for 10B, 11B and 16O in the thesis of S. G. Glendinning. We have since begun measurements on 13C. When this work is completed we will have studied neutron scattering from all 1-p shell nuclei except the nitrogen isotopes.

The boron scattering data have been submitted for publication in Nuclear Science and Engineering. Excerpts from the abstract from the thesis of S. G. Glendinning appear below:

> "Neutron scattering cross sections of high quality have been measured for 10B, 11B and 16O using the Triangle Universities Nuclear Laboratory neutron time-of-flight facility. .... The neutron data obtained are compared with high quality proton data for 10B to determine this dependence using the optical model, assuming that the isospin dependence may be expressed as a correction to the energy of the incident projectile. The energy correction is found to be 4.6   1.4 MeV lowering of the incident energy for protons. The neutron data obtained for 11B were compared to the 10B neutron and proton data in an attempt to extract the symmetry

terms (dependence on target isospin) but the data were insufficiently sensitive to the effect to yield good results. The spherical optical model alone was insufficient to predict the 160 data because of the many resonances in the energy region, ... The 11B data (elastic and inelastic) were also fit using the coupled-channel optical model. .... "

A 13C sample of mass 8.5 g was prepared by compressing 13C powder into a stainless steel can of wall thickness 0.006". The density of the sample was 1.178 g/cm , which is substantially greater than the density of uncompressed 13C powder (about 0.8 gm/cm). With our TOF system the elastic scattering peak is well separated, but the inelastic groups around 3.7 MeV are only partially resolved from the first-excited-state peak at 3.1 MeV. Data have been obtained between 10 and 18 MeV in 2 MeV steps in about 5° increments between 20° and 155°.

Global optical model parametrizations of nucleon scattering data from light nuclei [4] have not in general been as successful as for heavier nuclei. [5] In regions where resonance structure is absent, however, good fits can be obtained for individual nuclei. The 10B data are a case in point. The symmetry terms in the optical potential are zero by definition, and proton and neutron scattering parameters differ only in a Coulomb correction term for the proton well depths.

Fig. A3-1 shows the TUNL 10B neutron data, together with proton data from Ref. [4]. The optical model searches were made with the computer code GENOA of F. Perey. A standard spherical Woods-Saxon well shape was used with a surface imaginary potential. The fits are in general quite good and the proton and neutron parameters at a given energy differ only in a Coulomb correction term Vc. The parameters are:

Real well:

$V = 48.1 - 0.3\ E_{cm} - V_c$ MeV
$r = 1.34$ fm
$a = 0.55$ fm
$V_c = 1.54$ MeV protons

Imaginary well:

$W = 0.16 + 0.78\ E_{cm}$ MeV
$r = 1.41$ fm
$a = 0.34$ fm

Spin-orbit potential:

$V = 5.5$ MeV
$r = 1.15$ fm
$a = 0.57$ fm

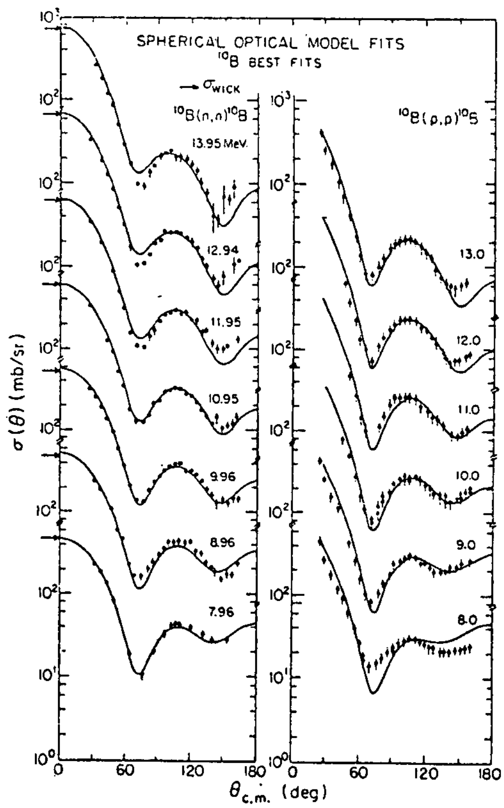

Fig. A3-1. Fit to 10B(N,N) data

In attempting to generalize to neighboring nuclei, the fits are less successful unless the geometries are allowed to vary. But even with fixed geometries, it is possible to obtain reasonable fits. Fig. A3-3 shows 9Be, 10B, and 11B neutron scattering data. For these fits

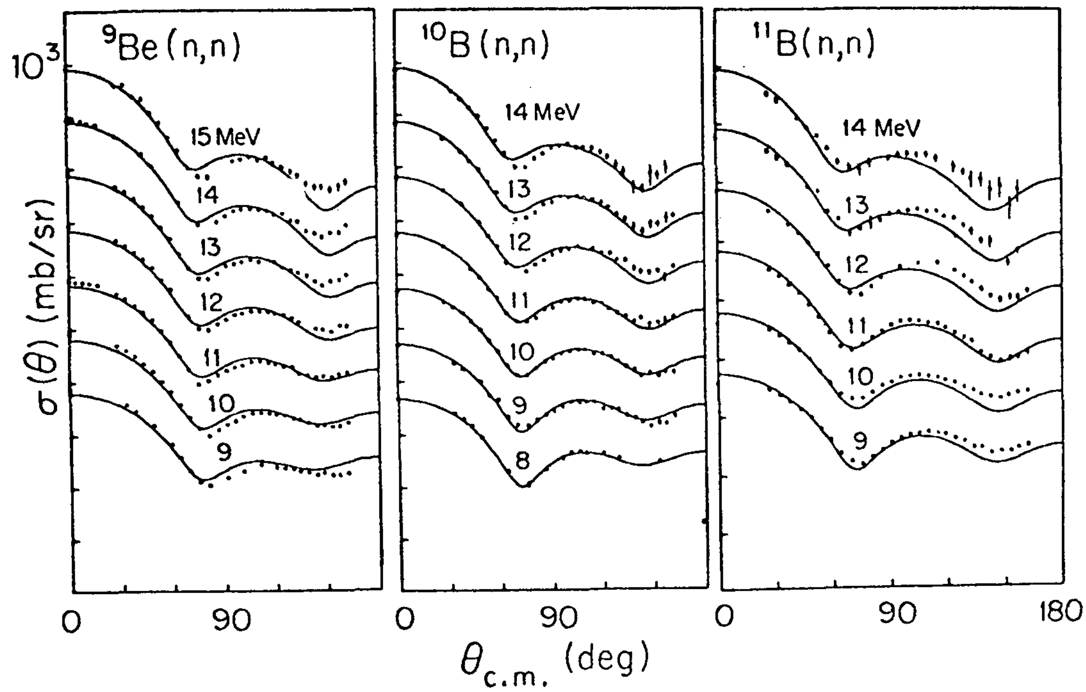

Fig. A3-2. Fixed geometry spherical OM fits

only the real and imaginary well depths were allowed to vary with energy. The parameters were:

Real well:

V = 47.2 - 0.32 Ecm - 27.8*(N-Z)/A MeV
r = 1.39 fm
a = 0.57 fm

Imaginary well:

W = 0.76 + 0.90 Ecm - 1.95*(N-Z)/A MeV
r = 1.45 fm
a = 0.30 fm

Spin orbit potential: same as for 10B.

The symmetry term is proportional to [(N-Z)/A] in the above potentials. For light nuclei the quantity [(N-Z)/A] is only 1/4 as large as that for heavy nuclei. This makes our data relatively insensitive to the size of the symmetry term. Nevertheless, this term in V is in rough agreement with values found for heavier nuclei. The W symmetry term is small. However, systematics for this term are not nearly as well established in the literature compared to those for V.

----

1. H. H. Hogue *et al.*, Nucl. Sci. and Eng. 69 (1979) 22
2. H. H. Hogue *et al.*, Nucl. Sci. and Eng. 68 (1978) 38
3. D. W. Glasgow *et al.*, Nucl. Sci. and Eng. 61 (1979) 521
4. B. A. Watson *et al.*, Phys. Rev. 182 (1969) 977
5. F. D. Bechetti and G. Greenlees, Phys. Rev. 182 (1969) 1190

4. Elastic and Inelastic Scattering of Neutrons from $^{54,56}Fe$ and $^{63,65}Cu$

Cross-section data have been obtained at 8, 10, 12, and 14 MeV for enriched samples of $^{54,56}Fe$, and $^{63,65}Cu$ and at 17 MeV for ^{54}Fe. Optical model analyses for $^{54,56}Fe$ and $^{63,65}Cu$ are being performed independent of the optical model studies for ^{54}Fe and ^{65}Cu that are discussed below in Section B where neutron polarization measurements for these two isotopes are presented. The main purpose of making two independent searches is to obtain the best representation of the cross section for these nuclei so that comparisons can be made to parameters obtained in studies using a similar approach, i.e., searches which employ only cross-section data. In addition, such representations are perhaps the most useful for interpolating or extrapolating cross sections to other energies for applied purposes. The second reason is to investigate the behavior of a spin-orbit term obtained from searching only on cross-section data and to compare this parameterization to that obtained in later searches which include the additional constraint of polarization data. The comparison should be particularly interesting for Fe and Cu at 14 MeV where it is known from the work in Section B that the cross section for "spin-down" neutrons is greater than that for "spin-up" neutrons over almost the entire angular range measured, i.e., 20° to 155°.

The status of the Fe and Cu data for the region between 8-14 MeV is that the time-of-flight spectra have been stripped a second time following a preliminary sensitivity test of optical model fitting. Examples of the results are shown in the left hand and middle panels of Fig. A4-1 for ^{54}Fe and ^{65}Cu. The curves are polynomial fits of the data.

Constrained Woods-Saxon optical models are being derived for these four nuclei. The energy dependence is contained in the well depths. First, best fits were derived, varying all parameters. These are shown in the right hand panels of Fig. A4-1 by the solid curves. Secondly, the geometry parameters were held at their average values and then the depths were permitted to vary. The energy dependence of the well-depth parameters are being fit presently with linear functions for comparison between isotopes and elements. Coupled channel calculations to describe the elastic and first inelastic scattering cross section have been initiated in collaboration with J.-P. Delaroche of Bruyeres le Chatel.

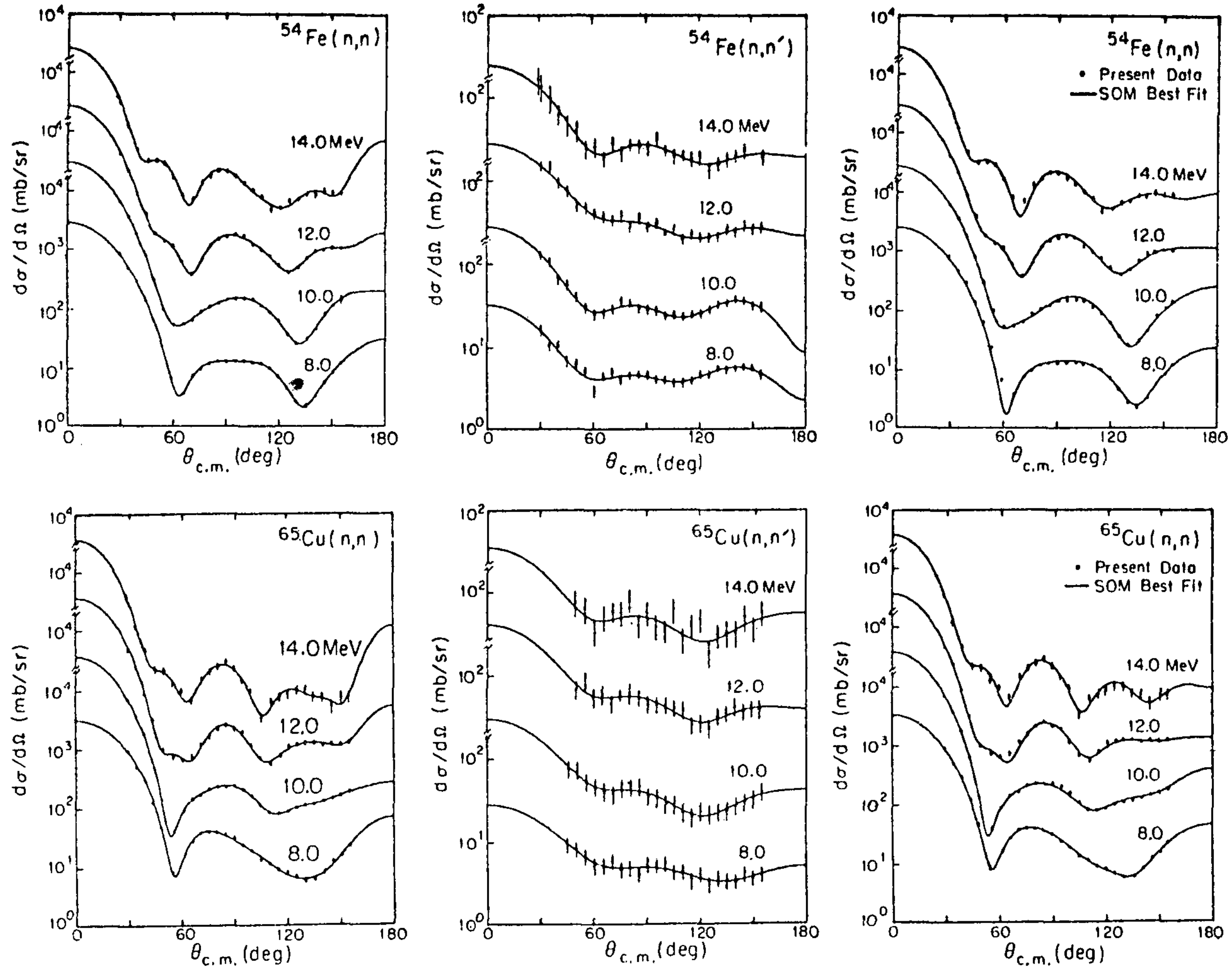

Fig. A4-1. Left panels: Comparison of TUNL data to polynomial fits for (n,n) from 54Fe and 65Cu. Middle Panels: Same for (n,n). Right panels: Results of single-energy spherical optical models fits compared to data from left panels.

5. Cross Section for Neutron Scattering from 58Ni, 60Ni, 116Sn, 120Sn, and 208Pb between 8 and 17 MeV

Cross-section data for 58Ni, 60Ni, 116Sn, 120Sn, and 208Pb were obtained for the fusion energy program as well as to complement the polarization data reported in Section B1. These data were obtained by the group listed in that part of the report and will be part of the thesis work of C. E. Floyd (208Pb) and P. P. Guss (Ni and Sn). Measurements were made for 58Ni and 60Ni at 8, 10, 12, and 14 MeV. The differential cross sections for 58Ni are shown in Fig. A5-1. The curves are polynomial fits of the data. Optical-model and coupled-channel calculations will be underway when the cross-section data for 60Ni have been adjusted with multiple-scattering corrections, as calculated in the Monte Carlo code EFFIGY.

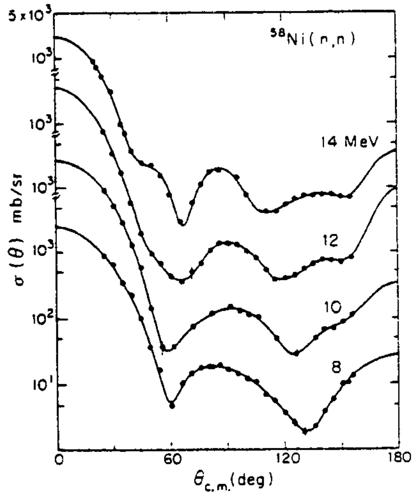

Fig. A5-1. Data for 58Ni

Cross section data were taken for isotopically enriched 116Sn, 120Sn and 208Pb. Angular distributions were obtained at energies of 10.0 and 14.0 MeV for all three nuclei and at 17.0 MeV for 120Sn and 208Pb. These data complement the polarization data described below, the earlier cross-section results of Finlay et al., [1,2] and the TUNL neutron continuum measurements from tin and lead. For 116Sn and 120Sn inelastic scattering was obtained for the 2+ states at 1.29 MeV and 1.17 MeV, respectively, and, according to Rapaport et al., for the 3- state at 2.26 MeV and 2.40 MeV, respectively.

In preliminary calculations, the elastic and the 2+ inelastic results measured for both tin isotopes have been found to be fairly well described by the vibrational model. Preliminary attempts to use the spherical optical model to describe both the cross section and polarization data discussed below have failed until now.

Before serious calculations for 208Pb are initiated, all of the on-line data (cross sections and polarizations) must be reduced and put into final form. However, our preliminary optical model calculations indicate that the cross-section and polarization data cannot be fitted simultaneously if "standard" parameters are used.

---

1. R. W. Finlay et al., Nucl. Phys. A338 (1980) 45
2. J. Rapaport et al., Nucl. Phys. A341 (1980) 56

6. Double Differential Neutron Scattering Cross Sections

To complement theoretical predictions of neutron emission cross sections, we have undertaken a program of (n,n') measurements on medium mass to heavy nuclei, with particular emphasis on inelastic scattering to the continuum region. Some details of experimental procedure were given in the report last year (TUNL XVIII, 1979, pg. 12).

Briefly, proton or deuteron beams were pulsed and bunched into about 2 ns bursts at a repetition rate of 1 MHz with typical beam currents on either tritium or deuterium gas targets of 1.5 A. Neutrons thus produced were scattered from appropriate samples into shielded detectors. Data at incident neutron energy of 7.5 MeV were taken with the 2H(d,n) source reaction and at 10 and 12 MeV with the 3H(p,n) source reaction. Neutron angular distributions were typically taken at five angles from 40° to 145° at each energy.

The data are being analyzed by use of computer code EFFIGYC, a Monte Carlo program aimed at producing a realistic simulation of the time-of-flight experiment and data reduction conditions. A major portion of the effort over the past year in the continuum project has been to write and adapt the code to the TUCC computer and accessories and to test the calculations. The code is elegant and massive. It includes the effects of the finite size of neutron production, the scattering sample and the detector, finite energy resolution, and multiple scattering and attenuation effects. In addition the code corrects for neutrons caused by "breakup" of bombarding particles in the source gas, transforms time-of-flight spectra to energy spectra, folding in the detector efficiency, and normalizes cross sections to absolute values. It uses estimated continuum cross sections for all incident and exit energies possible, measured cross sections for all discrete states, measured total cross sections for sample material, cross sections for the gas source reaction and geometric information about the time-of-flight system. Spectra are calculated and compared to experiment and the estimated cross section tables are updated. EFFIGYC iterates until the calculation agrees with experiment. Fig. A6-1 is an example of the results of such calculations. In this manner EFFIGYC calculates and applies corrections for experimental curves.

Comparison of the TUNL data obtained for Fe with other data and calculations is shown in Fig. A6-2. Agreement in magnitude of cross section is within the errors of previous experinments. Energy integrated yields exceed the upper limit of ENDF-B/V total cross sections minus discrete state cross sections by 20% or less.

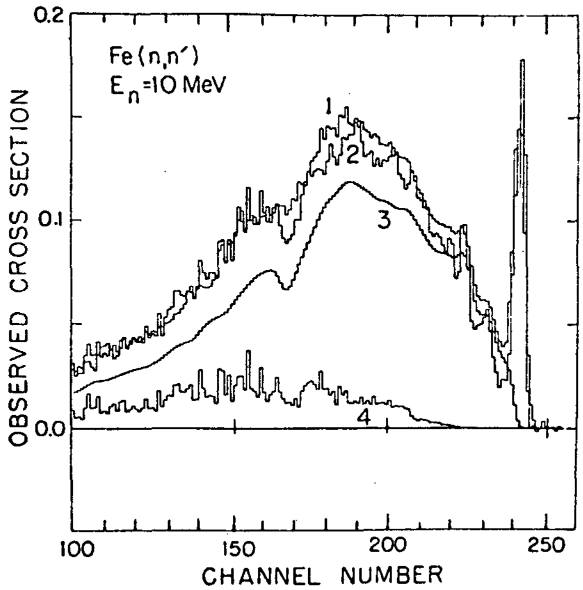

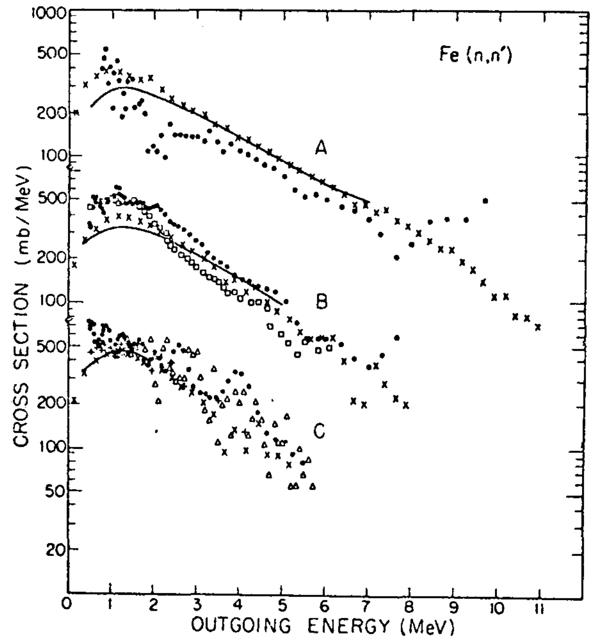

Fig. A6-1. Time-of-flight spectra for simulation calculation at 10 MeV. Spectrum (1) is the experimental spectrum compressed into 256 channels; (2) is the simulation of the experimental data; (3) is that part of the scattering involving single scattering of primary source neutrons; and (4) is the calculated scattering of all source gas breakup neutrons.

Fig. A6-2. Comparison of TUNL results to other data and calculations. Solid curve from ENDF/B-V. Upper set: TUNL data at 12 MeV, 125° (●); H. Vonach calculations (private comm.), interpolated between 11 and 14 MeV (X). Middle set: TUNL at 10 MeV, 100° (●); H. Vonach interpolated between 8 and 11 MeV (X); Biryukov data at 9 MeV (◻). Lower set: TUNL at 7.5 MeV, 95° (●); H. Vonach at 8 MeV (X); Kinney and Perey data at 7.5 MeV (△); Owen and Towle data at 7.0 MeV (+).

Data have been accumulated in two packages. The earliest set was obtained for Fe, Ni, Cu and Pb at 7.5, 10.0 and 12.0 MeV. In a second series of runs we obtained data for Si, Cr, Mo, Nb and W at 10 and 12 MeV. The delay in processing the data involves the expense of obtaining good statistics in the Monte Carlo calculations on the TUCC computer. At TUNL we have recently installed a VAX 11/780 computer which will be used for recording and analyzing raw data as well as running background jobs. We are presently adapting the code EFFIGYC to the VAX computer so that manipulation of the data can be performed without exorbitant expense.

7. <u>Breakup Cross Sections for 3H+p Neutrons</u>

An accurate determination of the zero degree neutron spectrum resulting from proton bombardment of tritium is of importance in making corrections to our neutron emission spectra data. For proton energies above 8.3 MeV the 3H+p neutron source is not monoenergetic and a continuum of neutrons arises from thre body breakup of the 3H+p system. The magnitude of the breakup spectrum was recently reported by Drosg *et al.* [1], but the shape of the spectrum was not particularly well characterized. We undertook a measurement of the breakup in order to better determine the shape and also to check the results of Ref. [1]. Data were obtained from 10 to 14 MeV using the time-of-flight system. The integrated breakup neutron cross sections extracted from the data are shown in Fig. A7-1. The agreement with Ref. [1] is quite good. We have found the tailing of the intense 3H(p,n)3He peak into the continuum region limits the accuracy of the integrated cross-section measurements. The overall precision of the data in Fig. A7-1 is estimated to be about 15-20%.

---

1. M. Drosg *et al.*, Nucl. Inst. Meth. <u>140</u> (1977) 515

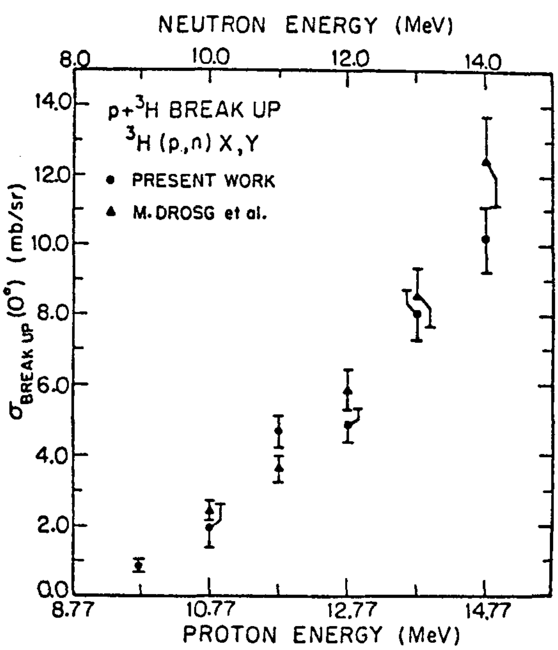

Fig. A7-2. Integrated breakup cross section

B. Neutron Polarization Studies

1. Scattering of Polarized Neutrons

a. Overview

The neutron polarization program has been a major effort at TUNL. Personnel involved are: C. E. Floyd, P. P. Guss, K. Murphy, C. R. Howell, R. Pedroni, G. Tungate, R. . Byrd, and R. L. Walter from Duke; T. B. Clegg and W. J. Thompson from UNC at Chapel Hill; C. R. Gould and D. Haas from NCSU; and a group from Tübingen, West Germany, E. Woye, W. Tornow and G. Mack. Our current interest in scattering of polarized neutrons from nuclei involves about 12 nuclei ranging from 1H to 208Pb. The work can be grouped into three areas of interest: (i) few nucleon studies (1H, 2H, 4He), involving targets that can be made into scintillator media; (ii) light nuclei (9Be and 12C), which can be interpreted only approximately with the standard optical model; and (iii) medium to heavy nuclei (40Ca, 54Fe, 58Ni, 65Cu, 116Sn, 120Sn, and 208Pb), for which an analysis in terms of the standard optical model should yield suitable tests concerning shapes, sizes and depths of the neutron-nucleus potential. It is significant that never before has such high accuracy been achieved for neutron analyzing power data at energies above 4 MeV. Our new data presents stringent tests for nucleon-nucleon models, three-nucleon models, the Lane optical model for 9Be(N,N)9Be, and previously unclear details of the nucleon-nucleus model.

All of these tests have been made possible through the use of the polarization transfer reaction $2H(\vec{d},\vec{n})3He$, which gives a high flux of polarized neutrons at 0°, the angle where the cross section conveniently is strongly peaked. Our success in being the first to accurately measure analyzing power distributions at energies above about 6 MeV for non-scintillating targets is due to a development at TUNL reported in a paper by Wender _et al_. [1] This development permits us to obtain 2-ns wide bursts of polarized protons or deuterons with an average beam of 100-200 nA on target. The repetition rates of 2 and 4 MHz are ideal for detecting 8-17 MeV neutrons with our time-of-flight apparatus.

Highlights of our scattering work during the past two years were reported in ten contributions (Refs. [2-11]) to the 5th International Symposium on Polarization Phenomena in Nuclear Physics. To exemplify the quality of the new data, a comparison is made in Fig. B1-1 between our results for 208Pb at 10 MeV (uncorrected for multiple scattering) and the only other existing polarization data for Pb(n,n) between 5 and 24 MeV. It is obvious that the new data clearly define the structure in the analyzing power function between 20° and 160°.

Much of the analyzing power data in this Section requires the cross-section information reported in Section A in order to extract nuclear parameters. On the other hand, much of the eventual understanding of the models which describe the data of Section A will revolve around their ability to predict analyzing power data. In this way, Sections A and B1 complement one another in such a manner that the division into two separate analyses may soon become superficial.

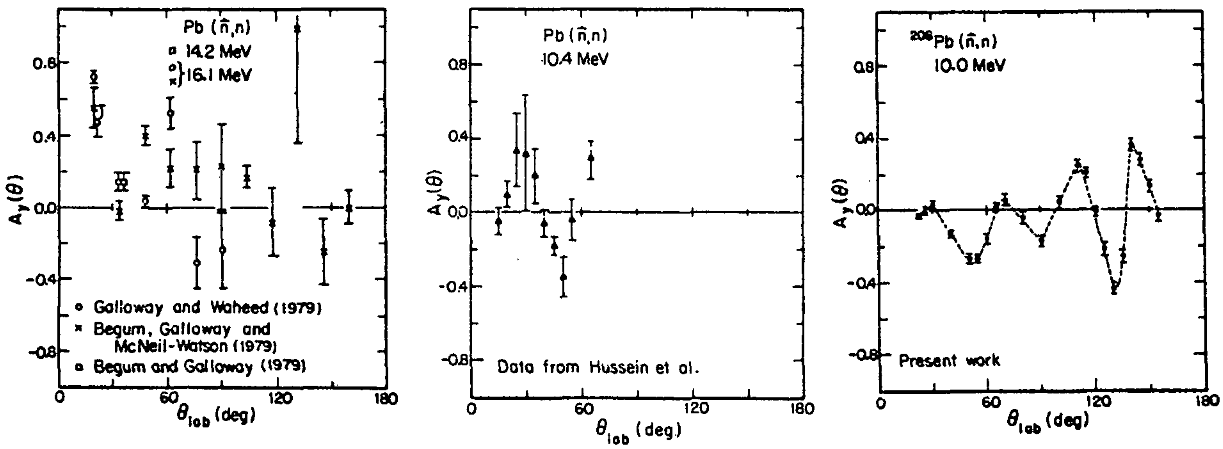

Fig. B1-1. Comparison of present A(θ) data (right panel) to earlier work

b. Review of Advances in Neutron Polarization Studies

A paper which summarized the major advances in neutron polarization studies in the past five years for energies between about 2 and 30 MeV was presented by us at the 5th International

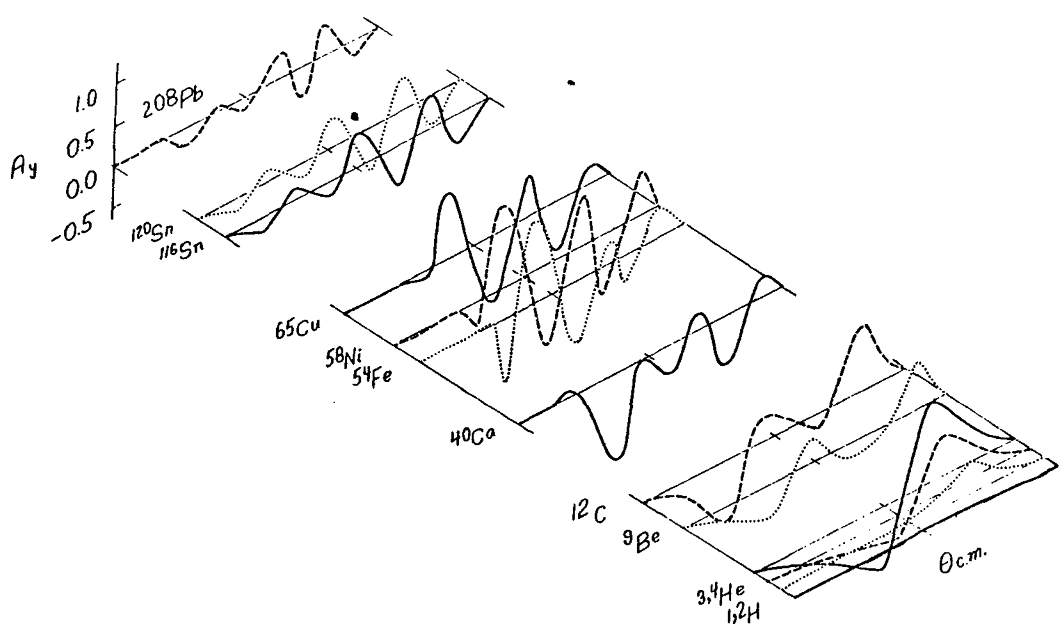

Fig. B1-2. Global view of observed analyzing power for 10-14 MeV neutron elastic scattering

Polarization Symposium in August in Santa Fe. [11] One topic was a summary of the analyzing power data obtained at TUNL for 10 to 14 MeV neutron-nucleus scattering. The results were presented as a composite graph which shows the expected smooth changes of A(θ) with mass number. This figure is reproduced in Fig. B1-2. One important aspect of these data, in comparison to that for proton-nucleus scattering, is that the magnitude of A(θ) for the heavier targets is not overwhelmed by the strong diluting effect of Rutherford scattering for this energy region.

c. Analyzing Power for n-p Scattering at 16.9 MeV

A paper describing the precision n-p analyzing power measurements and their comparison to theory has been published in Nuclear Physics A. [12] Excepts from the abstract follow:

> "The analyzing power A(θ) for neutron-proton scattering has been measured for θ = 90°(c.m.) from 13.5 to 16.9 MeV and from θ = 50° to 145°(c.m.) at 16.9 MeV. ...Overall uncertainties are about ±0.002. All the A(θ) data, but primarily those at 16.9 MeV, disagree with predictions based on the phase-shift sets which have been derived previously by way of global analyses of nucleon-nucleon scattering data. ...

Comparisons of the data to calculations using the most recent Paris Potential for nucleon-nucleon scattering show that the predictions are inadequate to explain the systematics of the data. The Paris group will investigate this discrepancy in an attempt to relate it to the aproximations in their model.

d. Scattering of Polarized Neutrons from 9Be

The first experiment using the TUNL pulsed polarized neutron scattering facility was the measurement of analyzing powers for scattering to the ground and 2.43 MeV (5/2-) states of 9Be at 9, 10, 11, 13, and 15 MeV neutron energies. The A(θ) data vary gently with angle and energy. The 9Be + nucleon system has been studied by two theoretical techniques at TUNL. A Lane model has been developed to describe the elastic and quasi-elastic processes in the (p,p), (n,n), and (p,n) reaction channels. [9,13] This model used one potential to simultaneously fit the (p,p), (n,n), and (p,n) cross sections as well as the (p,p) and (p,n) A(θ) data. In addition coupled channels calculations were made in an effort to predict the observed analyzing power for 9Be(n,n')9Be*(2.4 MeV). The calculations used the 9Be(p,p) model of Votava *et al*. [14]. The agreement was satisfactory for (n,n') although the magnitude of the A(θ) data was overestimated in the region between 80° and 120° for (n,n_0).

e. Analyzing Power for 12C(n,n) Scattering

One of the cooperative experiments with Tübingen was a study of A(θ) for elastic and inelastic (4.43 MeV state) scattering from

12C. The preliminary data and calculations were shown at Santa Fe. [Refs. 3,5] Until now, two models have been used by us to study the region between 11 and 15 MeV where the resonance effects do not have a strong influence. A standard spherical optical model was investigated. The results of a global optical model for the elastic scattering are compared to the data in Fig. B1-3. Here the cross section data are from

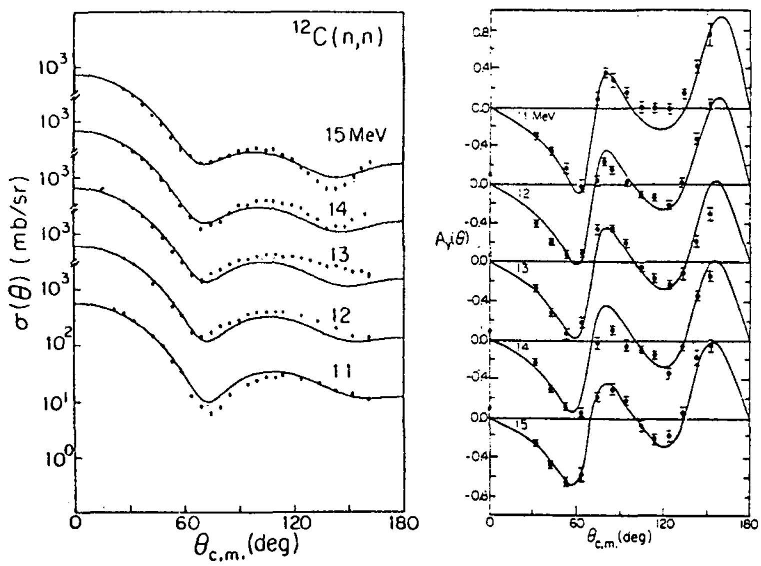

Fig. B1-3. Global predictions for 12C(n,n)

the TUNL report of Glasgow et al. [16] The new model provides a fair representation of the data, considering that standard Woods-Saxon form factors were employed. Interestingly, the diffuseness of the spin-orbit term favors values that are a factor of two or more smaller than those of heavier nuclei, i.e., less than 0.3 compared to about 0.6 fm. This same feature was obtained in the optical model search on 9Be. The second model included the 12C(n,n') reaction in the global analysis by using the coupled-channel code ECIS. Again the calculations give a fair representation to the data, both (n,n) and (n,n'). The deformation parameter obtained was similar to that seen in earlier carbon analyses.

f. Cross Section and Analyzing Power for 40Ca(n,n)

Cross-section and A(θ) data have been obtained at 10, 12 and 14 MeV. A comparison of the analyzing power to calculations using familiar optical models for neutron scattering is shown in Fig. B1-4. The agreement using the conventional optical model of Becchetti and Greenlees [17] is poorer than that shown here. The cross-section and A(θ) data have been employed in an optical model search using the code GENOA with the standard Woods-Saxon form factors. Again the results are in fair agreement with the data and are considerably improved over those in

Fig. B1-4. The feature of a small spin-orbit diffuseness (a = 0.3 fm) surfaced here also, indicating that some feature of the standard Thomas term for the nucleon-nucleus spin-orbit form factor is probably breaking down for light nuclei, as one doesn't expect to observe geometrical effects as sharp as 0.3 fm in the nuclear interaction.

g. Elastic and Inelastic Scattering from 54Fe, 58Ni, and 65Cu at 10 and 14 MeV

Analyzing power measurements have been conducted for elastic scattering of neutrons from 54Fe, 58Ni, and 65Cu at 10 MeV and 12 MeV. [7,8] The A(θ) results at 10 MeV for 54Fe and 65Cu are shown in Figs. B1-5 and B1-6. All data have been corrected for finite geometry and double scattering effects; triple scattering effects are presently being investigated. Our analyzing power data are not consistent with the anomalously high polarizations reported by Galloway and Waheed [18] for angles around 20°. Apparently there must have been instrumental asymmetries in the forward angle measurements of Ref. [18].

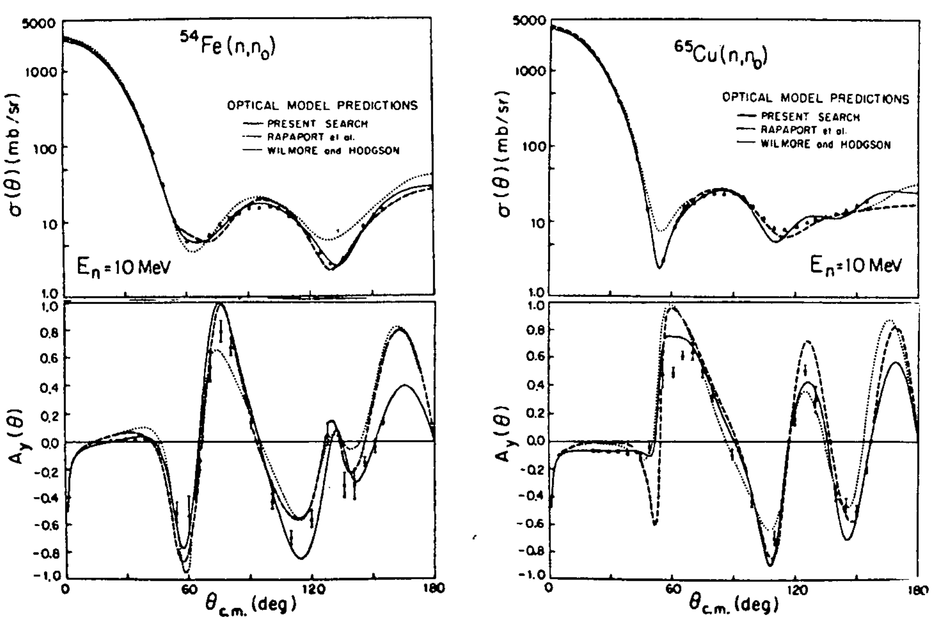

Figs. B1-5 and B1-6. Comparison of TUNL data to OM calculations

Our A(θ) values, together with the total cross section and the differential cross-section data of El-Kadi <u>et al</u>. (Section A4), have been fitted using the optical-model search code GENOA obtained from F. Perey. For our purposes, the Mott-Schwinger interaction between the neutron magnetic moment and the Coulomb field of the nucleus (Section B1-i) has been included in the code GENOA and used in the optical model calculations shown here. The data are compared in Figs. B1-5 and B1-6 with optical-model calculations based on a TUNL best fit and the global models of Rapaport <u>et al</u>. [19] (RKF) and Wilmore and Hodgson [20] (WH).

Due to the scarcity of accurate polarization data for neutrons, the spin-orbit terms in neutron models have typically been set to zero (as in Ref. [20]) or set to the proton parameters of Becchetti and Greenlees [17] (BG) (as in Ref. [19]). For the present comparisons shown, the BG spin-orbit values were used with the parameter set of WH. While both global sets reproduce the general features of the distributions, neither set predicts the analyzing powers at forward angles, where our data has its highest statistical accuracy. In our optical model search, the spin-orbit term has a well depth of about 6 MeV, a radius parameter of 1.1 fm, and a diffuseness of 0.5 to 0.6 fm. The data favor the inclusion of an imaginary spin-orbit term, a feature which has been hard to observe in low-energy proton-nucleus scattering.

h. Scattering from 116Sn, 120Sn and 208Pb

Neutron analyzing power data have been obtained for isotopically enriched 116Sn, 120Sn, and 208Pb at 10.0 and 14.0 MeV. [8] These Sn data nicely complement the cross sections for these same isotopes at 10.0, 14.0, and 17.0 MeV, also measured at TUNL. Coupled channel calculations are underway for the cross section and A(θ) for 116Sn and 120Sn. The analyzing power for 208Pb are yet to be corrected for double and triple scattering effects.

i. Effects of Mott-Schwinger Scattering

When a neutron scatters from a charged nucleus it experiences an electromagnetic interaction between its magnetic moment and the Coulomb field of the nucleus, which is moving in the rest frame of the neutron. This effect is termed Mott-Schwinger (M-S) scattering. To avoid a false parameterization of the nuclear potential, this electromagnetic interaction must be the optical search code GENOA in the Born approximation. [21] Calculations for 54Fe at 10 MeV are shown in Fig. B1-7 for angles less than 9°. In Fig. B1-8 we show optical model calculations

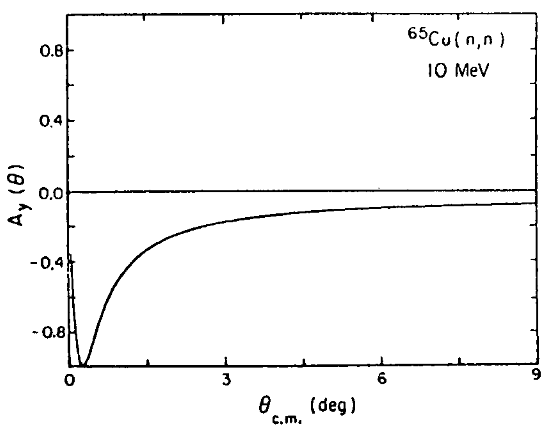

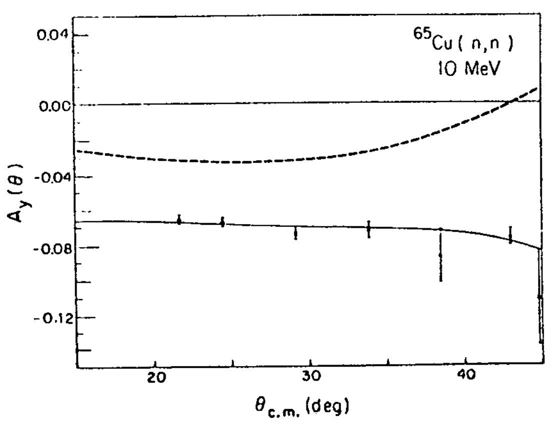

Figs. B1-7 and B1-8. Optical model calculations with (solid curve) and without (dashed curve) Mott-Schwinger interaction compared to present data which illustrate the effect on the analyzing power in the region between 15° and 45°. In this region the error in A(θ) is typically less than 0.004. The solid curve is an optical model fit including Mott-Schwinger effects. The effect of turning off the electromagnetic interaction is shown by the dashed curve. The effect of Mott-Schwinger scattering on the cross section is small for angles greater than a few degrees, at most exhibiting a small contribution in the diffraction minima.

This study was prompted by the concern that exclusion of Mott-Schwinger effects would result in spurious optical model parameters. Indeed, when the M-S interaction is omitted, the parameters are changed by up to 20%, primarily in the absorptive and spin-orbit terms. We conclude that M-S scattering must be included to avoid spurious parameters when fitting data sets which include accurate neutron A(θ) data.

j. Polarized Target for Total Cross Sections

We are presently developing a polarized target system for studies of the spin-spin interaction. The initial experiments will be neutron transmission measurements, i.e., total cross sections. The source of neutrons will be either the 2H(d,n)3He reaction as a "mono-energetic" source or the 9Be(d,n) reaction as a white source of polarized neutrons.

----

1. S. A. Wender, C. E. Floyd, T. B. Clegg and W. R. Wylie, Nucl. Instr. and Meth. 174 (1980) 341
2. The Influence of Multiple Scattering Corrections on High-Accuracy Neutron-Proton Analyzing power Data Measured at 16.9 MeV, W. Tornow and R. L. Walter, Proc. 5th Int. Symp. on Polarization Phenomena in Nuclear Physics, Santa Fe, N.M., 1980 (to be published)
3. Discrepancies in the Polarization of Elastically-Scattered Neutrons from 12C Around 16 MeV, W. Tornow, E. Woye, and R. L. Walter, *ibid*.
4. The Scattering of Polarized Neutrons from 9Be Between 9 and 15 MeV, C. E. Floyd, *et al*., *ibid*.
5. The Analyzing Power Ay(θ) for 12C(n,n0,1)12C from 9 to 16.8 MeV, E. Woye, *et al*., *ibid*.
   Optical-Model and Coupled-Channel Predictions to n-12C Analyzing Power Data, E. Woye, W. Tornow, and G. Mack, *ibid*.
6. The Analyzing Power for Elastic Scattering of 9.9, 11.9, and 13.9 MeV Neutrons from Ca, W. Tornow, *et al*., *ibid*.
7. Scattering of Polarized Neutrons from 54Fe and 65Cu at 10 MeV, C. E. Floyd, P. P. Guss, K. Murphy, R. C. Byrd, S. A. Wender, R. L. Walter, and T. B. Clegg, *ibid*.
8. Neutron Scattering from 58Ni and 208Pb at 10 MeV, P. P. Guss, *et al*., *ibid*.
9. A Program of Systematic Measurement and Analysis for the

Low-Energy Optical-Model Potential, R. L. Walter, *et al.*, *ibid.*
10. Lane Model Constraints on Nucleon-Nucleus Scattering Potentials, R. C. Byrd, R. L. Walter and S. R. Cotanch, *ibid.*
11. Recent Advances in Neutron Polarization, R.L. Walter, *ibid.*
12. Analyzing Power Measurements for n-p Scattering between 13.5 and 16.9 MeV, W. Tornow, *et al.*, Nucl. Phys. A340 (1980) 34
13. R. C. Byrd, R. L. Walter, and S. R. Cotanch, Phys. Rev. Lett. 43 (1979) 260
14. H.J. Votova, *et al.*, Nucl. Phys. A204 (1973) 529
15. J. S. Blair, *et al.*, Phys. Lett. 60B (1975) 25
16. D. W. Glasgow, *et al.*, Nucl. Sci. and Eng. 61 (1976) 521
17. F. D. Becchetti Jr. and G. W. Greenlees, Phys. Rev. 182 (1969) 1190
18. R. B. Galloway and A. Waheed, Phys. Rev. C20 (1979) 1711
19. J. Rapaport *et al.*, Nucl. Phys. A330 (1979) 15
20. D. Wilmore and P. E. Hodgson, Nucl. Phys. 55 (1964) 673
21. W. S. Hogan and R. G. Seyler, Phys. Rev. C177 (1969) 1706

2. Studies of (p,n) Reactions

The (p,n) program over the past year has involved contributions from a large number of TUNL staff and students. Direction has been provided by R. C. Byrd and R. L. Walter; the bulk of the development work on the polarized source and pulsed polarized beam facility was done by S. A. Wender, T. B. Clegg, C. E. Floyd, and C. R. Howell. On-line data acquisition rested primarily on K. Murphy, P. P. Guss and the above mentioned personnel.

a. Overview

The study of (p,n) reactions at TUNL has concentrated mainly on cross section and polarization measurements on light nuclei ($A < 16$) at bombarding energies below 20 MeV. A significant development in this program is the use of a calibrated detection system for our analyzing power measurements; we are therefore able to measure both cross section and analyzing power $A(\theta)$ at the same time.

The interpretation of the data for the lightest nuclei, ^{2}H and ^{3}H, is dictated partly by the few-nucleon nature of these systems. Our approach in the heavier cases has generally followed two somewhat complementary avenues. First, comparison of the values of the polarization P of the outgoing neutrons and the analyzing power A of the reaction for an incident polarized beam can provide useful information about the nuclear structure of intermediate states. [1] On the other hand, at higher excitation and bombarding energies these P-A differences disappear, along with the resonance structure to which they are related. At energies above about 10 MeV, therefore, we have attempted to describe our results using the Lane optical model. These coupled-channels analyses have included all available data for the (p,p), (n,n) and (p,n) cross section and polarization in this energy range.

Summaries of these two programs, i.e., the Lane model and comparison of polarizations to analyzing powers, have been presented at the Telluride Conference on (p,n) reactions [2,3] and at the Fifth Polarization Symposium at Santa Fe. [4,5] Briefly, these papers show that P-A splitting is caused by and evidence for isospin symmetry violation which allows different rates for spin up-to-down and down-to-up transitions in (p,n) reactions. Experimentally, (i) no substantial differences have been seen in P and A data for the ^{3}H(p,n)^{3}He and ^{9}Be(p,n)^{9}B reactions, (ii) possible differences exist in data for ^{7}Li, ^{11}B, and ^{13}C targets, but the P and A results are from different laboratories, and (iii) pronounced splitting was observed in TUNL data for ^{15}N(p,n)^{15}O below about 9 MeV.

b. The ^{2}H(p,n)2p Breakup Reaction

The final publication in an earlier study of (p,n) transverse polarization transfer measurements on light nuclei appeared during the past year; previous studies were covered in Ref. [6]. The abstract of our latest paper [7] is included here:

> "The transverse polarization transfer coefficient Kyy has been measured for the breakup reaction 2H(p,n)2p at θ=0° for five incident energies in the range from 10.6 to 15.1 MeV. ....The data are compared to predictions from a three-body separable-potential model calculation."

c. The 3H(p,n)3He Reaction: Comparison of Analyzing Power and Polarization

The final publications on our comparisons [9] between P and A were prepared jointly with T.R. Donoghue of the Ohio State University G.M. Hale of LASL. A pair of back-to-back papers have been submitted to Nuclear Physics A.

In summary, new R-matrix and shell-model calculations have been obtained near 2.5 MeV. These analyses, which include the effects of the Coulomb interaction, predict that A(θ) should be larger than P(θ) by about 0.02 to 0.05 out of a maximum value that is near 0.40 for 55° (c.m.). There is no evidence for unexplained (i.e., nuclear) charge symmetry breaking in this case. Fig. B2-1 reproduces an illustration of these conclusions from

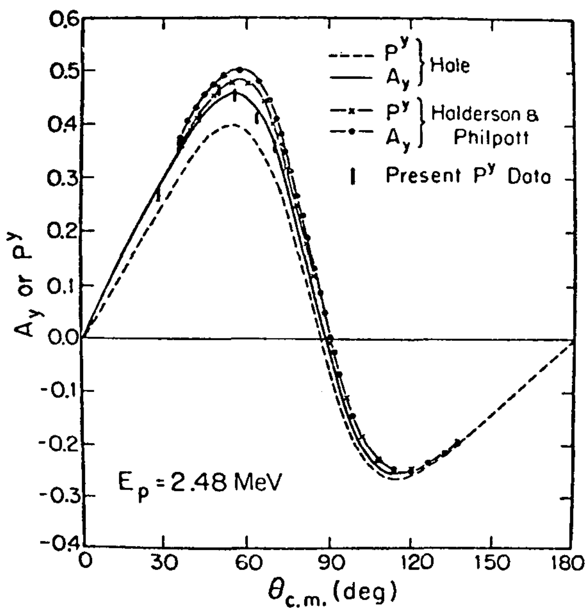

Fig. B2-1. Comparison of P(θ) data to calculations for P(θ) and A(θ) for the 3H(p,n)3He reaction

the polarization paper above, showing the P(θ) data, R-matrix calculations [10] by Hale, and shell-model results from Florida State. [12]

d. The 9Be(p,n)9B Reaction

The focus of recent data acquisition for this reaction has been on (1) analyzing power results measured with the pulsed polarized beam and (2) higher energy cross sections to support previous Lane model studies (see Refs. [4,5,13]). Preliminary results for the analyzing powers were presented [14] at the Spring meeting of the APS and at the Fifth Polarization Symposium. [15] New cross section results at 16.4 and 17.5 MeV have not yet been analyzed and will be included in a larger study of 9Be(p,n)9B cross section results from 8 to 17 MeV. Our data set of (p,n) analyzing powers for 9Be now includes new TOF data at 8.2, 9.2, 11.1, 13.5, and 15.0 MeV. This work extends the other results both to more backward angles and to higher energies. Results of two previous studies were published during the past year. Fig. B2-2 shows the overall Lane model description (see Overview and Refs. [4,5,13]) of the 9Be + nucleon system; the data shown are those which were included in the search. The (p,n) analyzing powers used here were the forward-angle results from TUNL. [18] The predictions of the new (n,n) analyzing powers from TUNL are shown in Fig. B2-3.

e. The 11B(p,n)11C and 13C(p,n)13N Reactions

Preliminary measurements for the targets 11B and 13C have been made this year as an extension of previous P-A comparisons. Analyzing powers for 13C(p,n) have been obtained at 6.88, 8.00 and 8.77 MeV for comparison to P(θ) data from ref. [20]. The comparison for 11B consists of an A(θ) distribution at 8.56 MeV to previous P(θ) data obtained at Livermore Laboratory. [20] The results were presented at the Fifth Polarization Conference. [19] We find possible evidence for small P-A splitting in these reactions. The principal difficulty with the evaluation results from resonance behavior; differences in target thickness or beam energy can yield spurious results. A considerable amount of thick-target cross-section data was obtained at 10.5, 11.5, 12.5, 13.5, 14.5, and 15.5 MeV; companion A(θ) angular distributons were taken at 8.5, 10.5, and 12.0 MeV. These results have not yet been analyzed, but it appears that the remaining resonances can be averaged sufficiently to allow an optical model analysis of the results. Such an analysis is particularly inviting, because the comparison cludes not only (p,p), (n,n) and (p,n) data for 11B targets, but also (p,p) and (n,n) data for 10B. Thin 11B targets are being made for further experiments.

f. The 13C(p,n)13N Reaction

A paper on cross sections was submitted to Nuclear Physics A as part of a study of cross sections and analyzing powers and their Lane model interpretation. Fig. B2-4 shows the Lane model results near 11 MeV; the "data" in this figure, except for the (p,n) P(θ) results of Walker *et al*., [20] has been smoothed over energy. The (p,p) results are from Weller *et al*., [22] and the "Watson" parameters are from a global optical model for light nuclei. [23]

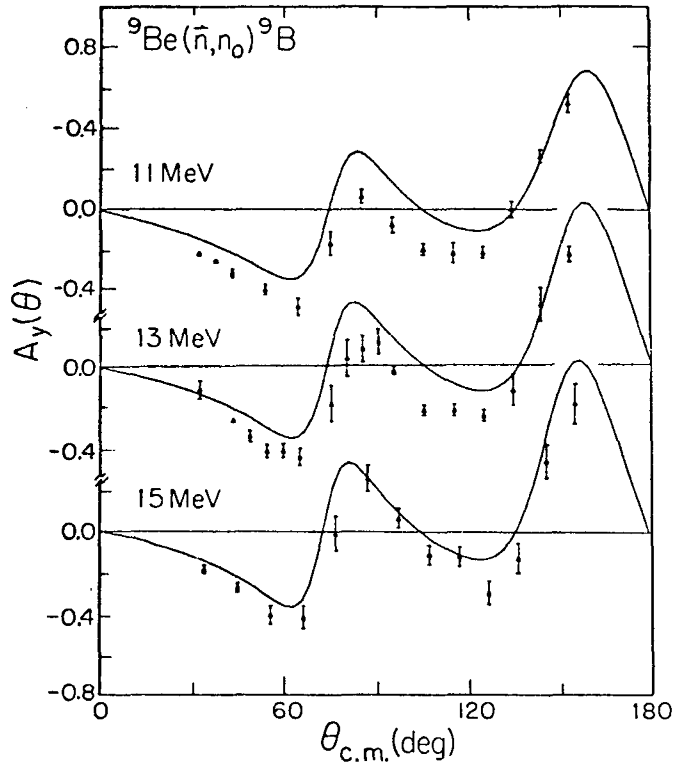

Fig. B2-3. Lane model predictions compared to data for the 9Be(n,n)9Be analyzing power. Calculations were made with the same potential used for Fig. B2-2.

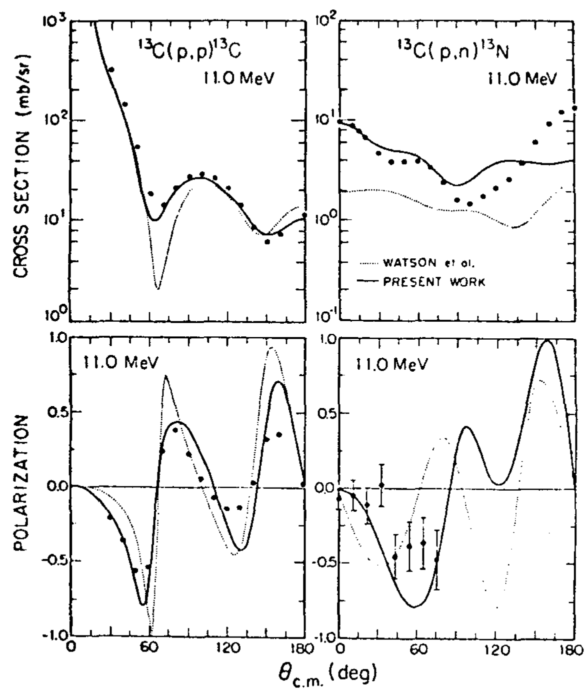

Fig. B2-4. Lane model description for 13C + nucleon system

g. The 15N(p,n)15O Reaction

Much of our interest in the 15N(p,n)15O system was stimulated by the dramatic observed differences between P and A below 9 MeV, a detailed report of which is now in preparation. Calculations by Philpott and Halderson [1] using a recoil-corrected continuum shell model have been able to reproduce the character of the observed differences (see Refs. [1-3,24]). The erratic quality of the (p,n) cross section data below 9 MeV led us to obtain supplementary data in this energy range. A considerable amount of effort went into evaluation of all previously available data. A paper on our results will appear in Nuclear Physics A. Fig. B2-5 shows the agreement between different data sets. The upper part gives the results before renormalization of the total cross sections of Barnett [26] and rejection of seriously discrepant data; the lower part shows the situation afterwards.

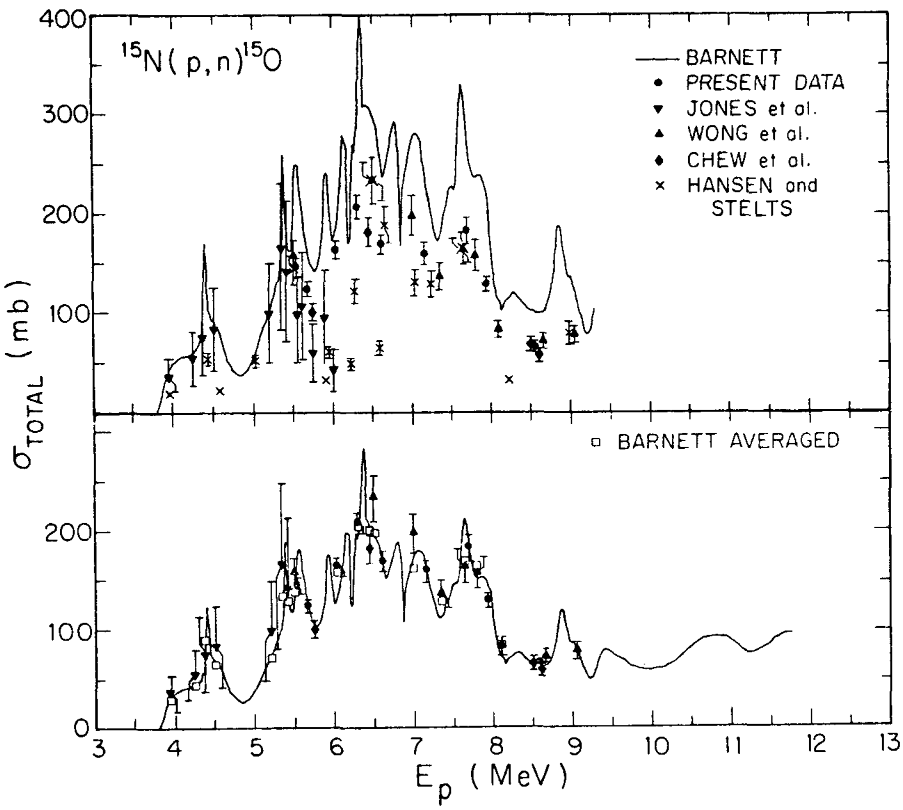

Fig. B2-5. Total cross section for the 15N(p,n)15O reaction below 9.3 MeV. The solid curve represents the data of Barnett; individual values are obtained from other authors. The upper panel shows data before renormalization of Barnett's results; the lower panel shows the agreement obtained by renormalization.

Above 9.3 MeV the Lane model study [18] of the 13C and 15N systems revealed the need for further cross section and analyzing power measurements at energies between 12 and 17 MeV. Differential cross sections were measured at 16.25 and 17.0 MeV and angular distributions of A(θ) were taken at 12.0, 15.0, and 16.8 MeV. Although some of the analyzing power data was presented at Santa Fe (see Ref. [15]), most of these new results have yet to be processed; it appears that they will be very useful in resolving the uncertainties in the energy dependence of the parameters of the Lane model analysis. [18]

---

1. R.J. Philpott and D. Halderson, in The (p,n) Reaction and the Nucleon-Nucleon Force, ed. C.D. Goodman, S.M. Austin, S.D. Bloom, J. Rapaport, and G.R. Satchler (Plenum, New York, 1980) p. 491
2. R.L. Walter and R.C. Byrd, "Polarization Observables in (p,n) Reactions," ibid., p. 469
3. R.C. Byrd and R.L. Walter, "Status of Comparisons Between Polarization and Analyzing Power in (p,n) Reactions," Proc. 5th Pol. Symp. (Santa Fe, N.M., 1980)
4. R.C. Byrd, R.L. Walter, and S.R. Cotanch, "Self-Consistent Application of the Lane Model," in The (p,n) Reaction..., p.481
5. R.C. Byrd, R.L. Walter, and S.R. Cotanch, "Lane Model Constraints on Nucleon-Nucleus Scattering Potentials," Proc. 5th Pol. Symp.,
6. P.W. Lisowski et al., Nucl. Phys. A264 (1976) 188
7. P.W. Lisowski et al., Nucl. Phys. A334 (1980) 45
8. M. Jain and G. Doolen, Phys. Rev. C8 (1973) 124
9. T.R. Donoghue et al., Phys. Rev. Lett. 37 (1976) 981
10. Sr. M.A. Doyle, et al., submitted to Nucl. Physics A
11. W. Tornow, et al/., submitted to Nucl. Phys. A
12. Dean Halderson and R.J. Philpott, Phys. Rev. Lett. 42 (1979) 36
13. R.C. Byrd, R.L. Walter, S.R. Cotanch, Phys. Rev. Lett. 43 (1979) 260
14. R.C. Byrd, et al., Bull. Am. Phys. Soc. 25 (1980) 592
15. K. Murphy, et al., "Analyzing Powers for (p,n) Reactions on Light Nuclei," Proc. 5th Pol. Symp.
16. R.C. Byrd, unpublished Ph.D. dissertation (Duke Univ., 1978)
17. R.C. Byrd et al., "Use of Neutron Time-of-Flight Techniques in (p,n) Ay Measurements," Proc. 5th Pol. Symp.
18. G. Mack et al., Nucl. Phys. A345 (1980) 241
19. K. Murphy et al., "Comparisons of Polarizations and Analyzing Powers for the 11B(p,n)11C and 13C(p,n)13N Reactions," Proc. 5th Pol. Symp.
20. B.D. Walker et al., Phys. Rev. 137 (1965) pp. 347ff and 1504ff
21. R.C. Byrd et al., Nucl. Phys. A351 (1981) 189
22. H.R. Weller et al., Phys. Rev. C18 (1978) 1120
23. B.A. Watson et al., Phys. Rev. 182 (1969) 977
24. D. Halderson and R.J. Philpott, Nucl. Phys. A345 (1980) 141
25. K. Murphy et al., "The 15N(p,n)15O Reaction Below 9.3 MeV," Nucl. Phys. A (in press)
26. A.R. Barnett, Nucl. Phys. A120 (1968) 342
27. C. Wong et al., Phys. Rev. 123 (1961) 598
28. R. LaCanna, Ph.D. dissertation (Stanford Univ., 1977)
29. E. Woye et al.,

"The Analyzing Power Ay(θ) for 12C(n,n0,1)12C from 9 to 16.8 MeV," Proc. 5th Pol. Sym.

30. R.L. Walter *et al.*, "Observation of Kyy(0°) for 15N(p,n)15O from 12.5 to 16.5 MeV," *ibid*.

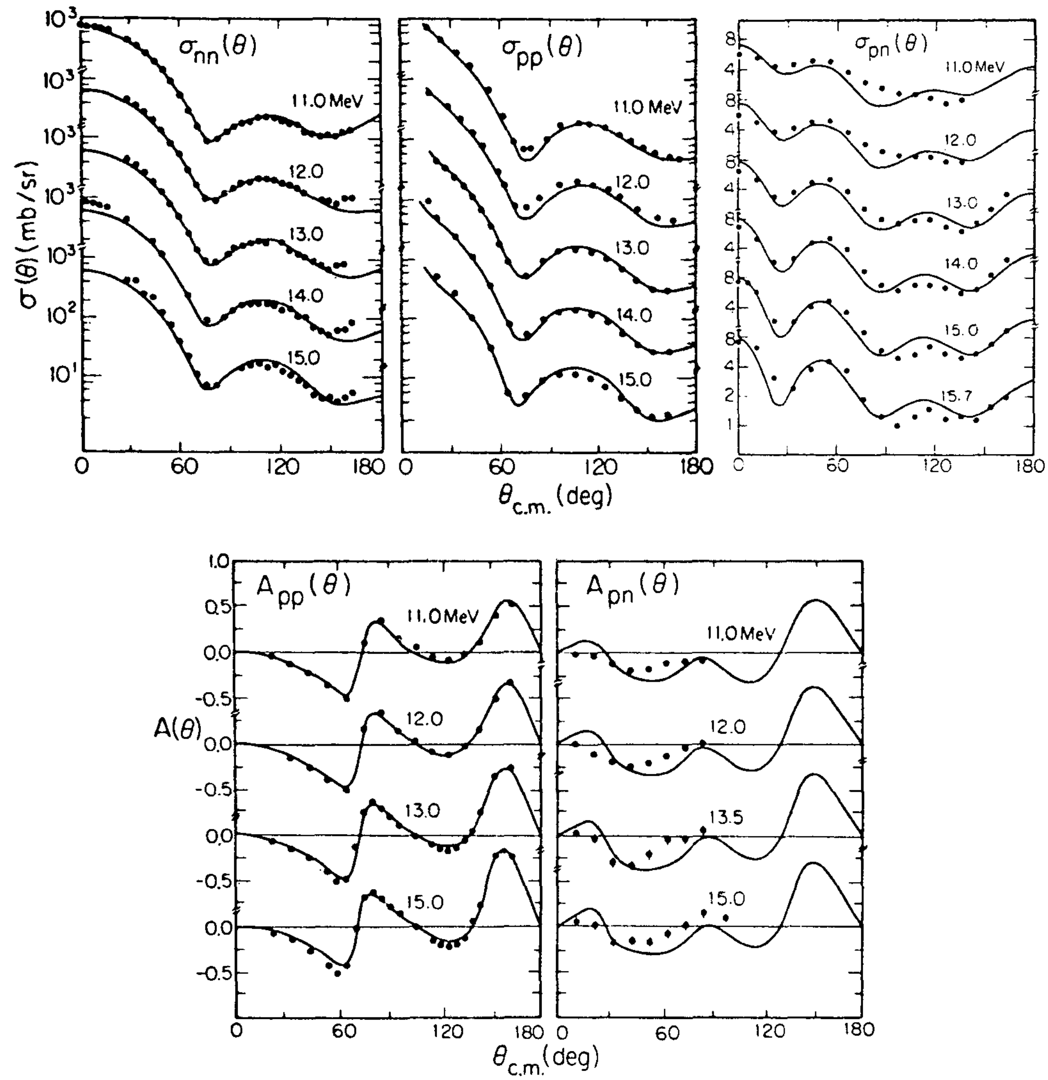

Fig. B2-2. Lane model analysis of the 9Be + nucleon system. Fits are obtained from a single coupled-channels calculation using an isospin-conserving potential.

3. Neutron Reaction Studies Involving Polarized Deuteron Beams

Polarization studies in (d,n) reactions have historically been a major interest at TUNL, although during the past couple of years this thrust has been small. With the success of the pulsed polarized beam facility at TUNL, analyzing power measurements can be performed for $(\vec{d},n)$ reactions to a high accuracy in a relatively short time. The first reaction study with the pulsed system was a measurement of A(θ) for the $^2H(\vec{d},n)^3He$ reaction at five energies between 5.5 and 11.5 MeV. The accuracy is typically ±0.003, an order of magnitude better than cross section data can be obtained. The data which were reported at Santa Fe are being prepared for submission to the 4-nucleon calculation of G. Hale at LASL. Data of this accuracy place stringent constraints on R-matrix or other model parameterizations.

Another parameter for the $^2H(d,n)^3He$ reaction has also been investigated; however, this was done primarily for applied reasons. In scattering experiments that utilize the polarized neutron beam produced in the $^2H(\vec{d},\vec{n})^3He$ polarization transfer reaction, the scatterer is placed along the original incident deuteron beam axis, i.e., at a reaction angle of 0° for the $^2H(d,n)$ reaction. The average polarization transfer coefficient is known for the angular region between 0° and 2° from previous work at TUNL. [1] However, in our scattering experiments the samples must be relatively large and placed relatively close to the $^2H + d$ source reaction in order to overcome counting rate problems. Typically the scatterer in the (n,n) experiments subtends an angle out to between 5° and 7° in the (n,γ) experiments, the angle is out to about 15°. It is therefore important to know the angular distribution of the polarization produced in the $^2H(\vec{d},\vec{n})$ reaction for angles out to 15°. The polarization transferred to the neutrons was determined by scattering from ^{12}C at 40° the angle where TUNL experiments have shown that the figure of merit for $^{12}C + n$ analyzing power is largest. The deuteron beam energy was 8 MeV, and that of the outgoing neutrons was about 11 MeV. The results were presented at Santa Fe [2] where it was shown that the "effective polarization" of the neutrons is probably equal to the value at 0° for the entire region all the way out to 15°. The observed value of 0.62 for our beam indicates that nearly 90% of the polarization of the deuteron beam is "effectively" transferred to the neutrons over the angular region subtended in the TUNL experiments. This result demonstrates another favorable feature of the $^2H(\vec{d},\vec{n})$ polarization transfer reaction as a source of polarized neutrons.

---

1. P. W. Lisowski *et al.*, Nucl Phys. A242 (1975) 298
2. Small Angle Neutron Polarization for $^2H(d,n)^3He$ at E_d = 8 MeV, W. Tornow, E. Woye, G. Mack, R. L. Walter, P. P. Guss, and R. C. Byrd (to be published)

C. RADIATIVE CAPTURE REACTIONS

1. Overview Related to (n,γ) Reactions

A large portion of the research program at TUNL involves nucleon capture studies. Previously this program has not been included in the present cross-section report, but the nature of some of the work makes it suitable to be included here. The program is under the direction of N. R. Roberson, H. R. Weller and D. R. Tilley and their collaborators are: C. Fitzpatrick, M. Jensen, S. King, S. Manglos, G. Mitev, L. Ward, S. A. Wender, M. Wright, H. Kitazawa [Tokyo Institute of Technology], H. Hasan and R. G. Seyler [Ohio State University]. The summary presented below is excerpted from the TUNL progress report for 1980. For additional details, see TUNL XIX, December 1980. One subsection of the progress report was singled out for inclusion in detail because it indicates the significance of a portion of the data for resolving a conflict in previous publications. Also shown are a collection of some of the (n,γ) cross section results (without description for brevity) which were merely lifted from the TUNL progress report.

Previous studies, mainly of nuclei with $A \leq 20$, have shown that polarized proton capture measurements can be used to extract E2 strength rather unambiguously. However, it has been found that when the resulting E2 cross sections are compared with those predicted by a simple direct (non-collective) capture model, there is rather good agreement. Therefore, it is difficult, if not impossible, to draw any firm conclusions about the effects of the GQR in the (p,γ) channel.

Polarized neutron capture measurements duplicate the physics of polarized proton capture measurements in many respects but with one important difference: The E2 effective charge for neutrons is down by Z/A^2 so that the troublesome direct E2 capture strength is virtually eliminated in most cases. If indeed most E2 strength were associated with direct capture, we would expect to see little or no E2 strength in neutron capture measurements. Our 13C(n,γ)14C results are, however, quite contrary to this expectation and indicate a substantial amount of E2 strength. Since direct capture in this case is near zero, the direct-semidirect (DSD) model must attribute all of this E2 strength to collective E2 states. Our latest calculations indicate that fair agreement with experiment is obtained if a volume type form factor is used with reasonable parameters for the isoscalar GQR. So it appears, at this time, as though (n,γ) measurements are a promising tool for observing the isoscalar GQR.

Since we have measured both the 13C(n,γ)14C and the 13C(p,γ_1)14N*(0^+,T=1) reactions, we are in a position to test the DSD model where p and n data leading to virtually the same giant resonance state are available. Another case: 14N(n,γ)15N, along with 14C(p,γ)15N, has also received our attention. In addition, we have been measuring 3He(n,γ)4He which can be related to T(p,γ)4He measurements done here and elsewhere.

Having both sets of data should provide more stringent tests of our reaction theories.

We have had considerable success in our continuing study of few-nucleon systems. In addition to measuring the first angular distribution for the 3He(n,γ)4He reaction, we have performed the first polarized neutron capture measurement for this reaction. It appears as though we can measure the angular distributions for this reaction with an accuracy greater than that achieved in previous works which used the 4He(γ,n)3He reaction to obtain this information. Our preliminary results indicate that the percentage of spin-flip E1 strength is similar in magnitude to that deduced from the T(p,γ)4He reaction. The same result holds for the percentage of E2 strength in the two experiments if triplet E2 strength is ignored. These results are especially interesting in view of the fact that our absolute cross section measurements on 3He(n,)4He indicate that the (γ,p) cross section on 4He is about 1.6-1.8 times as large as the (γ,n) cross section. These experiments (T(p,γ)4He and 3He(n,γ)4He) demonstrate the utility of polarized capture rather nicely since it is only the polarized capture data which are sufficiently sensitive to the ^{3}P E1 (spin-flip) capture strength to allow us to measure it.

A significant amount of the machine time given to capture experiments in the past year has been applied towards improving the quality of our (n,γ) and ($\vec{n}$,γ) data. Careful and complete measurements are required if we are going to extract definite results about the E2 strength in these reactions. In the future we are counting on the second large (10" x 10") NaI detector, presently being installed, to make it possible for us to significantly improve the quality and quantity of these data. Several promising changes including the addition of Boron Carbide shielding, better pile-up rejection circuitry, and the addition of gain monitoring electronics are underway.

3. The 3He(n,γ)4He Reaction

There has been considerable controversy over the magnitude of the photoneutron cross section of 4He. Our 3He(n,γ)4He cross section indicates a value of about 1.0 mb for the 4He(γ,n)3He reaction in the energy region of E_x = 23 to 33 MeV. This result, when combined with the previously reported (γ,p) cross section, implies a (γ,p) to (γ,n) cross section ratio of 1.6 to 1.9 in this energy region. In addition to determining the cross section more accurately, the yield curve was extended to En = 18 MeV. This extension allows a comparison of the 3He(n,γ) and 3H(p,γ) cross sections in a region where their ratio has been consistently measured to be approximately one. Fig. C3-1 shows our data together with the 3H(p,γ)4He data from Stanford. [1,2] Both of these are 90° yield curve measurements. Fig. C3-2 gives a comparison of our data to some of the (γ,n) measurements; [3,4,5] as well as the only other capture measurement. [6] A total (γ,n) cross section has been deduced by the principle of detailed balance, and by the relation σ_T = 8(π/3) (90). The angular distribution at Ex = 28 MeV verified this

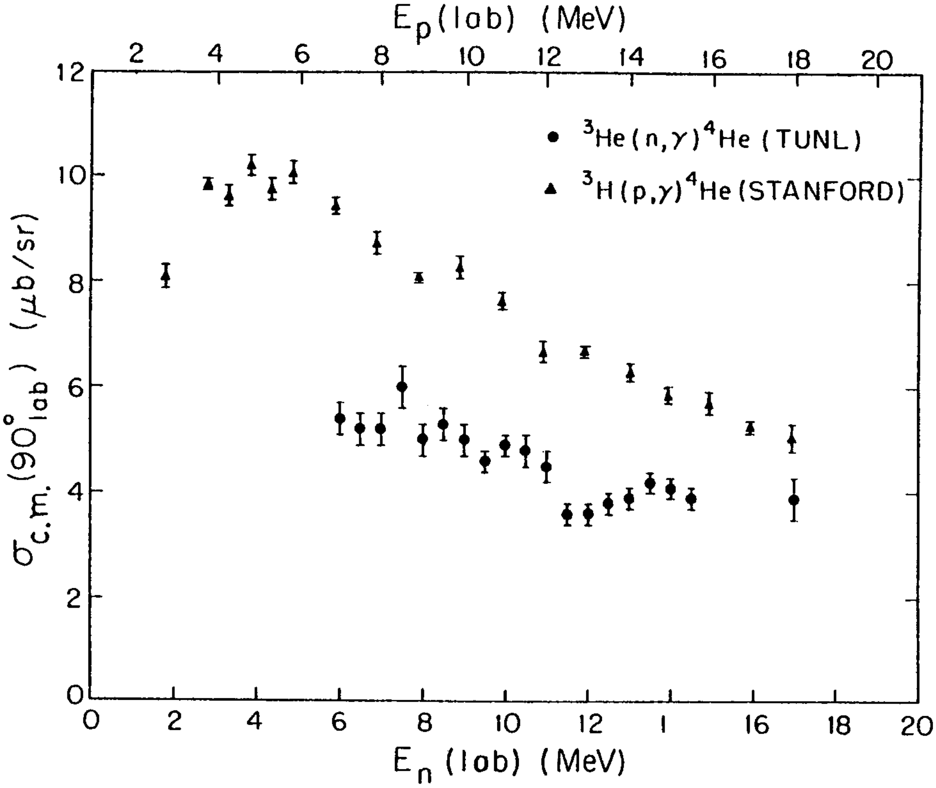

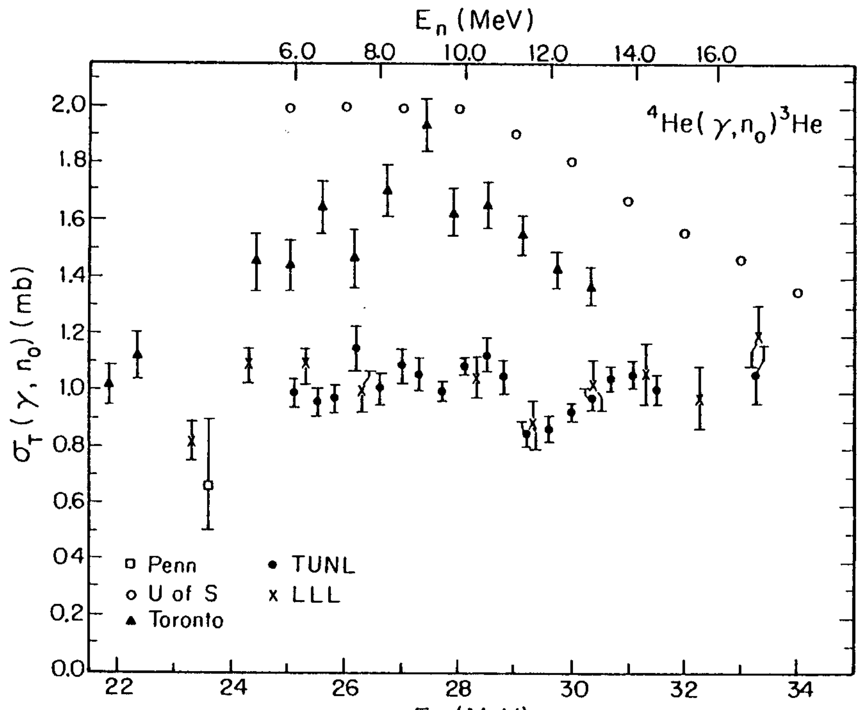

Fig. C3-2 and 3. Comparison of (γ,N) and (N,γ) data for mass four system.

relation to within 5%. Fig. C3-3 shows the angular distribution of cross section and analyzing power for the present experiment as well as for the 3H(p,γ)4He experiment performed at Stanford. [7] The a_k and b_k coefficients for each are shown for comparison.

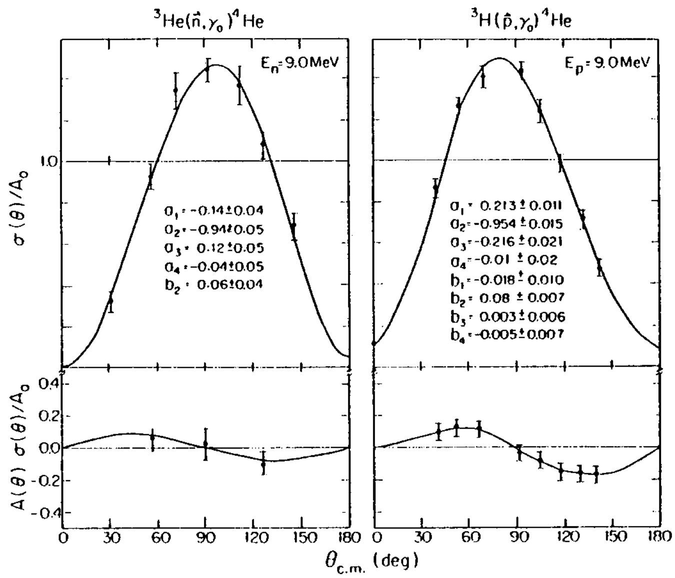

Fig. C3-3. Angular distributions of cross sections and analyzing power. The (p,γ) data are from Ref. [7].

---

1. TUNL XVIII Annual Report (1979)
2. Meyerhoff, Suffert, and Feldman, Nuclear Physics A148, 211 (1970)
3. Berman et al., Phys. Rev. C22 (1980) 2273
4. Malcom, et al., Physics Letters 47B (1973) 433
5. Irish, et al., Can. J. Phys., 53 (1975) 802
6. Zurmuhle, et al., Phys. Rev. 132 (1963) 751
7. G. King, III, Stanford, Ph.D. Thesis

4. Additional (n,γ) Cross Sections

Here we indicate the type of data that has been accumulated at TUNL recently. Note that the energy range covered in the experiments is 6 to 15 MeV.

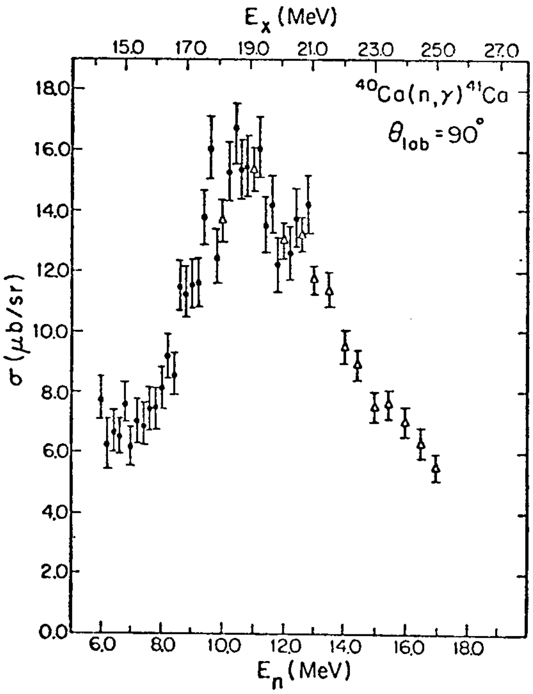

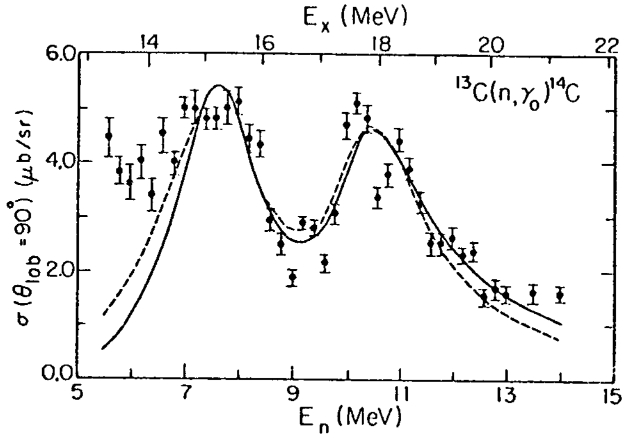

Fig. C4-1. Cross section at 90° lab for 13C(n,γ).

Fig. C4-2. Cross section at 90° for 40Ca(n,γ). Triangles are present data, solid circles earlier TUNLwork (1978).

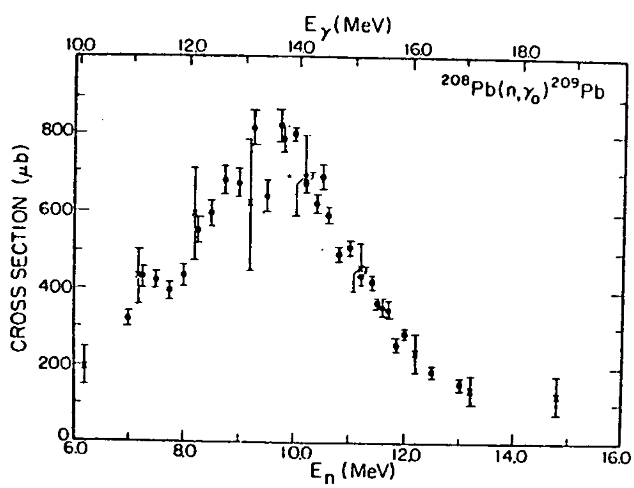

Fig. C4-3. Cross section for 208P(n,γ). Solid circles are present work, crosses from Rosen et al.

UNIVERSITY OF WASHINGTON

A. ALPHA,N YIELDS (Patrick J. Grant, Gene L. Woodruff, & David L. Johnson)

Calibration measurements of the efficiency of the 1.5m graphite stack with Fe multiplier are partially completed. At low neutron energies ($0 \leq E_n \leq 4.5$ MeV) the efficiency is 5.5% as determined by several independent methods. Efficiency measurements at higher energies are being performed using the $T(p,n)^3He$ and $D(T,n)\,\alpha$ reactions.

Yield measurements have been performed for (α,n) neutrons for O, Be, and F for α energies up to 10 MeV. Using the calibration data currently available, the yields for these elements are consistently about 20% higher than those reported in Ref. 1. The magnitudes of these yields are not expected to be significantly changed by the results of the calibrations at high neutron energies.

[1] J. K. Bair and J. Gomez del Campo, Nuc. Sci. Eng. 21, 18 (1979)

A. FAST NEUTRON PHYSICS

1. Polarization Effects in n-^{209}Bi Scattering between 2 and 4 MeV and a Limit on the Polarizability of the Neutron (M. Ahmed and F. W. K. Firk)

We have analyzed our results of the asymmetry of polarized neutrons elastically scattered from ^{209}Bi as a continuous function of energy between 2 and 4 MeV and at angles between 3° and 30° using the method of Hogan and Seyler and a modified form of Tanaka's optical potential. We have observed, for the first time, the energy-dependence of the polarization in Mott-Schwinger scattering, and have shown that at angles less than 10°, the observed polarization is essentially energy-independent. Our measurements at angles between 10° and 30° are sensitive to the form of the nuclear scattering amplitude, and we have therefore determined a set of optical model parameters (based on Tanaka's model) that accurately describe the angular- and energy-dependence of the polarization of these wider angles. We have therefore been able to set a limit on the polarizability of the neutron by fitting our data below 10° using the nuclear scattering amplitude determined at the wider angles. Our result for the polarizability coefficient is $\alpha < 3 \times 10^{-41}$ cm^3 with a 68% confidence limit. This is smaller by an order-of-magnitude than the value deduced from earlier studies of the angular distributions of the small-angle scattering of fast neutrons from heavy nuclei. It is larger than the value $< 6 \times 10^{-42}$ cm^3 deduced by Anikin and Kotukhov from studies of the anisotropy of the scattering of keV-neutrons from ^{Nat}U. We are continuing our studies of this fundamental quantity in an effort to improve our limiting value by at least a factor of ten.

2. Polarization Studies of n-^{Nat}Mg Scattering below 500 keV (J. Kruk and F. W. K. Firk)

We have made significant progress in our development of an effective polarized neutron source between 50 and 500 keV based on elastic scattering of unpolarized neutrons from natural Mg. We have constructed a new shielded detector housing of large volume that permits scattering studies to be made in the angular range 3° to 175°. We are measuring the source polarization absolutely for polarizers of widely differing sizes in order to optimize the flux and polarization. As an example of the polarization obtained in practice we observe a polarization of 50% for 250-keV neutrons scattered from a cylinder of natural Mg, 1/4" thick and 3" inside diameter. This system is being used to continue our neutron polarizability studies in the hundred-keV region.

B. PHOTONEUTRON REACTIONS

1. Non-E1 Absorption in ^{16}O between 17 and 21 MeV (F. W. K. Firk)

The polarization of photoneutrons emitted at 90° from the reaction $^{16}O(\gamma, \vec{n}_0)^{15}O$ in the photon energy range 17 to 21 MeV has been measured with good resolution using the well-known $^{12}C(\vec{n}, n)$ reaction as an analyzer. Clear evidence is obtained for non-E1 absorption at 17.15, 18.77, 19.15, 19.5 and 20.4 MeV. The states at 17.15 and 18.77 can be identified with the 1^+ states observed by Snover et al. in the $^{15}N(\vec{p}, \gamma_0)^{16}O$ reaction. Of particular interest is the observation that the maximum neutron polarization at 18.77 MeV is -60%, which agrees closely in magnitude and has the same sign as the value deduced from the proton study. These observations establish the isospin of the state unambiguously.